Temporal coordination of the metaphase to anaphase transition

Dissertation

der Mathematisch-Naturwissenschaftlichen Fakultät

der EBERHARD KARLS UNIVERSITÄT TÜBINGEN

zur Erlangung des Grades eines

Doktors der Naturwissenschaften

(Dr. rer. nat.)

vorgelegt von

Julia Luise Kamenz

aus Berlin

Tübingen

2014

Gedruckt mit Genehmigung der Mathematisch-Naturwissenschaftlichen Fakultät der Eberhard Karls Universität Tübingen.

Tag der mündlichen Qualifikation:	18.02.2015
Dekan:	Prof. Dr. Wolfgang Rosenstiel
1. Berichterstatter:	Dr. Silke Hauf
2. Berichterstatter:	Prof. Dr. Ralf-Peter Jansen
3. Berichterstatter:	Prof. Dr. Olaf Stemmann

Meiner Familie

ACKNOWLEDGEMENTS

Science can be great, exciting and truly enriching, but it can also be hard, frustrating and unforgiving. Sometimes it is an illuminating experiment, but much more often it is the good discussion over lunch, a new idea sketched on a napkin, late night pizza in the lab or a good laugh about the last messed up experiment, which makes all the difference. Therefore, I would like to thank all the people, who made the lab such an enjoyable place for the last six years and will hopefully continue to enrich my life inside and outside of the lab.

In particular, I would like to thank Silke for being such an outstanding mentor for almost 10 years by now. I am grateful for your inexhaustible trust and support, for coping with my slightly chaotic nature, and tolerating my (normally not so secret) secret projects. Your enthusiasm, curiosity and your approach to science have always inspired me.

Thanks to Steffi for making every day (and night) in the lab a bit more fun - for every of the countless coffees and chocolate breaks.
I would also like to thank all other Hauf lab members, who I had the pleasure to work with. Thanks to Katharina, Andre, Asha, Yu-Hua, Hanna, Sabine, Nadine, und Eva S. I am particularly thankful to Maria and Eva, for being there for me during all these years and for never giving up trying to make a more tidy person out of me. I am thankful to Armin for being the best Bachelor student one can imagine.
I would like to thank Remco and Stefan for these very fun and successful collaborations and for all their encouragement and support.

I would also like to thank Fabio, Verena, Stephi, Enno, Andi, Jörg, Ole, and Nicole for being such good friends.

Most importantly, I would like to thank my parents, my brother and my grandparents for their continuous support throughout all these years.

TABLE OF CONTENTS

LIST OF FIGURES

ABBREVIATIONS

A	alanine
APC/C	anaphase-promoting complex/cyclosome
Ark1	aurora-related kinase 1
Bub	budding uninhibited by benzimidazole
BubR1	bub1-related protein 1
cdc	cell division cycle
CDK	cyclin-dependent kinase
C. elegans	*Caenorhabditis elegans*
CPC	chromosomal passenger complex
cut	cell untimely torn
Cyc(B)	cyclin B
d	day
Da	Dalton
DAPI	4',6-diamidino-2-phenylindole
D-box	destruction box
D. melanogaster	*Drosophila melanogaster*
DMSO	Dimethyl-sulfoxide
DNA	deoxyribonucleic acid
DTT	Dithiothreitol
EDTA	Ethylenediaminetetraacetic acid
EMM	Edinburgh minimal medium
FRET	Förster resonance energy transfer
GFP	green-fluorescent protein
HEPES	2-[4-(2-hydroxyethyl)piperazin-1-yl]ethanesulfonic acid
K	Lysine
KMN	KNL1/Mis12 complex/Ndc80 complex
KNL1	Kinetochore-null protein
KT-MT	kinetochore-microtubule
L	liter
MBC	methyl-2-benizimidazole carbamate, carbendazim
MCC	mitotic checkpoint complex
min	minutes
mL	millilitre
μL	microliter

MPF	maturation promoting factor
MT	microtubule
ORF	open reading frame
Plo1	polo-kinase 1
PP1	protein phosphatase 1
PP2A	protein phosphatase 2A
rcc	raw camera counts
rpm	rounds per minute
S	serine
SAC	spindle assembly checkpoint
SCS	sister chromatid separation
Sec	securin
sec	seconds
Sep	separase
Slp1	sleepy homolog 1
SPB	spindle pole body
S. pombe	*Schizosaccharomyces pombe*
TRIS	Tris(hydroxymethyl)aminomethane
WCE	whole cell extract
X. laevis	*Xenopus laevis*
YE	yeast extract

SUMMARY

The cell cycle is an ordered sequence of events culminating in the formation of two identical daughter cells. Ensuring the order of the events is essential for genomic integrity and cell proliferation. The sudden and synchronous splitting of chromosomes during the metaphase to anaphase transition is one of the visually most dramatic events of the cell cycle. The transition is driven by the activity of the anaphase promoting complex/cyclosome (APC/C), an E3 ubiquitin ligase, which initiates the destruction of its two essential targets, cyclin B and securin. Cyclin B degradation inactivates the cyclin-dependent kinase 1 (CDK1) and triggers a multitude of processes during mitotic exit. Degradation of securin releases separase from its inhibition. Active separase subsequently triggers the highly synchronous separation of sister chromatids. The separation is irreversible and therefore needs to be highly accurate and tightly coordinated with mitotic exit. Yet, little is known about the molecular events that determine the timing of the single processes and coordinate the individual processes relative to each other.

I have systematically studied the dynamics of the metaphase to anaphase transition in the fission yeast *Schizosaccharomyces pombe* using live cell imaging assays with high temporal resolution. My analysis shows that the synchronicity of sister chromatid separation directly depends on the degradation kinetic of its upstream regulator securin, which suggests the absence of additional feedback regulation. Stochastic processes dominate the order in which sister chromatids separate, but an intrinsic bias in chromosome segregation exists, which is enhanced by decreased separase activity or securin degradation rates.

Sister chromatid separation has to be tightly coordinated with the cyclin B degradation-driven processes of mitotic exit. I find the temporal order of events during the metaphase to anaphase transition to be remarkably robust against changes in securin and cyclin B, even if the overall timing of the respective events is severely altered. Competition of securin and cyclin B for the shared degradation machinery as well as systematic variability in the protein thresholds at which certain events occur contribute to the observed temporal robustness.

I further investigated the consequences of potential misregulation between securin and cyclin B degradation-dependent events and show that high CDK1 activity at anaphase results in untimely destabilization of chromosome

attachment, activation of the mitotic checkpoint and inhibition of the APC/C. Yet, we find that inhibition of the APC/C occurs with slow kinetics, which might provide an additional buffer against the detrimental consequences of such a loss in coordination.

ZUSAMMENFASSUNG

Der Zellzyklus besteht aus einer Abfolge molekularer Prozesse, die letztendlich zur Entstehung von zwei identischen Tochterzellen führen. Um die Unversehrtheit der genetischen Information und somit die kontrollierte Zellvermehrung sicherzustellen, ist dabei entscheidend, dass eine strikte Reihenfolge der Prozesse eingehalten wird. Einer der eindrucksvollsten Vorgänge des Zellzykluses ist die abrupte und synchrone Teilung der Schwesterchromatiden, die während des Übergangs von der Metaphase in die Anaphase stattfindet. Der Übergang ist durch die Aktivität des Anaphase-fördernden Komplexes/Cyclosoms (APC/C) gesteuert, einer E3 Ubiquitinligase, die den Abbau der beiden Substrate, Securin und Cyclin B, initiiert. Der Abbau von Cyclin B verringert die Aktivität der Cyclin-abhängigen Kinase 1 (CDK1), was eine Vielzahl von Prozessen einleitet, die für das korrekte Beenden der Mitose notwendig sind. Der Abbau von Securin setzt Separase frei, welche zuvor von Securin inhibiert wurde. Die nun aktive Separase löst die hochsynchrone Teilung der Schwesterchromatiden aus. Die Teilung der Schwesterchromatiden ist unumkehrbar und muss daher präzise ausgeführt werden und zeitlich mit anderen Prozessen am Ende der Mitose koordiniert werden. Welche Mechanismen bestimmen, wann einzelne Prozesse stattfinden, und wie diese Prozesse relativ zueinander koordiniert werden, war bisher nicht bekannt.

Mit Hilfe von zeitlich hochaufgelöster Mikroskopie lebender Hefezellen (*Schizosaccharomyces pombe*) habe ich die dynamischen Vorgänge während des Übergangs von der Metaphase in die Anaphase untersucht. Meine Studien zeigen, dass die Synchronizität der Schwesterchromatidenteilung direkt von der Abbaurate des Securins abhängt. Dies legt nahe, dass keine zusätzlichen Rückkopplungsmechanismen existieren. Des Weiteren ist die Reihenfolge, in der sich die Schwesterchromatiden unterschiedlicher Chromosomen trennen, im Wesentlichen zufällig. Es gibt jedoch eine leichte Tendenz für eine bestimmte Reihenfolge in der Trennung der Chromosomen, die verstärkt wird, wenn die Aktivität von Separase oder die Abbaurate von Securin verringert wird.

Die Teilung der Schwesterchromatiden muss mit weiteren Vorgängen am Ende der Mitose – welche durch den Abbau von Cyclin B reguliert werden – koordiniert werden. Ich habe festgestellt, dass die zeitliche Abfolge dieser Prozesse erstaunlich robust gegenüber Proteinkonzentrationsschwankungen

von Securin und Cyclin B ist – und das obwohl diese Schwankungen den gesamten zeitliche Ablauf beachtlich verzögern können. Sowohl Kompetition um die Abbaumaschinerie, die für Securin und Cyclin B die gleiche ist, als auch eine systematische Variabilität im Grenzwert, den es für ein Protein zu erreichen gilt bevor ein bestimmter Prozess stattfinden kann, tragen zu dieser zeitlichen Robustheit bei.

Darüber hinaus habe ich untersucht, was die Konsequenzen sind, wenn die von Securin- und Cyclin B-Abbau eingeleiteten Prozesse fehlreguliert sind. Ich konnte zeigen, dass eine zu hohe Aktivität von CDK1 während der Anaphase dazu führt, dass einige Prozesse irrtürmlich stattfinden: die Anheftung der Chromosomen an die mitotische Spindel wird wieder gelöst, der Überwachungsmechanismus der Mitose, der eigentlich zu diesem Zeitpunkt inaktiv sein sollte, wird wieder aktiviert und der APC/C wird inhibiert. Ich habe jedoch auch festgestellt, dass die Inhibition des APC/C relativ langsam stattfindet. Diese Langsamkeit könnte einen weiteren Mechanismus darstellen, der das System robust gegenüber natürlich auftretenden Schwankungen macht.

1 Introduction

1.1 The cell cycle – a brief history

Already over 150 years ago Robert Remak and Rudolf Virchow suggested that the cell is the basic unit of every organism and that new cells only emerge from pre-existing cells ('omnis cellula ex cellula'). Thus, cell division is one of the most fundamental processes in nature and central to growth and development of every multicellular organism. In general, for a cell to divide, the genomic information has to be duplicated and equally distributed to the two newly arising daughter cells. In eukaryotes, unlike in prokaryotes, these events of DNA replication and segregation are separated in time and embedded in a large set of ordered events which comprise all necessary steps for accurate cell duplication, called the cell cycle (Hartwell et al., 1974). Cell division is often closely coordinated with cell growth, which ensures a constant ratio of DNA to cellular volume within a cell population (Mitchison, 2003). Hence, the cell cycle is classically viewed as alternating between the phase of DNA synthesis (S-phase) and the phase of DNA segregation and cytokinesis (M-phase). S- and M-phase are interspersed by two phases, G1 and G2, which are predominantly associated with cell growth.

1.1.1 What drives the cell cycle?

Although the reoccurring ordered stages leading up to cell division have already captured the interest of researchers like Walther Flemming and Eduard Strasburger in the 19th century, and terms describing the different cell cycle phases (e.g. mitosis, prophase, anaphase, telophase) have their origin in this period, researchers at that time were condemned to a phenomenological description of the process. First insights into the molecular mechanisms underlying the oscillatory behaviour of events during the cell cycle were gained in the 1970s when Masui and Markert realized that the cytoplasm of early frog (*Rana pipiens*) embryos was capable of inducing the maturation of immature oocytes (Masui and Markert, 1971). Consequently, they named the agent maturation promoting factor (MPF). Over the next years biochemical evidence accumulated that the activity of the MPF was oscillating during the cell cycle with high activity in mitotic and meiotic metaphases and low activity in the remaining cell cycle phases (Gerhart et al., 1984; Wasserman and Smith, 1978). In 1983 using protein gel-electrophoresis to separate proteins of cycling sea urchin

and clam extracts, Tim Hunt and colleagues reported two prominent protein bands, which seemed to appear and disappear periodically during the cell cycle. Based on the labelling of these bands on their blots, they named the proteins cyclin A and cyclin B (Evans et al., 1983). Although the authors of this paper already pointed out that 'the parallels between the behaviour of the MPF and cyclin are striking' (Evans et al., 1983) the direct link between cyclins and the MPF could not be made until some years later because the MPF proofed notoriously difficult to purify.

During the same period, a different view on the cell cycle emerged from two genetic screens, which were conducted by Lee Hartwell in budding yeast (*Saccharomyces cerevisiae*) (Hartwell et al., 1974; Hartwell et al., 1970) and later by Paul Nurse in fission yeast (*Schizosaccharomyces pombe*) (Nurse et al., 1976). These screens isolated temperature-sensitive mutants, which arrested uniformly at distinct stages of the cell cycle. Among these mutants, which were named cell division cycle (cdc) mutants, was the budding yeast mutant *cdc28*, which seemed to play a crucial role in the transition from G1 to S phase (also referred to as 'Start') (Hartwell et al., 1974) and the fission yeast mutant *cdc2*, which arrested at the transition from G2 to M phase (Nurse et al., 1976). The advent of molecular cloning enabled these researchers to demonstrate that *CDC28* and *cdc2*$^{+}$ encoded functionally homologous kinases (Beach et al., 1982). Finally, towards the end of the 1980s Lohka and Maller succeeded in purifying the MPF (Lohka et al., 1988) and it became evident that the MPF was a heterodimer consisting of cyclin B (Gautier et al., 1990) and Cdc2 (Gautier et al., 1988). Cdc2 was renamed into the cyclin-dependent kinase 1 (CDK1). Murray and Kirschner irrevocably established that cyclin B synthesis and degradation are essential for progression into and out of mitosis (Murray and Kirschner, 1989a; Murray et al., 1989) and shortly after, it was shown that the degradation was mediated by the ubiquitin/proteasome system (Glotzer et al., 1991; Hershko et al., 1991), specifically by a large E3 ubiquitin ligase, which was named the anaphase-promoting complex or cyclosome (Irniger et al., 1995; King et al., 1995; Sudakin et al., 1995). Rapidly the different experimental lines of evidence were now unified to a bigger picture (Murray and Kirschner, 1989b): The cell cycle is generally driven by the rise and fall of cyclins, which determine activity and specificity of the cyclin-dependent kinase. The kinase activity in turn regulates a multitude of events associated with DNA replication and DNA segregation in a spatial and temporal manner. The progression of this oscillator is furthermore controlled by several signalling pathways ('checkpoints'), which ensure faithful, orderly progression

through the cell cycle (Hartwell and Weinert, 1989; Hoyt et al., 1991; Li and Murray, 1991). These signalling pathways modulate the length of the different cell cycle phases in response to external cues, e.g. nutrient availability or growth factors, and they delay commitment to the next cell cycle phase until all crucial steps of the previous cell cycle phase have been achieved, e.g. not allowing mitosis before completion of DNA synthesis.

1.1.2 What holds sister chromatids together and what separates them?

Chromosomes and their intriguing movements had sparked the interest of scientists long before their importance as the units of inheritance was recognized. Already in the second half of the 19th century, researchers had been able to visualize chromosomes using specific dyes (hence, their name from the greek word chroma meaning colour and soma meaning body). Around 1880, Walther Flemming described that chromosomes split along their longitudinal axis and that the halves move to opposite poles of a dividing cell ((Flemming, 1882), page 215 et seq.). The term ‘anaphase’ was introduced by Eduard Strasburger shortly thereafter. Astonishingly, Flemming also suggested the existence of a temporary connection between sister chromatids, which would be resolved during anaphase (Flemming, 1879). A hundred years later, genetic screens in budding and fission yeast identified the first genes, which were essential for the faithful segregation of artificial or natural chromosomes (Hirano et al., 1986; Larionov et al., 1985; Maine et al., 1984; McGrew et al., 1989; Michaelis et al., 1997). Several of the identified gene products were later shown to assemble into a large ring-shaped complex, called cohesin complex. The cohesin ring topologically entraps the two DNA strands and connects sister chromatids from their synthesis in S-phase until anaphase (Ivanov and Nasmyth, 2005). The timely destruction of the Scc1 subunit at anaphase opens the cohesin ring and allows the longitudinal splitting of the chromosomes (Ciosk et al., 1998; Michaelis et al., 1997). But what was triggering the timely destruction of cohesin? The fact, that blocking the anaphase-promoting complex/cyclosome (APC/C) but not preventing cyclin B degradation inhibited sister chromatid separation suggested a so far unidentified target of the APC/C (Holloway et al., 1993; Surana et al., 1993). In 1996, several groups reported the identification of a protein in budding and fission yeast respectively, which efficiently inhibited sister chromatid separation if their degradation in anaphase was prevented (Cohen-Fix et al., 1996; Funabiki et al., 1996b; Yamamoto et al., 1996). Intriguingly, despite low overall sequence homology, the N-termini of these proteins contained the same short sequence motifs, which had

already been shown to be essential for the degradation of the B-type cyclins during mitosis (Funabiki et al., 1997). Because of its essential inhibitory function in preventing precocious sister chromatid separation this protein is commonly referred to as securin. Securin was found to closely associate with a large protease, separase (Ciosk et al., 1998; Funabiki et al., 1996a; Uhlmann et al., 2000). Elegant biochemical work showed, that once released from its inhibition, this protease hydrolyses specific peptide bonds of cohesin's Scc1 subunit. Mutations in the recognition motif around the cleavage site completely block sister chromatid separation. The importance of this cleavage was further demonstrated by showing that artificial cleavage of cohesin by an unrelated protease initiates chromosome splitting and anaphase-like movement of sister chromatids in the absence of separase activity (Oliveira et al., 2010; Pauli et al., 2008; Uhlmann et al., 1999; Uhlmann et al., 2000).

These proteins and complexes constitute the core of mitotic progression: APC/C, CDK1, cyclin B, separase and the cohesin complex are highly conserved and presumably have been present in the last eukaryotic common ancestor (Eme et al., 2011; Krylov et al., 2003). Proteins resembling cohesin subunits are even present in bacteria (Strunnikov, 2006). A potential exception to the general rule that the APC/C controls anaphase has recently been uncovered in *Giardia intestinalis*, a highly diverged eukaryotic parasite, where it seems that the cyclin B fluctuations are independent of the APC/C (Gourguechon et al., 2013).

1.2 Mitosis

Only once the cell has ensured that its genomic information has been correctly duplicated during S-phase, it has reached an adequate size, and environmental conditions are favourable, it will commit to the next and final phases of the cell cycle, mitosis and cytokinesis (constituting M-phase). Mitosis comprises a highly ordered sequence of events, which culminates in the separation and segregation of the duplicated chromosomes and the emergence of two nuclei. With a few prominent exceptions, e.g. the syncytial cell during early development of *Drosophila melanogaster*, nuclear division is followed and closely linked to cellular division. Biochemically, mitosis is defined by the high activity of the CDK1/cyclin B complexes, which orchestrate mitotic progression by phosphorylating over 100 targets (Chi et al., 2008; Holt et al., 2009; Mitchison, 2003; Strunnikov, 2006; Ubersax et al., 2003). During the initial rise of CDK1 activity in early mitosis (prophase), chromosomes

condense and in many organisms the nuclear envelope is disassembled. Centrosomes separate and initiate the nucleation of microtubules in order to establish the mitotic spindle (Walczak et al., 2010). The kinetochore, a large proteinaceous structure which mediates the contact between the spindle microtubules and the centromeric region of sister chromatids, assembles fully (Cheeseman, 2014; Gascoigne and Cheeseman, 2013). Via a stochastic 'search-and-capture' mechanism, spindle microtubules attach to the kinetochores (Kirschner and Mitchison, 1986). An error-correction mechanism destabilizes kinetochore-microtubule interactions, if tension, which results from the attachment of the two sister kinetochores to microtubules emanating from the opposing spindle poles, is not established (Maresca and Salmon, 2010; Nezi and Musacchio, 2009). Until all chromosome have become properly attached an additional surveillance mechanism, the spindle assembly checkpoint (SAC), delays further progression through mitosis. The alignment of all chromosomes to the equatorial plane of the spindle marks the entry into metaphase. At this point the spindle assembly checkpoint is satisfied and the anaphase-promoting complex/cyclosome (APC/C) becomes active. The APC/C mediates the degradation of its two essential targets securin, an inhibitor of sister chromatid separation, and cyclin B, the activator of the cyclin-dependent kinase (Primorac and Musacchio, 2013). Destruction of securin releases separase, which then proteolytically cleaves the Scc1 subunit of the cohesin complex, which has held sister chromatids together from S phase on (Uhlmann, 2003). Degradation of cyclin B results in a gradual decrease in CDK1 activity, which orchestrates the events of mitotic exit, e.g. anaphase B spindle elongation, spindle disassembly, chromosome decondensation (Sullivan and Morgan, 2007) (Figure 1). Eventually the contractile ring, a membrane-associated structure of actin and myosin filaments, forms at the position of the midspindle (Barr and Gruneberg, 2007). Ingression of the contractile ring results in constriction (cytokinesis) and in the final abscission of the two cell halves (Agromayor and Martin-Serrano, 2013).

1.3 The metaphase to anaphase transition

The rapid and synchronous splitting of sister chromatids and their fast movement to opposite poles is visually the most impressive event of the cell cycle. The loss of cohesion and hence, the splitting of chromosomes is irreversible. Once the split has been made, cells need to make sure that the chromosomes reliably reach the opposite ends of the cell and are packaged into separate nuclei. Any error during

these final steps of nuclear division jeopardizes the inheritance of the genetic material.

The metaphase to anaphase transition is a highly dynamic process in which a multitude of events occur in a very short amount of time. Despite the dynamical nature of the process, the events driven by the destruction of securin and cyclin B need to occur in an orderly fashion and have to be coordinated with respect to each other, e.g. the splitting of the chromosomes has to be coordinated with changes in the spindle apparatus. Research so far mainly focused on how the initiation of the metaphase to anaphase transition is controlled by the timely activation of the APC/C; much less is known about what determines the timing of the individual events during the transition and how the relative timing of the events during the metaphase to anaphase transition is coordinated.

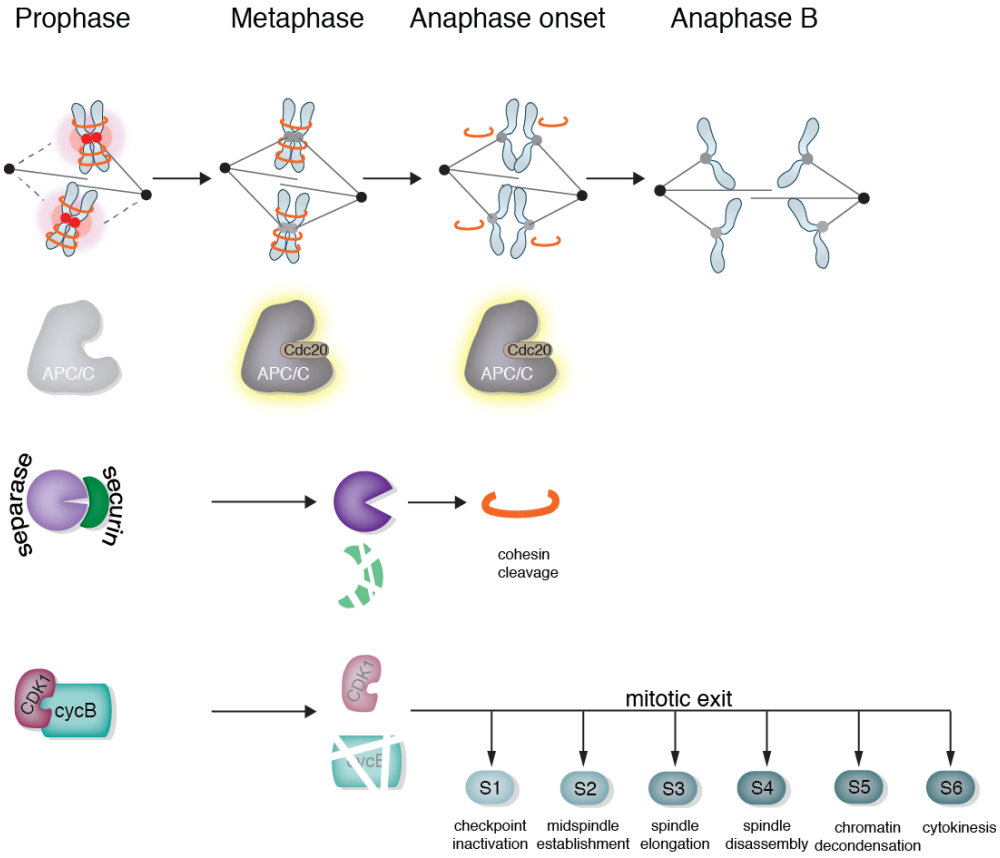

Figure 1-1 The metaphase to anaphase transition

In prophase, when chromosomes have not yet become attached to the mitotic spindle, the anaphase-promoting complex/cyclosome (APC/C) does not exhibit activity towards securin and cyclin B (cycB). Hence, separase is inhibited and the cyclin-dependent kinase (CDK1) active. Once all chromosomes are attached to the mitotic spindle in metaphase, the APC/C in conjunction with its co-activator Cdc20 targets securin and cyclin B for proteasomal degradation. Free separase now cleaves the cohesin complex and promotes sister chromatid separation. Cyclin B destruction and concomitant inactivation of CDK1 results in the dephosphorylation and activation of multiple substrates (S1, S2, etc.), which orchestrate events of mitotic exit, e.g. checkpoint inactivation, midspindle establishment and spindle elongation.

1.4 The anaphase-promoting complex/cyclosome

The anaphase-promoting complex/cyclosome (APC/C) is a multi-subunit ubiquitin-ligase (E3), which marks proteins for proteasomal degradation by attaching poly-ubiquitin chains (Chang and Barford, 2014; Peters, 2006; Pines and Hagan, 2011; Primorac and Musacchio, 2013). The APC/C belongs to the family of cullin RING (Really Interesting New Gene) ubiquitin ligases (CRLs), which catalyse the direct transfer of ubiquitin from a ubiquitin-conjugating enzyme (E2) to a lysine residue of the substrate without an E3-ubiquitin intermediate. Besides the catalytic core, which is formed by a cullin domain (Apc2) and a RING domain (Apc11) subunit, the APC/C consists of at least 10 additional subunits (Chang and Barford, 2014), some of which are present in multiple copies, yielding a molecular machinery of about 1.2 MDa. Inhibition or depletion of the APC/C efficiently blocks cells in metaphase (Hirano et al., 1988; Irniger et al., 1995; O'Donnell et al., 1991; Tugendreich et al., 1995). Similarly, proteasome inhibition leads to the persistence of APC/C substrates and blocks anaphase and exit from mitosis in a variety of organisms (Genschik et al., 1998; Ghislain et al., 1993; Gordon et al., 1993; Wojcik et al., 1996). This indicates that proteasome-mediated destruction ultimately inactivates APC/C substrates. However, ubiquitination alone, without proteasome-mediated degradation, may suffice to inactivate APC/C substrates in some cases (Li and Blow, 2004; Nishiyama et al., 2000). The APC/C has many substrates (reviewed in (Manchado et al., 2010a; Peters, 2002; Pines, 2006)) and the time of degradation varies between substrates, e.g. cyclin A degradation starts with nuclear envelope breakdown, securin and cyclin B become degraded during the metaphase to anaphase transition, while other proteins only become degraded in anaphase B and telophase (Lindon, 2008; Sullivan and Morgan, 2007). Partially this temporal order is mediated by distinct specificity factors (co-activators) of the APC/C, which recognize different substrates and mediate their interaction with the APC/C. Two co-activators are highly conserved: Cdc20 (also called Slp1 (sleepy 1) in *S. pombe*, Hct1 in *S. cerevisiae,* fizzy (fzy) in *D. melanogaster* and p55 in *H. sapiens*) and Cdh1 (also called Ste9 (sterile 9) in *S. pombe* and fzr (fizzy-related) in *D. melanogaster*). Both co-activators share common structural elements: an N-terminal C-box (consensus DRF/YIPXR) and a C-terminal IR-tail mediate the contact with the APC/C, while a WD40 domain, which exhibits a seven-bladed propeller fold, facilitates substrate recognition (Burton and Solomon, 2001; Burton et al., 2005; da Fonseca et al., 2011; Eytan et al., 2006; Hilioti et al., 2001; Kraft et al., 2005; Pfleger et al., 2001; Vodermaier et al., 2003). Beyond

substrate recruitment, C-box mediated binding of the co-activator also stimulates APC/C activity by inducing a conformational change in the catalytic module of the complex (Chang and Barford, 2014; Kimata et al., 2008; Van Voorhis and Morgan, 2014). Distinct motifs have been associated with preferential recognition by the APC/C in association with either Cdc20 or Cdh1. The destruction box motif (D-box, consensus RXXLXXXXN) has been first characterized in cyclins and is generally thought to mediate the degradation by the APC/C^{Cdc20} (King et al., 1996; Murray and Kirschner, 1989b). Nevertheless, the D-box can also be recognized by Cdh1 (Glotzer et al., 1991). Proteins carrying a KEN-motif (consensus KEN) seem to be mainly degraded by the APC/C^{Cdh1} (Pfleger and Kirschner, 2000). Furthermore, several other non-canonical degradation sequences have been identified (Chang and Barford, 2014) and multiple low-affinity interactions between substrates, the APC/C and its co-activators have been suggested to provide further specificity (Matsusaka et al., 2014; Matyskiela et al., 2009).

The co-activators associate with the APC/C at different stages during the cell cycle. Cdc20 acts as a co-activator for the APC/C from early mitosis on, whereas Cdh1 associates with the APC/C only once Cdh1 has been sufficiently stripped of CDK1-mediated phosphorylations (Blanco et al., 2000; Jaspersen et al., 1999; Kramer et al., 2000; Zachariae et al., 1998) around anaphase (Floyd et al., 2008; Gurden et al., 2010; Hagting et al., 2002). Cdc20 and Cdh1 might co-exist for some time during anaphase (Floyd et al., 2008; Gurden et al., 2010) until Cdc20 is inactivated by auto- and Cdh1-mediated degradation (Foe et al., 2011; Robbins and Cross, 2010).

In addition to consecutive binding of substrates to the APC/C, differential processivity of substrate ubiquitination has been suggested to provide order in substrate degradation (Rape et al., 2006). Processivity is defined by how many ubiquitin molecules are transferred onto a substrate within a single round of binding to the APC/C. Hence, processivity is determined by the dissociation rate of the substrate from the APC/C (k_{off}) and the catalytic rate of substrate ubiquitination (k_{cat}). Only substrates, which carry multiple ubiquitin molecules (n>4), either as a poly-ubiquitin chain or as mono-ubiquitinations of multiple lysines, are efficiently targeted for proteasomal degradation (Dimova et al., 2012; Thrower et al., 2000). Hence, highly processive substrates like securin or cyclin B, which become poly-ubiquitinated within a single round of association with the APC/C, are more likely to be degraded efficiently in the presence of many competitive target substrates. Low processivity (distributive) substrates dissociate quickly and therefore have to undergo several

rounds of APC/C binding before degradation (Rape et al., 2006). Distributive substrates are also more likely to be targeted by deubiquitinating enzymes, which counteracts their efficient degradation (Rape et al., 2006). The processivity observed *in vitro* correlates to some extent with the order at which substrates degrade *in vivo* (Lindon and Pines, 2004; Rape et al., 2006).

1.4.1 Activation of the anaphase-promoting complex/cyclosome and anaphase commitment

The APC/C should only initiate anaphase once all chromosomes have become properly attached to the mitotic spindle. At least two mechanisms control APC/C activity in this regard: a 'timer' and a checkpoint. The mitotic checkpoint (or spindle assembly checkpoint, SAC) monitors the attachment of chromosomes to the mitotic spindle in early mitosis and inhibits the co-activator Cdc20 as long as not all chromosomes are properly attached (Lara-Gonzalez et al., 2012; Musacchio and Salmon, 2007). While targeted by the checkpoint, Cdc20 cannot mediate the degradation of securin and cyclin B, but can mediate the degradation of early mitotic substrates like cyclin A or Nek2A (den Elzen and Pines, 2001; Geley et al., 2001; Hames et al., 2001). Hence, the checkpoint makes anaphase dependent on proper chromosome attachment. However, even if the checkpoint is absent, there is a delay between entry into mitosis and initiation of anaphase. This delay is for example important to create the oscillatory behaviour between high and low CDK activity in the early embryonic cell cycles of *Xenopus* laevis, which lack a mitotic checkpoint (Yang and Ferrell, 2013). The time of the delay seems, at least in part, to be determined by the progressive accumulation of phosphorylations on the APC/C, which are catalyzed by cyclin-dependent kinase 1 (CDK1) and are required for the activity of the APC/C (Felix et al., 1990; Kraft et al., 2003; Lahav-Baratz et al., 1995; Rudner and Murray, 2000; Sudakin et al., 1995; Yang and Ferrell, 2013). Additional timer mechanisms may operate as well: in fission yeast, the Cdc20 ortholog Slp1 is only synthesized after cells enter mitosis (Yamada et al., 2000) and presumably needs to accumulate to a certain level to allow APC/C activation (Wolthuis et al., 2008).

The contributions of these different mechanisms for achieving sufficient mitotic APC/C activity are largely unknown for most organisms. In *Drosophila melanogaster*, *Xenopus laevis* embryos and yeast, anaphase in an unperturbed mitosis seems to be determined by the timer. In these cells, the checkpoint is not absolutely essential for faithful mitotic progression. In the absence of a checkpoint the timer mechanism

provides enough time to attach all chromosomes before anaphase is initiated (Buffin et al., 2007; Rahmani et al., 2009). In contrast, anaphase onset in other vertebrate cells is determined by the checkpoint. Abolishing the checkpoint leads to significantly earlier anaphase onset. Because in these cells the timer mechanism alone does not provide sufficient time for the cell to accomplish correct chromosome attachment, checkpoint defects result in dramatic chromosome missegregation (Canman et al., 2002; Gorbsky et al., 1998; Meraldi et al., 2004). In human cells, the attachment of the last chromosome almost instantaneously leads to cyclin B degradation (Clute and Pines, 1999). This indicates that once the checkpoint is satisfied, checkpoint silencing and APC/C^{Cdc20} activation towards securin and cyclin B is a very rapid process. The rapid silencing may encompass a feedback loop (Ciliberto and Shah, 2009; Foster and Morgan, 2012; Mansfeld et al., 2011; Reddy et al., 2007; Stegmeier et al., 2007; Uzunova et al., 2012). In any case, both mechanisms, the timer and the checkpoint, need to be satisfied before the APC/C can start to degrade securin and cyclin B and the cell can commit to anaphase.

1.4.2 The spindle assembly checkpoint controls the activation of the anaphase-promoting complex/cyclosome

Correct kinetochore-microtubule attachment and APC/C activation is under the surveillance of the spindle assembly checkpoint. In response to incorrectly attached kinetochores this signalling pathway recruits conserved core checkpoint proteins (Aurora B kinase, Mps1 kinase, Bub1, Bub3, Mad1, Mad2, Mad3/BubR) to the kinetochore and creates an inhibitory signal, which blocks degradation of securin and cyclin B by the APC/C. Recruitment of checkpoint proteins is hierarchical (Heinrich et al., 2012). At the top of the recruitment cascade stand the Aurora B kinase and the Mps1 kinase. Aurora B promotes the localization of the Mps1 kinase at the kinetochore, thereby providing a link between the error-correction mechanism and spindle assembly checkpoint signalling. Artificial tethering of Mps1 to the kinetochore bypasses the requirement for Aurora B activity for a functional checkpoint in yeast and mammalian cells (Heinrich et al., 2012; Ito et al., 2012; Saurin et al., 2011) suggesting that Mps1 recruitment is the only essential function of Aurora B for checkpoint signalling. By phosphorylating the N-terminus of KNL1 Mps1 recruits the Bub1/Bub3 complex (Krenn et al., 2012; London et al., 2012; Primorac et al., 2013; Shepperd et al., 2012; Yamagishi et al., 2012), which in turn is important for the recruitment of Mad3/BubR1 as well as the Mad1:Mad2 complex (London and Biggins, 2014). The Mad1:Mad2 complex, a heterotetrameric complex consisting of

two Mad1 molecules and two Mad2 molecules in their active, closed conformation (C-Mad2), catalyses the formation of a Mad2-Cdc20 complex by converting additional Mad2 molecules from an inactive, open conformation (O-Mad2) into the closed form bound to Cdc20 (Luo et al., 2002; Luo et al., 2004; Mapelli and Musacchio, 2007).Yet, formation of Mad2-Cdc20 constitutes only the first step towards the inhibition of APC/C^{Cdc20}. Subsequently, Mad2-Cdc20 associates with the Mad3/BubR1-Bub3 complex (although Bub3 seems not to be present in the complex in fission yeast (Sczaniecka et al., 2008)) to form the inhibitory mitotic checkpoint complex (MCC). The MCC associates with the APC/C thereby blocking substrate degradation. Recent evidence indicates that the MCC is able to bind and inhibit a second Cdc20 molecules that binds in a different mode than the first (Izawa and Pines, 2014) (Figure2).

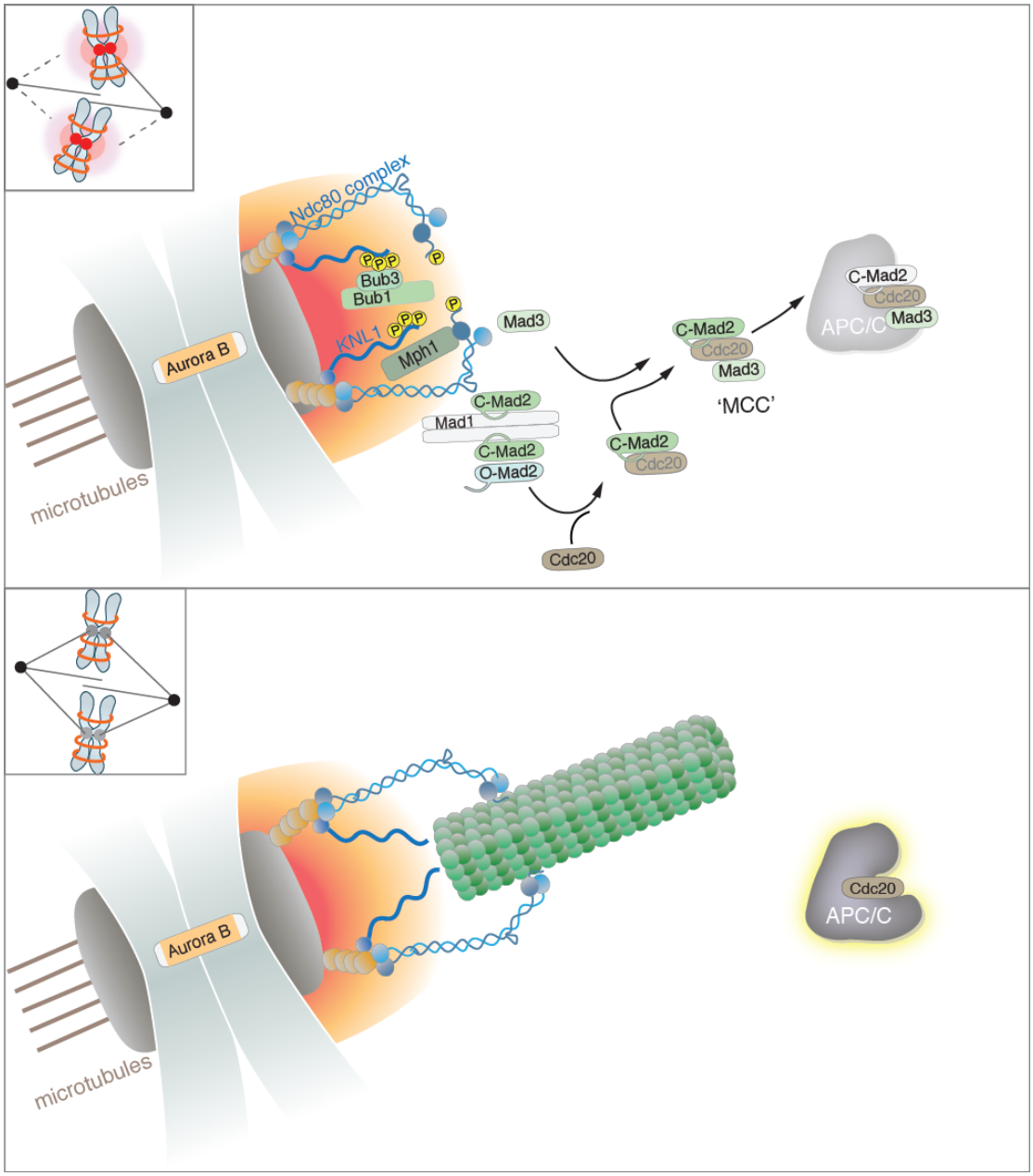

Figure 1-2 Kinetochore-microtubule attachment and spindle assembly checkpoint signalling

During pro- and metaphase Aurora B localizes to the inner centromere and creates a phosphorylation gradient (red/orange). If proper kinetochore-microtubule (KT-MT) attachment and therefore tension is lacking, proteins of the Ndc80 complex (blue) are phosphorylated ('P' = phosphorylation), which results in destabilization of KT-MT interactions. Mph1 (the Mps1 ortholog in *S. pombe*) is recruited to the kinetochore and phosphorylates KNL1. KNL1 phosphorylation recruits Bub1 and Bub3 to the kinetochore, which in turn recruits BubR1/Mad3 as well as the Mad1:Mad2 complex. The Mad1:Mad2 complex then triggers the formation of Mad2-Cdc20 by conversion of O-Mad2 (Mad2 in the open confirmation) into C-Mad2 (Mad2 in the closed confirmation). Subsequent binding of Mad3/BubR1 to the Mad2-Cdc20 complex creates the inhibitory mitotic checkpoint complex (MCC), which inhibits the anaphase promoting complex/cyclosome (APC/C). If proper KT-MT attachment is established, the distance between the inner centromere and the outer kinetochore is increased, proteins are dephosphorylated, the interaction between the KMN network and microtubules is stabilized and checkpoint proteins dissociate from the kinetochore (adapted from Heinrich/Hauf, 2012 and Welburn/Cheeseman, 2010).

1.5 Cyclin B degradation and mitotic exit

In 1884 Eduard Strasburger stated that he would now join Fleming's view, that 'the anaphases of the daughter nuclei reversely recapitulate the prophase of the mother's nucleus'. While in some aspects this is a valid statement, e.g. during mitotic entry cyclin B activity raises from low to high, while during mitotic exit the opposite is the case, it is probably not true on a molecular basis, e.g. chromosome condensation and chromosome decondensation likely comprise distinct molecular machineries (Magalska et al., 2014). Nevertheless the view that cyclin B destruction simply reverses the events of mitotic entry has persisted. Hence, insight into how the processes during anaphase and mitotic exit are regulated has generally been sparse. Cyclin B binds to and activates CDK1. The CDK1-dependent phosphorylations are required to establish and maintain the mitotic state. Phosphorylations on specific substrates by CDK1 not only promote mitotic events, e.g. establishment of the mitotic spindle, but phosphorylations of other substrates at the same time inhibit events of mitotic exit, e.g. spindle elongation. Hence, loss of CDK1 activity and dephosphorylation of CDK1 substrates are essential for anaphase progression. Expression of non-degradable cyclin B, which locks cells in a state of high CDK1 activity, blocks mitotic exit in fission yeast, flies and vertebrates (Gallant and Nigg, 1992; Holloway et al., 1993; Parry and O'Farrell, 2001; Sigrist et al., 1995; Wolf et al., 2006; Yamano et al., 1996). Because securin is still degraded in this situation, cells arrest with separated but condensed sister chromatids and short metaphase-like spindles ('pseudo-metaphase') (Gallant and Nigg, 1992; Hagting et al., 2002; Holloway et al., 1993; Parry et al., 2003; Sigrist et al., 1995; Yamano et al., 1996). Yet, loss of CDK1 activity alone might not suffice to drive mitotic exit. Vertebrate cells arrested in metaphase by deletion of the APC/C activator Cdc20 or chemical proteasome inhibition remain in the mitotic state despite treatment with CDK1 inhibitors (Manchado et al., 2010b; Skoufias et al., 2007; Wu et al., 2009). This suggests that at least in vertebrates an additional substrate of the APC/C might exist, which needs to be degraded in order to allow mitotic exit. Yet, whether or not cells are able to undergo mitotic exit in the presence of proteasome inhibition has remained controversial (see (Potapova et al., 2009; Potapova et al., 2006; Schmitz et al., 2010)). Similarly, vertebrate cells which are treated with CDK1 inhibitors in the presence of the phosphatase inhibitor okadaic acid maintain the mitotic state

(Skoufias et al., 2007; Wu et al., 2009). Indeed, the temporal coordination of phosphatase activity, which counteracts the CDK1 phosphorylations has recently emerged as a crucial factor during mitotic exit (reviewed in (Mochida and Hunt, 2012; Wurzenberger and Gerlich, 2011)). The best-characterized system in this regard is budding yeast, where the timely activation of the Cdc14 phosphatase is essential for mitotic exit (Stegmeier and Amon, 2004). Inactivation of Cdc14 results in segregated chromosomes but absence of central spindle assembly, anaphase B spindle elongation or mitotic exit, a phenotype which is reminiscent of the pseudo-metaphase phenotype caused by expression of non-degradable cyclin B in other organisms (Higuchi and Uhlmann, 2005b; Pereira and Schiebel, 2003; Visintin et al., 1998). Conversely, overexpression of Cdc14 can efficiently drive mitotic exit in the presence of spindle poison (Tinker-Kulberg and Morgan, 1999; Visintin et al., 1998). Interestingly, activation of Cdc14 is tightly coupled to sister chromatid separation in budding yeast, as I will discuss later. Yet, the central role of Cdc14 seems not to be conserved (Mocciaro and Schiebel, 2010) and no single phosphatase was identified, which adopts the central role of Cdc14 in other organisms. Instead, most likely several phosphatases contribute to mitotic exit progression, most prominently PP1 (Wu et al., 2009) and PP2A in complex with its regulatory subunits B55α and B55δ (Manchado et al., 2010b; Mochida et al., 2009; Schmitz et al., 2010). Yet, the crucial targets of these phosphatases have remained unknown and even the contribution of the different phosphatase activities to mitotic exit seem to differ in different organisms or even different tissues (Mochida and Hunt, 2012; Wurzenberger and Gerlich, 2011). Both, the activities of PP1 and PP2A-B55 complexes, are negatively regulated by CDK1 activity during early mitosis. While PP1 inhibition occurs via direct phosphorylation by CDK1 (Dohadwala et al., 1994; Kwon et al., 1997), inhibition of PP2A-B55 is more complex: During mitotic entry CDK1 activates another kinase, Greatwall/MASTL, which phosphorylates two small proteins, α-endosulphine (ensa) and cyclic AMP-regulated phosphoprotein19 (arpp19). The phosphorylated proteins then inhibit PP2A-B55 (Mochida et al., 2009). Reversal of this inhibition and downregulation of MASTL seems to be crucial for mitotic exit. Consistently, MASTL depletion efficiently drives mitotic exit in the absence of APC/C activity, when cells are treated with CDK1 inhibitors (Manchado et al., 2010b).

The gradual decrease of cyclin B and CDK1 activity during the metaphase to anaphase transition and the concomitant activation of counteracting phosphatases

orchestrate a multitude of events. Of particular consideration for the temporal coordination of the metaphase to anaphase transition are early cyclin B degradation-dependent events, which have to occur in close temporal proximity to sister chromatid separation. One of the earliest events in this context is the stabilization of kinetochore-microtubule interaction and the inactivation of the mitotic checkpoint, which are thought to depend on the loss of CDK1 activity (Oliveira and Nasmyth, 2010; Vázquez-Novelle et al., 2010). At the time when sister chromatids split, the so-called central spindle needs to be rapidly assembled in the region of overlapping anti-parallel MTs. Protein complexes in the central spindle stabilize and elongate the spindle (anaphase B) and are later important for cytokinesis. Other early events, include the recruitment of chromatin regulators to chromosomes early in anaphase, which set the stage for later chromosome decondensation and reassembly of the nuclear envelope (Vagnarelli et al., 2006; Vagnarelli et al., 2011).

1.5.1 Stabilization of kinetochore-microtubule attachments and inactivation of the mitotic checkpoint

In order to faithfully segregate sister chromatids into the two newly arising daughter cells, the kinetochores of the sister chromatid have to become stably attached to microtubules (MT) from opposite spindle poles. The attachment platform at the kinetochore is formed by the KMN network, a kinetochore protein complex, which consists of three subcomplexes, the KNL1 complex, the MIS12 complex and the NDC80 complex (Varma and Salmon, 2012). Chromosome capture by the mitotic spindle is thought to be intrinsically random: attachment of the sister chromatids to MTs from opposite poles is achieved by a trial and error mechanism. Correct bi-oriented attachment becomes stabilized while improper attachment between kinetochores and the microtubules is rapidly destabilized. Failures to correct improper attachment can result in genomic instability (Cimini et al., 2001). The status of the kinetochore-microtubule (KT-MT) attachment is inferred by the amount of tension applied to the kinetochores, which results in a stretched conformation of the kinetochore (Maresca and Salmon, 2009; Nannas and Murray, 2014; Uchida et al., 2009). Tension arises from the counteracting forces of correctly attached spindle microtubules and cohesion between sister chromatids. Low tension results in the destabilization of KT-MT interactions, which allows for a new attempt for correct attachment. The activity of the Aurora B kinase, as part of the chromosomal passenger complex (CPC), is central to this error-correction mechanism (Carmena et al., 2012). The CPC localizes to the inner centromere in early mitosis and is thought

to establish a phosphorylation gradient (Wang et al., 2011). If tension is lacking across the kinetochore, Aurora B phosphorylates proteins of the KMN network, which destabilizes the interaction between the KMN network and the microtubules (Welburn et al., 2010). If the kinetochores come under tension, the distance between the inner centromere and the outer kinetochores increases, and proteins of the outer kinetochore are no longer phosphorylated by Aurora B, resulting in stable KT-MT attachment.

In anaphase, cohesion and with it the necessary counteracting force for maintaining tension at the kinetochore is lost. Hence, attachments would become unstable, unless the destabilizing activity is removed after chromosome alignment in metaphase, but before anaphase onset (Oliveira and Nasmyth, 2010; Vázquez-Novelle et al., 2010). Similarly, if the mitotic checkpoint was still on duty when cohesion is lost, it would recognize the now tension-less kinetochores as mal-attached and re-engage. Because cohesin has already been removed, re-establishment of tension is impossible at this stage and cell cycle progression would be permanently blocked. In principle the checkpoint maintains the capacity to detect chromosome attachment errors even once it has been silenced in metaphase (Clute and Pines, 1999; Dick and Gerlich, 2013; Hagting et al., 2002). This has been demonstrated by treating cells with microtubule drugs after the APC/C^{Cdc20} had become active and cyclin B and securin degradation had started. The drug treatment efficiently stopped substrate degradation, indicating that the mitotic checkpoint had been re-engaged and APC/C^{Cdc20} activity was blocked (Clute and Pines, 1999; Hagting et al., 2002). Destroying the KT-MT interaction of a single chromosome during the metaphase to anaphase transition by laser-cutting yielded similar results (Dick and Gerlich, 2013). This demonstrates that mitotic checkpoint silencing is reversible at least for some time after the cell has committed to anaphase and activated APC/C^{Cdc20}. Hence, it is thought to be crucial to permanently inactivate the mitotic checkpoint machinery prior to, or concomitantly with, sister chromatid separation. Indeed one study reported that human cells become unresponsive to the loss of KT-MT interactions about 5 minutes prior to anaphase onset (Dick and Gerlich, 2013).

The loss of CDK1-dependent phosphorylations is a prime candidate mechanism for regulating mitotic checkpoint inactivation and stabilization of kinetochore-microtubule attachment. A drug-induced checkpoint arrest is rapidly overcome by treatment with CDK1 inhibitors (D'Angiolella et al., 2003), indicating that CDK1 activity is necessary

for mitotic checkpoint function. Unlike in an unperturbed anaphase, checkpoint proteins are re-recruited to the kinetochore upon sister chromatid separation in the presence of non-degradable cyclin B (Parry et al., 2003). This suggests that mal-attached kinetochores are recognized by the checkpoint in this situation. In addition, when CDK1/cyclin B activity stays high, kinetochore-microtubule interactions are unstable after anaphase in several organisms (Parry et al., 2003; Wolf et al., 2006). Artificial cleavage of cohesin in the absence of APC/C activity relocalizes checkpoint proteins to the kinetochore in budding yeast and in flies (Mirchenko and Uhlmann, 2010; Oliveira et al., 2010). Thus, under high CDK1 activity the kinetochore remains competent for sensing the loss of tension even when sister chromatids split.

As one of the central proteins of the error-correction mechanism as well as the mitotic checkpoint, Aurora B seems an ideal candidate for linking these processes to CDK1 activity. Prior to anaphase, Aurora B as part of the chromosomal passenger complex localizes to the centromere, from where it translocates onto the spindle midzone at around anaphase (reviewed in (Carmena et al., 2012)). The relocalization is mediated by dephosphorylation of CDK1-dependent phosphosites on the CPC subunit INCENP (Hummer and Mayer, 2009; Pereira and Schiebel, 2003). Preventing anaphase removal of the CPC from the centromere re-recruits a subset of checkpoint proteins to the kinetochore (Vázquez-Novelle and Petronczki, 2010). Nevertheless, kinetochores remain stably attached to the microtubules and cyclin B continues to decline, indicating that the APC/C^{Cdc20} remains active. This suggests that Aurora B translocation might contribute but is not absolutely necessary for checkpoint inactivation and stabilization of kinetochore-microtubule attachment in human cells (Vázquez-Novelle and Petronczki, 2010). Which additional mechanisms could contribute? CDK1-dependent phosphorylation of Cdc20 (Chung and Chen, 2003; D'Angiolella et al., 2003) and the checkpoint kinase Mps1 (Morin et al., 2012) are important for checkpoint function in vertebrates. Interestingly, Mps1 phosphorylation is necessary for the recruitment of the checkpoint proteins Mad1 and Mad2 to the kinetochore (Morin et al., 2012). Unlike other checkpoint proteins, these two proteins were not recruited to the kinetochore when anaphase took place while Aurora B was forced to localize to the centromere (Vázquez-Novelle and Petronczki, 2010). It is possible that Mps1 inactivation and removal of Aurora B are concomitantly required to inactivate the checkpoint. However, additional regulatory mechanisms are possible. Phosphorylation of the checkpoint kinase Bub1 by CDK1 promotes checkpoint function in fission yeast (Yamaguchi et al., 2003) and dephosphorylation

may be required to inactivate the checkpoint. Furthermore, the outer kinetochore complexes, which are needed for the recruitment of checkpoint proteins to the kinetochore and therefore for checkpoint activity, begin to disassemble during anaphase (Gascoigne and Cheeseman, 2013). Disassembly of the recruitment platform could make the kinetochore refractory to association of at least some components.

Despite all these evidences, it has remained unclear, whether maintaining CDK1 activity while sister chromatids separate is sufficient to not only recruit checkpoint proteins to the kinetochore but also to create a sufficient inhibitory signal in order to block APC/C activity. This has formally only been shown in budding yeast, where slow re-accumulation of securin is detected in a checkpoint-dependent manner when the CDK1 counteracting phosphatase, Cdc14, is mutated (Mirchenko and Uhlmann, 2010). On the contrary, in the human system complete degradation of endogenous cyclin B and securin have been observed in the presence of non-degradable cyclin B (Hagting et al., 2002; Wolf et al., 2006). It is possible, that the inhibition of the APC/C could not be read out by this assay, because cyclin B and securin levels were already greatly diminished at the time point of sister chromatid separation. Although keeping CDK1 activity high (by non-degradable cyclin B1) clearly leads to an abnormal anaphase, there is also experimental evidence that CDK1-dependent phosphorylations may normally not have dropped much by the time that sister chromatids separate. A fluorescence based sensor for CDK1 activity only started to significantly decrease at the time of sister chromatid separation when the cyclin B level had already been reduced to 50 % (Gavet and Pines, 2010). There is also controversy about the residual amount of cyclin B that is remaining at the time of sister chromatid separation, with reported values between 0 and 80 % (Clute and Pines, 1999; Vázquez-Novelle and Petronczki, 2010), probably due to technical differences between the experiments. To clarify the regulation of checkpoint activity during anaphase, it will be important to 1) establish whether under conditions of high CDK1 activity, the APC/C can indeed become inhibited in organisms other than budding yeast, and 2) to analyse the kinetics of such a potential inhibition (is the inhibition fast enough to put the transition at risk?).

1.5.2 Establishment of the central spindle in anaphase

During metaphase, spindle length is constant and the kinetochore microtubules as well as the interdigitating antiparallel spindle microtubules (interpolar MTs) are highly dynamic. The microtubules of the mitotic spindle and their associated proteins are

reorganized at anaphase onset in order to fulfil their functions in spindle elongation and cytokinesis. Interpolar MTs are stabilized (Brust-Mascher and Scholey, 2011) and the so-called central spindle is assembled at the spindle midzone (Figure 1). The central spindle is a proteinaceous structure comprised of interdigitating microtubules, microtubule-associated proteins, motor proteins and regulatory subunits. Its core consists of three subcomplexes, the PRC1/KIF4A complex, the centralspindlin complex and the chromosomal passenger complex (CPC). PRC1 (Ase1 in budding yeast and fission yeast) is a conserved microtubule-associating protein (MAP) with the ability to bundle antiparallel MTs (Mollinari et al., 2002; Schuyler et al., 2003). PRC1 depletion causes aberrant anaphase spindles, loss of interdigitating MTs between the spindle halves and failure in the completion of cytokinesis (Juang et al., 1997; Mollinari et al., 2002). Accumulation of PRC1 at the spindle midzone in anaphase depends on its association with the kinesin-4 KIF4A in HeLa cells (Kurasawa et al., 2004; Zhu and Jiang, 2005) as well as the centralspindlin complex and the CPC in *C. elegans* (Verbrugghe and White, 2004).

The centralspindlin complex is a heterotetrameric complex made of two molecules of the kinesin-6 MKLP1 (ZEN-4 in *C. elegans*) and two molecules of the Rho family GTPase activating protein MgcRacGAP (CYK-4). It also exhibits MT bundling activity (Mishima et al., 2002) and is further involved in the assembly of the contractile ring (Glotzer, 2005; Lewellyn et al., 2011). The CPC exhibits important regulatory roles at the spindle midzone. Both subunits of centralspindlin are substrates of the Aurora B kinase and its activity is essential for stable recruitment of the centralspindlin complex to the spindle midzone (Hauf et al., 2003; Kaitna et al., 2000; Severson et al., 2000).

The recruitment of each of the three core complexes to the spindle midzone is independently regulated by CDK1 phosphorylation/dephosphorylation. In human cells, the binding of Kif4A to PRC1 and subsequent localization to the plus-ends of interpolar microtubules is restricted to anaphase by CDK1-dependent phosphorylation (Zhu and Jiang, 2005). Additionally, PRC1 dephosphorylation promotes oligomerization, which is important for its MT-bundling activity at the midzone (Zhu and Jiang, 2005; Zhu et al., 2006). In budding yeast, central spindle localization of the PRC1 ortholog Ase1 depends on dephosphorylation of CDK1 phosphorylation sites by Cdc14 (Khmelinskii et al., 2007). Dephosphorylation of Ase1 also promotes accumulation of the kinesin-5 Cin8, which is important for spindle elongation in budding yeast. Fission yeast Ase1 is dephosphorylated and

subsequently recruits the kinesin-6 Klp9, which is important for anaphase B spindle elongation (Fu et al., 2009). Furthermore, dephosphorylation of CDK1-dependent sites is also important for PRC1 functioning as a recruitment platform for other regulatory proteins, like Polo-kinase Plk1 (Neef et al., 2007). Localization of the centralspindlin complex was shown to be regulated by CDK1 and to be counteracted by the phosphatase CDC-14 in *C. elegans* (Mishima et al., 2004). In human cells association of the CPC and the kinesin-6 MKLP2 is required for their localization to the central spindle (Gruneberg et al., 2004; Hummer and Mayer, 2009). CDK1 phosphorylation of the CPC subunit INCENP prevents the association of the CPC with MKLP2 and thereby restricts CPC translocation to anaphase (Hummer and Mayer, 2009; Vázquez-Novelle and Petronczki, 2010). Dephosphorylation of the INCENP homologue Sli15 by Cdc14 regulates CPC translocation in budding yeast (Pereira and Schiebel, 2003).

In summary, a multitude of dephosphorylation events regulate the assembly of the central spindle during the metaphase to anaphase transition. In addition, the proper localization and enrichment of the complexes mutually depend on each other. The independent phosphoregulation of the complexes in combination with their localization dependencies might ensure that spindle elongation occurs rapidly and only once CDK1 activity has decreased enough to allow all complexes to be dephosphorylated and recruited into one stable assembly. Additionally, the potential dual role of CPC translocation in checkpoint inactivation and central spindle assembly could provide an elegant mechanism for coordinating these events in time. Additionally, assembly of the central spindle recruits several factors important for cytokinesis (e.g. Plk1, ECT2) (reviewed in (Barr and Gruneberg, 2007)). This may ensure that cytokinesis can only be executed in cells that have been competent for anaphase B spindle elongation and thereby ensure proper temporal order.

1.6 Securin degradation and sister chromatid separation

Securin is a stoichiometric inhibitor of separase and is the crucial APC/C substrate to initiate sister chromatid separation. Securin tightly associates with separase and blocks accessibility to the catalytic site of the protease (Ciosk et al., 1998; Funabiki et al., 1996a; Hornig et al., 2002; Hornig and Uhlmann, 2004; Waizenegger et al., 2002). Securin orthologs in different species exhibit poor sequence conservation and were not identified by sequence homology but solely by their conserved function as separase inhibitors and the presence of at least one D-box (Jager et al., 2001;

Kitagawa et al., 2002; Leismann et al., 2000; Zou et al., 1999). APC/C^{Cdc20}-mediated degradation of securin releases separase from the inhibition and allows cohesin cleavage (Nasmyth, 2002; Uhlmann, 2001). Expression of non-degradable securin efficiently blocks sister chromatid separation in all organisms studied (Cohen-Fix et al., 1996; Funabiki et al., 1996b; Hagting et al., 2002; Leismann et al., 2000; Zou et al., 1999; Zur and Brandeis, 2001). Interestingly, securin seems to live a double life as both inhibitor and activator of separase. In budding yeast and human cells, securin deletion leads to reduced abundance and catalytic activity of separase (Hornig et al., 2002; Jallepalli et al., 2001). In flies and fission yeast, securin deletion is lethal. This is not due to precocious separase activation in the absence of securin, but due to reduced separase activity and insufficient chromosome disjunction (Funabiki et al., 1996a; Stratmann and Lehner, 1996). The activating role is attributed to a chaperone-like function of securin, which promotes proper folding of the large protease and prevents aggregation. In fungi, which undergo closed mitosis, securin additionally promotes the nuclear import of separase (Hornig et al., 2002; Jensen et al., 2001; Kumada et al., 1998). Despite these seemingly crucial functions, securin is dispensable for the viability of budding yeast and mice (Alexandru et al., 1999; Wang et al., 2001; Yamamoto et al., 1996) and for the continued proliferation capacity of vertebrate cell lines (Jallepalli et al., 2001; Mei et al., 2001). Hence, additional mechanisms must be able to control timely sister chromatid separation.

In budding yeast, timely sister chromatid separation in securin-deleted cells is ensured by polo-kinase, which promotes cohesin cleavage (Alexandru et al., 1999,Hornig, 2004 #397). This pathway of cohesin removal is not under control of the mitotic checkpoint and hence strains lacking securin exhibit higher sensitivity to microtubule drugs (Alexandru et al., 1999; Yamamoto et al., 1996). In vertebrates in contrast, cohesin cleavage and sister chromatid separation are still controlled by the mitotic checkpoint in the absence of securin (Jallepalli et al., 2001; Mei et al., 2001). This can be explained by findings that cyclin B is able to bind to and inhibit separase (Gorr et al., 2005; Stemmann et al., 2001). Binding of cyclin B requires CDK1-dependent phosphorylation of separase at S1126 (in human cells or an analogous position in Xenopus) (Stemmann et al., 2001) and is mutually exclusive with binding of securin (Gorr et al., 2005). Expression of non-phosphorylatable separase (S1126A) in the absence of securin leads to precocious sister chromatid separation during prolonged pro-/metaphase (Huang et al., 2005; Shindo et al., 2012). Premature sister chromatid separation was also observed when separase S1126A

was overexpressed in the presence of securin but not at endogenous expression level (Holland and Taylor, 2006). Thus in vertebrates, securin and cyclin B are both inhibitors of separase, but cyclin B seems to have lower affinity and may not contribute significantly to separase inhibition under physiological conditions (Shindo et al., 2012). Instead separase inhibition by cyclin B might act as a safety net preventing precocious separase activation in case the concentration of separase exceeds the one of its primary inhibitor, securin.

The decreasing CDK1 to phosphatase activity ratio during mitotic exit orders a number of important processes (see part 1.5). In contrast, the declining level of securin has only one known function: the activation of separase. The time gap between the start of securin degradation and sister chromatid separation can be substantial – ranging from a few to more than 20 minutes, depending on the cell type and experimental conditions (Chang et al., 2003; Clute and Pines, 1999; Hagting et al., 2002; Pereira and Maiato, 2012). Yet, what exactly defines the time point as well as the high synchronicity of sister chromatid separation during securin degradation has not been conclusively answered.

The stoichiometric inhibition of separase by securin could provide a simple mechanism to define the time point of sister chromatid separation. Judged by its resistance to high-salt washes, securin seems to exhibit a high affinity towards separase (Gorr et al., 2005; Holland and Taylor, 2006). Hence, as long as securin is in excess it might be able to rapidly reassociate with separase and inhibit it despite ongoing degradation. Consistently, in human cell lines unbound securin disappears faster than separase-bound securin during anaphase (Hellmuth et al., 2014; Shindo et al., 2012). Interestingly, this may not (only) be a consequence of fast re-association, but seems to be caused by differential regulation of the two securin pools. The unbound pool of securin is phosphorylated, which makes it susceptible to degradation, whereas the complexed pool is kept hypo-phosphorylated by separase-mediated recruitment of the PP2A phosphatase and is thereby stabilized (Hellmuth et al., 2014). In both scenarios, either fast rebinding of securin to separase or preferential degradation of unbound securin, separase could only become active and initiate anaphase once the excess of securin has been degraded. Consistent with this it has been observed that higher levels of securin correlate with later sister chromatid separation (Hagting et al., 2002). Importantly, both mechanisms also shift the release of separase into a regime of faster securin degradation, which could promote more efficient release of separase. Indeed, preventing the preferential degradation of

securin in human cells seemed to decrease the abruptness of cohesin cleavage and sister chromatid separation (Hellmuth et al., 2014).

1.6.1 Positive feedback may increase the synchronicity of sister chromatid separation

The separation of all chromosomes is characteristically synchronous, indicating that the underlying cohesin cleavage is fast and efficient. In budding yeast a positive feedback loop has been proposed to ensure this rapid and timely activation of separase (Holt et al., 2008). Dephosphorylation of securin by the budding yeast phosphatase Cdc14 accelerates securin ubiquitinylation *in vitro*. Cdc14 is activated by separase. Hence, an initial separase release might enhance securin degradation and thereby promoting the release of more separase. This mechanism could result in a switch-like activation of separase (Holt et al., 2008) (Figure 3, upper panel). Consistent with this idea, a non-phosphorylatable securin mutant, which blocks the feedback loop, exhibited less synchronous sister chromatid separation (Holt et al., 2008). Budding yeast separase has also been suggested to inhibit PP2A, which counteracts the Cdc5 phosphorylations on cohesin. Since cohesin phosphorylation promotes its cleavage, this is a coherent feed forward mechanism, where separase mediates cohesin cleavage directly and promotes it indirectly through enhancing cohesin phosphorylation. This mechanism would not necessarily promote abrupt sister chromatid separation but could constitute a noise filter, which prevents precocious activation of the positive feedback loop (Yaakov et al., 2012). However, later findings have raised doubt about the existence or physiological significance of the proposed positive feedback loop: The non-phosphorylatable securin mutant exhibits degradation kinetics, which are very similar to wild type securin (Lu et al., 2014) and the kinetic of cohesin cleavage was hardly changed by the presence of the non-phosphorylatable securin mutant (Yaakov et al., 2012). In fission yeast securin is also phosphorylated in mitosis (Kumada et al., 1998), but the function of these phosphorylations is unclear.

1.7 Coordination of events during the metaphase to anaphase transition

As discussed above, the key regulator of anaphase commitment is the anaphase-promoting complex/cyclosome, whose essential substrates are securin and cyclin B. In human cell lines the destruction of securin and cyclin B exhibit highly similar kinetics (Chang et al., 2003; Clute and Pines, 1999; Hagting et al., 2002; Zur and

Brandeis, 2002) and both proteins seem to be highly processive substrates for the APC/C *in vitro* (Rape et al., 2006). This ensures that securin degradation-dependent sister chromatid separation and cyclin B degradation-dependent early anaphase events occur at roughly the same time. Yet, sister chromatid separation has to be exactly timed in relation to early cyclin B degradation driven events. Considering the noise in protein abundance, which is a consequence of unavoidable stochasticity in transcription and translation (Sanchez et al., 2013), it seems unlikely that the simultaneous start of securin and cyclin B degradation suffices to ensure precise coordination. Indeed, in several organisms additional mechanisms have been identified, which contribute to the robust timing of the events.

In budding yeast, expression of non-degradable securin or depletion of separase inhibits not only sister chromatid separation but completely blocks progression into anaphase (Cohen-Fix et al., 1996; Queralt et al., 2006; Surana et al., 1993). The block was not observed, when sister chromatid separation was inhibited by expression of either uncleavable cohesin (Uhlmann et al., 1999) or a separase mutant, which had the essential catalytic residue mutated (Sullivan and Uhlmann, 2003). This argued for an additional non-catalytic function of separase in budding yeast and subsequently the crucial role of separase in activating the Cdc14 phosphatase was identified (Stegmeier et al., 2002). Up to anaphase, Cdc14 is sequestered in the nucleolus. Upon securin degradation free separase induces the release of Cdc14 from the nucleolus by down-regulating the $PP2A^{Cdc55}$ phosphatase (Azzam et al., 2004; Queralt et al., 2006). Since budding yeast Cdc14 is crucial to counteract CDK1-mediated phosphorylations (Stegmeier and Amon, 2004), the separase-mediated activation of Cdc14 tightly couples sister chromatid separation to mitotic checkpoint inactivation, anaphase spindle elongation and the regulation of mitotic exit. For example, the dephosphorylation and subsequent translocation of the chromosomal passenger complex to the central spindle is promoted by Cdc14 (Pereira and Schiebel, 2003). In a *cdc14-1* mutant background, SAC proteins abnormally re-localize to the kinetochore upon sister chromatid separation and securin re-accumulates suggesting that the checkpoint is re-engaged (Mirchenko and Uhlmann, 2010). Furthermore, the early release of Cdc14 promotes the desphosphorylation of proteins that are important for central spindle establishment and spindle elongation, like Fin1, Ask1 and Ase1. Concordantly, interfering with this release pathway results in reduced viability and anaphase spindle instability (Higuchi and Uhlmann, 2005a). Although the direct link between separase and Cdc14

provides an elegant mechanism for ensuring temporal order during anaphase, its generality is unclear. Homologues of Cdc14 have been identified in fission yeast, invertebrates and vertebrates, yet the essential role in promoting mitotic exit might be restricted to budding yeast (Mocciaro and Schiebel, 2010).

In other organisms tight direct coupling mechanisms seem to be absent. Artificial uncoupling of cyclin B and securin degradation underscore the general independence of the events: In contrast to budding yeast, blocking separase release generally does not prevent mitotic exit: in the presence of non-degradable securin, metazoan cells or fission yeast still attempt to elongate their spindle and to undergo cytokinesis despite sister chromatids not being separated (Funabiki et al., 1996b; Hagting et al., 2002; Zur and Brandeis, 2001). Vice versa, in the presence of physiological levels of non-degradable cyclin B, sister chromatids separate, but spindle elongation and later events like cytokinesis fail (Parry and O'Farrell, 2001; Wolf et al., 2006; Yamano et al., 1996). Nevertheless, more subtle regulation might exist. In vertebrates, moderate overexpression of non-degradable cyclin B is able to block sister chromatid separation (Wolf et al., 2006). This is consistent with the inhibitory role of cyclin B on separase (Gorr et al., 2005) (Figure 3, lower panel). Yet, expression of the separase S1126A mutant, which is unable to bind cyclin B, showed no alteration in timing or kinetic of cohesin cleavage (Shindo et al., 2012). Hence, it seems that under physiological conditions securin degradation alone controls separase activation, whereas in the case of excess cyclin B or in the absence of securin, cyclin B can take over the role of inhibitor. Interestingly, CDK1 not only inhibits separase, but separase binding to CDK1/cyclin B also inhibits CDK1 activity in vertebrates (Gorr et al., 2005). This inhibition could as well constitute a mechanism for fine-tuning the events during anaphase. Consistent with this idea, studies showed that separase association with cyclin B significantly increases at later points of the metaphase to anaphase transition (Hellmuth et al., 2014; Shindo et al., 2012). At this time, separase is enriched on chromosomes, which may lead to a spatially restricted down-regulation of CDK1 activity during exit from mitosis. Strikingly, when separase was replaced by its S1126A mutant, which is unable to bind CDK1/cyclin B, dephosphorylation of a CDK1-dependent site on the CPC-subunit INCENP was impaired and translocation of the CPC to the spindle midzone was delayed (Shindo et al., 2012). Additionally, chromosome movement by the anaphase spindle was attenuated (Shindo et al., 2012). The spatially restricted inhibition of CDK1 by separase could ensure that down-regulation of CDK1 activity and CPC translocation

occur concomitantly with sister chromatid separation. Based on this study, a theoretical model further suggested that the localization of the midspindle component PRC1 might be delayed in the absence of the separase-cyclin B interaction due to inefficient down-regulation of CDK1 and slower activation of the counteracting phosphatase PP2A-B55 (Cundell et al., 2013). Yet, one should keep the stochiometries of these proteins in mind: Quantitative studies suggests that there is at least 10 times more cyclin B than securin and separase in a human cell (Kulak et al., 2014). Even if all separase was binding and inhibiting the cyclin B/CDK1 complex this could only inhibit only a fraction of the overall available pool. Therefore it seems unlikely that separase plays a crucial role in down-regulating the global CDK1 activity, particularly in the early phase of the metaphase to anaphase transition when the concentration of cyclin B/CDK1 is high. Instead separase might have very specific functions in decreasing CDK1 activity spatially, as has been suggested in the case of the CPC translocation (Shindo et al., 2012).

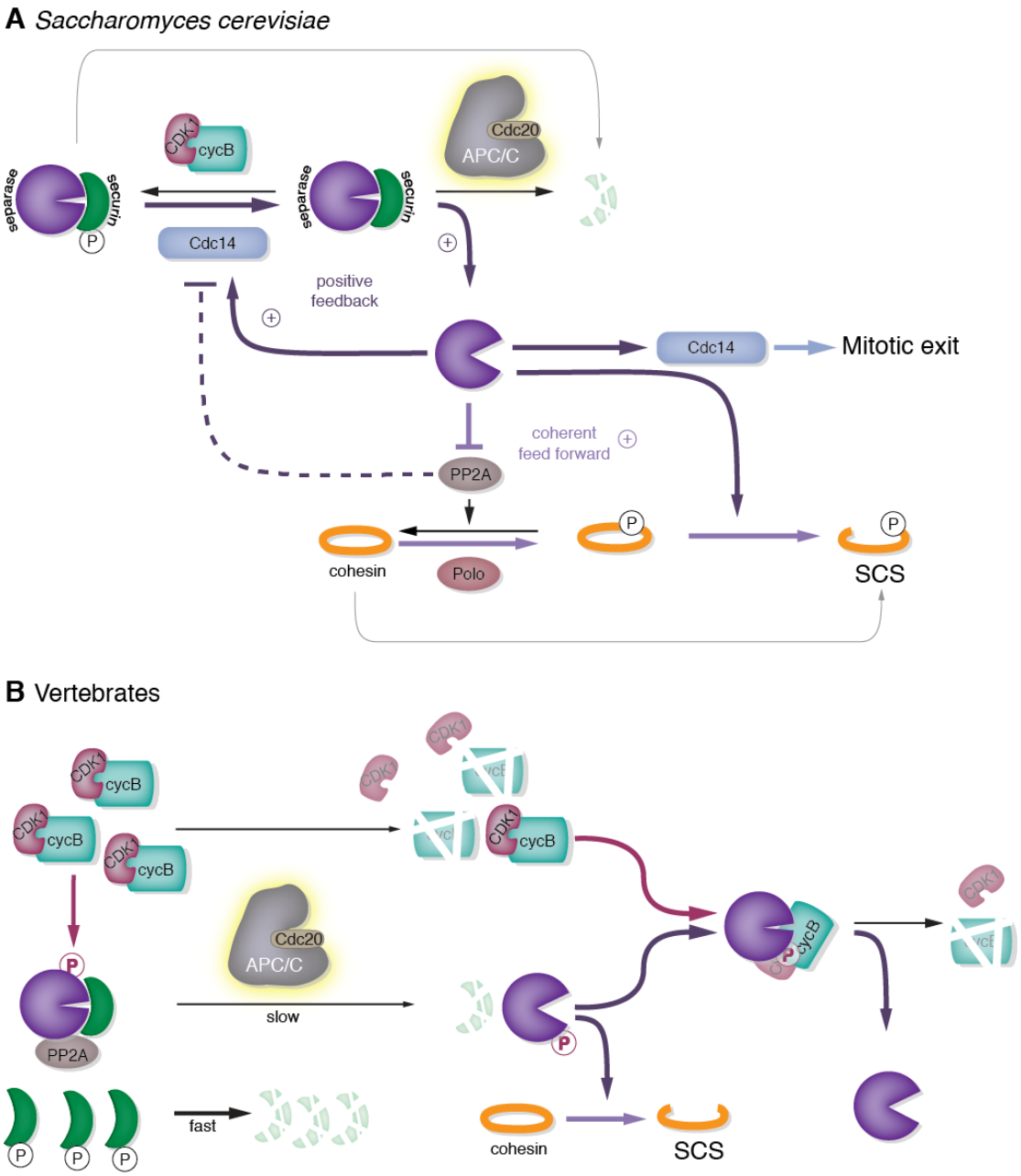

Figure 1-3 Crosstalk between securin degradation and CDK1 inactivation in different organisms

(A) In budding yeast the activation of the Cdc14 phosphatase by separase provides crucial crosstalk between sister chromatid separation (SCS) and mitotic exit. Separase-mediated activation of Cdc14 promotes mitotic exit by counteracting CDK1 phosphorylations. Furthermore, dephosphorylation of securin by Cdc14 is thought to accelerate securin degradation and separase release. Separase also inhibits the PP2A phosphatase, which further contributes to Cdc14 activation as well as cohesin phosphorylation. (B) In vertebrates, phosphorylation of securin promotes faster degradation. The separase-bound pool of securin is kept hypo-phosphorylated by separase-mediated recruitment of the PP2A phosphatase and hence is degraded with slower kinetics. Separase is phosphorylated by cyclin B/CDK1. Phosphorylated separase can be bound by cyclin B/CDK1 after securin is degraded, which results in inhibition of separase as well as of CDK1. 'P' = phosphorylation.

1.8 Aim of this study

During the metaphase to anaphase transition the destruction of two proteins, securin and cyclin B, translates into an ordered sequence of events, which ensures that the genomic information is securely segregated into the two newly arising daughter cells. Failure to maintain this order can result in genomic instability or cell death. Although the key proteins of the metaphase to anaphase transition and the general molecular principles have been identified, we are still lacking a comprehensive dynamical understanding of what determines the timing of single events and how a robust relative timing of multiple events is ensured. I was particularly interested in addressing the question how sister chromatid separation, the presumably only event mediated by securin degradation, is coordinated with the events of mitotic exit, which are orchestrated by cyclin B degradation.

Sister chromatid separation is driven by the destruction of the separase inhibitor securin, mediated by the anaphase-promoting complex/cyclosome (APC/C), which activates separase and leads to cohesin cleavage. As my first aim, I wanted to determine how abundances and activities of these different components determine the timing and synchronicity of sister chromatid separation. To this end, I planned to measure the concentrations of the different proteins and develop live cell imaging assays, which would enable me to follow the dynamics of securin degradation and sister chromatid separation during unperturbed mitosis as well as after targeted perturbations.

Subsequently, I wanted to expand on these findings to address how temporal order between sister chromatid separation and events of mitotic exit is ensured. Crosstalk between the degradation pathways has been found to contribute to the temporal order in other organisms, but seemed to be absent in fission yeast. Nevertheless, the transition had been found to be astonishingly robust against changes in protein abundance (Moriya et al., 2011). Hence, I aimed to identify the mechanisms, which contribute to the robust temporal order of events in the absence of crosstalk in fission yeast.

2 Results

2.1 Synchronous sister chromatid splitting in anaphase without obligatory positive feedback

Julia Kamenz[1,3,4], Tamara Mihaljev[2], Stefan Legewie[2,*] , Silke Hauf[1,3,4,*]

[1]*Friedrich Miescher Laboratory of the Max Planck Society, Tuebingen, Germany*

[2]*Department of Biological Sciences and* [3]*Virginia Bioinformatics Institute, Virginia Tech, Blacksburg, VA, United States*

[4]*Institute of Molecular Biology (IMB), Mainz, Germany*

Correspondence: silke@vt.edu, s.legewie@imb-mainz.de

Submitted as manuscript to **Journal of Cell Biology**

Author contributions:

I conceived the study together with Silke Hauf, designed, performed and analysed all experiments, and constructed and analysed computational models. In addition, I wrote the manuscript together with Silke Hauf and Stefan Legewie.

Tamara Mihaljev developed imaging analysis software and together with **Stefan Legewie** performed computational modelling and analyses.

Silke Hauf conceived and supervised the study.

Synchronous sister chromatid splitting in anaphase occurs without obligatory positive feedback

Julia Kamenz[1,3,4,*], Tamara Mihaljev[2], Stefan Legewie[2,*], Silke Hauf[1,3,4,*]

[1]*Friedrich Miescher Laboratory of the Max Planck Society, Tuebingen, Germany*

[2]*Institute of Molecular Biology (IMB), Mainz, Germany*

[3]*Department of Biological Sciences and* [4]*Virginia Bioinformatics Institute, Virginia Tech, Blacksburg, United States*

*Correspondence: silke@vt.edu, S.Legewie@imb-mainz.de, jkamenz@vt.edu

Running head: Abrupt sister separation without feedback

Total number of characters: 19,604

Abstract

Major cell cycle transitions involve positive feedback, which contributes to the abruptness and irreversibility of the transition. At the onset of anaphase, chromosomes split abruptly and synchronously, which is triggered by the protease separase. Whether this necessitates positive feedback regulation is unclear. Here, we systematically analysed the dynamics of sister chromatid separation in fission yeast at the single-cell level. All chromosomes split during a narrow time window. Separase activity and the degradation kinetics of its inhibitor, securin, are the main determinants of this synchronicity. Mathematical modelling on the basis of our findings suggests that synchronicity is established in the absence of feedback regulation. Hence, sister chromatid splitting, being already irreversible by nature, may be one of the few major cell cycle transitions that can operate without positive feedback. Inducing less synchronous sister chromatid separation caused a more pronounced order in the segregation of the different chromosomes, which we suggest is determined by the amount of centromeric cohesin on different chromosomes.

Introduction

The sudden and highly synchronous splitting of sister chromatids at anaphase onset is visually one of the most remarkable transitions in the cell cycle. Until anaphase, sister chromatids are held together by a large ring-shaped complex, called the cohesin complex, which topologically entraps the two identical DNA double strands (Nasmyth and Haering, 2009). The physical association ensures correct attachment of the sister chromatids to opposite poles of the mitotic spindle and hence, is a prerequisite for the equal distribution of genetic information to the two newly arising daughter cells (Tanaka et al., 2000). At anaphase, cohesion between sister chromatids is irreversibly lost. This is caused by proteolytic cleavage of cohesin's Scc1 subunit by the protease separase (Hauf et al., 2001; Oliveira et al., 2010; Uhlmann et al., 2000). Separase becomes active when its inhibitor securin is targeted for proteasomal degradation, following ubiquitinylation by the anaphase-promoting complex (APC/C) (Peters, 2002). Across organisms, the separation of all chromosomes takes place within a narrow time window. Yet, the causal degradation of securin proceeds substantially slower. Complete securin degradation in human cell lines takes about 20 min, whereas separation of the more than 40 chromosomes is completed in only 1 to 2 min (Hagting et al., 2002). Similar relative time scales have been observed in mouse oocytes (McGuinness et al., 2009) and budding yeast (compare (Lyons and Morgan, 2011; Pearson et al., 2001) and (Lu et al., 2014)).

To explain the sudden onset of sister chromatid separation, a switch-like increase in separase activity has been suggested (Hellmuth et al., 2014; Holt et al., 2008). Consistently, cohesin cleavage can be observed to increase sharply just before sister chromatids separate (Shindo et al., 2012; Yaakov et al., 2012). Positive feedback regulation is one of the regulatory mechanisms that can induce switch-like changes. Many cell cycle transitions employ positive feedback, which ensures both an abrupt and irreversible transition (Ferrell, 2013; Johnson and Skotheim, 2013; Kapuy et al., 2009). The loss of chromosome cohesion that brings the two sister chromatids apart is already irreversible by nature and sister chromatid separation therefore does not require

positive feedback for irreversibility. Yet, it remains possible that feedback regulation is necessary for the abruptness of cohesin cleavage by separase. A candidate positive feedback loop, where separase accelerates securin destruction, has been identified in budding yeast (Holt et al., 2008). In this organism, separase mediates the release of the Cdc14 phosphatase from nucleolar sequestration (Stegmeier et al., 2002; Sullivan and Uhlmann, 2003). Cdc14 dephosphorylates N-terminal sites in securin, which accelerates securin ubiquitinylation in vitro (Holt et al., 2008). Newer data, however, indicates that the degradation rates of non-phosphorylatable and wild type securin are similar (Lu et al., 2014) and that the rate of cohesin cleavage is not strongly affected by the expression of non-phosphorylatable securin (Yaakov et al., 2012). Furthermore in human cells, dephosphorylation of separase-bound securin by the phosphatase PP2A-B55 seems to decelerate (rather than accelerate) its degradation (Hellmuth et al., 2014). It therefore remains unclear whether this proposed feedback is physiologically important and functionally conserved across eukaryotes.

The abruptness of cohesin cleavage could be induced by switch-like activation of separase or by a switch-like modification of cohesin that facilitates cleavage. Cohesin's Scc1 subunit is phosphorylated by Polo-like kinases (Cdc5 in budding yeast and Plk1 in human cells), which enhances cleavage by separase in vitro (Alexandru et al., 2001; Hauf et al., 2005; Uhlmann et al., 2000). In budding yeast, separase may enhance cohesin phosphorylation by inhibiting the counteracting PP2A phosphatase Cdc55 (Yaakov et al., 2012). This does not constitute a positive feedback loop, but instead forms a coherent feed-forward regulation, where direct cohesin cleavage by separase is enhanced through a separase-mediated increase in cohesin phosphorylation. Such a feed-forward regulation can buffer against spurious separase activation, but is not expected to result in more abrupt cohesin cleavage compared to a situation where phosphorylation is constitutive and not regulated by separase (Mangan and Alon, 2003; Yaakov et al., 2012). Furthermore, unlike in budding yeast (Alexandru et al., 2001), mutation of Plk1-dependent phosphorylation sites in human Scc1 did not detectably impair sister chromatid separation (Hauf et al., 2005). Hence, we currently do not have a clear picture of the conserved

mechanisms that induce synchronous sister chromatid separation.

To address this, we implemented live cell imaging assays with high temporal resolution in fission yeast. We characterized the kinetics of both sister chromatid separation and the underlying securin degradation in wild type cells and then introduced perturbations to ask how strongly both dynamics were affected. We find that synchronicity of sister chromatid separation strongly correlates with securin degradation kinetics. Combining our quantitative results with computational models suggests that synchronous sister chromatid separation occurs in the absence of positive feedback regulation.

Results and Discussion

The separation of sister chromatids is highly synchronous and exhibits stochasticity

We had previously observed that in fission yeast securin (Cut2) degradation runs to completion in about 4 min and that splitting of chromosome I occurs around 1.5 min after the start of securin degradation ((Kamenz and Hauf, 2014) and Fig. S1A – D). To analyze the time window in which all three chromosomes split, we used fluorescent fusion proteins localized close to the centromeres of the three chromosomes (Sakuno et al., 2009; Straight et al., 1996; Yamamoto and Hiraoka, 2003) (Fig. 1A, B). We measured the time difference of sister chromatid separation between two chromosomes with high temporal resolution (7 seconds) by time-lapse microscopy (Fig. 1C). For both chromosome pairs (chromosome I versus II and chromosome II versus III) the time differences showed narrow Gaussian distributions with means close to 0 seconds (0 seconds representing simultaneous splitting of both chromosomes) and a standard deviation of 16.4 and 16.9 seconds, respectively (Fig. 1D, Table S1). Similar results were obtained when cells were grown in minimal instead of rich medium (Fig. S1E). Hence, in fission yeast - like in other organisms - securin degradation is relatively slow and progresses for a significant period of time before sister chromatids separate abruptly and synchronously. Chromosome I showed a slight, but significant tendency to separate before chromosome II, whereas chromosome III tended to

separate later (Fig. 1E and S1F, Table S1). Order in chromosome segregation has cytologically been observed in several organisms (Vig, 1983). In budding yeast, an invariant order was initially proposed (Holt et al., 2008) but subsequently questioned (Lyons and Morgan, 2011). Our data suggest a preferential order, but stochastic processes prevail so that this order is not absolute.

Reduced separase activity decreases the synchronicity of sister chromatid separation

The separation of sister chromatids is triggered by separase-mediated cohesin cleavage. To obtain a quantitative understanding of this process, we developed a hybrid deterministic-stochastic model which simulates stochastic cohesin cleavage in response to a deterministic, gradual increase in separase activity (Fig. 1F, Fig. S2, Supplementary Information). In a first model, we had active separase stochastically cleave cohesin molecules on either of two chromosomes, i.e. separase could rapidly diffuse between the two chromosomes (Fig. S2A). The likelihood of cohesin cleavage on one chromosome depends on the amount of cohesin on this chromosome at a given time. We assumed that a chromosome separates when the number of cohesin complexes has decayed to zero, or to another defined (low) number, and could thereby simulate the time of sister chromatid separation. Interestingly, in the rapid separase diffusion scenario cohesin disappeared from chromosomes with highly predictable kinetics and the two simulated chromosomes separated very synchronously (Fig. S2A-D). Hence, if realistic modeling assumptions were made, this model showed little variability in chromosome separation compared to our observations in vivo (Fig. 1D, Fig. S2C, see Supplementary Information for a detailed explanation).

We therefore constructed an alternative model, where active separase molecules randomly associate with one of the two chromosomes and then cleave cohesin complexes only on this chromosome (Fig. S2E-H). This behavior is supported by findings that separase associates with chromosomes in mitosis (Shindo et al., 2012; Sun et al., 2009; Yuan et al., 2009) and that DNA facilitates cohesin cleavage by separase (Shindo et al., 2012; Sun et al., 2009). This model shows rapid cohesin cleavage and a higher variability in the time window in which the two

chromosomes split (Fig. S2F-H). Furthermore, whereas in the rapid diffusion model the synchrony of chromosome segregation was highly sensitive to where we set the cohesin threshold (the number of cohesin molecules at which sister chromatids separate), the DNA association model showed a more robust behavior (Fig. S2D,H). We therefore favor the second model, and employed it for subsequent stochastic simulations; but the rapid diffusion model yielded qualitatively similar results (not shown).

When we decreased the activity of separase in the model, the variability in the time between separation of the two chromosomes was enhanced and the distribution broadened (Fig. 1F). To ask whether this occurs in vivo, we used the temperature-sensitive separase mutant *cut1-206* (Hirano et al., 1986) grown at semi-permissive temperature. For both chromosome pairs, their separation became significantly more asynchronous (Fig. 1G, Table S1). Similar observations have been made in budding yeast (Holt et al., 2008; Lyons and Morgan, 2011), where slower separase activity correlated with slower cohesin cleavage (Yaakov et al., 2012). Hence, the effects of lowering separase activity are consistent with a simple stochastic model of cohesin cleavage.

Separase-mediated feedback is unlikely to contribute to switch-like separase activation

Because of the high synchronicity of sister chromatid separation, it has been suggested that the regulation involves positive feedback. In particular, budding yeast separase is thought to enhance securin degradation through promoting the de-phosphorylation of CDK1-dependent phosphorylation sites on securin. The enhanced securin degradation would then lead to more abrupt separase release (Holt et al., 2008). Consistently, persistent CDK1 activity (through expression of a non-destructible version of the cyclin Clb5) made budding yeast sister chromatid separation more asynchronous (Holt et al., 2008), but whether this is caused by disruption of the proposed feedback or by another mechanism is unclear. We conducted a similar experiment in fission yeast and conditionally expressed a non-degradable version of cyclin B (ΔN-cyclin B) at close to endogenous levels (Kamenz and Hauf, 2014). As a consequence, a fraction of cells is

unable to exit mitosis (Yamano et al., 1996), whereas some cells with (presumably) low levels of non-degradable cyclin B remain unaffected. The time window of sister chromatid splitting in both classes of cells was similar (Fig. 2A, B), and was similar to wild type cells (Fig. 2C, Table S1). If the type of feedback regulation described in budding yeast would operate, we would have further expected that disrupting the feedback loop by either preventing cyclin B degradation or separase release would slow down securin degradation (Fig. 2D,E). However, expression of non-degradable cyclin B does not greatly influence securin degradation in fission yeast ((Kamenz and Hauf, 2014), Fig. S3A), nor does blocking separase release by expression of non-degradable securin (ΔN-securin) (Fig. 2F,G). We conclude that regulation by cyclin B or Cdk1 activity is not an integral part of the mechanism that promotes synchronous sister chromatid separation in fission yeast and that a separase-mediated feedback loop similar to the one proposed in budding yeast is unlikely to operate.

Securin degradation kinetics modulate the synchronicity of sister chromatid separation

A positive feedback loop would not necessarily need to act upstream and promote separase-release from securin (Fig. 2D), but could also operate downstream, for example in the form of autocatalytic separase activation (Fig. 3A,D). Separase is known to cleave autocatalytically (Chestukhin et al., 2003; Waizenegger et al., 2000; Zou et al., 2002), but the interpretation of the phenotype from expression of non-cleavable separase is difficult and there is no clear evidence that cleavage enhances activity (Holland et al., 2007; Papi et al., 2005). Nevertheless, to analyze the possibility for downstream feedback, we simulated a system of securin degradation and separase release without feedback (Fig. 3A-B) and in the presence of autocatalytic feedback (Fig. 3D-E). As expected, separase activity increases more slowly in the absence of feedback (Fig. 3B) than if feedback is present (Fig. 3E).

We employed a temperature-sensitive allele of the APC/C subunit APC6 (*cut9-665,* (Hirano et al., 1986)) to discriminate between regulation with or without feedback. Because the feedback amplification is downstream of APC/C-mediated securin degradation, the model predicted that

feedback would allow a sharp increase in separase activity, even if APC/C activity is reduced (Fig. 3E, Fig. S3B). In contrast, simulating lower APC/C activity without feedback leads to slower separase release (Fig. 3B). Using these separase release kinetics as input in our stochastic model predicts that sister chromatid separation becomes more asynchronous when APC/C activity is reduced in the absence of feedback (Fig. 3C), but not in the presence of feedback (Fig. 3F, Supplementary Information). Experimental measurements in the *cut9-665* strain showed that impaired APC/C activity resulted in slower securin degradation (Fig. S3C,E) and, more importantly, in significantly more asynchronous sister chromatid separation (Fig. 3G,I, Table S1). Slowing down securin degradation by partial inhibition of the proteasome with Bortezomib (Velcade) (Takeda et al., 2011) had the same effect (Fig. 3H,I, Table S1, Fig. S3D,E). Furthermore, the extent to which sister chromatid separation became asynchronous correlated with the degree to which securin degradation was slowed down (Fig. 3J and S3E). Because of the direct and pronounced effect of securin degradation kinetics onto the synchronicity of sister chromatid separation, we consider strong positive feedback downstream of separase unlikely. These results also make it unlikely that modification of cohesin can make sister chromatid separation abrupt, independent of the activity or kinetics of separase release.

Different amounts of centromeric cohesin can explain the segregation bias

When we induced more asynchronous chromosome segregation by slowing down securin degradation or decreasing separase activity, we noticed that the mean time difference between separation of chromosome II and III shifted considerably away from 0 sec (Fig. 4A and B). In our model, we can establish a bias towards earlier separation of one chromosome when assuming different initial amounts of cohesin on the two chromosomes (Fig. 4C). Consistent with the data, the simulations also showed that any existing bias would be further enhanced when securin degradation is attenuated (Fig. 4C). In our model, the larger the difference in the initial cohesin amount, the more pronounced the bias and the stronger the shift in the time difference when slowing down separase release (Fig. 4D). We observe the same correlation in our data (Fig. 4B).

Hence, it is conceivable that different initial amounts of cohesin are the underlying source of the observed segregation bias. The absence of a change in the time difference for chromosome I and II in our experiments (Fig. 4B) can be explained if these two chromosomes have a similar number of cohesin complexes (Fig. 4D). This is consistent with chromosome I and II also showing on average a smaller time difference in their separation in the wild type (6.8 and 4.6 sec in rich and minimal medium, respectively) compared to chromosome II and III (11.5 and 10.5 sec). Our current model does not explain why the asynchronicity in separation of chromosome I and II increases more strongly when securin degradation is slowed down than those of chromosome II and III (Fig. 4B, σ). Hence, we speculate that additional sources of stochasticity exist. We could imagine, for example, that the cohesin threshold is influenced by the number of kinetochore microtubules (and therefore the force exerted) on a given chromosome. The number of microtubules per kinetochore can vary between two and four in fission yeast (Ding et al., 1993).

With respect to the order in separation, it is suggestive that, although chromosome III is the shortest of the three chromosomes, it possesses by far the largest centromeric region (110 kbp compared to 35 kbp and 65 kbp for chromosomes I and II, respectively; Fig. 1B), and centromeric regions are known to be highly enriched for cohesin (Schmidt et al., 2009; Tomonaga et al., 2000). Hence, chromosome III may tend to separate later because of a higher cohesin load. The smaller difference in centromere size between chromosome I and II might explain why we observed a smaller mean time difference and no significant shift of the mean for this chromosome pair (Fig. 4A, B, Table S1). Interestingly, a link between the size and functionality of centromeric regions and the order of chromosome separation has been made decades ago through cytological observations in a number of species (Vig and Willcourt, 1998). In metazoan cells, order in separation may define chromosomal positions in interphase (Gerlich et al., 2003) and thereby contribute to proper genome regulation.

Mechanisms for abrupt separase release in the absence of feedback regulation

Since we did not find evidence for positive feedback in synchronizing sister chromatid separation

(Fig. 2 and 3), we asked which other mechanisms could contribute to rapid separase release and therefore to a narrow time window of sister chromatid separation. Any viable model also needs to explain the time delay between the onset of APC/C activity and sister chromatid separation (Fig. S1C, (Hagting et al., 2002; McGuinness et al., 2009)). In all organisms examined, securin is present in excess over separase (Ciosk et al., 1998; Shindo et al., 2012, J.K., ms. in preparation). Possibly the simplest assumption is that both separase-bound and free securin are degraded with similar kinetics, and that separase, which is released due to degradation of securin-separase complexes, is quickly rebound by free securin molecules and re-inhibited as long as securin is still in excess (Fig. 5A). If rebinding is fast, this mechanism can account both for the time delay, and for rapid separase release and synchronous sister chromatid separation (Figure 5B, C; Supplementary Text). Similar sequestration mechanisms by stoichiometric inhibitors have been shown to efficiently promote switch-like behavior in other systems (Buchler and Cross, 2009; Ferrell et al., 2014; Legewie et al., 2008).

It has recently been reported for human cells that, unlike in the simple model above, separase-bound and free securin are not degraded with similar kinetics, but that unbound securin is preferentially degraded (Hellmuth et al., 2014). Preferential degradation of securin could occur when the APC/C is present at a limiting concentration and has a higher affinity for free securin than for the securin-separase complex (Fig. 5D, Supplementary Information). Thus, by sequestering the APC/C, free securin effectively acts as a stoichiometric inhibitor of securin-separase complex degradation. This mechanism similarly provides a time-delay, ensures fast separase release and can promote more synchronous sister chromatid separation (Fig. 5E, F). Both mechanisms, preferential degradation and fast-rebinding, still exhibit sensitivity to the attenuation of securin degradation (Fig. S3F, G, Supplementary Information) and hence, are consistent with our experimental data (Fig. 3G-J).

Taken together, our parallel analysis of the kinetics of securin degradation and the synchronicity of sister chromatid separation did not reveal evidence for positive feedback, and our combined

deterministic and stochastic modeling suggests that positive feedback is not required for synchronous sister chromatid separation. Instead, simple assumptions about securin-separase association or securin degradation are sufficient to explain rapid separase release, which ensures a high synchronicity of sister chromatid separation. Hence, although positive feedback loops are ubiquitous in the cell cycle and regulate major transitions from one phase to the next (Ferrell, 2013; Johnson and Skotheim, 2013; Kapuy et al., 2009), such regulation may not be necessary and may not be implemented for this particular transition. Irreversibility is already ensured thermodynamically through loss of cohesion and the switch-like increase in separase activity can be implemented by mechanisms other than a positive feedback loop.

Materials and Methods

S. pombe strains

All strains are listed in Supplementary Table 2. To fluorescently label the region close to the centromere of chromosome III, the plasmid pRS14 was used to integrate a ~224x*tetO* array 556 bp 5' of *meu27* following the previously described method (Rohner et al., 2008). The resulting strain was crossed to a strain expressing the TetR-tdTomato fusion protein integrated at the Z-locus (Sakuno et al., 2009). For inducible expression of non-degradable securin (*ΔN-Cut2*) the coding sequence of amino acids 81 to 301 of Cut2 (Funabiki et al., 1996) was cloned into the pDual vector (Matsuyama et al., 2004) under the control of the *nmt81* promoter and integrated into the *leu1* locus. *S. pombe* strains with the following modifications and mutations have been described previously: *dh1L-tdTomato* (Sakuno et al., 2009), *cen2-GFP* (Yamamoto and Hiraoka, 2003), *cut9-665* and *cut1-206* (Hirano et al., 1986), *cut2-GFP<<kanR* and the inducible version of non-degradable cyclin B (*leu1+<<Pnmt81-ΔN67-cdc13*) (Kamenz and Hauf, 2014).

Pre-culturing and live cell imaging

Prior to imaging cells were cultured either in rich medium (YE + adenine) or Edinburgh minimal medium (EMM) with the necessary supplements (Moreno et al., 1991) at 30 °C, except for the strains carrying the temperature-sensitive alleles *cut9-665* or *cut1-206*, which were cultured at 25 °C. We used cells grown in EMM for the proteasome inhibition, because this led to a more effective inhibition in our hands, while the *cut9-665* and *cut1-206* phenotypes were more pronounced after growth in rich medium. The *nmt81* promoter was repressed by addition of 16 μM thiamine to EMM and induced by transferring the cells into EMM without thiamine for 14-18 hours. Prior to imaging, all strains were transferred into EMM, mounted in lectin-coated (35 μg/ml, Sigma L1395) culture dishes (8-well, Ibidi) and pre-incubated on the microscope stage at 30 °C for 30 min. For partial inhibition of the proteasome, Bortezomib (Velcade, LC laboratories, B-1408) was added to a final concentration of 100 μM. Live cell imaging was carried out at 30 °C on

a DeltaVision Core system (Applied Precision/GE Healthcare) equipped with a climate chamber (EMBL) using a 60x/1.4 Apo oil objective (Olympus). Images were acquired using the 'optical axis integration' modus of the softWoRx software over a range of 4 μm. To measure the time difference between the separation of two chromosomes, images were acquired every 7 seconds for 1 hour, then the image field was changed and acquisition was continued for another hour. To visualize securin-GFP dynamics, images were acquired every 15 seconds for 2 hours.

Data processing and analysis

Images were deconvolved using softWoRx software. The time point of sister chromatid separation was scored manually and was defined as the last time point at which sister chromatids were still associated before anaphase A movement became visible. Kymographs were assembled using MATLAB (kymograph assembly software available on www.hauflab.org) and the contrast was enhanced for easier visualization of the separation events.

To determine the kinetics of securin degradation, we used softWoRx software to measure signal intensities, and custom MATLAB software to additionally process the data. The nuclear background signal of tetR-tdTomato was used to define the nucleus as a region of interest (ROI) and the average GFP signal intensity of the ROI was determined for each time point. The extracellular background was determined by averaging the signal intensity of three ROIs placed outside of the cell and was subtracted from the GFP signal. If there were more than one ROI (e.g. after nuclear division), the average of the two measurements was calculated before subtraction. Mean and standard deviation of a cell population are shown in Fig. 2F. The following steps were performed for the extraction of features from these time courses (Figs. 2G, 3J, S1B-D, S3A and S3E): A local time course slope was calculated by taking a derivative over 7 consecutive points of the spline (the time point +/- the next 3 time points). The onset of securin degradation was determined as the time point before which this local slope repeatedly (over 5 time points) dropped below a threshold (20% of a reference slope calculated when securin decayed to half of its initial level). The curves were normalized by setting the onset securin level to 100 % and the minimum

of the smoothed curve to 0 %. In these curves, the normalized degradation rate was then approximated as the linear decay between 60 and 40 % (Figs. 2G, 3J, S3A and S3E). Moreover, the percentage of securin left at sister chromatid separation (Fig. S1B), the time between degradation onset and sister chromatid separation (Fig. S1C), and time points at which 90 % of securin had been degraded (Fig. S1D) were calculated.

Statistical analysis

Statistical analysis was performed using MATLAB and results are listed in Supplementary Table S1. Values were binned with a bin width of 7 seconds and the bin counts translated into percentages of the total number of cells counted. The Gaussian distribution describing each data set was then calculated by $y = \frac{bin\ width * 100\%}{\sigma\sqrt{2\pi}} e^{-\frac{(x-\mu)^2}{2\sigma^2}}$ where μ is the mean of the data and σ is $\frac{|\mu - p_{15.8}| + |\mu - p_{84.1}|}{2}$, with $p_{15.8}$ and $p_{84.1}$ being the interpolated 15.87 and 84.13 percentile, respectively. This method to calculate σ was robust against experimental outliers and hence yielded a good overall fit of the data. Data sets were compared by two-sample Kolmogorov-Smirnov test.

Acknowledgments

We thank Fabio Zanini for advice, Susan Gasser and her group for reagents, Ruslan Aydarkhanov for discussions, Andrea Ciliberto for comments on the manuscript and the QBio Summer School at the Kavli Institute for Theoretical Physics (KITP) for training. This work was supported by the Max Planck Society (J.K., S.H.), Virginia Tech (J.K., S.H.), the German Federal Ministry of Education and Research (e:Bio Junior Group grant to S.L.) and the Boehringer Ingelheim Fonds (fellowship to J.K.).

Author contributions

J.K. and S.H. conceived the project and all authors discussed the results; J.K. designed, performed and analysed all experiments; S.L. created and analysed deterministic simulations; J.K. and T.M. created and analysed stochastic simulations; J.K. and S.H. wrote the paper with input by S.L.

Competing Interest

None declared.

References

Alexandru, G., F. Uhlmann, K. Mechtler, M.A. Poupart, and K. Nasmyth. 2001. Phosphorylation of the cohesin subunit Scc1 by Polo/Cdc5 kinase regulates sister chromatid separation in yeast. *Cell*. 105:459-472.

Buchler, N.E., and F.R. Cross. 2009. Protein sequestration generates a flexible ultrasensitive response in a genetic network. *Molecular systems biology*. 5:272.

Chestukhin, A., C. Pfeffer, S. Milligan, J.A. DeCaprio, and D. Pellman. 2003. Processing, localization, and requirement of human separase for normal anaphase progression. *Proc Natl Acad Sci U S A*. 100:4574-4579.

Ciosk, R., W. Zachariae, C. Michaelis, A. Shevchenko, M. Mann, and K. Nasmyth. 1998. An ESP1/PDS1 complex regulates loss of sister chromatid cohesion at the metaphase to anaphase transition in yeast. *Cell*. 93:1067-1076.

Ding, R., K.L. McDonald, and J.R. McIntosh. 1993. Three-dimensional reconstruction and analysis of mitotic spindles from the yeast, Schizosaccharomyces pombe. *J Cell Biol*. 120:141-151.

Ferrell, J.E. 2013. Feedback loops and reciprocal regulation: recurring motifs in the systems biology of the cell cycle. *Current opinion in cell biology*. 25:676-686.

Ferrell, J.E., Jr, and S.H. Ha. 2014. Ultrasensitivity part II: multisite phosphorylation, stoichiometric inhibitors, and positive feedback. *Trends in biochemical sciences*. 39:556-569.

Funabiki, H., H. Yamano, K. Kumada, K. Nagao, T. Hunt, and M. Yanagida. 1996. Cut2 proteolysis required for sister-chromatid seperation in fission yeast. *Nature*. 381:438-441.

Gerlich, D., J. Beaudouin, B. Kalbfuss, N. Daigle, R. Eils, and J. Ellenberg. 2003. Global chromosome positions are transmitted through mitosis in mammalian cells. *Cell*. 112:751-764.

Hagting, A., N. Den Elzen, H. Vodermaier, I. Waizenegger, J.-M. Peters, and J. Pines. 2002. Human securin proteolysis is controlled by the spindle checkpoint and reveals when the APC/C switches from activation by Cdc20 to Cdh1. *The Journal of cell biology*. 157:1125-1137.

Hauf, S., E. Roitinger, B. Koch, C.M. Dittrich, K. Mechtler, and J.M. Peters. 2005. Dissociation of cohesin from chromosome arms and loss of arm cohesion during early mitosis depends on phosphorylation of SA2. *PLoS biology*. 3:e69.

Hauf, S., I.C. Waizenegger, and J.M. Peters. 2001. Cohesin cleavage by separase required for anaphase and cytokinesis in human cells. *Science*. 293:1320-1323.

Hellmuth, S., F. Bottger, C. Pan, M. Mann, and O. Stemmann. 2014. PP2A delays APC/C-dependent degradation of separase-associated but not free securin. *The EMBO journal*. 33:1134-1147.

Hirano, T., S. Funahashi, T. Uemura, and M. Yanagida. 1986. Isolation and characterization of Schizosaccharomyces pombe cutmutants that block nuclear division but not cytokinesis. *The EMBO journal*. 5:2973-2979.

Holland, A.J., F. Bottger, O. Stemmann, and S.S. Taylor. 2007. Protein phosphatase 2A and separase form a complex regulated by separase autocleavage. *The Journal of biological chemistry*. 282:24623-24632.

Holt, L.J., A.N. Krutchinsky, and D.O. Morgan. 2008. Positive feedback sharpens the anaphase switch. *Nature*. 454:353-357.

Johnson, A., and J.M. Skotheim. 2013. Start and the restriction point. *Current opinion in cell biology*. 25:717-723.

Kamenz, J., and S. Hauf. 2014. Slow checkpoint activation kinetics as a safety device in anaphase. *Current biology : CB*. 24:646-651.

Kapuy, O., E. He, S. Lopez-Aviles, F. Uhlmann, J.J. Tyson, and B. Novak. 2009. System-level feedbacks control cell cycle progression. *FEBS letters*. 583:3992-3998.

Legewie, S., D. Dienst, A. Wilde, H. Herzel, and I.M. Axmann. 2008. Small RNAs establish delays and temporal thresholds in gene expression. *Biophysical journal*. 95:3232-3238.

Lu, D., J.Y. Hsiao, N.E. Davey, V.A. Van Voorhis, S.A. Foster, C. Tang, and D.O. Morgan. 2014. Multiple mechanisms determine the order of APC/C substrate degradation in mitosis. *J Cell Biol*. 207:23-39.

Lyons, N.A., and D.O. Morgan. 2011. Cdk1-dependent destruction of Eco1 prevents cohesion

establishment after S phase. *Molecular cell*. 42:378-389.

Mangan, S., and U. Alon. 2003. Structure and function of the feed-forward loop network motif. *Proc Natl Acad Sci U S A*. 100:11980-11985.

Matsuyama, A., A. Shirai, Y. Yashiroda, A. Kamata, S. Horinouchi, and M. Yoshida. 2004. pDUAL, a multipurpose, multicopy vector capable of chromosomal integration in fission yeast. *Yeast*. 21:1289-1305.

McGuinness, B.E., M. Anger, A. Kouznetsova, A.M. Gil-Bernabe, W. Helmhart, N.R. Kudo, A. Wuensche, S. Taylor, C. Hoog, B. Novak, and K. Nasmyth. 2009. Regulation of APC/C activity in oocytes by a Bub1-dependent spindle assembly checkpoint. *Curr Biol*. 19:369-380.

Moreno, S., A. Klar, and P. Nurse. 1991. Molecular genetic analysis of fission yeast Schizosaccharomyces pombe. *Methods in enzymology*. 194:795-823.

Nasmyth, K., and C.H. Haering. 2009. Cohesin: its roles and mechanisms. *Annual review of genetics*. 43:525-558.

Oliveira, R.A., R.S. Hamilton, A. Pauli, I. Davis, and K. Nasmyth. 2010. Cohesin cleavage and Cdk inhibition trigger formation of daughter nuclei. *Nature cell biology*. 12:185-192.

Papi, M., E. Berdougo, C.L. Randall, S. Ganguly, and P.V. Jallepalli. 2005. Multiple roles for separase auto-cleavage during the G2/M transition. *Nature cell biology*. 7:1029-1035.

Pearson, C.G., P.S. Maddox, E.D. Salmon, and K. Bloom. 2001. Budding yeast chromosome structure and dynamics during mitosis. *J Cell Biol*. 152:1255-1266.

Peters, J.M. 2002. The anaphase-promoting complex: proteolysis in mitosis and beyond. *Molecular cell*. 9:931-943.

Rohner, S., S.M. Gasser, and P. Meister. 2008. Modules for cloning-free chromatin tagging in Saccharomyces cerevisae. *Yeast*. 25:235-239.

Sakuno, T., K. Tada, and Y. Watanabe. 2009. Kinetochore geometry defined by cohesion within the centromere. *Nature*. 458:852-858.

Schmidt, C.K., N. Brookes, and F. Uhlmann. 2009. Conserved features of cohesin binding along fission yeast chromosomes. *Genome biology*. 10:R52.

Shindo, N., K. Kumada, and T. Hirota. 2012. Separase sensor reveals dual roles for separase coordinating cohesin cleavage and cdk1 inhibition. *Developmental cell*. 23:112-123.

Stegmeier, F., R. Visintin, and A. Amon. 2002. Separase, polo kinase, the kinetochore protein Slk19, and Spo12 function in a network that controls Cdc14 localization during early anaphase. *Cell*. 108:207-220.

Straight, A.F., A.S. Belmont, C.C. Robinett, and A.W. Murray. 1996. GFP tagging of budding yeast chromosomes reveals that protein-protein interactions can mediate sister chromatid cohesion. *Current biology : CB*. 6:1599-1608.

Sullivan, M., and F. Uhlmann. 2003. A non-proteolytic function of separase links the onset of anaphase to mitotic exit. *Nature cell biology*. 5:249-254.

Sun, Y., M. Kucej, H.Y. Fan, H. Yu, Q.Y. Sun, and H. Zou. 2009. Separase is recruited to mitotic chromosomes to dissolve sister chromatid cohesion in a DNA-dependent manner. *Cell*. 137:123-132.

Takeda, K., A. Mori, and M. Yanagida. 2011. Identification of genes affecting the toxicity of anti-cancer drug bortezomib by genome-wide screening in S. pombe. *PloS one*. 6:e22021.

Tanaka, T., J. Fuchs, J. Loidl, and K. Nasmyth. 2000. Cohesin ensures bipolar attachment of

microtubules to sister centromeres and resists their precocious separation. *Nature cell biology*. 2:492-499.

Tomonaga, T., K. Nagao, Y. Kawasaki, K. Furuya, A. Murakami, J. Morishita, T. Yuasa, T. Sutani, S.E. Kearsey, F. Uhlmann, K. Nasmyth, and M. Yanagida. 2000. Characterization of fission yeast cohesin: essential anaphase proteolysis of Rad21 phosphorylated in the S phase. *Genes & development*. 14:2757-2770.

Uhlmann, F., D. Wernic, M.A. Poupart, E.V. Koonin, and K. Nasmyth. 2000. Cleavage of cohesin by the CD clan protease separin triggers anaphase in yeast. *Cell*. 103:375-386.

Vig, B.K. 1983. Sequence of centromere separation: occurrence, possible significance, and control. *Cancer genetics and cytogenetics*. 8:249-274.

Vig, B.K., and M. Willcourt. 1998. Decondensation of pericentric heterochromatin alters the sequence of centromere separation in mouse cells. *Chromosoma*. 107:417-423.

Waizenegger, I.C., S. Hauf, A. Meinke, and J.M. Peters. 2000. Two distinct pathways remove mammalian cohesin from chromosome arms in prophase and from centromeres in anaphase. *Cell*. 103:399-410.

Yaakov, G., K. Thorn, and D.O. Morgan. 2012. Separase biosensor reveals that cohesin cleavage timing depends on phosphatase PP2A(Cdc55) regulation. *Developmental cell*. 23:124-136.

Yamamoto, A., and Y. Hiraoka. 2003. Monopolar spindle attachment of sister chromatids is ensured by two distinct mechanisms at the first meiotic division in fission yeast. *The EMBO journal*. 22:2284-2296.

Yamano, H., J. Gannon, and T. Hunt. 1996. The role of proteolysis in cell cycle progression in Schizosaccharomyces pombe. *The EMBO journal*. 15:5268-5279.

Yuan, K., N. Li, Y. Huo, F. Yan, Y. Yang, T. Ward, C. Jin, and X. Yao. 2009. Recruitment of separase to mitotic chromosomes is regulated by Aurora B. *Cell cycle*. 8:1433-1443.

Zou, H., O. Stemman, J.S. Anderson, M. Mann, and M.W. Kirschner. 2002. Anaphase specific auto-cleavage of separase. *FEBS letters*. 528:246-250.

Figure Legends

Figure 1. The separation of sister chromatids is highly synchronous and largely stochastic

(A) Schematic of the imaging assay used to assess the synchronicity of chromosome segregation. **(B)** Fluorescent labeling of chromosomes close to their centromeric regions. Localization of the tandem-repeats of the tet- or lac-operon relative to the centromere with its central core (cnt) and different numbers of dg/dh repeat pairs (brackets: total chromosome size/size of the centromeric region). Chromosome II was marked with GFP (Yamamoto and Hiraoka, 2003), whereas chromosome I and III were marked with tdTomato ((Sakuno et al., 2009) and this study). **(C)** Representative kymograph of mitotic progression. Arrowheads indicate when the sister chromatids of chromosome I (magenta) and chromosome II (green) split (vertical scale bar, 5 μm). **(D)** Frequency distributions and Gaussian fits (continuous lines) of the time difference between the separation of chromosome I and II or chromosome II and III for cells grown in rich medium prior to imaging. Cells grown in minimal medium are shown in Fig. S1E. **(E)** Gaussian fits of the frequency distributions for the separation of chromosome I and III relative to chromosome II. The distributions were significantly different (Kolmogorov-Smirnov test, Table S1). **(F)** Stochastic model for separase-mediated cleavage of cohesin on two chromosomes. Time window of sister chromatid separation between two chromosomes with the same number of initial cohesin complexes (right graph) when assuming the indicated time courses of separase activity (left graph) in wild type (grey) or separase mutant (purple). See Supplementary Information for details. **(G)** Frequency distributions and Gaussian fit (continuous lines) of the time difference between the separation of chromosome I and II or chromosome II and III for cells carrying the temperature-sensitive separase allele *cut1-206* grown in rich medium prior to imaging. The fitted Gaussian distributions of wild type cells from (D) are shown for comparison (green and grey, respectively). Insets show the standard deviation, σ, of the Gaussian fits.

Figure 2. Loss of Cdk1 activity is dispensable for synchronous sister chromatid separation

(A) Representative kymographs of cells with fluorescently labeled chromosomes I and II after expression of non-degradable cyclin B (Cdc13), ΔN-cyclin B, in minimal medium. The cell on the left displays a 'pseudo-metaphase' phenotype and does not exit mitosis. The cell on the right progresses through mitosis unhindered (vertical scale bars, 5 μm). **(B)** Frequency distributions and Gaussian fits (continuous lines) of the time difference between the separation of chromosome I and II for the experiment described in (A). The Gaussian fit of wild type cells grown under similar conditions (green) is shown for comparison. **(C)** Comparison of the Gaussian fits from (B). **(D)** Schematic for a separase-mediated positive feedback loop, where unbound separase enhances securin degradation. **(E)** Simulation of the securin degradation (green) and separase release (grey) dynamics with (dashed) or without (continuous) feedback for the model shown in (D). The increase in APC/C activity (grey) is assumed to be sigmoidal. See Supplementary Information for details. **(F)** Securin-GFP degradation was followed by live cell imaging in wild type cells (green, n=27) or in cells failing to separate their chromosomes after induction of non-degradable securin (Cut2), ΔN-securin (grey, n=21). The individual time courses were normalized and aligned to start of securin degradation. Shown is the average +/- standard deviation of the cell population (filled area). **(G)** Quantification of the degradation rate for the experiment shown in (F) with mean and standard deviation.

Figure 3. Securin degradation kinetics modulate the synchronicity of sister chromatid separation

(A, B) Deterministic model for separase release (solid lines) mediated by securin degradation (dashed lines), assuming high (grey) or low (orange) APC/C activity. **(C)** Stochastic modeling of sister chromatid separation using the separase release curves from (B) as input (see Supplementary Information for details). The continuous lines are the Gaussian fits of the distribution. **(D, E)** Deterministic model as in (A) with the additional assumption of autocatalytic

separase activation. **(F)** Stochastic modeling of sister chromatid separation using the separase release curves from (E) as input. **(G, H)** Frequency distributions and Gaussian fits (continuous lines) of the time difference between the separation of chromosome I and II or chromosome II and III. Cells were either carrying a temperature-sensitive allele of the APC/C subunit Cut9 (*cut9-665*) and were grown in rich medium before imaging, or cells were grown in minimal medium and treated with 100 μM of the proteasome inhibitor Bortezomib 30 min prior to imaging. The fitted Gaussian distribution of wild type cells grown under similar conditions and without inhibitor is shown for comparison. **(I)** Standard deviation, σ, of the Gaussian fits shown in (G) and (H). **(J)** Standard deviation, σ, of the Gaussian fits in the different genetic backgrounds and media conditions (rich, minimal) relative to the measured normalized degradation rate for securin in these backgrounds (see Fig. S3 C-E, Materials and Methods).

Figure 4. Slow securin degradation or low separase activity enhances separation bias between chromosome II and III

(A) Comparison of the Gaussian fits of the frequency distributions for wild type cells and the different perturbations (taken from Fig. 1, 3 and S1). The dashed lines give the distribution for wild type cells grown in minimal medium prior to imaging (Fig. S1). **(B)** Standard deviation, σ, and mean of the Gaussian fits shown in (A) for cells grown in rich (larger dots) or minimal medium (smaller dots) prior to imaging. **(C)** Stochastic modeling as in Fig. 3C using the separase release curves from the deterministic modeling shown in Fig. 3B, but now assuming different numbers of initial cohesin complexes (250 and 1000, respectively) on the two chromosomes. **(D)** The number of cohesin complexes loaded on one chromosome and the kinetics of separase release were varied in the stochastic model. For simplification, logistic functions of varying steepness were used as input functions for the separase release (see Supplementary Information). The mean and the standard deviation, σ, were plotted for each combination of cohesin molecule numbers and separase release kinetics. Dots of the same color exhibit the same number of initial cohesin complexes and the continuous lines show the linear regression for each of these data sets. The

further a dot is to the right on the graph, the slower were the kinetics of separase release.

Figure 5. Fast securin rebinding or preferential degradation can explain rapid separase activation

(A, B) Deterministic model for separase release mediated by securin degradation. Separase release curves are shown for no (grey), slow (light blue) or fast (dark blue) rebinding of securin to separase molecules, which were released due to degradation of the securin-separase complex. **(C)** Stochastic modeling of sister chromatid separation using the separase release curves from (B) as input. See Supplementary Information for details. **(D, E)** Deterministic model for separase release, assuming preferential degradation of free over separase-bound securin and a limiting pool of the APC. The separase release curves are shown assuming an identical association constant (k_{on}) for the free and separase-bound securin to the APC/C^{Cdc20} (grey) or a 10x (magenta) or 100x (purple) larger k_{on} for the free securin species. **(F)** Stochastic modeling of sister chromatid separation using the separase release curves from (E) as input.

Figure 1

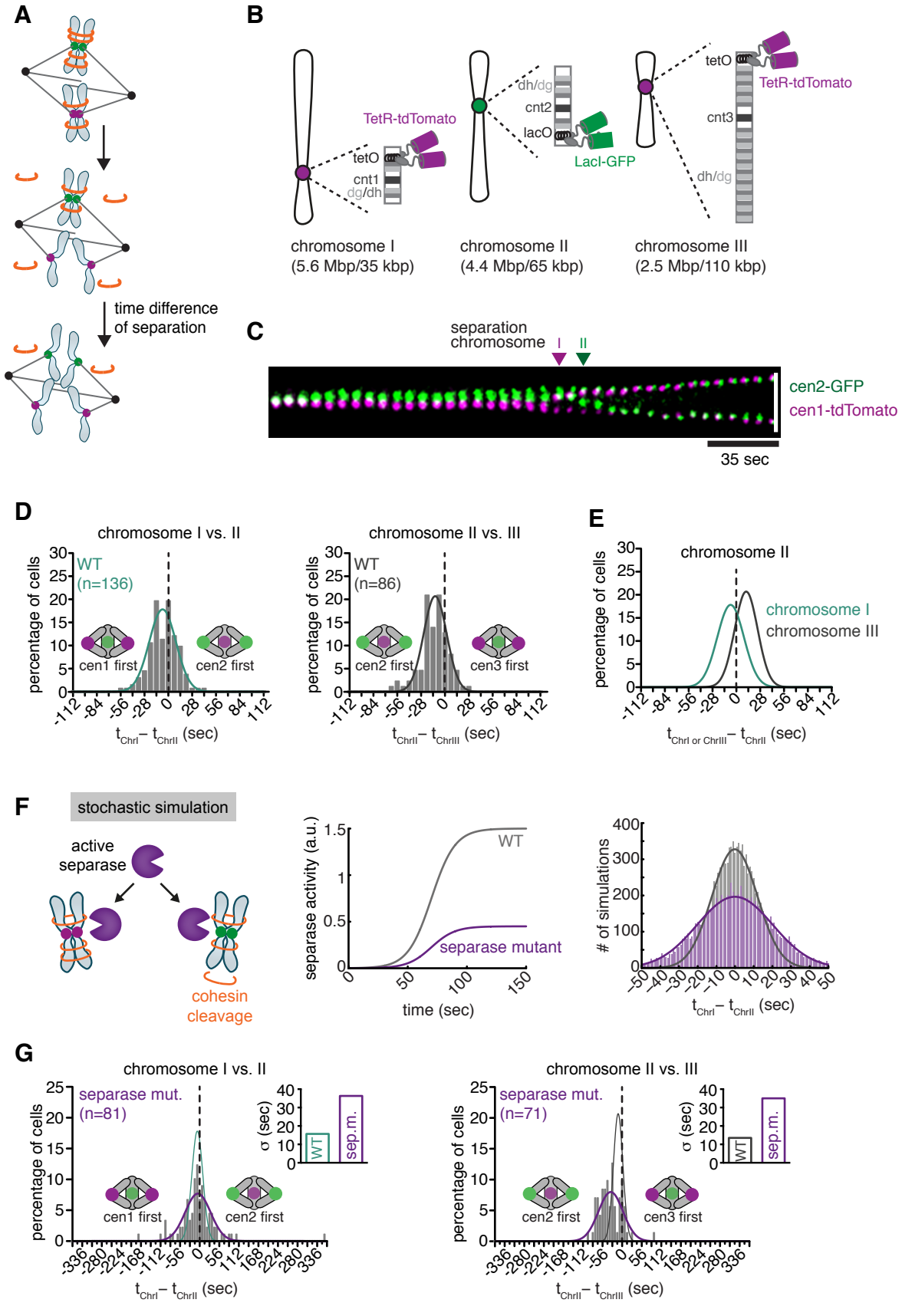
A
time difference of separation
B
TetR-tdTomato
tetO
cnt1
dg/dh
dh/dg
cnt2
lacO
LacI-GFP
tetO
TetR-tdTomato
cnt3
dh/dg
chromosome I (5.6 Mbp/35 kbp)
chromosome II (4.4 Mbp/65 kbp)
chromosome III (2.5 Mbp/110 kbp)
C
separation chromosome I II
cen2-GFP
cen1-tdTomato
35 sec
D
chromosome I vs. II
WT (n=136)
cen1 first
cen2 first
percentage of cells
tChrI – tChrII (sec)
chromosome II vs. III
WT (n=86)
cen2 first
cen3 first
tChrII – tChrIII (sec)
E
chromosome II
chromosome I
chromosome III
tChrI or ChrIII – tChrII (sec)
F
stochastic simulation
active separase
cohesin cleavage
separase activity (a.u.)
WT
separase mutant
time (sec)
# of simulations
tChrI – tChrII (sec)
G
chromosome I vs. II
separase mut. (n=81)
cen1 first
cen2 first
σ (sec)
WT
sep.m.
tChrI – tChrII (sec)
chromosome II vs. III
separase mut. (n=71)
cen2 first
cen3 first
tChrII – tChrIII (sec)

Figure 2

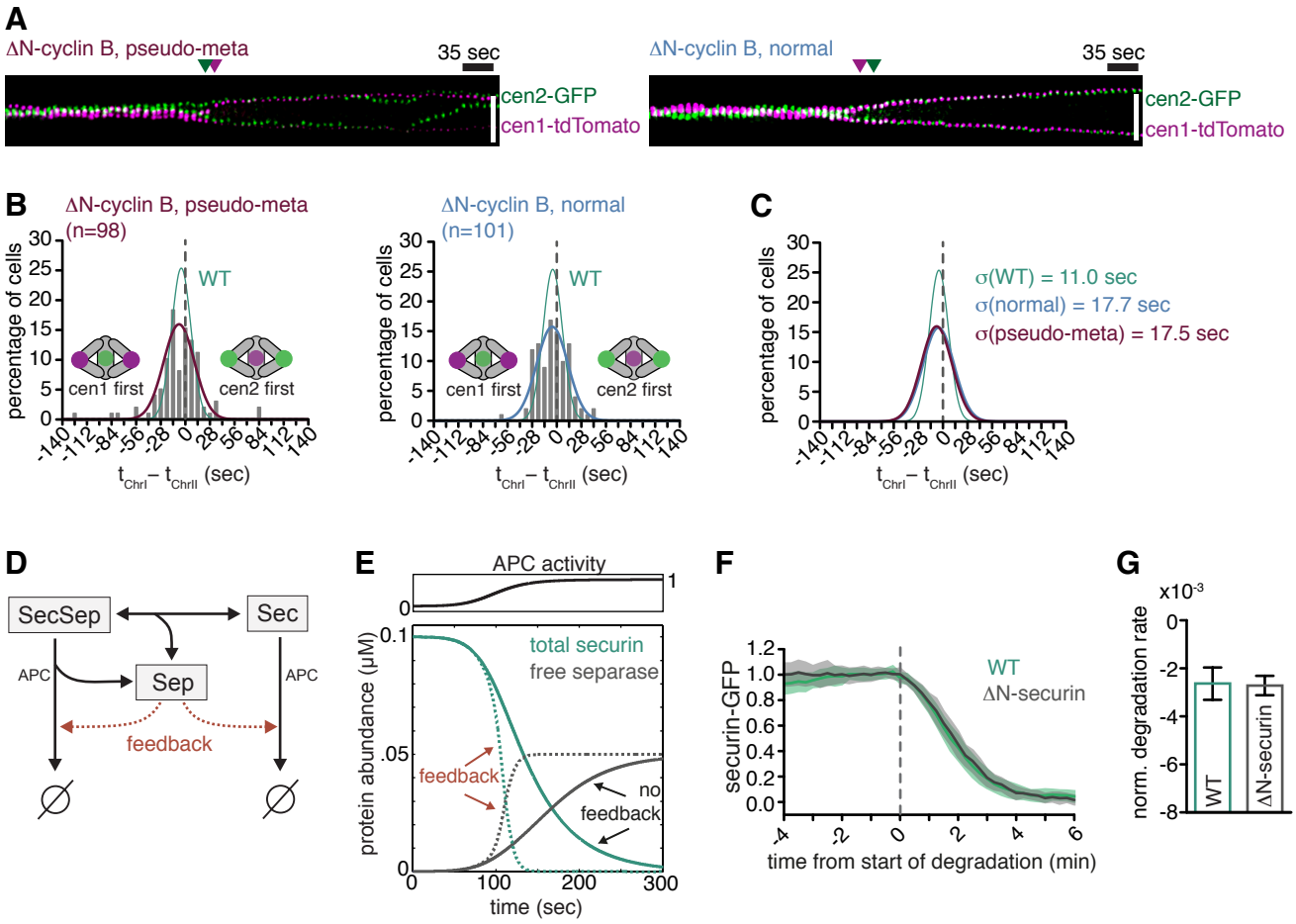
A
ΔN-cyclin B, pseudo-meta
35 sec
cen2-GFP
cen1-tdTomato
ΔN-cyclin B, normal
35 sec
cen2-GFP
cen1-tdTomato
B
ΔN-cyclin B, pseudo-meta (n=98)
WT
cen1 first
cen2 first
percentage of cells
t_ChrI – t_ChrII (sec)
ΔN-cyclin B, normal (n=101)
WT
cen1 first
cen2 first
percentage of cells
t_ChrI – t_ChrII (sec)
C
σ(WT) = 11.0 sec
σ(normal) = 17.7 sec
σ(pseudo-meta) = 17.5 sec
percentage of cells
t_ChrI – t_ChrII (sec)
D
SecSep
Sec
Sep
APC
APC
feedback
E
APC activity
total securin
free separase
feedback
no feedback
protein abundance (μM)
time (sec)
F
WT
ΔN-securin
securin-GFP
time from start of degradation (min)
G
x10-3
norm. degradation rate
WT
ΔN-securin

Figure 3

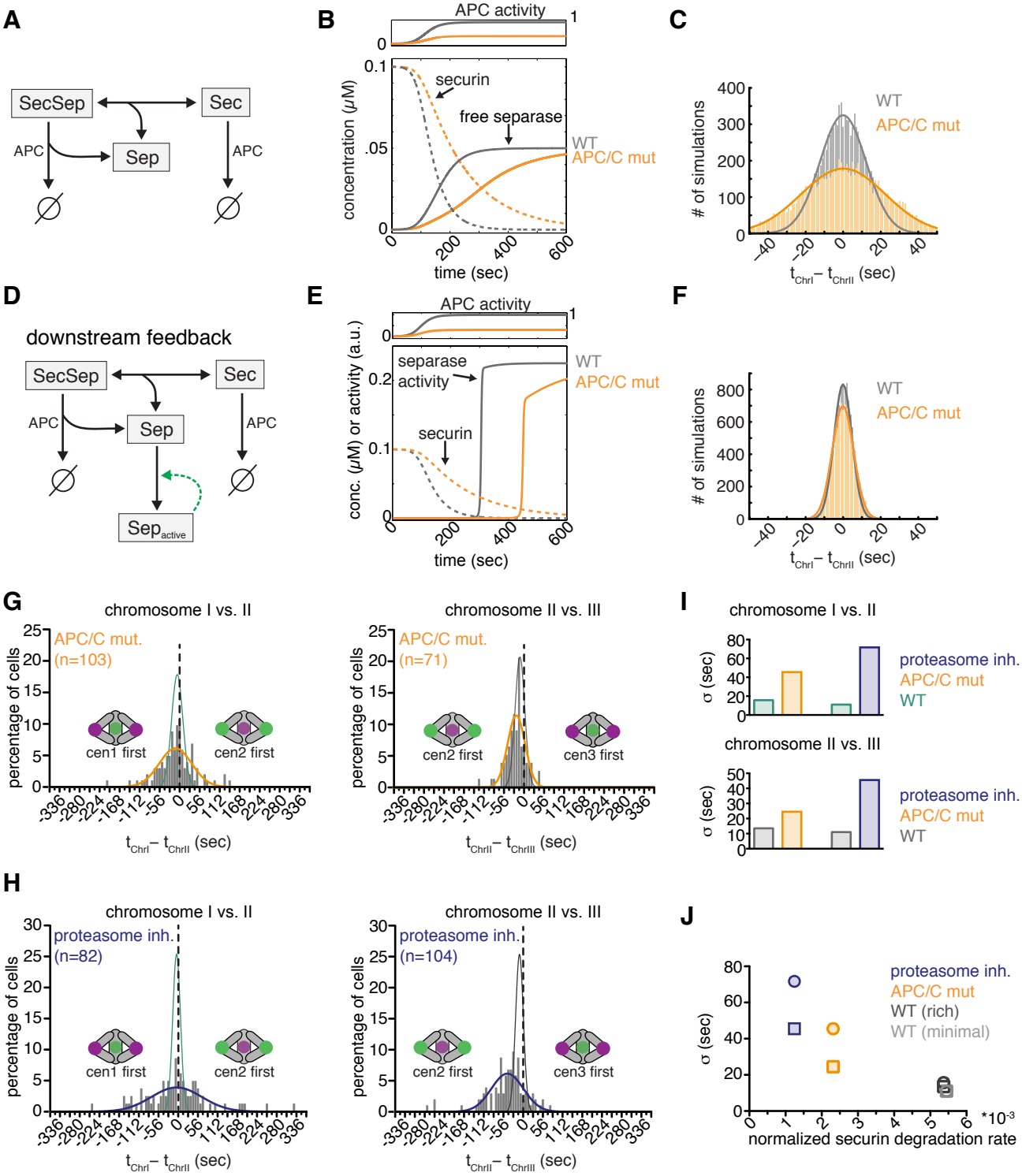
A
SecSep
Sec
Sep
APC
APC
B
APC activity
securin
free separase
WT
APC/C mut
concentration (μM)
time (sec)
C
WT
APC/C mut
# of simulations
t_ChrI – t_ChrII (sec)
D
downstream feedback
SecSep
Sec
Sep
APC
APC
Sep_active
E
APC activity
separase activity
securin
WT
APC/C mut
conc. (μM) or activity (a.u.)
time (sec)
F
WT
APC/C mut
# of simulations
t_ChrI – t_ChrII (sec)
G
chromosome I vs. II
APC/C mut. (n=103)
cen1 first
cen2 first
percentage of cells
t_ChrI – t_ChrII (sec)
chromosome II vs. III
APC/C mut. (n=71)
cen2 first
cen3 first
t_ChrII – t_ChrIII (sec)
I
chromosome I vs. II
proteasome inh.
APC/C mut
WT
σ (sec)
chromosome II vs. III
proteasome inh.
APC/C mut
WT
σ (sec)
H
chromosome I vs. II
proteasome inh. (n=82)
cen1 first
cen2 first
percentage of cells
t_ChrI – t_ChrII (sec)
chromosome II vs. III
proteasome inh. (n=104)
cen2 first
cen3 first
t_ChrII – t_ChrIII (sec)
J
proteasome inh.
APC/C mut
WT (rich)
WT (minimal)
σ (sec)
*10^-3
normalized securin degradation rate

Figure 4

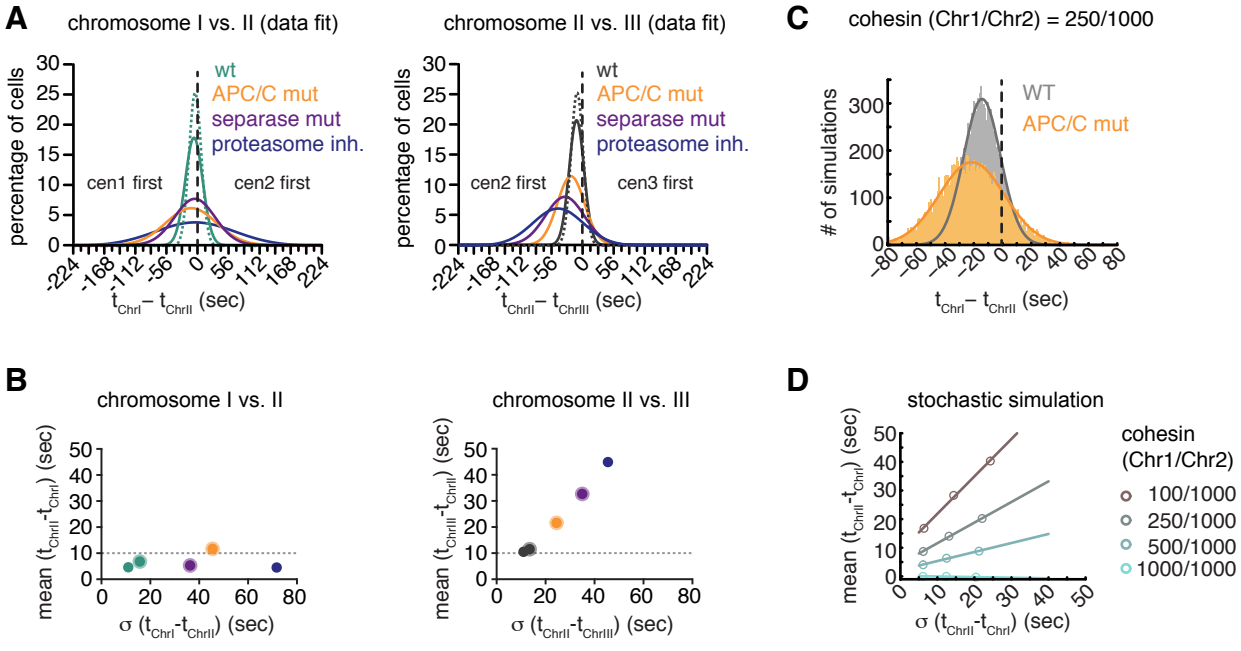
A
chromosome I vs. II (data fit)
chromosome II vs. III (data fit)
percentage of cells
wt
APC/C mut
separase mut
proteasome inh.
cen1 first
cen2 first
cen3 first
tChrI – tChrII (sec)
tChrII – tChrIII (sec)
C
cohesin (Chr1/Chr2) = 250/1000
# of simulations
WT
APC/C mut
tChrI – tChrII (sec)
B
chromosome I vs. II
chromosome II vs. III
mean (tChrI-tChrII) (sec)
mean (tChrII-tChrIII) (sec)
σ (tChrI-tChrII) (sec)
σ (tChrII-tChrIII) (sec)
D
stochastic simulation
mean (tChrII-tChrI) (sec)
σ (tChrII-tChrI) (sec)
cohesin
(Chr1/Chr2)
100/1000
250/1000
500/1000
1000/1000

Figure 5

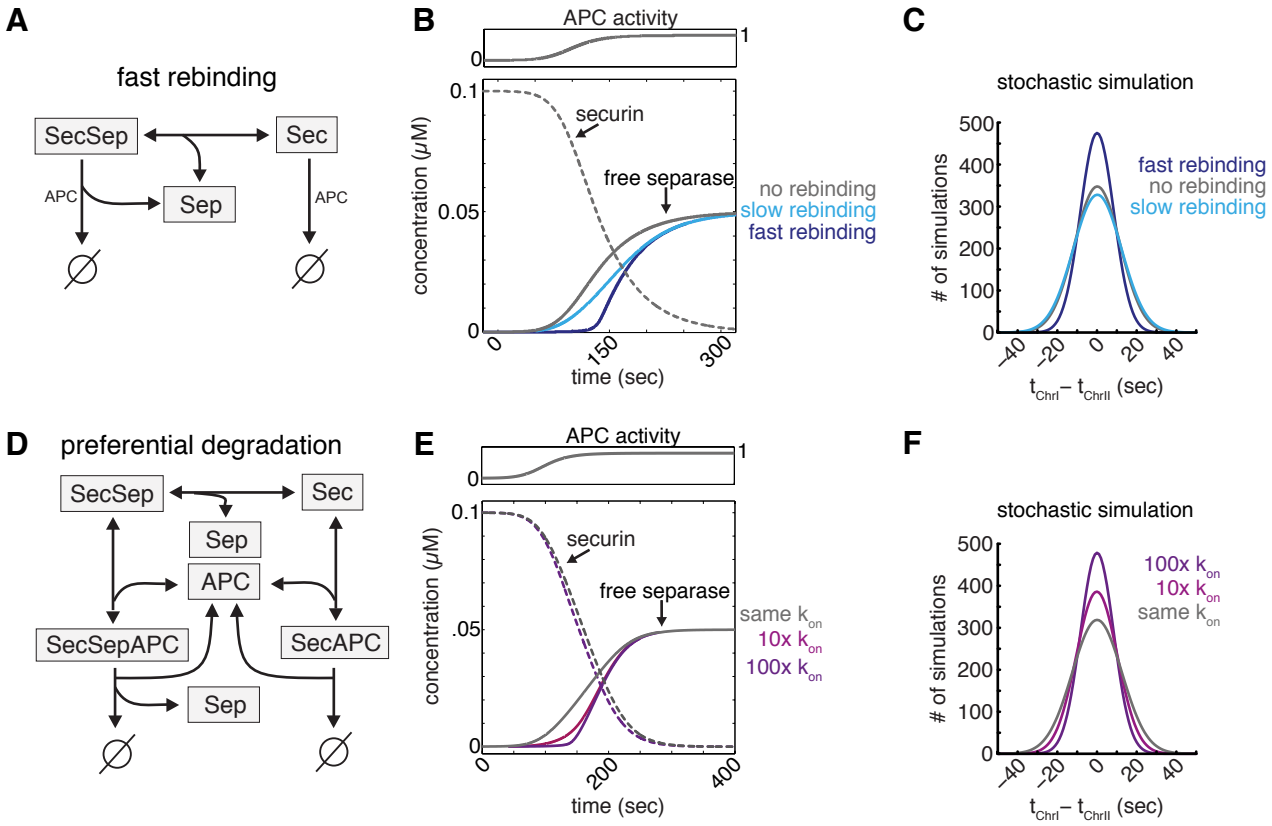
A
fast rebinding
SecSep
Sec
APC
Sep
APC
B
APC activity
1
0
0.1
securin
free separase
concentration (μM)
0.05
0
no rebinding
slow rebinding
fast rebinding
0
150
300
time (sec)
C
stochastic simulation
500
400
300
200
100
0
# of simulations
fast rebinding
no rebinding
slow rebinding
−40
−20
0
20
40
tChrI – tChrII (sec)
D
preferential degradation
SecSep
Sec
Sep
APC
SecSepAPC
SecAPC
Sep
E
APC activity
1
0
0.1
securin
free separase
concentration (μM)
.05
0
same kon
10x kon
100x kon
0
200
400
time (sec)
F
stochastic simulation
500
400
300
200
100
0
# of simulations
100x kon
10x kon
same kon
−40
−20
0
20
40
tChrI – tChrII (sec)

Figure S1

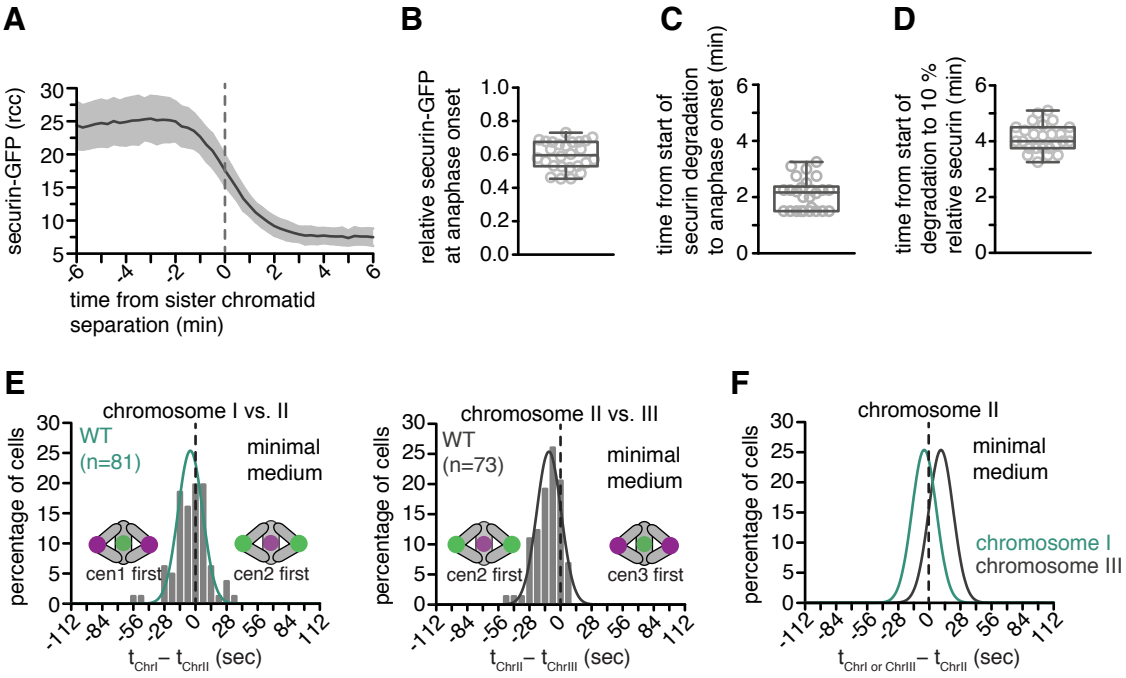
A
securin-GFP (rcc)
time from sister chromatid separation (min)
B
relative securin-GFP at anaphase onset
C
time from start of securin degradation to anaphase onset (min)
D
time from start of degradation to 10 % relative securin (min)
E
chromosome I vs. II
WT
(n=81)
minimal medium
cen1 first
cen2 first
percentage of cells
tChrI – tChrII (sec)
chromosome II vs. III
WT
(n=73)
minimal medium
cen2 first
cen3 first
tChrII – tChrIII (sec)
F
chromosome II
minimal medium
chromosome I
chromosome III
tChrI or ChrIII – tChrII (sec)

Figure S2

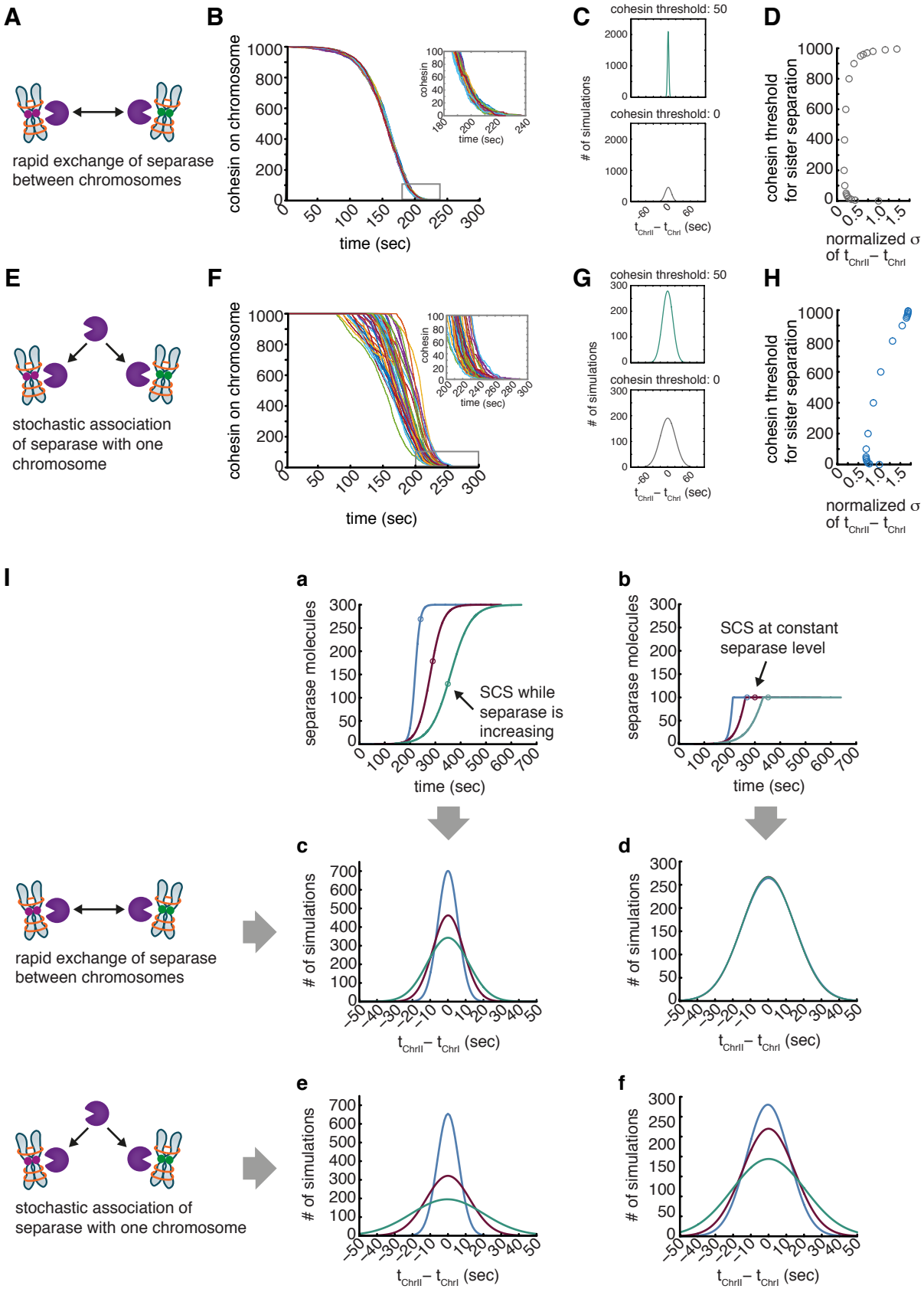
A
rapid exchange of separase between chromosomes
B
cohesin on chromosome
time (sec)
cohesin
time (sec)
C
cohesin threshold: 50
cohesin threshold: 0
# of simulations
$t_{ChrII} - t_{ChrI}$ (sec)
D
cohesin threshold for sister separation
normalized σ of $t_{ChrII} - t_{ChrI}$
E
stochastic association of separase with one chromosome
F
cohesin on chromosome
time (sec)
cohesin
time (sec)
G
cohesin threshold: 50
cohesin threshold: 0
# of simulations
$t_{ChrII} - t_{ChrI}$ (sec)
H
cohesin threshold for sister separation
normalized σ of $t_{ChrII} - t_{ChrI}$
I
a
separase molecules
SCS while separase is increasing
time (sec)
b
separase molecules
SCS at constant separase level
time (sec)
rapid exchange of separase between chromosomes
c
# of simulations
$t_{ChrII} - t_{ChrI}$ (sec)
d
# of simulations
$t_{ChrII} - t_{ChrI}$ (sec)
stochastic association of separase with one chromosome
e
# of simulations
$t_{ChrII} - t_{ChrI}$ (sec)
f
# of simulations
$t_{ChrII} - t_{ChrI}$ (sec)

Figure S3

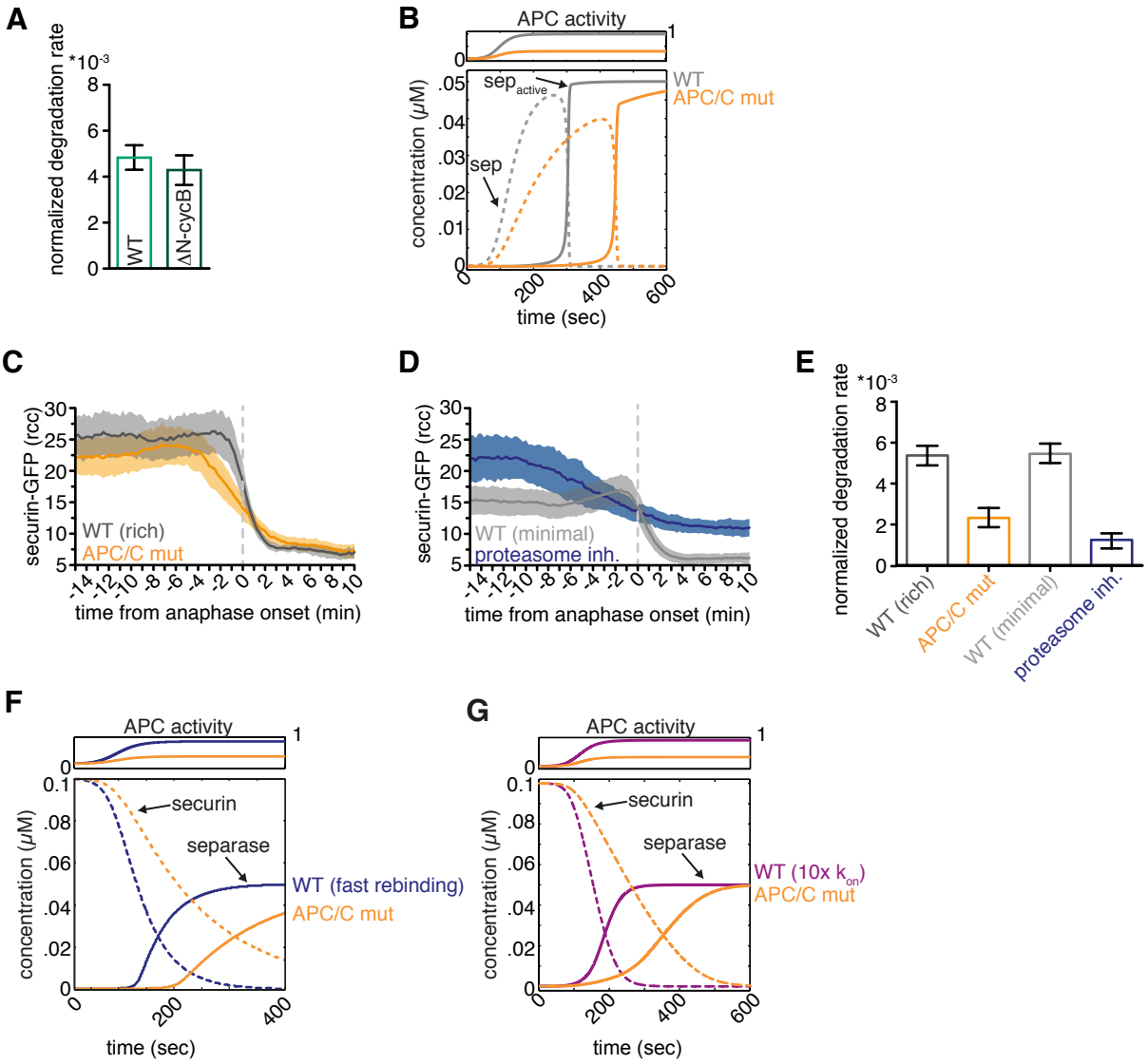
A
normalized degradation rate
*10-3
WT
ΔN-cycB
B
APC activity
concentration (μM)
sepactive
sep
WT
APC/C mut
time (sec)
C
securin-GFP (rcc)
WT (rich)
APC/C mut
time from anaphase onset (min)
D
securin-GFP (rcc)
WT (minimal)
proteasome inh.
time from anaphase onset (min)
E
normalized degradation rate
*10-3
WT (rich)
APC/C mut
WT (minimal)
proteasome inh.
F
APC activity
concentration (μM)
securin
separase
WT (fast rebinding)
APC/C mut
time (sec)
G
APC activity
concentration (μM)
securin
separase
WT (10x kon)
APC/C mut
time (sec)

Supplementary Table S1 Statistical analysis

		n	mean (sec)	stdev (sec)	σ of the gaussian fit (sec)	p-value (Kolmogorov-Smirnov)	tested against
WT (rich medium)	chromosome I vs. II	132	-6.8	16.4	15.7		
	chromosome III vs. II	86	11.5	16.9	13.5	1.5*10-9	WT, rich medium, chromosome I vs. II
WT (minimal medium)	chromosome I vs. II	81	-4.6	15.6	11		
	chromosome III vs. II	73	10.5	11.8	11	9.9*10^-7	WT, minimal medium, chromosome I vs. II
separase mutant (*cut1-206,* rich medium)	chromosome I vs. II	89	-5.3	58.5	36.3	0.031	WT, rich medium, chromosome I vs. II
	chromosome III vs. II	71	32.7	31.9	35	3.2*10^-9	WT, rich medium, chromosome III vs. II
APC/C mutant (*cut9-665*, rich medium)	chromosome I vs. II	103	-11.7	51.6	45.5	0.0038	WT, rich medium, chromosome I vs. II
	chromosome III vs. II	78	21.6	31.9	24.5	0.0034	WT, rich medium, chromosome III vs. II
proteasome inhibition (minimal medium)	chromosome I vs. II	82	-4.5	89.9	71.7	7.5*10^-4	WT, minimal medium, chromosome I vs. II
	chromosome III vs. II	104	44.9	58.2	45.5	3.5*10^-11	WT, minimal medium, chromosome III vs. II
ΔN-cyclin B normal (minimal medium)	chromosome I vs. II	101	-5.1	18.1	17.7	0.29	WT, minimal medium, chromosome I vs. II
ΔN-cyclin B pseudo-meta (minimal medium)	chromosome I vs. II	98	-7.2	27.35	17.5	0.4	WT, minimal medium, chromosome I vs. II

Supplementary Table S2 *S. pombe* strains

Figure 1C		
SI541	*h+*	*leu1 ade6-M216 (ura4-D18) cen2<<lacO-kanR-ura+ his7+<<Pdis1-GFP-lacI-NLS dh1L<<ura4+<<tetO Z<<natR<<Padh31-tetR-tdTomato*
Figure 1D-E		
SI541	*h+*	*leu1 ade6-M216 (ura4-D18) cen2<<lacO-kanR-ura+ his7+<<Pdis1-GFP-lacI-NLS dh1L<<ura4+<<tetO Z<<natR<<Padh31-tetR-tdTomato*
SL239'	*h+*	*leu1 ade6-M216 cen2<<lacO-kanR-ura+ his7+<<dis1-GFP-lacI-NLS Z<<natR<<Padh31-tetR-tdTomato cen3<<LEU2+<<tetO*
Figure 1G		
SM388	*h?*	*leu1 ade6-M21? (ura4-D18) cen2<<lacO-kanR-ura+ his7+<<Pdis1-GFP-lacI-NLS dh1L<<ura4+<<tetO Z<<natR<<Padh31-tetR-tdTomato cut1-206*
SM387	*h?*	*ade6-M21? leu1 cen2<<lacO-kanR-ura+ his7+<<dis1-GFP-lacI-NLS Z<<natR<<Padh31-tetR-tdTomato cen3<<LEU2+<<tetO cut1-206*
Figure 2A-B		
SL274	*h+*	*leu1 ade6-M216 (ura4-D18) cen2<<lacO-kanR-ura+ his7+<<dis1-GFP-lacI-NLS dh1L<<ura4+<<tetO Z<<natR<<Padh31-tetR-tdTomato leu1+<<Pnmt81-ΔN67-cdc13*
Figure 2C		
SL274	*h+*	*leu1 ade6-M216 (ura4-D18) cen2<<lacO-kanR-ura+ his7+<<dis1-GFP-lacI-NLS dh1L<<ura4+<<tetO Z<<natR<<Padh31-tetR-tdTomato leu1+<<Pnmt81-ΔN67-cdc13*
SI541	*h+*	*leu1 ade6-M216 (ura4-D18) cen2<<lacO-kanR-ura+ his7+<<Pdis1-GFP-lacI-NLS dh1L<<ura4+<<tetO Z<<natR<<Padh31-tetR-tdTomato*
Figure 2F-G		
SL249	*h-*	*leu1 ade6-M216 cut2+-GFP<<kanR dh1L<<ura4+<<tetO Z<<natR<<Padh31-tetR-tdTomato*
SL275	*h-*	*leu1 ade6-M216 cut2+-GFP<<kanR dh1L<<ura4+<<tetO Z<<natR<<Padh31-tetR-tdTomato leu1+<<Pnmt81-ΔN80-cut2*
Figure 3G, I		
SI541	*h+*	*leu1 ade6-M216 (ura4-D18) cen2<<lacO-kanR-ura+ his7+<<Pdis1-GFP-lacI-NLS dh1L<<ura4+<<tetO Z<<natR<<Padh31-tetR-tdTomato*
SL231	*h+*	*leu1 ade6-M216 cen2<<lacO-kanR-ura+ his7+<<dis1-GFP-lacI-NLS dh1L<<ura4+<<tetO Z<<natR<<Padh31-tetR-tdTomato plo1+-GFP<<kanR cut9-665*
SL239'	*h+*	*leu1 ade6-M216 cen2<<lacO-kanR-ura+ his7+<<dis1-GFP-lacI-NLS Z<<natR<<Padh31-tetR-tdTomato cen3<<LEU2+<<tetO*
SM386	*h?*	*ade6-M216 leu1 cen2<<lacO-kanR-ura+ his7+<<dis1-GFP-lacI-NLS Z<<natR<<Padh31-tetR-tdTomato cen3<<LEU2+<<tetO cut9-665*
Figure 3H, I		
SI541	*h+*	*leu1 ade6-M216 (ura4-D18) cen2<<lacO-kanR-ura+ his7+<<Pdis1-GFP-lacI-NLS dh1L<<ura4+<<tetO Z<<natR<<Padh31-tetR-tdTomato*
SL239'	*h+*	*leu1 ade6-M216 cen2<<lacO-kanR-ura+ his7+<<dis1-GFP-lacI-NLS Z<<natR<<Padh31-tetR-tdTomato cen3<<LEU2+<<tetO*
Figure 3J		
SI541	*h+*	*leu1 ade6-M216 (ura4-D18) cen2<<lacO-kanR-ura+ his7+<<Pdis1-GFP-lacI-NLS dh1L<<ura4+<<tetO Z<<natR<<Padh31-tetR-tdTomato*
SL231	*h+*	*leu1 ade6-M216 cen2<<lacO-kanR-ura+ his7+<<dis1-GFP-lacI-NLS dh1L<<ura4+<<tetO Z<<natR<<Padh31-tetR-tdTomato plo1+-GFP<<kanR cut9-665*
SL239'	*h+*	*leu1 ade6-M216 cen2<<lacO-kanR-ura+ his7+<<dis1-GFP-lacI-NLS Z<<natR<<Padh31-tetR-tdTomato cen3<<LEU2+<<tetO*
SM386	*h?*	*ade6-M216 leu1 cen2<<lacO-kanR-ura+ his7+<<dis1-GFP-lacI-NLS Z<<natR<<Padh31-tetR-tdTomato cen3<<LEU2+<<tetO cut9-665*
SL249	*h-*	*leu1 ade6-M216 cut2+-GFP<<kanR dh1L<<ura4+<<tetO Z<<natR<<Padh31-tetR-tdTomato*
SL258'	*h-*	*leu1 ade6-M216 cut2+-GFP<<kanR dh1L<<ura4+<<tetO Z<<natR<<Padh31-tetR-tdTomato cut9-665*
Figure 4A, B		
SI541	*h+*	*leu1 ade6-M216 (ura4-D18) cen2<<lacO-kanR-ura+ his7+<<Pdis1-GFP-lacI-NLS dh1L<<ura4+<<tetO Z<<natR<<Padh31-tetR-tdTomato*
SM388	*h?*	*leu1 ade6-M21? (ura4-D18) cen2<<lacO-kanR-ura+ his7+<<Pdis1-GFP-lacI-NLS dh1L<<ura4+<<tetO Z<<natR<<Padh31-tetR-tdTomato cut1-206*
SL231	*h+*	*leu1 ade6-M216 cen2<<lacO-kanR-ura+ his7+<<dis1-GFP-lacI-NLS dh1L<<ura4+<<tetO Z<<natR<<Padh31-tetR-tdTomato plo1+-GFP<<kanR cut9-665*
SL239'	*h+*	*leu1 ade6-M216 cen2<<lacO-kanR-ura+ his7+<<dis1-GFP-lacI-NLS Z<<natR<<Padh31-tetR-tdTomato cen3<<LEU2+<<tetO*
SM387	*h?*	*ade6-M21? leu1 cen2<<lacO-kanR-ura+ his7+<<dis1-GFP-lacI-NLS Z<<natR<<Padh31-tetR-tdTomato cen3<<LEU2+<<tetO cut1-206*
SM386	*h?*	*ade6-M216 leu1 cen2<<lacO-kanR-ura+ his7+<<dis1-GFP-lacI-NLS Z<<natR<<Padh31-tetR-tdTomato cen3<<LEU2+<<tetO cut9-665*

Figure S1A-D

SL249	*h-*	*leu1 ade6-M216 cut2+-GFP<<kanR dh1L<<ura4+<<tetO Z<<natR<<Padh31-tetR-tdTomato*

Figure S1E-F

SI541	*h+*	*leu1 ade6-M216 (ura4-D18) cen2<<lacO-kanR-ura+ his7+<<Pdis1-GFP-lacI-NLS dh1L<<ura4+<<tetO Z<<natR<<Padh31-tetR-tdTomato*
SL239'	*h+*	*leu1 ade6-M216 cen2<<lacO-kanR-ura+ his7+<<dis1-GFP-lacI-NLS Z<<natR<<Padh31-tetR-tdTomato cen3<<LEU2+<<tetO*

Figure S3A

SL249	*h-*	*leu1 ade6-M216 cut2+-GFP<<kanR dh1L<<ura4+<<tetO Z<<natR<<Padh31-tetR-tdTomato*
SL253	*h-*	*leu1 ade6-M216 cut2+-GFP<<kanR dh1L<<ura4+<<tetO Z<<natR<<Padh31-tetR-tdTomato leu1+<<Pnmt81-deltaN67-cdc13*

Figure S3C-E

SL249	*h-*	*leu1 ade6-M216 cut2+-GFP<<kanR dh1L<<ura4+<<tetO Z<<natR<<Padh31-tetR-tdTomato*
SL258'	*h-*	*leu1 ade6-M216 cut2+-GFP<<kanR dh1L<<ura4+<<tetO Z<<natR<<Padh31-tetR-tdTomato cut9-665*

Supplementary Information for

Synchronous sister chromatid splitting in anaphase occurs without obligatory positive feedback

by Julia Kamenz, Tamara Mihaljev, Stefan Legewie and Silke Hauf

Contents

Supplementary figure legends

Figure S1. Securin degradation is slow compared to sister chromatid separation

(A) The nuclear securin-GFP abundance of individual wild type cells grown in rich medium prior to imaging was followed by live cell imaging (grey, n=26). The cen1-tdTomato marker was used to determine anaphase onset and individual time courses were aligned to this point (vertical dashed line). Shown is the average (line) +/- the standard deviation (filled area) of securin-GFP degradation in a population of cells. **(B)** Quantification of the amount of securin-GFP present at the time of anaphase onset relative to the amount present at start of degradation. Data from the experiment shown in (A). Box-Whisker blot with the single-cell measurements as circles. The lines extending from the box represent the minimum and maximum values of the data set. **(C, D)** Quantification of the time from start of securin-GFP degradation until anaphase onset (C) or until 90 % of securin-GFP had been degraded (D). Same representation as described in (B). **(E)** Frequency distributions and Gaussian fits (continuous lines) of the time difference between the separation of chromosome I and II or chromosome II and III for cells grown in minimal medium prior to imaging. **(F)** Comparison of the Gaussian fits of the frequency distributions for the separation of chromosome I and III relative to chromosome II as shown in (E). The distributions are significantly different (Kolmogorov-Smirnov test, Table S1).

Figure S2. Comparison of stochastic models for cohesin cleavage

(A) Schematic representation of the minimal stochastic model that allows rapid diffusion of separase from one chromosome to the other (see Supplementary Information). **(B)** Single time courses of cohesin loss for one chromosome using the model depicted in (A). The inset shows the lower part of the curve indicated by the grey box. See Supplementary Information for model implementation and parameter values. **(C)** Time difference between sister chromatid separation of two chromosomes, determined by the model in (A, B) for two different cohesin thresholds. **(D)** Standard deviation, σ, of the time difference between separation of two chromosomes (x-axis), which is a measure of synchrony, with respect to the number of cohesin molecules that needs to be reached in the model for sister chromatids to separate ('cohesin threshold', y-axis). Data was

extracted from time courses as those shown in (B). To allow for better comparison between model variants, the standard deviations were normalized to the standard deviation of the case, when the cohesin threshold was set to zero. Note that the standard deviation strongly decreases when the cohesin threshold is set larger than zero. **(E)** Schematic representation of the stochastic model, where free separase randomly associates with one of the chromosomes and then only cleaves cohesin on this chromosome (see Supplementary Information). **(F)** Single time courses of cohesin loss for one chromosome using the model depicted in (E). See Supplementary Information for model implementation and parameter values. **(G)** Time difference between sister chromatid separation of two chromosomes, determined by the model in (E, F) for two different cohesin thresholds. **(H)** Relation between chromosome segregation synchrony (x-axis) and cohesin threshold (y-axis), similar to (D), is shown for the model with stochastic separase association to the chromosomes. Note that the standard deviation is less sensitive to changing cohesin thresholds (H) when compared to the simpler stochastic model (C). **(I)** Comparison of the two stochastic model variants with respect to changes in input characteristics. Different release kinetics of separase were used as input (panels a and b). If rapid diffusion of separase between chromosomes is allowed (panels c and d), the timing variance of sister chromatid separation is predominantly determined by the amount of separase at the time when sisters split. Hence, differences in the variance are observed when sister chromatids separate while separase still increases (panel a) but not when sister chromatids separate once separase has reached a constant level, irrespective of the previous kinetics of separase increase (panel b). In contrast, for the model, which assumes stochastic association of separase with one of the chromosomes (panels e and f), the variance is in part determined by the initial kinetics of separase increase. Hence, the variance differs even when the end level of separase is the same (panel f).

Figure S3. Modulation of securin degradation kinetics by impairing APC/C or proteasome activity

(A) Quantification of the degradation rates in the presence (ΔN-cycB, n=22) or absence (WT, n=31) of non-degradable cyclin B. The corresponding securin degradation curves have been shown previously in Kamenz and Hauf, 2014, Figure 1E. **(B)** Deterministic

model of released separase (dashed lines) and active separase (solid lines) for the model with autocatalytic separase activation (shown in Fig. 3D) assuming high (grey) or low (orange) APC/C activity. **(C)** The nuclear securin-GFP abundance of individual wild type cells (grey, n=19) or cells carrying the temperature sensitive *cut9-665* allele (orange, n=25) grown initially in rich medium at 25 °C were followed by live cell imaging at 30 °C. The cen1-tdTomato marker was used to determine anaphase onset and individual time courses were aligned to this point (vertical dashed line). Shown is the average (line) +/- standard deviation (filled area) of securin-GFP degradation in a population of cells. **(D)** The nuclear securin-GFP abundance of individual wild type cells (grey, n=41) grown in minimal medium or cells additionally treated with 100 μM of the proteasome inhibitor Bortezomib (Velcade) (blue, n=18) were followed by live cell imaging. Shown is the average (line) +/- standard deviation (filled area) of securin-GFP degradation in a population of cells. **(E)** Quantification of the degradation rates for the experiments shown in (C) and (D). Error bars represent the standard deviation of the cell population. **(F)** Deterministic model of securin degradation (dashed lines) and separase release (solid lines) for the model with fast rebinding of separase as shown in Figure 5B (blue line) assuming high (blue) or low (orange) APC/C activity. **(G)** Deterministic model of securin degradation (dashed lines) and separase release (solid lines) for the model with preferential degradation of free securin as shown in Figure 5E (purple line, 100x k_{on}) assuming high (purple) or low (orange) APC/C activity.

Deterministic modeling of separase release

1. Minimal stoichiometric inhibition model

Model description: The minimal stoichiometric inhibition model between securin-separase is depicted in Fig. 3A: securin (Sec) and separase (Sep) reversibly form a complex (SecSep). Upon initiation of anaphase, the anaphase-promoting complex (APC) activity increases from 0 to a positive value and securin is regulated by APC-mediated degradation. The differential equations describing complex formation and APC-mediated degradation are given by (1)

$$\frac{dSec}{dt} = -k_{on} \cdot Sec \cdot Sep + k_{off} \cdot SecSep - k_{APC,Sec} \cdot Sec$$

$$\frac{dSep}{dt} = -k_{on} \cdot Sec \cdot Sep + k_{off} \cdot SecSep + k_{APC,SecSep} \cdot SecSep$$

$$\frac{dSecSep}{dt} = k_{on} \cdot Sec \cdot Sep - k_{off} \cdot SecSep - k_{APC,SecSep} \cdot SecSep$$

Before the initiation of anaphase, the APC activity is assumed to be negligible (i.e., $k_{APC,Sec} = 0$ and $k_{APC,SecSep} = 0$), and the SecSep complex is assumed to be in equilibrium with the free proteins. Based on biochemical evidence (J.K., unpublished observations and (Hellmuth et al., 2014; Shindo et al., 2012)), we will assume that securin is in excess over separase before anaphase, and that the amount of free separase is negligible, i.e., the total concentrations of securin (Sec_{tot}) and separase (Sep_{tot}) are assumed to be much larger than the dissociation constant of the complex ($K_D = k_{off} / k_{on}$). Hence, the initial equilibrium can be approximated as (2)

$$Sec \approx Sec_{tot} - Sep_{tot}$$

$$Sep \approx 0$$

$$SecSep \approx Sep_{tot}$$

Gradual separase release in the absence of securin rebinding: Owing to the fast time scale of securin degradation, it is conceivable that the re-association kinetics of securin-separase binding (k_{on}) cannot catch up with the fast degradation-mediated separase release ($k_{APC,SecSep}$). Under these conditions, the amount of free separase simply equals the inverse of the SecSep complex concentration (3)

$$Sep(t) \approx SecSep(0) - SecSep(t) = Sep_{tot} - SecSep(t)$$

and the SecSep dynamics will be mainly determined by the degradation term (4)

$$\frac{dSecSep}{dt} \approx -k_{APC,SecSep} \cdot SecSep$$

Assuming a step-like activation of the APC activity from $k_{APC,SecSep} = 0$ to $k_{APC,SecSep} > 0$ at t = 0, one derives for the separase release (5)

$$Sep(t) \approx Sep_{tot} \cdot \left(1 - e^{k_{APC,SecSep} t}\right)$$

Hence, separase will be released gradually (immediately starting at t = 0). Moreover, the

separase release dynamics depend in a linear manner on the APC concentration, because $k_{APC,SecSep}$ is proportional to the amount of the APC according to classical enzyme kinetics.

Switch-like separase release upon fast securin rebinding to separase: When reformation of the SecSep complex is fast, separase that is released due to degradation of SecSep will be immediately re-bound by any remaining pool of free securin. In the extreme case, the amount of free separase will thus remain zero as long as the total amount of securin ($Sec_{tot}(t) = Sec(t) + SecSep(t)$) exceeds the separase pool (6)

$Sep(t) \approx 0$ if $Sep_{tot} < Sec_{tot}(t)$

Free separase will become non-zero once degradation has reduced the amount of securin below the separase concentration (7)

$Sep(t) \approx Sep_{tot} - Sec_{tot}(t)$ if $Sep_{tot} > Sec_{tot}(t)$

Thus, the system exhibits a waiting time t_W (or a temporal threshold) for the separase release which can be calculated by setting $Sec_{tot}(t) = Sep_{tot}$. The degradation of the total securin pool is determined by the following differential equation (8)

$$\frac{dSec_{tot}}{dt} = \frac{dSec}{dt} + \frac{dSecSep}{dt} = -k_{APC,Sec} \cdot Sec - v_{APC,SecSep} \cdot SecSep$$

Assuming the same degradation rate for free and complexed securin ($dSec_{tot}/dt = - k_{APC} Sec_{tot}$), and a step-like increase of the APC activity at t = 0 one derives (9)

$$Sec_{tot}(t) = Sec_{tot}(0) \cdot e^{k_{APC}t}$$

$$t_W = \frac{1}{k_{APC}} \ln\left(\frac{Sep_{tot}}{Sec_{tot}(0)}\right)$$

$$s_0 = Sep_{tot} \cdot k_{APC}$$

Here, s_0 is the initial slope of separase release just after the waiting time t_W. The steepness of separase release after the waiting time can be enhanced by two factors: (i) increasing the total amount of separase; (ii) increasing APC activity. For a gradual (not step-like) increase in APC activity, the steepness of the switch can be further enhanced by appropriately choosing the securin/separase–ratio to position t_W into a region of fast securin decay (Eq. 7).

Numerical simulations: The numerical simulations in Fig. 3B, 5B and S3F were

performed using Eq. 1. The initial steady state was calculated by setting $k_{APC,Sec}$ = $k_{APC,SecSep}$ = 0. Anaphase was simulated by assuming a sigmoidal increase in APC activity, i.e., (10)

$$k_{APC}(t) \approx k_{APC,max} \cdot \frac{t^n}{t^n + {t_{50}}^n}$$

The following parameter values were assumed in Fig. 3B: total separase concentration Sep_{tot} = 0.05 μM; total securin concentration Sec_{tot} = 0.1 μM; $k_{APC,max}$ = 0.02 sec^{-1} (wt) or 0.0066 sec^{-1} (APC/C mut); k_{on} = 1 μM^{-1} sec^{-1}; k_{off} = 10^{-4} sec^{-1}; t_{50} = 100 sec; n = 10.

The following parameter values were assumed in Fig. 5B: total separase concentration Sep_{tot} = 0.05 μM; total securin concentration Sec_{tot} = 0.1 μM; $k_{APC,max}$ = 0.02 sec^{-1}; k_{on} = 0.01 μM^{-1} sec^{-1} (no rebinding), 1 μM^{-1} sec^{-1} (slow rebinding) or 100 μM^{-1} sec^{-1} (fast rebinding); k_{off} = 10^{-6} sec^{-1} (no rebinding), 10^{-4} sec^{-1} (slow rebinding) or 10^{-2} sec^{-1} (fast rebinding); t_{50} = 100 sec; n = 10.

The following parameter values were assumed in Fig. S3F: total separase concentration Sep_{tot} = 0.05 μM; total securin concentration Sec_{tot} = 0.1 μM; $k_{APC,max}$ = 0.02 sec^{-1} (wt) or 0.0066 sec^{-1} (APC/C mut); k_{on} = 100 μM^{-1} sec^{-1}; k_{off} = 10^{-2} sec^{-1}; t_{50} = 100 sec; n = 10.

2. Model with positive feedback on securin degradation

Model description: The model with feedback on securin degradation is depicted in Fig. 2D. Separase, once released from securin, accelerates the degradation of the securin pool. The differential equations describing this scenario are given by (11)

$$\frac{dSec}{dt} = -k_{on} \cdot Sec \cdot Sep + k_{off} \cdot SecSep - k_{APC} \cdot Sec \cdot (k_{basal} + k_{FB} \frac{Sep^h}{Sep^h + {K_{FB,50}}^h})$$

$$\frac{dSep}{dt} = -k_{on} \cdot Sec \cdot Sep + k_{off} \cdot SecSep + k_{APC} \cdot SecSep \cdot (k_{basal} + k_{FB} \frac{Sep^h}{Sep^h + {K_{FB,50}}^h})$$

$$\frac{dSecSep}{dt} = k_{on} \cdot Sec \cdot Sep - k_{off} \cdot SecSep - k_{APC} \cdot SecSep \cdot (k_{basal} + k_{FB} \frac{Sep^h}{Sep^h + {K_{FB,50}}^h})$$

The positive feedback was assumed to be non-linear and is described using the Hill equation. The APC activity is assumed to be zero in the basal state, implying that the basal concentrations of securin, separase and of the SecSep complex are the same as in Eq. 2.

Approximation for the time course behavior with positive feedback: The re-binding dynamics of securin and separase will be assumed to be slow, implying that separase is released in a gradual manner starting from t = 0 (Eqs. 3-5). Assuming a step-wise activation of the APC at t = 0, one derives for the total securin pool ($Sec_{tot}(t)$ = Sec(t) + SecSep(t)) and for the released amount of separase (12)

$$Sec_{tot}(t) \approx Sec_{tot}(0) \cdot e^{k_{APC,effective}t}$$

$$Sep(t) \approx Sep_{tot} \cdot \left(1 - e^{k_{APC,effective}t}\right)$$

For sufficiently nonlinear feedback (high exponent *h*), the feedback term is initially negligible (as long as $Sep(t) < K_{FB,50}$). The kinetics of securin degradation and separase release are thus determined by the following effective APC rate constant (13)

$$k_{APC,effective} \approx k_{APC} \cdot k_{basal}$$

Once the concentration of free separase reaches the threshold ($Sep(t) = K_{FB,50}$), the securin degradation and separase release kinetics will be dominated by the feedback term which is assumed to strongly exceed the basal contribution. Hence, we have (14)

$$k_{APC,effective} \approx k_{APC} \cdot k_{FB} \frac{Sep^h}{Sep^h + {K_{FB,50}}^h}$$

Thus, securin degradation and separase release show two temporal regimes, a slow feedback-less regime and a fast feedback-dominated regime. The transition point between these two regimes is determined by the threshold $K_{FB,50}$, and may be visible as a kink in the time course. Expressing a non-degradable securin mutant (Fig. 2F) blocks separase release, and should abolish the fast phase of securin degradation.

Numerical simulations: Numerical simulations were performed using the ODE system in Eq. 11. The initial steady state was calculated by setting $k_{APC,Sec} = k_{APC,SecSep} = 0$. Anaphase was simulated by assuming a sigmoidal increase in APC activity (Eq. 10). The following parameter values were assumed in Fig. 2E: total separase concentration Sep_{tot} = 0.05 μM; total securin concentration Sec_{tot} = 0.1 μM; k_{APC} = 0.02 sec^{-1}; k_{on} = 1 μM^{-1} sec^{-1}; k_{off} = 10^{-4} sec^{-1}; t_{50} = 100 sec; n = 10; k_{basal} = 1; k_{FB} = 10 (dotted lines) or k_{FB} = 0 (solid lines); $K_{FB,50}$ = 0.02 μM; h = 2.

3. Model with separase auto-amplification

Model description: The model with feedback amplification of separase activity is depicted in Fig. 3D. Free separase (Sep), once released from securin (Sec), performs auto-cleavage to generate a highly active separase species (Sep_{active}) which is more efficient in auto- and cohesin cleavage. The differential equations describing this scenario are given by (15)

$$\frac{dSec}{dt} = -k_{on} \cdot Sec \cdot Sep + k_{off} \cdot SecSep - k_{APC} \cdot Sec$$

$$\frac{dSep}{dt} = -k_{on} \cdot Sec \cdot Sep + k_{off} \cdot SecSep + k_{APC} \cdot SecSep - \left(k_{a,1} \cdot Sep^{h} + k_{a,2} \cdot {Sep_{active}}^{h}\right) \cdot Sep$$

$$\frac{dSecSep}{dt} = k_{on} \cdot Sec \cdot Sep - k_{off} \cdot SecSep - k_{APC} \cdot SecSep$$

$$\frac{dSep_{active}}{dt} = \left(k_{a,1} \cdot Sep^{h} + k_{a,2} \cdot {Sep_{active}}^{h}\right) \cdot Sep$$

Auto-cleavage occurs with an exponent h that prevents premature amplification and may arise from oligomerization of separase.

The APC activity (k_{APC}) and the irreversible cleavage reactions ($k_{a,1}$, $k_{a,2}$) are assumed to be zero in the basal state. Balancing of these slow irreversible reactions by securin and separase synthesis and degradation is thus not modeled explicitly. The basal concentrations of securin, separase and of the SecSep complex are therefore the same as in Eq. 2.

Numerical simulations: The ODE system in Eq. 15 was integrated numerically. The re-binding dynamics of securin and separase were assumed to be slow, implying that separase is released in a gradual manner (Eqs. 3-5). For nonlinear auto-cleavage (h>1), the auto-cleavage term is initially negligible, and free separase primarily accumulates as the less active form, Sep (Fig. S3B). As soon as Sep and Sep_{active} reach a critical value, there is rapid conversion of Sep into Sep_{active}. Efficient feedback amplification requires that almost all securin has been degraded by the APC before this critical value is reached (Fig. 3E), because otherwise the feedback is soon slowed down by the rate-limiting degradation step. In the former case, the kinetic profile of Sep to Sep_{active} conversion depends on the feedback auto-cleavage rate constants ($k_{a,1} >> k_{a,2}$), and is almost independent of the APC activity (compare grey and orange solid lines in Fig.

S3B). The separase activity towards cohesin (shown in Fig.. 3E) was assumed to be the same as the auto-cleavage activity, i.e., (16)

$$A = k_{a,1} \cdot Sep^h + k_{a,2} \cdot {Sep_{active}}^h$$

Anaphase was simulated by assuming a sigmoidal increase in APC activity (Eq. 10). The following parameter values were assumed in Fig. 3E and S3B: total separase concentration Sep_{tot} = 0.05 μM; total securin concentration Sec_{tot} = 0.1 μM; k_{APC} = 0.02 sec^{-1} (wt) or 0.0066 sec^{-1} (APC/C mut); k_{on} = 10^{-3} μM^{-1} sec^{-1}; k_{off} = 10^{-7} sec^{-1}; t_{50} = 100 sec; n = 10; $k_{a,1}$ = 0.1; $k_{a,2}$ = 300; h = 2.

4. Model with enzyme competition and preferential degradation

Model description: The model with enzyme competition is depicted in Fig. 5D. Free securin (Sec) and the securin-separase complex (SecSep) compete for binding to the APC. Biochemical evidence suggests that the APC/C is present at a lower concentration than securin in fission yeast (Kulak et al., 2014; Marguerat et al., 2012). Under these conditions, the APC may be sequestered in the enzyme-substrate complexes (SecAPC and SecSepAPC), which may give rise to switch-like behavior (see below).

The differential equations describing this scenario are given by (17)

$$\frac{dSec}{dt} = -k_{on,SecSep} \cdot Sec \cdot Sep + k_{off,SecSep} \cdot SecSep - k_{on,SecAPC} \cdot \alpha \cdot Sec \cdot (APC_{tot} - SecAPC - SecSepAPC) + k_{off,SecAPC} \cdot SecAPC$$

$$\frac{dSep}{dt} = -k_{on,SecSep} \cdot Sec \cdot Sep + k_{off,SecSep} \cdot SecSep + k_{cat,SecAPC} \cdot SecSepAPC$$

$$\frac{dSecSep}{dt} = k_{on,SecSep} \cdot Sec \cdot Sep - k_{off,SecSep} \cdot SecSep - k_{on,SecAPC} \cdot SecSep \cdot (APC_{tot} - SecAPC - SecSepAPC) + k_{off,SecAPC} \cdot SecSepAPC$$

$$\frac{dSecAPC}{dt} = k_{on,SecAPC} \cdot \alpha \cdot Sec \cdot (APC_{tot} - SecAPC - SecSepAPC) - (k_{off,SecAPC} + k_{cat,SecAPC}) \cdot SecAPC$$

$$\frac{dSecSepAPC}{dt} = k_{on,SecAPC} \cdot SecSep \cdot (APC_{tot} - SecAPC - SecSepAPC) - (k_{off,SecAPC} + k_{cat,SecAPC}) \cdot SecSepAPC$$

The free APC species was not described explicitly, and enters the differential equations only in the form of the mass conservation relation APC = APC_{tot} - SecAPC – SecSepAPC, where APC_{tot} is the total active APC/C concentration.

The same enzyme kinetic parameters ($k_{on,SecAPC}$, $k_{off,SecAPC}$, $k_{cat,SecAPC}$) were assumed for the APC-dependent ubiquitination of Sec and SecSep. The only difference between the two enzymatic processes is the preferential degradation factor α which enhances the binding of free securin to the APC relative to the SecSep complex.

Switch-like time course behavior with preferential degradation: Assuming that the binding and dissociation dynamics of the SecSep complex are slow, we can neglect the exchange between Sec and SecSep species, and model the enzymatic processes using a quasi-steady state assumption. For the initial rates of degradation one derives (18)

$$v_{Sec}(0) = k_{cat,Sec} APC_{tot} \frac{\frac{Sec(0)}{K_{M,Sec}}}{1+\frac{Sec(0)}{K_{M,Sec}}+\frac{SecSep(0)}{K_{M,SecSep}}}$$

$$v_{SecSep}(0) = k_{cat,Sec} APC_{tot} \frac{\frac{SecSep(0)}{K_{M,SecSep}}}{1+\frac{Sec(0)}{K_{M,Sec}}+\frac{SecSep(0)}{K_{M,SecSep}}}$$

These equations differ from the classical Michaelis-Menten formulation by an additional competition term in the denominator because both enzymatic reactions share the common APC enzyme. The Michaelis-Menten constants $K_{M,Sec} = (k_{off,SecAPC} + k_{cat,SecAPC}) / (\alpha \cdot k_{off,SecAPC})$ and $K_{M,SecSep} = (k_{off,SecAPC} + k_{cat,SecAPC}) / (k_{off,SecAPC})$ differ by the preferential degradation factor α.

For strong preferential degradation ($K_{M,Sec} << K_{M,SecSep}$), the APC is initially sequestered by degrading free securin, and not available for degradation of the SecSep complex, i.e., (19)

$$v_{Sec}(0) \approx k_{cat,Sec} APC_{tot} \frac{\frac{Sec(0)}{K_{M,Sec}}}{1+\frac{Sec(0)}{K_{M,Sec}}}$$

$$v_{SecSep}(0) \approx 0$$

Thus, the degradation of the SecSep complex and the release of separase will only start with a delay. We can solve for the waiting time t_W that it takes to initiate SecSep complex degradation by approximating the free securin degradation time course as $Sec(t) = Sec(0) - v_{Sec}(0) \cdot t$ and by setting Sec(t) = 0. Then, we obtain (20)

$$t_W = \frac{K_{M,Sec}}{k_{cat,Sec} APC_{tot}} \left(1 + \frac{Sec(0)}{K_{M,Sec}}\right)$$

As expected, the waiting time is longer for lower catalytic efficiencies ($k_{cat,Sec} \cdot APC_{tot}/K_{M,Sec}$) and if the APC is strongly saturated ($Sec(0) >> K_{M,Sec}$). After the waiting time, only complexed securin is left, and the APC switches from one substrate to another (21)

$$v_{Sec}(0) = 0$$

$$v_{SecSep}(0) = k_{cat,SecSep} APC \frac{\frac{SecSep(0)}{K_{M,SecSep}}}{1+\frac{SecSep(0)}{K_{M,SecSep}}}$$

We can neglect any rebinding of separase to securin because the free securin has previously been degraded. Therefore, free separase suddenly starts to accumulate efficiently after the waiting time.

Numerical simulations: The ODE system in Eq. 17 was integrated numerically to generate Fig. 5E and S3G. The initial steady state was calculated by setting $APC_{tot} = 0$. Anaphase was simulated by assuming a sigmoidal increase in the APC concentration, i.e., (22)

$$APC_{tot}(t) \approx APC_{tot,max} \cdot \frac{t^n}{t^n + {t_{50}}^n}$$

Due to mass conservation, it is implicitly assumed that newly generated APC initially exists in the free form. The re-binding dynamics of securin and separase were assumed to be slow.

The following parameter values were assumed in Fig. 5E: total separase concentration Sep_{tot} = 0.05 μM; total securin concentration Sec_{tot} = 0.1 μM; $APC_{tot,max}$ = 0.02 μM; k_{on} = 0.1 μM^{-1} sec^{-1}; $k_{off} = 10^{-3}$ sec^{-1}; t_{50} = 100 sec; n = 10; α = 1 (same k_{on}), α = 10 (10x k_{on}) or α = 100 (100x k_{on}).

The following parameter values were assumed in Fig. S3G: total separase concentration Sep_{tot} = 0.05 μM; total securin concentration Sec_{tot} = 0.1 μM; $APC_{tot,max}$ = 0.02 μM or $APC_{tot,max}$ = 0.0066 μM; k_{on} = 0.1 μM^{-1} sec^{-1}; $k_{off} = 10^{-3}$ sec^{-1}; t_{50} = 100 sec; n = 10; α = 10 (10x k_{on}).

Stochastic modeling of sister chromatid separation

1. Minimal stochastic model of cohesin cleavage

In order to account for the observed stochasticity and synchronicity of sister chromatid separation, we computationally modeled the loss of cohesin from two chromosomes using the Gillespie algorithm (Gillespie, 1977). The probability that a cohesin molecule on a chromosome is cleaved was assumed to depend on the amount of separase, the number of cohesin molecules on the chromosomes (Chr1 and Chr2) and on the reaction constant of the cohesin cleavage (k_{degr}). Accordingly, the total reaction rate is described by

(23) $\alpha_0 = kdegr * separase(t) * (Chr1(t) + Chr2(t))$

At each time point the waiting time (τ) until the next cleavage reaction takes place is calculated by

(24) $\tau = \frac{1}{\alpha_0} * \ln\left(\frac{1}{rand(0,1)}\right)$

The probability that this reaction is a cleavage of a cohesin molecule on chromosome I or II are given by

(25) $p(Chr1) = \frac{Chr1(t)}{Chr1(t)+Chr2(t)}$ and $p(Chr2) = \frac{Chr2(t)}{Chr1(t)+Chr2(t)}$, respectively

Equations 23-25 were applied repeatedly until all cohesin links on both chromosomes were cleaved. The starting number of cohesin complexes on each chromosome was assumed to be 1000 unless stated differently. This is an estimate based on several mass spectrometric studies (Carpy et al., 2014; Kulak et al., 2014; Marguerat et al., 2012). The reaction constant was assumed to be k_{degr}=0.0012 molecules^{-2}*seconds^{-1} to obtain simulation results comparable to experiments. The cohesin threshold (the number of cohesin molecules that are allowed to remain on a chromosome for sister chromatid separation to occur) was set to zero, unless stated differently.

The amount of free separase at a given time point (separase(t)) was provided to the model either in the form of a logistic function in the simplified case or as the solution of the deterministic simulation of the upstream processes. This hybrid implementation allowed us to probe the impact of altered separase release kinetics on the variance in

the time of sister chromatid separation.

Hybrid modeling approaches require that the stochastic subsystem (Eqs. 23-25) is updated sufficiently often to ensure that the deterministic input does not increase strongly during the waiting time τ. We ensured frequent updating by including a fast auxiliary reaction in the stochastic system. This auxiliary reaction did not affect cohesin cleavage and was set to occur before a change in separase(t) has a significant impact on the total reaction rate (Eq. 23). We confirmed the validity of our hybrid modeling approach by comparing the hybrid simulation results with those of a full stochastic model that incorporates securin degradation, separase release and cohesin cleavage (not shown).

We assumed that sister chromatid separation of each individual chromosome occurs when a defined threshold of cohesin molecules had been reached and then calculated the time difference between separation of the two chromosomes. We noticed that the initial model (defined in Eqs. 23-25) exhibited very little variation in the time difference of sister chromatid separation between different chromosomes. One underlying assumption of our initial model (Eq. 23-25) was that separase rapidly diffuses from one chromosome to the other. Thus, any variance created during the early steps of cohesin cleavage, when separase abundance is low, is efficiently buffered because separase efficiently re-samples both chromosomes in later cohesin cleavage steps. Through this mechanism, the cohesin amounts on the two chromosomes during the time course are kept highly similar. In order to yield a variance comparable to experiments, we would need to assume that cleavage of few cohesin links was sufficient for sister chromatid separation, or that sister chromatid separation required cleavage of virtually all cohesin links (Fig. S2D). The former scenario seemed unlikely because a sizable fraction of cohesin may need to be cleaved before chromosome segregation can occur (Shindo et al., 2012; Yaakov et al., 2012) On the other hand, a requirement for enzymatic removal of all cohesin links seems unlikely as well, considering that strong spindle pulling forces act on the kinetochore of sister chromatids and that phenotypes of cohesin loss are readily observed with cohesin mutants or cohesin regulators, even though it is unlikely that the entire protein pool has become inactive (Feytout et al., 2011; Kawashima et al., 2007) .

2. Separase-DNA association model of stochastic cohesin cleavage

To overcome the above-mentioned limitations, we altered the model by assuming that free separase stochastically associates with one of the chromosomes (the rate of association is k_{assoc}=0.005 molecules*s^{-1}) and only the chromosome-associated pool of separase is allowed to cleave cohesin specific to this chromosome (k_{degr}=0.005 $molecules^{-2}$*s^{-1}). For simplicity, we neglect dissociation of separase from the chromosome that it has first associated with. We therefore assume that separase processively acts on many cohesin links on a chromosome and that separase remains associated with a chromosome by virtue of its DNA binding properties (Sun et al., 2009).

In this model, the amount of free nucleoplasmic separase(t) that is not associated with one of the chromosomes was described using a mass conservation relation: separase(t) equals the total pool of active enzyme $separase_{tot}$(t), given by the deterministic input, minus the chromosome-associated pools of separase ($separase_{Chr1}$(t) and $separase_{Chr2}$(t))

(26) $separase(t) = separase_{tot}(t) - separase_{Chr1}(t) - separase_{Chr2}(t)$

The reaction rate for association of separase with the two chromosomes was

(27) $\alpha_1 = k_{assoc} * separase(t)$

and the reaction rates for the cohesin cleavage on each of the chromosomes were calculated by

(28) $\alpha_2 = k_{degr} * separase_{Chr1}(t) * Chr1(t)$ and $\alpha_3 = k_{degr} * separase_{Chr2}(t) * Chr2(t)$

Accordingly, the total reaction rate and the waiting time (τ) until the next reaction are described by

(29) $\alpha_0 = 2 * \alpha_1 + \alpha_2 + \alpha_3$

(30) $\tau = \frac{1}{\alpha_0} * \ln\left(\frac{1}{rand(0,1)}\right)$

and the probability for the individual reactions occurring after this waiting times are calculated by

(31) $p(separase_{Chr1}) = \frac{a_1}{a_0}$ and $p(separase_{Chr2}) = \frac{a_1}{a_0}$ for the association of a separase molecule to one of the chromosomes, and

(32) $p(Chr1) = \frac{a_2}{a_0}$ and $p(Chr2) = \frac{a_3}{a_0}$, for the cleavage of cohesin on chromosome I or II, respectively.

Equations 26-32 were employed to generate all simulations shown in the main figures using the hybrid modeling approach described above. The cohesin threshold was set to 25 in all simulations, unless stated differently.

The separase-DNA association model resulted in a larger variance in the time difference of sister chromatid separation between two chromosomes (more asynchronous sister separation), which was more robust against the chosen cohesin threshold at which sister chromatid separation occurred (Supplementary Figure S2 D, H). Interestingly, because in this model initial variability in separase association with one of the chromosomes is only slowly compensated by the increasing amounts of separase on both chromosomes, the variance now not only depends on the amount of separase at the cohesin threshold but also on the kinetics of separase release at earlier time points (Fig. S2I). To simulate the system's behavior in a separase mutant with lower separase activity (Fig. 1F), k_{degr} was reduced to 0.0015 molecules^{-2}*s^{-1}.

Logistic functions were calculated by

(33) $f(x) = \frac{300}{1+e^{-k(x-x_0)}}$

and used as a simplified model for the separase release kinetics in Figure 1F and 4D and Supplementary Figure S2. The following parameters were used:

- Figure 1F: x_0=120, k=0.1,
- Figure 4D: x_0=220 and k=0.1,k=0.04 or k=0.025
- Figure S2F-H. x_0=220, k=0.04
- Figure S2I: x_0=220, k=0.1 (blue curve), x_0=280, k=0.04 (maroon curve), or x_0=360, k=0.025 (green curve)

Supplemental References

Carpy, A., K. Krug, S. Graf, A. Koch, S. Popic, S. Hauf, and B. Macek. 2014. Absolute proteome and phosphoproteome dynamics during the cell cycle of Schizosaccharomyces pombe (Fission Yeast). *Molecular & cellular proteomics : MCP*. 13:1925-1936.

Feytout, A., S. Vaur, S. Genier, S. Vazquez, and J.P. Javerzat. 2011. Psm3 acetylation on conserved lysine residues is dispensable for viability in fission yeast but contributes to Eso1-mediated sister chromatid cohesion by antagonizing Wpl1. *Molecular and cellular biology*. 31:1771-1786.

Gillespie, D.T. 1977. Exact stochastic simulation of coupled chemical reactions. *The Journal of Physical Chemistry*. 81:2340-2361.

Hellmuth, S., F. Bottger, C. Pan, M. Mann, and O. Stemmann. 2014. PP2A delays APC/C-dependent degradation of separase-associated but not free securin. *The EMBO journal*. 33:1134-1147.

Kamenz, J., and S. Hauf. 2014. Slow checkpoint activation kinetics as a safety device in anaphase. *Current biology : CB*. 24:646-651.

Kawashima, S.A., T. Tsukahara, M. Langegger, S. Hauf, T.S. Kitajima, and Y. Watanabe. 2007. Shugoshin enables tension-generating attachment of kinetochores by loading Aurora to centromeres. *Genes & development*. 21:420-435.

Kulak, N.A., G. Pichler, I. Paron, N. Nagaraj, and M. Mann. 2014. Minimal, encapsulated proteomic-sample processing applied to copy-number estimation in eukaryotic cells. *Nature methods*. 11:319-324.

Marguerat, S., A. Schmidt, S. Codlin, W. Chen, R. Aebersold, and J. Bahler. 2012. Quantitative analysis of fission yeast transcriptomes and proteomes in proliferating and quiescent cells. *Cell*. 151:671-683.

Shindo, N., K. Kumada, and T. Hirota. 2012. Separase sensor reveals dual roles for separase coordinating cohesin cleavage and cdk1 inhibition. *Developmental cell*. 23:112-123.

Sun, Y., M. Kucej, H.Y. Fan, H. Yu, Q.Y. Sun, and H. Zou. 2009. Separase is recruited to mitotic chromosomes to dissolve sister chromatid cohesion in a DNA-dependent manner. *Cell*. 137:123-132.

Yaakov, G., K. Thorn, and D.O. Morgan. 2012. Separase biosensor reveals that cohesin cleavage timing depends on phosphatase PP2A(Cdc55) regulation. *Developmental cell*. 23:124-136.

2.2 Properties of the degradation machinery ensure temporal coupling during anaphase

Julia Kamenz[1,2,3], Tamara Mihaljev[4], Armin Kubis[1], Stefan Legewie[4,*], Silke Hauf[1,2,3,*]

[1]*Friedrich Miescher Laboratory of the Max Planck Society, Tuebingen, Germany*

[2]*Department of Biological Sciences and* [3]*Virginia Bioinformatics Institute, Virginia Tech, Blacksburg, VA, United States*

[4]*Institute of Molecular Biology (IMB), Mainz, Germany*

*Correspondence: silke@vt.edu, s.legewie@imb-mainz.de

To be submitted as manuscript to **Molecular Cell**

Author contributions:

I designed, performed and analysed all experiments with the exception of Figures 1E, 1G, 4D, 4E and S2E (lower panel), which were performed by **Armin Kubis**. In addition, I contributed to writing the manuscript together with Silke Hauf and Stefan Legewie.

Tamara Mihaljev developed imaging analysis software and together with **Stefan Legewie** performed the computational modelling and analyses.

Silke Hauf conceived and supervised the study.

Properties of the degradation machinery ensure temporal coupling during anaphase

Julia Kamenz[1,2,3], Tamara Mihaljev[4], Armin Kubis[1], Stefan Legewie[4,*], Silke Hauf[1,2,3,*]

[1]*Friedrich Miescher Laboratory of the Max Planck Society, Tuebingen, Germany*

[2]*Department of Biological Sciences and* [3]*Virginia Bioinformatics Institute, Virginia Tech, Blacksburg, VA, United States*

[4]*Institute of Molecular Biology (IMB), Mainz, Germany*

*Correspondence: silke@vt.edu, S.Legewie@imb-mainz.de

Running head: Temporal coordination of anaphase

Summary

The splitting of chromosomes in anaphase and their distribution to the two daughter cells is a critical event in the cell cycle that needs to be faithfully completed to maintain genome stability. Chromosome splitting requires the degradation of securin, but proper distribution of the split chromosomes to the daughter cells requires the degradation of cyclin B. How robust temporal coordination can be achieved by parallel securin and cyclin B degradation without explicit crosstalk between the two pathways is unclear. Here, we show that competition of cyclin B and securin for a shared degradation machinery helps, but is not sufficient, to buffer variation in their levels. In addition, the threshold of securin at which sister chromatid separation occurs is flexible and scales with securin degradation rate. Such threshold shifts can provide a second mechanism enforcing temporal robustness. Our work reveals simple, universal mechanisms that ensure coordination of highly dynamic parallel pathways without requiring direct crosstalk.

Highlights

- Variations in the securin to cyclin B ratio occur physiologically and are tolerated
- Securin and cyclin B compete for APC/C-mediated degradation in anaphase
- The securin threshold for sister chromatid separation is flexible
- Both mechanisms can contribute to robust temporal coupling

Introduction

As our knowledge of the molecules participating in cellular signalling pathways becomes more complete, the challenge shifts towards understanding the principles that allow groups of molecules to regulate cellular processes. These networks do not only need to produce a certain outcome, but need to produce it in a timely fashion. Here, we focus on a window of a few minutes in dividing cells, during which chromosomes split and become distributed into the emerging daughter cells (Nasmyth et al., 2000; Sullivan and Morgan, 2007).

The splitting of chromosomes is an abrupt irreversible event that needs to run to faithful completion (one set of chromosomes in each daughter cell) in order to preserve the genome for subsequent generations. While the splitting of chromosomes is regulated by degradation of the protein securin, many other events in mitotic exit, which need to be coordinated in time with chromosome splitting, depend on the degradation of cyclin B (Peters, 2006). The degradation of both securin and cyclin B is initiated when they are ubiquitinylated by the anaphase-promoting complex/cyclosome (APC/C (Chang and Barford, 2014; Pines, 2011; Primorac and Musacchio, 2013)) and are thereby targeted to the proteasome for degradation (Figure 1A). Degradation of securin releases separase, a protease that separates the chromosome halves by cleaving the cohesin complex that holds sister chromatids together (Uhlmann et al., 2000; Waizenegger et al., 2000). Cyclin B is the activating subunit of CDK1 (cyclin-dependent kinase 1) and its degradation lowers CDK1 activity, which is necessary for conversion back to the interphasic state ('mitotic exit') (Ghiara et al., 1991; Murray et al., 1989). Some of the events during mitotic exit are directly relevant to sister chromatid separation: degradation of cyclin B is needed to stabilize kinetochore-microtubule attachments, so that sister chromatids do not fall off the microtubule ends once sister chromatids have split (Higuchi and Uhlmann, 2005; Oliveira et al., 2010; Parry et al., 2003; Parry and O'Farrell, 2001; Vazquez-Novelle et al., 2014). Degradation of cyclin B is also needed to inactivate the spindle assembly checkpoint which - if not inactivated - can abnormally halt cell cycle progression in response to sister chromatid splitting (Clijsters et al., 2014; Kamenz and

Hauf, 2014; Rattani et al., 2014; Vazquez-Novelle et al., 2014). Both events, stabilization of kinetochore microtubules and inactivation of the checkpoint, need to happen before or around the time of sister chromatid splitting. In addition, degradation of cyclin B is needed for spindle elongation and eventually for spindle breakdown, decondensation of chromosomes, nuclear envelope reformation and cytokinesis (Sullivan and Morgan, 2007; Zachariae and Nasmyth, 1999). These events need to happen concomitantly with or well after sister chromatid splitting. Hence, cyclin B degradation starts a series of events, which need to be timed with respect to chromosome splitting so that segregation can be completed faithfully. Since the APC/C initiates degradation of securin and cyclin B at the same time (Hagting et al., 2002; Homer et al., 2005; van Zon et al., 2010), some level of coordination is ensured. Here, we ask whether this simple mechanism is sufficient.

It is generally assumed, and supported by experimental evidence (Bouchoux and Uhlmann, 2011; Hellmuth et al., 2014; Shindo et al., 2012; Wolf et al., 2006), that sister chromatid separation and mitotic exit events occur at certain threshold levels of securin and cyclin B. In such a scenario, the timing of events is expected to be sensitive to the abundance of securin and cyclin B. If the level of only one protein changes, the relative timing between sister chromatid separation and mitotic exit events should be perturbed. The levels of securin and cyclin B will never be entirely constant because of intrinsic cellular ‘noise’, i.e. protein abundance fluctuations that result from the stochasticity of transcription (Raj and van Oudenaarden, 2008). Small fluctuations may only result in slight temporal shifts, which could be tolerated. However, we show here that the securin to cyclin B ratio can change substantially in situations of DNA damage. How temporal coordination of securin and cyclin B dependent events can be maintained in such a situation is unclear.

Some organisms have evolved crosstalk between the two degradation pathways. In budding yeast, separase, once released from securin, activates the CDK1-counteracting phosphatase Cdc14 and thereby helps to lower CDK1-dependent phosphorylations (Queralt et al., 2006; Stegmeier et al., 2002; Sullivan and Uhlmann, 2003). In addition, the chromosome separation

event itself supports mitotic exit (Lu and Cross, 2009). In vertebrate cells, cyclin B/CDK1 can bind to separase that has lost securin (Gorr et al., 2005; Stemmann et al., 2001). Once bound, cyclin B/CDK1 and separase mutually inhibit each other (Gorr et al., 2005; Holland et al., 2007). This seems to serve two functions: (i) if securin levels have decreased, but cyclin B levels are still high, or if securin is entirely absent, cyclin B can block separase activity (Hagting et al., 2002; Herbert et al., 2003; Madgwick et al., 2004) and (ii) once separase is released from securin its binding to cyclin B/CDK1 may locally lower CDK1 activity at kinetochores and ensure the complete separation of sister chromatids (Shindo et al., 2012). Although elegant, such cross-talk between securin and cyclin B-dependent processes does not seem very strong and not universal. In budding yeast, the expression of non-degradable securin indeed blocks both sister chromatid separation and mitotic exit (Cohen-Fix and Koshland, 1999; Cohen-Fix et al., 1996; Queralt et al., 2006) and overexpression of separase can drive mitotic exit (Tinker-Kulberg and Morgan, 1999; Visintin et al., 1998). However, in human cells, Drosophila, and fission yeast expression of non-degradable securin (Funabiki et al., 1996; Hagting et al., 2002; Leismann and Lehner, 2003; Zur and Brandeis, 2001) or inactive separase (Hirano et al., 1986; Siomos et al., 2001; Wirth et al., 2006) only blocks sister chromatid separation, but not mitotic exit (leading to cell death because cell division randomly cleaves the DNA). Similarly, expression of non-degradable cyclin B in budding yeast, flies, human cells or fission yeast prevents mitotic exit, but chromosomes still split (Rimmington et al., 1994; Sigrist et al., 1995; Surana et al., 1993; Wolf et al., 2006; Yamano et al., 1996). How the timing of sister chromatid separation and mitotic exit events can be tightly coordinated without strong, direct crosstalk and despite possible changes in the securin to cyclin B ratio is unclear.

Results

Changes in the cyclin B to securin ratio are well tolerated

The APC/C initiates the degradation of securin and cyclin B at the same time ((Hagting et al., 2002; Homer et al., 2005; van Zon et al., 2010), Figure 1A). Parallel degradation could be sufficient for a constant temporal order between sister chromatid separation and mitotic exit events if the abundances of securin and cyclin B were fairly stable or coregulated. We therefore determined the abundance of securin and cyclin B in fission yeast and asked how well these levels are maintained under different conditions. By quantitative immunoblotting of cells from an asynchronous culture, securin (Cut2) had a cellular concentration of about 19 nM, whereas the concentration of cyclin B (Cdc13) was around 188 nM (Figure 1B, Supplementary Figure 1A,B). Hence, fission yeast cyclin B is about ten-times more abundant than securin, which is corroborated by quantitative mass spectrometry measurements, which found *S. pombe* cyclin B to securin ratios between 4.7 and 7.4 to 1 (Carpy et al., 2014; Kulak et al., 2014; Marguerat et al., 2012).

We next asked whether the ratio of securin and cyclin B was stable. When synchronizing cells by temporary arrest just prior to mitosis (using the temperature sensitive *cdc25-22* mutation, (Russell and Nurse, 1986)) we noted that the abundance of cyclin B in arrested cells and in the first mitosis after release was higher than during the subsequent mitosis, which was not the case for securin (Figure 1C, Supplementary Figure 1 C and D; also observed by (Booher et al., 1989)). This suggested that the ratio between cyclin B and securin was not stably maintained under all conditions. The effect was not restricted to the *cdc25-22* mutant strain. We observed a similar – about two- to three-fold – increase in cyclin B, but not securin, when we induced cell cycle arrest by the DNA-damaging agent bleomycin (Figure 1C, Supplementary Figure 1 C and D). Importantly, the increase in the cyclin B to securin ratio does not seem to affect cell division: cells undergoing mitosis after release from a *cdc25-22* arrest (with excess amounts of cyclin B) do not

show any obvious mitotic defects and many laboratories have used this synchronization protocol to study mitosis. This suggests that variations in the cyclin B to securin ratio do occur and are well tolerated.

To systematically explore the tolerance towards variations in securin and cyclin B levels, we placed exogenous promoters 5' of the open reading frame of *cut2+* and *cdc13+* and raised the level of securin to about 4- and 8-times the wild type amount (Figure 1D) and the level of cyclin B to about 20-times the wild type amount (Figure 1E). None of the strains showed any obvious growth defects (Figure 1F and G). Since the abundance of the respective other protein (cyclin B or securin) was not changed (Figure 1D and E), this confirms that considerable variations in the cyclin B to securin ratio are tolerated. Experiments using overexpression from multi-copy plasmids also concluded that fission yeast securin can be increased by at least 30-times and cyclin B by at least 5-times, before any detrimental effects occur (Moriya et al., 2011).

Sister chromatid separation and mitotic exit occur independently in *S. pombe*

Crosstalk between securin and cyclin B degradation-dependent events is thought to be absent in fission yeast. Expression of a non-degradable version of cyclin B (ΔN-Cdc13) prevents mitotic exit, but sister chromatids separate (Yamano et al., 1996), whereas expression of non-degradable securin (ΔN-Cut2) blocks sister chromatid separation, but cells exit mitosis (Funabiki et al., 1996). Such lack of crosstalk should make the system susceptible to variations in the cyclin B to securin ratio. We therefore wondered whether the expression of the non-degradable versions of securin or cyclin B could delay (albeit not prevent) events in the other pathway, which would have been missed by the end-point assays that were originally used. We therefore reanalyzed these situations by live cell imaging in single cells. We used the kinetochore protein Mis12 fused to GFP as a marker for sister chromatid separation and the Polo kinase Plo1 fused to mCherry as a marker for CDK1 activity. Plo1 binds to spindle pole bodies (SPBs) in a CDK1-dependent manner and is removed from SPBs as cells exit mitosis (Dischinger et al., 2008; Mulvihill et al., 1999). Hence, Plo1 removal from SPBs functions as a readout for cyclin B-degradation dependent

events.

As expected, mitotic exit was blocked by non-degradable cyclin B and the localization of Plo1 to SPBs persisted for more than 20 min (and often more than one hour) (Kamenz and Hauf, 2014). In contrast, there was only a slight delay in when sister chromatid separation happened with respect to entry into mitosis (Figure 2A and B). When we expressed non-degradable securin, chromosomes failed to split (Figure 2A). However, Plo1 was removed from SPBs with similar timing as in wild type cells (Figure 2C). Together, this implies that securin and cyclin B degradation-dependent processes occur largely independently and exacerbates the question how increases in securin or cyclin B can be so well tolerated (Figure 1F and G).

Increases in either securin or cyclin B abundance delay both securin and cyclin B degradation-dependent events

We could imagine two scenarios why increases in securin or cyclin B are tolerated: either the timing of events does in fact not need to be closely coupled, or timing is coupled through mechanisms other than direct crosstalk. To distinguish between these two possibilities, we monitored sister chromatid separation and removal of Plo1 from SPBs by live cell imaging in cells with increased amounts of cyclin B or securin. Having 20-times the amount of cyclin B delayed the removal of Plo1, as we had expected given the dependence of Plo1 localization on CDK1 activity. However, sister chromatid separation (which depends on securin degradation, not on cyclin B degradation) was delayed as well (Figure 3A and B). The delay was almost entirely maintained when the spindle assembly checkpoint was inactivated, and hence is unlikely to be the result of an extended prometaphase (Supplementary Figure S3A). The same effect was observed in strains with higher than normal amounts of securin: not only sister chromatid separation, but also Plo1 removal from SPBs was delayed (Figure 3D and E). The delay time of both events was similar, so that the time between sister chromatid separation and Plo1 removal from SPBs stayed remarkably constant, both in cells with more cyclin B and in cells with more securin (Figure 3C and F). Hence, although we had only increased the amount of one protein,

both pathways seemed affected. The coordinated timing can also be observed in single cells of the same genotype: cells with delayed sister chromatid separation tend to show a delayed removal of Plo1 from SPBs (Figure 3G and H). This variation within a single population could be caused by variable levels ('noise') of securin and cyclin B, which we assume would be buffered in a similar way as in cells with a larger excess of securin or cyclin B. It was important to exclude that the concomitant delays are a consequence of a delay in APC/C activation (which would delay both securin- and cyclin B-degradation-dependent events). Ideally, one would like to measure the time from the onset of APC/C activity to sister chromatid separation and Plo1 removal. For technical reasons, this was only feasible in cells with 4-times and 8-times the amount of securin (see Material and Methods). Corroborating our earlier results, we observed that the excess of securin delayed not only sister chromatid separation but also Plo1 removal with respect to the onset of APC/C activity (Figure 3I, Supplementary Figure 3B – D).

Competition for the degradation machinery can partially explain temporal coordination

These data raised the question why we did not see any obvious delay of sister chromatid separation in cells with non-degradable cyclin B (Figure 2B), whereas an excess amount of cyclin B delayed sister chromatid separation (Figure 3B), or – similarly – why non-degradable securin did not obviously delay Plo1 removal (Figure 2C) although the overexpression of securin does (Figure 3E). The difference between these situations is the type of cyclin B or securin that we express. The non-degradable versions lack the N-terminus containing the degradation signal (D-box). This region is important to target these proteins to the APC/C activator Slp1 (Cdc20 or Fizzy/Fzy in other organisms) (Pfleger et al., 2001; Tian et al., 2012) and both proteins are strongly expected to bind to the same site on Slp1 (Tian et al., 2012). We therefore surmised that additional copies of full length securin or cyclin B have the potential to compete for binding sites on Slp1, whereas non-degradable versions would be inert with respect to the degradation machinery. Because additional copies of cyclin B would not only compete with other cyclin B but also with securin molecules, overproduction of one protein (cyclin B or securin) has the potential

to slow down ubiquitinylation and therefore degradation of the other (Figure 4A). Such 'queuing' for the same degradation machinery has been shown to have the capacity to couple otherwise unrelated pathways (Cookson et al., 2011; Prindle et al., 2014).

Theoretically, competition could happen at three levels: (i) binding of securin and cyclin B to Slp1 or Slp1/APC/C, (ii) binding of the Slp1/securin and Slp1/cyclin B complexes to the APC/C, or (iii) binding of ubiquitinylated securin and cyclin B to the proteasome. We increased the amount of proteasome in the nucleus and did not observe faster securin degradation (Supplementary Figure 4E - J). Hence, we suspect that under normal conditions Slp1 or APC/C are more likely to be limiting. We created a computational model to ask in which concentration regime competition can be observed and for simplicity lumped Slp1 and APC/C binding into a single step (APC/C binding, Figure 4A). We initially assumed a similar affinity of cyclin B and securin for APC/C, and observed competition for realistic protein concentrations and parameter values (Figure 4B). We then asked in which range the concentration of the APC/C needs to be in order to observe competition effects with 8-times the wild type amount of securin or 20-times the wild type amount of cyclin B (Figure 4C). When APC/C concentrations are above 1 μM the effects are minimal, but they become strong at APC/C concentrations below 200 nM. We previously measured Slp1 and APC/C concentrations in the range of 10 to 50 nM (Heinrich et al., 2013), and, hence, competition is conceivable in vivo. To experimentally test this, we followed securin degradation in single cells with 20-times the amount of cyclin B. Indeed, securin degradation was considerably slowed down (Figure 4D). Concomitantly, sister chromatid separation was delayed (Figure 4D and E), as we had seen before (Figure 3B). We have been unable to perform the reverse experiment for securin-overexpressing cells, because - unlike for securin - putting fluorescent protein tags onto cyclin B interferes with the protein function (Supplementary Figure S2).

We conclude that competition for the same degradation machinery can - at least partly (see below) - buffer the effect of variations in the securin to cyclin B ratio. Interestingly, in mouse oocytes in prophase of meiosis I an excess of securin causes cyclin B to become stabilized,

which leads to an earlier entry into M-phase, whereas depletion of securin increases cyclin B degradation and delays entry into M-phase, demonstrating a similar competition effect (Marangos and Carroll, 2008). Hence, competition between securin and cyclin B for APC/C-mediated degradation seems universal.

We employed securin degradation measurements in wild type, cyclin B overexpression (Figure 4D) and securin overexpression conditions (Figure 5A) to quantitatively calibrate our model. We estimated kinetic parameters by fitting the model to changes in the securin degradation slope and to the time it took to deplete the securin pool to 10 % of its initial value (t_{10}). With an equal affinity of securin and cyclin B to the APC/C (as we had initially assumed), securin degradation (t_{10}) in cells with 20-times the amount of wild type cyclin B took much longer than observed experimentally (Supplementary Figure S4A). In order to fit the data, the APC/C needed to have a lower affinity (i.e., a higher K_M-value) for cyclin B than for securin (Supplementary Figure S4B, C). Based on these fitting results, we predicted that 8-fold overexpression of securin does not greatly affect the slope of cyclin B degradation (Supplementary Figure S4D). This model prediction is supported by immunoblotting cell extracts from a highly synchronized culture, which shows that the cyclin B degradation dynamics are not strongly altered by 8x securin overexpression (Supplementary Figure S4E-G). Taken together, our data suggest that securin and cyclin B compete for a limiting pool of Slp1 or the APC/C.

Competition for the degradation machinery is not sufficient for temporal coordination if events happen at fixed thresholds

Sister chromatid separation and cyclin B degradation-dependent events are thought to happen when defined threshold concentrations of securin and cyclin B are reached in the degradation process: In human cells, securin is initially in excess over separase and sister chromatid separation occurs when the excess pool of securin has been largely degraded and separase starts to be released (Hellmuth et al., 2014). In other words, the amount of separase sets a threshold under which securin needs to drop to allow sister chromatid separation. Similar

thresholds exist for cyclin B-degradation dependent events: different levels of cyclin B block mitotic exit at different stages (Parry and O'Farrell, 2001; Sigrist et al., 1995; Wolf et al., 2006) and in budding yeast certain CDK1 substrates are dephosphorylated at different thresholds of the CDK1 kinase to Cdc14 phosphatase ratio (Bouchoux and Uhlmann, 2011). Despite this evidence, if we assume in our best-fit competition model that downstream events happen at fixed threshold concentrations of cyclin B and securin, we do not observe temporal coordination of sister chromatid separation and Plo1 removal (Figure 4F and G, Supplementary Note). Instead, the model predicts that the time difference between sister chromatid separation and Plo1 removal shortens, and even reverses, as securin increases, whereas the time difference becomes overly large when cyclin B increases (Figure 4H), which is in contrast to our observations (Figure 3). We excluded that this result is specific to the best-fit parameter values by testing other parameter combinations that quantitatively describe the securin degradation kinetics (not shown). In addition, re-calibrating the model under the assumption of fixed thresholds failed to find solutions that describe the temporal invariance and securin degradation dynamics that we observed (not shown).

The securin threshold for sister chromatid separation is variable

Since fixed thresholds can apparently not explain the relatively constant time difference between sister chromatid separation and Plo1 removal from SPBs, we asked whether the assumption of a fixed threshold is appropriate. In fission yeast wild type cells, sister chromatid separation occurs when around 25 to 30 % of nuclear securin has been degraded ((Kamenz and Hauf, 2014), Figure 5A, G and H). When we increased the abundance of securin to 4-times or 8-times its wild type level, the amount of separase stayed constant (Supplementary Figure S5A). Yet, as securin levels increased, sister chromatid separation occurred at higher securin levels (Figure 5A). In fact, cells with 4- or 8-times the normal amount of securin separated sister chromatids at securin levels that were higher than the securin level that reliably blocks sister chromatid separation in wild type cells (Figure 5A). The correlation between securin abundance and the securin level at sister

chromatid separation, was also observed within the population of wild type cells (Figure 5B). Because securin retains separase in the nucleus (Hornig et al., 2002; Marangos and Carroll, 2008), a potential reason for this result could have been that cells with more securin accumulate more separase in the nucleus. If this was the case, one could have imagined that separase would now start to be released at higher securin levels than in the wild type. We therefore used quantitative fluorescence microscopy to determine the relative amount of securin and separase in the nucleus, using GFP-fusions at the endogenous locus (Figure 5D and E). In otherwise wild type cells, the securin to separase ratio was around 2:1 (Figure 5F). The nuclear abundance of separase increased only slightly in cells with 8-times the endogenous amount of securin (Figure 5D and E) – not enough to explain the substantially higher securin level, at which sister chromatids separate. Together, these results suggested that the securin level at which sister chromatid separation happens is not simply determined by the amount of separase. The securin to separase ratio of about 2 in wild type cells supports this notion: if it was necessary to degrade the excess amount of securin, we would predict that 50 % of securin needs to be degraded for anaphase to occur, whereas the actual amount that needs to be degraded is in the order of 25 - 30 % ((Kamenz and Hauf, 2014), Figure 5A and H). The notion that the threshold is not stable was further corroborated by experiments that slowed down securin degradation, either by cyclin B competition (Figure 4D), or by APC/C inhibition (Figure 5G and H, Supplementary Figure 5G and H), or by proteasome inhibition (Supplementary Figure S5K and L). In all these cases, more securin needed to be degraded before sister chromatid separation occurred, opposite to the effect in securin overexpression.

Securin thresholds closely follow a scaling rule

Because, we had initially found that fixed thresholds cannot explain our observations (Figure 4F - H) and we now indeed observed a variable threshold (Figure 5A and G), we went back to modeling to understand which rules the threshold shifts needed to obey to ensure temporal coordination when the system is perturbed (Supplementary Note). It can be shown analytically

that elegant solutions of global temporal invariance exist if the securin and cyclin B thresholds are proportional to certain features of the securin and cyclin B degradation dynamics. In particular, the thresholds should either scale with the initial concentrations of securin and cyclin B or with the initial slope of degradation for securin and cyclin B (Supplementary Note). In our measurements, we observed a correlation between the securin degradation rate and the amount of securin at sister chromatid separation, both on the population level (Figure 5I) and in single cells (Figure 5C). (Note that the absolute degradation rate increases when securin is overexpressed. Supplementary Figure 5C and D). Remarkably, the relationship is close to the linear dependency between threshold and degradation slope that is predicted by the scaling rule. In addition to the scaling rule, temporal invariance required that cyclin B and securin degradation run to completion within a comparable time frame, i.e. the catalytic efficiency of the APC/C towards the two substrates needed to be similar (Figure 5J and Supplementary Note). This is consistent with the requirements that we had determined when fitting the competition model to our experimental data (Supplementary Fig. S4C).

Since we can not yet follow cyclin B degradation in single cells and therefore cannot directly observe any potential threshold shifts, we asked which threshold shifts would be expected for an invariant timing. To this end, we extended the competition model, and assumed sister chromatid separation to happen at the experimentally measured threshold levels, while Plo1 removal was presumed to occur three minutes later, as we had observed (Fig. 3C and F). Similar to the threshold shifts for securin, we would predict that the threshold for cyclin B degradation-dependent events needs to move up if cyclin B abundance is increased and down if cyclin B degradation is slowed down (Figure 5K). This further supports that competition of securin and cyclin B for degradation, combined with systematic threshold shifts, can quantitatively account for temporal invariance.

Unbalancing the degradation kinetics of securin and cyclin B disturbs temporal order

Our findings suggested that competition for the degradation machinery, together with flexible

thresholds, can provide robustness in the order of anaphase events against protein abundance changes of cyclin B and securin. Since all the perturbations that we had introduced so far, preserved the timing between sister chromatid separation and Plo1 removal, we asked which other perturbations may disrupt it. Interestingly, several *S. pombe* APC/C mutants were identified in a screen for the 'cut' (cell untimely torn) phenotype (Hirano et al., 1986), which means that they undergo cytokinesis and septation without having separated sister chromatids. This is surprising, given that mutations in the APC/C are expected to impair both degradation of securin and of cyclin B. Apparently, these specific mutants impair securin degradation more than they impair cyclin B degradation (Chang et al., 2001). Hence, they offer a possibility to analyze timing in a situation where securin and cyclin B degradation are unbalanced. Imaging one such temperature-sensitive mutant (*cut9-665*) at semi-permissive temperature revealed that the time window between sister chromatid separation and Plo1 removal now indeed shortened (Figure 6A), indicating that this time difference is not always invariant. Strikingly, if we impaired securin and cyclin B degradation in equal measure by reducing the amount of the APC/C activator Slp1 (Figure S5), the timing between these two events was not shortened, but remained 3 min as in the wild type (Figure 6A). These results are corroborated by genetic evidence that increased amounts of securin are lethal in the *cut9-665* mutant, whereas high amounts of cyclin B are tolerated (Figure 6B, (Matsumura et al., 2003)). In contrast, cells with reduced Slp1 levels tolerate both higher securin and higher cyclin B levels (Figure 6C). This indicates that comparable perturbations in the ubiquitinylation pathway are better buffered if they impair securin and cyclin B degradation similarly. Altogether, our results suggest a surprising robustness of the timing between securin and cyclin B degradation-dependent events that results purely from the features of the degradation pathway, without invoking direct crosstalk.

Discussion

For proper progression through the cell cycle, cellular events need to happen in a certain order. How such order is achieved has attracted considerable attention (Bhaduri and Pryciak, 2011; Coudreuse and Nurse, 2010; Hartwell and Weinert, 1989; Koivomagi et al., 2011; Murray, 1991; Pagliuca et al., 2011). With respect to cell division, several groups have examined how order in the degradation of different APC/C substrates comes about (Enquist-Newman et al., 2008; Lu et al., 2014; Rape et al., 2006; Sedgwick et al., 2013; Williamson et al., 2011) or how events are ordered downstream of the degradation of cyclins (Bouchoux and Uhlmann, 2011; Cundell et al., 2013; Wolf et al., 2006).

Here, we have addressed the related but not identical question how events that depend on the parallel degradation of either securin or cyclin B can maintain their order, even when the abundance ratio between these two proteins changes. So far, the implicit assumption has been that the similar onset of degradation for securin and cyclin B is sufficient to ensure that downstream processes are coordinated in time. However, this would only be true if the levels and ratio of securin and cyclin B were constant, which they are not (Figure 1C). Hence, other mechanisms are required. As one mechanism, we have identified competition between securin and cyclin B for the degradation machinery. Increased abundance of one protein slows down the degradation of the other (Figure 4). Given that this is a very intuitive mechanism, it is surprising that (at least to our knowledge) endogenous securin and cyclin B have never been formally shown to compete for degradation at the metaphase to anaphase transition. The possibility, however, was already suggested by experiments showing that the expression of an N-terminal cyclin B fragment (containing the D-box) impairs the degradation of both securin and cyclin B (Holloway et al., 1993; Yamano et al., 1996). In addition, securin and cyclin B have been shown to compete for degradation prior to M-phase in mouse oocytes (Marangos and Carroll, 2008). In contrast, we did not observe any difference in interphase abundance of securin when cyclin B was overexpressed or vice versa (Figure 1D and E), suggesting that their degradation prior to

metaphase is low or requires different factors for the two proteins.

Competition for the same biochemical pathway is a very simple, yet effective coupling mechanism (Cookson et al., 2011; Prindle et al., 2014). Importantly, however, our experiments also indicate that competition for degradation alone is not sufficient to explain the robust temporal order between sister chromatid separation and Plo1 removal from SPBs, which depends on the degradation of cyclin B (Figure 4F - H). Our computational analysis indicated that a mechanism, which allows the threshold for downstream events to scale with the degradation kinetics, could further contribute to the robust temporal order of events. Indeed, we show that the securin threshold at which sister chromatid separation occurs closely follows this scaling rule for several perturbations that we investigated. Interestingly, similar flexible thresholds for the point of sister chromatid separation during securin degradation have been observed in human cells (D. Izawa and J. Pines, personal communication) and in budding yeast (Lu et al., 2014), indicating that this is a universal mechanism. Other authors have suggested that flexible thresholds point to another mechanism, in addition to securin degradation, that controls sister chromatid separation (Lu et al., 2014). We, in contrast, favor the idea that sister chromatid separation is solely controlled by securin degradation. However, the relation between securin abundance and sister chromatid separation is clearly more complex than simply assuming that the excess of securin over separase needs to be degraded for sister chromatid separation to occur. Our idea that the level of securin and separase, and not another mechanism, determines the onset of sister chromatid separation is influenced by our findings that (a) the time of sister chromatid separation is considerably delayed by additional securin (Figure 5A), and (b) higher expression of separase, in addition to higher expression of securin, reverses the delay in sister chromatid separation (Kamenz and Hauf, 2014). Hence, the ratio between securin and separase plays a predominant role in determining the timing of sister chromatid separation. If this is the case, then why does sister chromatid separation not always occur at the same securin to separase ratio? One hint comes from our findings that securin seems to be present in double the amount of separase; yet, only 25 – 30 % of securin need to be degraded for anaphase to occur. This suggests that a pool

of securin - that is visible as securin-GFP at the onset of sister chromatid separation - is not able to inhibit separase. We can envision two mechanisms, which could create such an inhibition-deficient pool: (1) Since securin degradation is a two-step process of ubiquitinylation and degradation, it is possible that ubiquitinylation alone renders securin (at least partially) incapable of separase inhibition, so that the protein may be functionally inactive before being degraded. (2) Alternatively or additionally, the rate of binding of securin to separase may be slow. Therefore, once the APC/C has become active and some separase-bound securin has been degraded, separase may not efficiently be re-inhibited by the free pool of securin. Therefore, even if securin is still present in excess, separase activity cannot be suppressed. A similar situation would arise if separase became refractory to securin-mediated inhibition after having been released. For any of these mechanisms, a higher abundance of securin at the onset of APC/C-mediated degradation would also result in a higher abundance of the non-inhibitory pools of securin as degradation proceeds. Hence, sister chromatid separation would occur at a higher level of securin-GFP, just as we observed it (Figure 5A). The plausibility of these mechanisms is corroborated by findings that in human cells sister chromatid separation can occur while a pool of free, unbound securin is still present (Hellmuth et al., 2014) and by findings that cyclin B can be inactivated by ubiquitinylation alone – at least in some situations (Li and Blow, 2004; Nishiyama et al., 2000). In the future, it will be important to directly test whether one of these mechanisms operates and is functionally relevant in vivo.

So far, we have only analysed one cyclin B degradation-dependent event: Plo1 removal from SPBs. It remains unknown whether other cyclin B degradation-dependent events are similarly tightly coupled to sister chromatid separation in time. Given the complexity of mitotic exit regulation by multiple phosphatases (Wurzenberger and Gerlich, 2011), it is conceivable that other events follow different regulatory pathways. Cyclin B degradation-dependent events later in mitotic exit may not require tight coordination with sister chromatid separation or their timely execution could be regulated by other mechanisms. Chromosome decondensation, for example, has been shown to be inhibited on chromosomes that remain in the center of the spindle and

have not yet reached the pole (Afonso et al., 2014). The last stage of cytokinesis, abscission, is also delayed if chromosome separation is incomplete (Mendoza et al., 2009; Norden et al., 2006). Although a variety of mechanisms may play a role in coordinating anaphase events, it is interesting to note that a drop in Plo1 activity during mitotic exit has been implicated in activating a specific PP2A phosphatase, which presumably initiates later events of mitotic exit (Grallert et al., 2014). Assuming that Plo1 activity is linked to its localization, this suggests that the tight coordination between sister chromatid separation and Plo1 localization that we have uncovered here, plays a wider role in setting the timing of downstream events.

For many mitotic exit events – for example, the stabilization of kinetochore-microtubule attachment or the inactivation of the spindle assembly checkpoint – it is still unclear when exactly they take place and how variable their timing can be to still preserve faithful chromosome segregation and cell division. Due to the tight coupling that we have identified here, it has been difficult for us to uncouple these events in order to study the consequences. Yet, our finding that the temporal order starts to break down in the *cut9-665* mutant and that this mutant also is highly sensitive to changes in the expression level of securin suggests that the coupling mechanisms that we have uncovered here are important and that the same onset of securin and cyclin B degradation is insufficient for the faithful completion of mitosis.

Materials and Methods

S. pombe strains

All strains are listed in Supplementary Table 1. To increase the expression of securin-GFP (*cut2+-GFP<<kanR,* (Kamenz and Hauf, 2014)), securin (*cut2+*) or cyclin B (*cdc13+*), the *adh1* promoter was integrated 5' of the open reading frame (ORF) of the respective gene by PCR-based gene targeting (Bahler et al., 1998) (*Padh1*-GGATCTGCCGGTCTCC-ORF). Integration of the *Padh1* 5' of the *cut2+-GFP<<kanR* gave raise to strains with differently elevated expression level (4-times(M13) and 8-times(M6) increase, respectively) due to different mutations that these strains had acquired in the *Padh1* region. The *cut1+-13myc<<kanR, the mis12+-GFP<<kanR, rpn10+-GFP<<kanR, rpn11+-GFP<<kanR, and the cdc13+-mCherry<<kanR* strain were likewise created by PCR-based gene targeting. For inducible expression of non-degradable securin (*ΔN-Cut2*) the coding sequence of amino acids 81 to 301 of Cut2 (Funabiki et al., 1996) was cloned into the pDual vector (Matsuyama et al., 2004) under the control of the *nmt81* promoter and integrated into the *leu1* locus. *S. pombe* strains with the following modifications and mutations have been described previously: *cdc25-22* (Russell and Nurse, 1986)*, cdc25-22 ura4::pcn1p::EGFP-pcn1* (Carpy et al., 2014; Meister et al., 2003), *dh1L-tdTomato* (Sakuno et al., 2009), *cut9-665* (Hirano et al., 1986), *Prad21-slp1+* (Yokobayashi and Watanabe, 2005), *plo1+-mCherry<<natR* (Heinrich et al., 2012), *cut2-GFP<<kanR* and the inducible version of non-degradable cyclin B (*leu1+<<Pnmt81-ΔN67-cdc13*) (Kamenz and Hauf, 2014).

Pre-culturing and live cell imaging

Cells were cultured either in rich medium (YE + adenine) or Edinburgh minimal medium (EMM) with the necessary supplements (Moreno, 1991) at 30 °C; strains carrying the temperature-sensitive mutants c*ut9-665* or *cdc25-22* were cultured at 25 °C. Prior to imaging all strains were grown in EMM (+ supplements) – with the exception of the *cut9-665* and the *Prad21+-slp1* strains, because the effect of APC/C inhibition was more pronounced when cells were grown in

rich medium. If necessary, the *nmt81* promoter was repressed by addition of 16 μM thiamine to EMM and induced by washing cells and transferring them into media without thiamine for 14-18 hours. Prior to imaging, all strains were transferred into EMM, mounted in lectin-coated (35 μg/ml, Sigma L1395) culture dishes (8-well, Ibidi) and incubated on the microscope stage at 30 °C for 30 min. To partially inhibit the proteasome, Bortezomib (Velcade, LC laboratories, B-1408) was added to a final concentration of 10 μM. Live cell imaging was carried out at 30 °C on a DeltaVision Core system (Applied Precision/GE Healthcare) equipped with a climate chamber (EMBL) using a 60x/1.4 Apo oil objective (Olympus). To follow the securin degradation kinetics, images were acquired every 15 seconds for 2 hours using the 'optical axis integration' mode of the SoftWorx software over a range of 4 μm. To follow Plo1-mCherry and Mis12-GFP, a z-stack of 8 planes spaced by 0.4 μm was acquired every 20 seconds for 1 hour, the field of view was then changed and the acquisition continued for an additional hour.

Data processing and image analysis

The analysis of the securin degradation kinetics relative to the time of sister chromatid separation is described in (Kamenz, Mihaljev, Legewie, Hauf, 2014, submitted). For the analysis of sister chromatid separation relative to Plo1 removal, the time point of sister chromatid separation was scored manually by following the kinetochore dynamics of the Mis12-GFP signal. The last time point at which sister chromatids were still associated before anaphase A movement became visible was defined as sister chromatid separation. For the analysis of Plo1 removal, images were deconvolved using SoftWorx software, and a maximum projection was calculated. For each time point a region of interest (ROI) was defined by the cell outline and the maximum intensity of the area was measured. For further processing of the measurements, custom-written MATLAB software was used. Every single cell measurement was normalized to the minimum and maximum value of the time course. The data were smoothed by calculating the average intensity of 7 consecutive time points and the first time derivative was computed using linear regression on 5 consecutive time points. The second derivative was computed using linear regression on 4

consecutive points of the first derivative. Progressing backwards in time, Plo1 removal was defined as the time point were the first derivative became significantly negative (<-0.005 was used as a threshold value) and the second derivative significantly positive (>0.001). For determining the start of securin degradation in strains, which, in addition to the Mis12-GFP, also overexpressed securin-GFP by 4- or 8-times, a sum projection of the z-stack was calculated. (Only in the securin-GFP overexpression strains the intensity was significantly higher than the Mis12-GFP intensity and could be reliably determined). For every time point a ROI defining the nucleus was placed manually and the average signal intensity was measured. If there were more than one ROI for a time point (because of nuclear division) the area measurements were averaged. The data was further smoothed by calculating the average intensity of 5 consecutive time points and the time derivative was calculated by linear regression on 5 consecutive time points. Start of securin degradation was defined as the nearest time point before sister chromatid separation at which the time derivative raised about a given threshold. The threshold needed to be slightly adjusted between experimental replicates of different days: for the 4-times securin-GFP overexpression it ranged between -0.7 rcc s^{-1} and -1.5 rcc s^{-1}, for the 8-time securin-GFP overexpression it ranged between -2.0 rcc s^{-1} and -2.5 rcc s^{-1}.

Quantification the nuclear mitotic concentration of separase- and securin-GFP by wide-field fluorescence deconvolution microscopy (WiFDeM)

The general procedure for the quantification of the GFP-intensity has been described previously (Heinrich et al., 2013), but here cells were mounted in lectin-coated (35 mg/ml; Sigma L1395) culture dishes (8-well, Ibidi) instead of microfluidic devices.

Cell synchronization

To synchronize at the G2/M transition, *cdc25-22* cells were cultured at 25 °C in minimal medium (EMM) into logarithmic growth phase. To arrest cells at the G2/M transition cultures were shifted to the restrictive temperature of 36.5 °C for 5 h. Cells were released from the arrest by quickly cooling the culture to 25 °C (Figure 1C, Supplementary Figure 1C-F) or 20 °C (Supplementary

Figure 4E-G) using an ice-water bath and were further incubated in a shaking-water bath at the respective temperature until harvest. For arresting cells in G2 in response to DNA damage, cultures were split 120 min after release and 5 mU/mL bleomycin (Dot Scientific, DSB40060) in 0.154 M NaCl was added to one culture. As a control the same amount of 0.154 M NaCl solution was added to the other culture.

Cell extracts, immunoblotting and antibodies

Protein extraction under denaturing conditions using trichchloroacetic acid (TCA) was performed as described (Heinrich et al., 2012). Mouse anti-Myc (Sigma, M4439), mouse anti-Cdc13 (cyclin B, Novus, NB200-576), rabbit anti-Cdc2 (CDK1, Santa Cruz, SC-53), anti-tubulin (Sigma, T5168), and rabbit anti-Cut2 (securin,(Kamenz and Hauf, 2014)) antibodies were used as primary antibodies. Anti-mouse or anti-rabbit HRP-conjugates (Dianova, 115-035-003, 111-035-003) were used as secondary antibodies and were read out using chemiluminescence.

Quantitative immunoblotting

Fission yeast securin and cyclin B were recombinantly expressed in *E. coli* as Hisx6-MBP-fusion proteins and affinity purified. The affinity tag was cleaved off and securin was further purified by cation exchange chromatography. Cyclin B precipitated after the cleavage of the affinity tag. Therefore, the precipitate was resuspended in 8 M Urea. Protein concentrations were determined using the Bradford protein assay. The purity of cyclin B was estimated by gel electrophoresis and Coomassie brilliant blue staining to be only 90 %. Because we previously observed that the immunoblotting efficiency differs between loading purified proteins or proteins in a cell extract, we mixed the different dilutions of recombinant securin and cyclin B into a cell extract of a strain, which expressed the larger securin-GFP and cyclin B-mCherry fusion proteins. This enabled us to compare the cellular concentration of securin and cyclin B from cells grown asynchronously in rich medium to our recombinant protein standards. Note that securin is more readily re-synthesized after mitosis than cyclin B (Supplementary Fig. S1C). Since the experiment was

performed using asynchronous cells, we probably slightly underestimate the cyclin B to securin ratio.

Acknowledgments

We thank Andreas Boland for advice and Yoshinori Watanabe for reagents. This work was supported by the Max Planck Society (J.K., S.H.), Virginia Tech (J.K., S.H.), the German Federal Ministry of Education and Research (e:Bio Junior Group grant to S.L.) and the Boehringer Ingelheim Fonds (fellowship to J.K.).

Author contributions

J.K. and S.H. conceived the project and all authors discussed the results; J.K. designed, performed and analysed all experiments with the exception of Figures 1E, 1G, 4D, 4E and S2E (lower panel), which were performed by A.K.; T.M. and S.L. created and analysed all deterministic simulations; S.H. and S.L. wrote the paper with input by J.K.

Competing Interest

None declared.

References

Afonso, O., Matos, I., Pereira, A.J., Aguiar, P., Lampson, M.A., and Maiato, H. (2014). Feedback control of chromosome separation by a midzone Aurora B gradient. Science *345*, 332-336.

Bahler, J., Wu, J.Q., Longtine, M.S., Shah, N.G., McKenzie, A., 3rd, Steever, A.B., Wach, A., Philippsen, P., and Pringle, J.R. (1998). Heterologous modules for efficient and versatile PCR-based gene targeting in Schizosaccharomyces pombe. Yeast *14*, 943-951.

Bhaduri, S., and Pryciak, P.M. (2011). Cyclin-specific docking motifs promote phosphorylation of yeast signaling proteins by G1/S Cdk complexes. Current biology : CB *21*, 1615-1623.

Booher, R.N., Alfa, C.E., Hyams, J.S., and Beach, D.H. (1989). The fission yeast cdc2/cdc13/suc1 protein kinase: regulation of catalytic activity and nuclear localization. Cell *58*, 485-497.

Bouchoux, C., and Uhlmann, F. (2011). A quantitative model for ordered Cdk substrate dephosphorylation during mitotic exit. Cell *147*, 803-814.

Carpy, A., Krug, K., Graf, S., Koch, A., Popic, S., Hauf, S., and Macek, B. (2014). Absolute proteome and phosphoproteome dynamics during the cell cycle of Schizosaccharomyces pombe (Fission Yeast). Mol Cell Proteomics *13*, 1925-1936.

Chang, L., and Barford, D. (2014). Insights into the anaphase-promoting complex: a molecular machine that regulates mitosis. Current opinion in structural biology *29C*, 1-9.

Chang, L., Morrell, J.L., Feoktistova, A., and Gould, K.L. (2001). Study of cyclin proteolysis in anaphase-promoting complex (APC) mutant cells reveals the requirement for APC function in the final steps of the fission yeast septation initiation network. Mol Cell Biol *21*, 6681-6694.

Clijsters, L., van Zon, W., Riet, B.T., Voets, E., Boekhout, M., Ogink, J., Rumpf-Kienzl, C., and Wolthuis, R.M. (2014). Inefficient degradation of cyclin B1 re-activates the spindle checkpoint right after sister chromatid disjunction. Cell cycle *13*.

Cohen-Fix, O., and Koshland, D. (1999). Pds1p of budding yeast has dual roles: inhibition of anaphase initiation and regulation of mitotic exit. Genes & development *13*, 1950-1959.

Cohen-Fix, O., Peters, J.M., Kirschner, M.W., and Koshland, D. (1996). Anaphase initiation in Saccharomyces cerevisiae is controlled by the APC-dependent degradation of the anaphase inhibitor Pds1p. Genes & development *10*, 3081-3093.

Cookson, N.A., Mather, W.H., Danino, T., Mondragon-Palomino, O., Williams, R.J., Tsimring, L.S., and Hasty, J. (2011). Queueing up for enzymatic processing: correlated signaling through coupled degradation. Mol Syst Biol *7*, 561.

Coudreuse, D., and Nurse, P. (2010). Driving the cell cycle with a minimal CDK control network. Nature *468*, 1074-1079.

Cundell, M.J., Bastos, R.N., Zhang, T., Holder, J., Gruneberg, U., Novak, B., and Barr, F.A. (2013). The BEG (PP2A-B55/ENSA/Greatwall) pathway ensures cytokinesis follows chromosome separation. Molecular cell *52*, 393-405.

Dischinger, S., Krapp, A., Xie, L., Paulson, J.R., and Simanis, V. (2008). Chemical genetic analysis of the regulatory role of Cdc2p in the S. pombe septation initiation network. Journal of cell science *121*, 843-853.

Enquist-Newman, M., Sullivan, M., and Morgan, D.O. (2008). Modulation of the mitotic regulatory network by APC-dependent destruction of the Cdh1 inhibitor Acm1. Molecular cell *30*, 437-446.

Funabiki, H., Yamano, H., Kumada, K., Nagao, K., Hunt, T., and Yanagida, M. (1996). Cut2 proteolysis required for sister-chromatid seperation in fission yeast. Nature *381*, 438-441.

Ghiara, J.B., Richardson, H.E., Sugimoto, K., Henze, M., Lew, D.J., Wittenberg, C., and Reed, S.I. (1991). A cyclin B homolog in S. cerevisiae: chronic activation of the Cdc28 protein kinase by cyclin prevents exit from mitosis. Cell *65*, 163-174.

Gorr, I.H., Boos, D., and Stemmann, O. (2005). Mutual inhibition of separase and Cdk1 by two-step complex formation. Molecular cell *19*, 135-141.

Grallert, A., Boke, E., Hagting, A., Hodgson, B., Connolly, Y., Griffiths, J.R., Smith, D.L., Pines, J., and Hagan, I.M. (2014). A PP1-PP2A phosphatase relay controls mitotic progression. Nature.

Hagting, A., Den Elzen, N., Vodermaier, H.C., Waizenegger, I.C., Peters, J.M., and Pines, J. (2002). Human securin proteolysis is controlled by the spindle checkpoint and reveals when the APC/C switches from activation by Cdc20 to Cdh1. The Journal of cell biology *157*, 1125-1137.

Hartwell, L.H., and Weinert, T.A. (1989). Checkpoints: controls that ensure the order of cell cycle events. Science *246*, 629-634.

Heinrich, S., Geissen, E.M., Kamenz, J., Trautmann, S., Widmer, C., Drewe, P., Knop, M., Radde, N., Hasenauer, J., and Hauf, S. (2013). Determinants of robustness in spindle assembly checkpoint signalling. Nature cell biology *15*, 1328-1339.

Heinrich, S., Windecker, H., Hustedt, N., and Hauf, S. (2012). Mph1 kinetochore localization is crucial and upstream in the hierarchy of spindle assembly checkpoint protein recruitment to

kinetochores. Journal of cell science *125*, 4720-4727.

Hellmuth, S., Bottger, F., Pan, C., Mann, M., and Stemmann, O. (2014). PP2A delays APC/C-dependent degradation of separase-associated but not free securin. The EMBO journal *33*, 1134-1147.

Herbert, M., Levasseur, M., Homer, H., Yallop, K., Murdoch, A., and McDougall, A. (2003). Homologue disjunction in mouse oocytes requires proteolysis of securin and cyclin B1. Nature cell biology *5*, 1023-1025.

Higuchi, T., and Uhlmann, F. (2005). Stabilization of microtubule dynamics at anaphase onset promotes chromosome segregation. Nature *433*, 171-176.

Hirano, T., Funahashi, S., Uemura, T., and Yanagida, M. (1986). Isolation and characterization of Schizosaccharomyces pombe cutmutants that block nuclear division but not cytokinesis. The EMBO journal *5*, 2973-2979.

Holland, A.J., Bottger, F., Stemmann, O., and Taylor, S.S. (2007). Protein phosphatase 2A and separase form a complex regulated by separase autocleavage. J Biol Chem *282*, 24623-24632.

Holloway, S.L., Glotzer, M., King, R.W., and Murray, A.W. (1993). Anaphase is initiated by proteolysis rather than by the inactivation of maturation-promoting factor. Cell *73*, 1393-1402.

Homer, H.A., McDougall, A., Levasseur, M., Yallop, K., Murdoch, A.P., and Herbert, M. (2005). Mad2 prevents aneuploidy and premature proteolysis of cyclin B and securin during meiosis I in mouse oocytes. Genes & development *19*, 202-207.

Hornig, N.C., Knowles, P.P., McDonald, N.Q., and Uhlmann, F. (2002). The dual mechanism of separase regulation by securin. Current biology : CB *12*, 973-982.

Kamenz, J., and Hauf, S. (2014). Slow checkpoint activation kinetics as a safety device in anaphase. Current biology : CB *24*, 646-651.

Koivomagi, M., Valk, E., Venta, R., Iofik, A., Lepiku, M., Morgan, D.O., and Loog, M. (2011). Dynamics of Cdk1 substrate specificity during the cell cycle. Molecular cell *42*, 610-623.

Kulak, N.A., Pichler, G., Paron, I., Nagaraj, N., and Mann, M. (2014). Minimal, encapsulated proteomic-sample processing applied to copy-number estimation in eukaryotic cells. Nat Methods *11*, 319-324.

Leismann, O., and Lehner, C.F. (2003). Drosophila securin destruction involves a D-box and a KEN-box and promotes anaphase in parallel with Cyclin A degradation. Journal of cell science *116*, 2453-2460.

Li, A., and Blow, J.J. (2004). Non-proteolytic inactivation of geminin requires CDK-dependent ubiquitination. Nature cell biology *6*, 260-267.

Lu, D., Hsiao, J.Y., Davey, N.E., Van Voorhis, V.A., Foster, S.A., Tang, C., and Morgan, D.O. (2014). Multiple mechanisms determine the order of APC/C substrate degradation in mitosis. The Journal of cell biology *207*, 23-39.

Lu, Y., and Cross, F. (2009). Mitotic exit in the absence of separase activity. Molecular biology of the cell *20*, 1576-1591.

Madgwick, S., Nixon, V.L., Chang, H.Y., Herbert, M., Levasseur, M., and Jones, K.T. (2004). Maintenance of sister chromatid attachment in mouse eggs through maturation-promoting factor activity. Dev Biol *275*, 68-81.

Marangos, P., and Carroll, J. (2008). Securin regulates entry into M-phase by modulating the stability of cyclin B. Nature cell biology *10*, 445-451.

Marguerat, S., Schmidt, A., Codlin, S., Chen, W., Aebersold, R., and Bahler, J. (2012).

Quantitative analysis of fission yeast transcriptomes and proteomes in proliferating and quiescent cells. Cell *151*, 671-683.

Matsumura, T., Yuasa, T., Hayashi, T., Obara, T., Kimata, Y., and Yanagida, M. (2003). A brute force postgenome approach to identify temperature-sensitive mutations that negatively interact with separase and securin plasmids. Genes Cells *8*, 341-355.

Matsuyama, A., Shirai, A., Yashiroda, Y., Kamata, A., Horinouchi, S., and Yoshida, M. (2004). pDUAL, a multipurpose, multicopy vector capable of chromosomal integration in fission yeast. Yeast *21*, 1289-1305.

Meister, P., Poidevin, M., Francesconi, S., Tratner, I., Zarzov, P., and Baldacci, G. (2003). Nuclear factories for signalling and repairing DNA double strand breaks in living fission yeast. Nucleic acids research *31*, 5064-5073.

Mendoza, M., Norden, C., Durrer, K., Rauter, H., Uhlmann, F., and Barral, Y. (2009). A mechanism for chromosome segregation sensing by the NoCut checkpoint. Nature cell biology *11*, 477-483.

Moriya, H., Chino, A., Kapuy, O., Csikasz-Nagy, A., and Novak, B. (2011). Overexpression limits of fission yeast cell-cycle regulators in vivo and in silico. Mol Syst Biol *7*, 556.

Mulvihill, D.P., Petersen, J., Ohkura, H., Glover, D.M., and Hagan, I.M. (1999). Plo1 kinase recruitment to the spindle pole body and its role in cell division in Schizosaccharomyces pombe. Molecular biology of the cell *10*, 2771-2785.

Murray, A.W. (1991). Coordinating cell cycle events. Cold Spring Harbor symposia on quantitative biology *56*, 399-408.

Murray, A.W., Solomon, M.J., and Kirschner, M.W. (1989). The role of cyclin synthesis and degradation in the control of maturation promoting factor activity. Nature *339*, 280-286.

Nasmyth, K., Peters, J.M., and Uhlmann, F. (2000). Splitting the chromosome: cutting the ties that bind sister chromatids. Science *288*, 1379-1385.

Nishiyama, A., Tachibana, K., Igarashi, Y., Yasuda, H., Tanahashi, N., Tanaka, K., Ohsumi, K., and Kishimoto, T. (2000). A nonproteolytic function of the proteasome is required for the dissociation of Cdc2 and cyclin B at the end of M phase. Genes & development *14*, 2344-2357.

Norden, C., Mendoza, M., Dobbelaere, J., Kotwaliwale, C.V., Biggins, S., and Barral, Y. (2006). The NoCut pathway links completion of cytokinesis to spindle midzone function to prevent chromosome breakage. Cell *125*, 85-98.

Oliveira, R.A., Hamilton, R.S., Pauli, A., Davis, I., and Nasmyth, K. (2010). Cohesin cleavage and Cdk inhibition trigger formation of daughter nuclei. Nature cell biology *12*, 185-192.

Pagliuca, F.W., Collins, M.O., Lichawska, A., Zegerman, P., Choudhary, J.S., and Pines, J. (2011). Quantitative proteomics reveals the basis for the biochemical specificity of the cell-cycle machinery. Molecular cell *43*, 406-417.

Parry, D.H., Hickson, G.R., and O'Farrell, P.H. (2003). Cyclin B destruction triggers changes in kinetochore behavior essential for successful anaphase. Current biology : CB *13*, 647-653.

Parry, D.H., and O'Farrell, P.H. (2001). The schedule of destruction of three mitotic cyclins can dictate the timing of events during exit from mitosis. Current biology : CB *11*, 671-683.

Peters, J.M. (2006). The anaphase promoting complex/cyclosome: a machine designed to destroy. Nature reviews Molecular cell biology *7*, 644-656.

Pfleger, C.M., Lee, E., and Kirschner, M.W. (2001). Substrate recognition by the Cdc20 and Cdh1 components of the anaphase-promoting complex. Genes & development *15*, 2396-2407.

Pines, J. (2011). Cubism and the cell cycle: the many faces of the APC/C. Nature reviews Molecular cell biology *12*, 427-438.

Primorac, I., and Musacchio, A. (2013). Panta rhei: the APC/C at steady state. The Journal of cell biology *201*, 177-189.

Prindle, A., Selimkhanov, J., Li, H., Razinkov, I., Tsimring, L.S., and Hasty, J. (2014). Rapid and tunable post-translational coupling of genetic circuits. Nature *508*, 387-391.

Queralt, E., Lehane, C., Novak, B., and Uhlmann, F. (2006). Downregulation of PP2A(Cdc55) phosphatase by separase initiates mitotic exit in budding yeast. Cell *125*, 719-732.

Raj, A., and van Oudenaarden, A. (2008). Nature, nurture, or chance: stochastic gene expression and its consequences. Cell *135*, 216-226.

Rape, M., Reddy, S.K., and Kirschner, M.W. (2006). The processivity of multiubiquitination by the APC determines the order of substrate degradation. Cell *124*, 89-103.

Rattani, A., Vinod, P.K., Godwin, J., Tachibana-Konwalski, K., Wolna, M., Malumbres, M., Novak, B., and Nasmyth, K. (2014). Dependency of the spindle assembly checkpoint on Cdk1 renders the anaphase transition irreversible. Current biology : CB *24*, 630-637.

Rimmington, G., Dalby, B., and Glover, D.M. (1994). Expression of N-terminally truncated cyclin B in the Drosophila larval brain leads to mitotic delay at late anaphase. Journal of cell science *107 (Pt 10)*, 2729-2738.

Russell, P., and Nurse, P. (1986). cdc25+ functions as an inducer in the mitotic control of fission yeast. Cell *45*, 145-153.

Sakuno, T., Tada, K., and Watanabe, Y. (2009). Kinetochore geometry defined by cohesion within the centromere. Nature *458*, 852-858.

Sedgwick, G.G., Hayward, D.G., Di Fiore, B., Pardo, M., Yu, L., Pines, J., and Nilsson, J. (2013). Mechanisms controlling the temporal degradation of Nek2A and Kif18A by the APC/C-Cdc20 complex. The EMBO journal *32*, 303-314.

Shindo, N., Kumada, K., and Hirota, T. (2012). Separase sensor reveals dual roles for separase coordinating cohesin cleavage and cdk1 inhibition. Developmental cell *23*, 112-123.

Sigrist, S., Jacobs, H., Stratmann, R., and Lehner, C.F. (1995). Exit from mitosis is regulated by Drosophila fizzy and the sequential destruction of cyclins A, B and B3. The EMBO journal *14*, 4827-4838.

Siomos, M.F., Badrinath, A., Pasierbek, P., Livingstone, D., White, J., Glotzer, M., and Nasmyth, K. (2001). Separase is required for chromosome segregation during meiosis I in Caenorhabditis elegans. Current biology : CB *11*, 1825-1835.

Stegmeier, F., Visintin, R., and Amon, A. (2002). Separase, polo kinase, the kinetochore protein Slk19, and Spo12 function in a network that controls Cdc14 localization during early anaphase. Cell *108*, 207-220.

Stemmann, O., Zou, H., Gerber, S.A., Gygi, S.P., and Kirschner, M.W. (2001). Dual inhibition of sister chromatid separation at metaphase. Cell *107*, 715-726.

Sullivan, M., and Morgan, D.O. (2007). Finishing mitosis, one step at a time. Nature reviews Molecular cell biology *8*, 894-903.

Sullivan, M., and Uhlmann, F. (2003). A non-proteolytic function of separase links the onset of anaphase to mitotic exit. Nature cell biology *5*, 249-254.

Surana, U., Amon, A., Dowzer, C., McGrew, J., Byers, B., and Nasmyth, K. (1993). Destruction of the CDC28/CLB mitotic kinase is not required for the metaphase to anaphase transition in

budding yeast. The EMBO journal *12*, 1969-1978.

Tian, W., Li, B., Warrington, R., Tomchick, D.R., Yu, H., and Luo, X. (2012). Structural analysis of human Cdc20 supports multisite degron recognition by APC/C. Proc Natl Acad Sci U S A *109*, 18419-18424.

Tinker-Kulberg, R.L., and Morgan, D.O. (1999). Pds1 and Esp1 control both anaphase and mitotic exit in normal cells and after DNA damage. Genes & development *13*, 1936-1949.

Uhlmann, F., Wernic, D., Poupart, M.A., Koonin, E.V., and Nasmyth, K. (2000). Cleavage of cohesin by the CD clan protease separin triggers anaphase in yeast. Cell *103*, 375-386.

van Zon, W., Ogink, J., ter Riet, B., Medema, R.H., te Riele, H., and Wolthuis, R.M. (2010). The APC/C recruits cyclin B1-Cdk1-Cks in prometaphase before D box recognition to control mitotic exit. The Journal of cell biology *190*, 587-602.

Vazquez-Novelle, M.D., Sansregret, L., Dick, A.E., Smith, C.A., McAinsh, A.D., Gerlich, D.W., and Petronczki, M. (2014). Cdk1 inactivation terminates mitotic checkpoint surveillance and stabilizes kinetochore attachments in anaphase. Current biology : CB *24*, 638-645.

Visintin, R., Craig, K., Hwang, E.S., Prinz, S., Tyers, M., and Amon, A. (1998). The phosphatase Cdc14 triggers mitotic exit by reversal of Cdk-dependent phosphorylation. Molecular cell *2*, 709-718.

Waizenegger, I.C., Hauf, S., Meinke, A., and Peters, J.M. (2000). Two distinct pathways remove mammalian cohesin from chromosome arms in prophase and from centromeres in anaphase. Cell *103*, 399-410.

Williamson, A., Banerjee, S., Zhu, X., Philipp, I., Iavarone, A.T., and Rape, M. (2011). Regulation of ubiquitin chain initiation to control the timing of substrate degradation. Molecular cell *42*, 744-757.

Wirth, K.G., Wutz, G., Kudo, N.R., Desdouets, C., Zetterberg, A., Taghybeeglu, S., Seznec, J., Ducos, G.M., Ricci, R., Firnberg, N.*, et al.* (2006). Separase: a universal trigger for sister chromatid disjunction but not chromosome cycle progression. The Journal of cell biology *172*, 847-860.

Wolf, F., Wandke, C., Isenberg, N., and Geley, S. (2006). Dose-dependent effects of stable cyclin B1 on progression through mitosis in human cells. The EMBO journal *25*, 2802-2813.

Wurzenberger, C., and Gerlich, D.W. (2011). Phosphatases: providing safe passage through mitotic exit. Nature reviews Molecular cell biology *12*, 469-482.

Yamano, H., Gannon, J., and Hunt, T. (1996). The role of proteolysis in cell cycle progression in Schizosaccharomyces pombe. The EMBO journal *15*, 5268-5279.

Yokobayashi, S., and Watanabe, Y. (2005). The kinetochore protein Moa1 enables cohesion-mediated monopolar attachment at meiosis I. Cell *123*, 803-817.

Zachariae, W., and Nasmyth, K. (1999). Whose end is destruction: cell division and the anaphase-promoting complex. Genes & development *13*, 2039-2058.

Zur, A., and Brandeis, M. (2001). Securin degradation is mediated by fzy and fzr, and is required for complete chromatid separation but not for cytokinesis. The EMBO journal *20*, 792-801.

Figure Legends

Figure 1: Variations in the securin to cyclin B ratio are well tolerated

(A) Schematic representation of the metaphase to anaphase transition. Despite being mediated by the degradation of either securin or cyclin B sister chromatid separation and events of mitotic exit need to be coordinated relative to each other in time. (B) Quantification of the average securin and cyclin B concentration per cell determined by quantitative immunoblotting of asynchronous cell extracts against the recombinant protein standards. Shown are the mean (bar graph) and the single measurements of the three replicates (diamonds). The corresponding immunoblots are shown in Figure S1 A and B. (C) Quantification of the relative protein abundances of securin and cyclin B in the first mitosis (15 minutes) and second mitosis (150 minutes) after release from G2/M arrest (using the temperature-sensitive *cdc25-22* allele) and after delaying entry into the second mitosis using the irradiation-mimetic bleomycin (150 minutes and 240 minutes, respectively). All measurements were normalized to the 150 minute sample of the control (reference). Shown is the mean and standard deviation of the technical replicates. Corresponding immunoblots of the time course, the quantification and the quantification of cell cycle progression are shown in Figure S1 C – F. (D,E) Immunoblots of the strains overexpressing securin-GFP and cyclin B compared to the strains expressing securin-GFP and cyclin B under the endogenous promoter. No co-regulation of cyclin B or securin-GFP is observed, when securin-GFP or cyclin B abundance is increased, respectively. Parts of the immunoblot in D have also been shown in (Kamenz and Hauf, 2014). (F,G) Growth assays on rich medium for overexpression strains of securin and cyclin B.

Figure 2: Absence of direct crosstalk between sister chromatid separation and mitotic exit

(A) Kymographs of the mitotic progression of a wild type cell or cells where mitotic exit or sister chromatid separation was blocked by the expression of non-degradable cyclin (ΔN-cycB) or non-

degradable securin (ΔN-securin), respectively (vertical scale bar, 5 μm). The kinetochore protein Mis12 fused to GFP was used as a marker for sister chromatid separation (SCS). The polo-kinase Plo1 fused to mCherry localizes to the spindle pole bodies (SPB) in a CDK1 activity-dependent manner and is used to judge mitotic entry (SPB separation, ME) as well as the timing of mitotic exit (Plo1 removal, Plo1). (B) Quantification of single cell measurements of the timing from mitotic entry to sister chromatids in the absence (n=31) or presence (n=31) of non-degradable cyclin B. Shown is the median (bar graph) and the interquartile range (error bars). (C) Quantification of single cell measurements of the timing from mitotic entry to Plo1 removal in the absence (n=23) or presence (n=18) of non-degradable securin. Shown are the median (bar graph) and the interquartile range (error bars).

Figure 3: The time between sister chromatid segregation and Plo1 removal from SPBs is unaffected by variations of the securin to cyclin B ratio

(A, B) Quantification of the time from mitotic entry to sister chromatid separation and Plo1 removal within single cells expressing endogenous level of cyclin B (n=32) or overexpressing cyclin B 20-times (n=24). Shown are the median (bar graph) and the interquartile range (error bars). The delay was largely independent of the spindle assembly checkpoint (Supplementary Figure S3 A). (C) Time difference between sister chromatid separation and Plo1 removal for the single cell measurements shown in A and B. Shown are a Box-Whisker plot (black, the whiskers represent the minimum and maximum value) and the single measurements (grey circles). (D-F) Equivalent measurements as shown in A-C for cells expressing securin-GFP from the endogenous promoter (n=31), overexpressing securin-GFP 4-times (n=38) or overexpressing securin-GFP 8-times (n=32). Similar results were obtained, when the time was measured relative to the start of securin degradation, which we were only able to determine in the securin-GFP overexpression strains (Supplementary figure S3 B – D). (G) Single cell correlation between the time from mitotic entry to sister chromatid separation and the time from mitotic entry to Plo1 removal for cells expressing cyclin B from the endogenous promoter (grey) or overexpressing

cyclin B 20-times (blue) for the data shown in (A,B). (H) Single cell correlation between the time from mitotic entry to sister chromatid separation and the time from mitotic entry to Plo1 removal for cells expressing securin-GFP from the endogenous promoter (grey) or overexpressing securin-GFP 8-times (green) for the data shown in (D,E). The correlation is also observed when the time is related to the start of securin degradation for the strains overexpressing securin-GFP 4-times or 8-times (I), and hence is not solely due to variability of the prometaphase timing.

Figure 4: Queuing for the degradation machinery partially explains tolerance to variability in the securin to cyclin B ratio

(A) Schematic representation of the competition model, in which securin (Sec) and cyclin B (Cyc) compete for the binding to the APC/C (APC). For simplicity the proteasomal degradation is assumed to be fast and hence not explicitly implemented. (B) Deterministic simulations of the competition model depicted in (A). Comparison of the degradation kinetics of securin (green) and cyclin B (blue) in the wild type (dashed lines) and in response to overexpressing securin 8-times (solid lines, left panel) or overexpressing cyclin B 20-times (solid lines, right panel). Nuclear concentrations for securin and cyclin B were considered. See Supplementary information for details on the model parameters. (C) Predicted change in the degradation rate for securin (green) and cyclin B (blue) in response to overexpressing cyclin B 20-times or securin 8-times, respectively. At APC/C concentrations smaller than 1 μM both securin and cyclin B degradation are impacted due to competition. (D) Securin-GFP degradation was followed by live cell imaging in cells expressing either endogenous level of cyclin B (light green, n=21) or overexpressing cyclin B 20 times (dark green, n=19). The individual time courses of securin-GFP intensity (in raw camera counts, rcc) were aligned to sister chromatid separation and the time axis of the averaged time courses was shifted so that 0 min reflects the average time of the start of securin degradation (see Materials and Methods). Shown is the average (solid line) +/- standard deviation of the cell population (filled area). (E) Quantification of the time from start of securin degradation to sister chromatid separation for the data in (D). Median (bar graph) and interquartile range (error

bars) are shown. (F, G) The temporal invariance can not be recapitulated in a competition model assuming fixed threshold values for sister chromatid separation (orange circles) and Plo1 removal (blue circles). Shown are the simulations of securin and cyclin B degradation similar to (B) but using the best solution after parameter optimization. In this simulation overexpression of securin leads to a reversal in the order of events (Δt= - 6 sec) and overexpression of cyclin B results in a larger delay of Plo1 removal (Δt= 3220 sec). (H) Shown is the behavior of the time difference between sister chromatid separation and Plo1 removal (Δt) depending on the relative increase in securin (upper panel) or cyclin B level (lower panel). The timing and the order of events strongly depends on the securin and cyclin B level under the assumptions of fixed thresholds.

Figure 5: The residual level of securin at sister chromatid separation correlates with the degradation rate

(A) Securin-GFP degradation was followed by live cell imaging in cells either expressing securin-GFP from the endogenous promoter (1 x, dark green, n=32), overexpressing securin-GFP 4-times (4 x, green, n=28) or overexpressing securin-GFP 8-times (8 x, light green, n=26). The individual time courses of securin-GFP intensity (in raw camera counts, rcc) were aligned to sister chromatid separation and the time axis of the averaged time courses was shifted so that 0 min reflects the average time of the start of securin degradation. Shown is the average (solid line) +/- standard deviation of the cell population (filled area). (B) Single cell correlation between the abundance of securin-GFP at metaphase and the abundance of securin-GFP at the time of sister chromatid separation for cells expressing securin-GFP from the endogenous promoter as shown in (A). (C) Single cell correlation between the abundance of securin-GFP at the time of sister chromatid separation and the absolute degradation rate for cells expressing securin-GFP from the endogenous promoter as shown in (A). (D) Representative images of mitotic cells expressing Cut11-mCherry, which localizes to the nuclear rim and to the spindle pole bodies in mitosis, and the indicated GFP-fusion proteins. One strain additionally overexpressed untagged securin 8-times (horizontal scale bar, 5 µm). (E) Quantification of the mitotic nuclear GFP intensity (raw

camera counts, rcc) from cells expressing the indicated GFP-fusion proteins as shown in (D). Shown are Box-Whisker plots (the whiskers represent the minimum and maximum value) for one representative experiment. (F) Mitotic nuclear ratio between securin and separase. Shown are the average and the standard error of the mean for 3 independent experiments. Securin is about twice as abundant as separase in the prometaphase nucleus. (G) Sister chromatid separation occurred at lower securin abundance when securin degradation was impaired. Securin-GFP degradation was followed by live cell imaging in wild type cells (green, n=9) or in cells carrying the temperature-sensitive allele of the APC/C subunit APC6 (*cut9-665*, orange, n=18). The individual time courses of securin-GFP intensity (in raw camera counts, rcc) were aligned to sister chromatid separation and the time axis of the averaged time courses was shifted so that 0 min reflects the average time of the start of securin degradation. Shown is the average (solid line) +/- standard deviation of the cell population (filled area). (H) Quantification of the ratio between the securin-GFP abundance in metaphase and at the time of sister chromatid separation in the wild type (green) and for the APC/C mutant *cut9-665* (orange). Shown are the mean (bar graph) and the standard error of the mean (error bars) for 3 (wild type) or 5 (APC/C mutant) independent experiments. (I) Ratio between the securin-GFP abundance in metaphase and at the time of sister chromatid separation (norm. securin threshold) in the indicated perturbations relative to the normalized degradation rate. (J) Shown is the behavior of the time difference between sister chromatid separation and Plo1 removal (Δt) depending on the relative increase in securin (upper panel) or cyclin B level (lower panel) under the assumption of adaptive thresholds. Temporal invariance can only be maintained over a large range of concentrations when the catalytic efficiencies of the APC/C towards securin and cyclin B are similar. (K) Shown are the simulations of securin (green) and cyclin B (blue) degradation in the wild type situation (dashed line) or in response to overexpression of securin (solid lines, left panel) or cyclin B (solid lines, right panel) using the best solution after parameter optimization now including the timing and the securin threshold of sister chromatid separation in the securin overexpression strains. Under these conditions an invariant timing between sister chromatid separation (orange circle) and Plo1

removal (blue circle) can be achieved.

Figure 6: Unbalancing securin and cyclin B degradation disrupts the invariant timing

(A) Single cell measurement for the time difference between sister chromatid separation and Plo1 removal in wild type cells, cells which express reduced level of the APC/C co-activator Cdc20 (*Prad21-slp1+*) or cells carrying the temperature-sensitive mutant allele *cut9-665*. Shown are a Box-Whisker plot (black, the whiskers represent the minimum and maximum value) and the single measurements (grey circles). (B,C) Genetic analyses of crosses between the different securin and cyclin B overexpression strains as indicated and strains, which either carry temperature-sensitive mutant allele *cut9-665* (B) or express reduced level of the APC/C co-activator Cdc20 (*Prad21-slp1+,* C). The colored circles indicate the genotype as shown in the figure legend. Dashed circles additionally indicate spores, which did not form a colony.

Figure 1

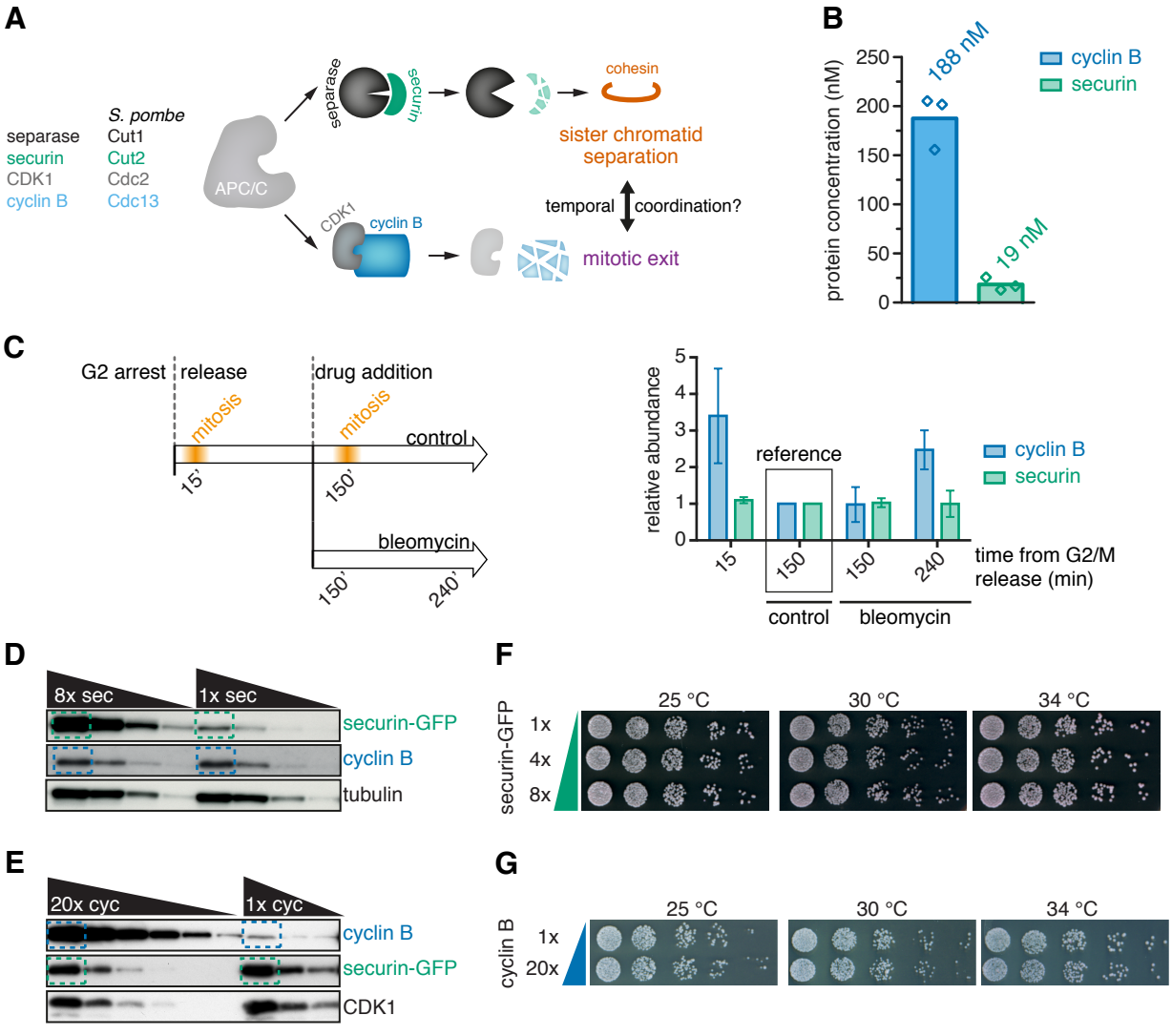
A
S. pombe
separase Cut1
securin Cut2
CDK1 Cdc2
cyclin B Cdc13
APC/C
separase
securin
cohesin
sister chromatid separation
temporal coordination?
CDK1
cyclin B
mitotic exit
B
protein concentration (nM)
250
200
150
100
50
0
188 nM
19 nM
cyclin B
securin
C
G2 arrest
release
drug addition
mitosis
mitosis
control
15'
150'
bleomycin
150'
240'
relative abundance
5
4
3
2
1
0
reference
cyclin B
securin
15
150
150
240
time from G2/M release (min)
control
bleomycin
D
8x sec
1x sec
securin-GFP
cyclin B
tubulin
F
25 °C
30 °C
34 °C
securin-GFP
1x
4x
8x
E
20x cyc
1x cyc
cyclin B
securin-GFP
CDK1
G
25 °C
30 °C
34 °C
cyclin B
1x
20x

Figure 2

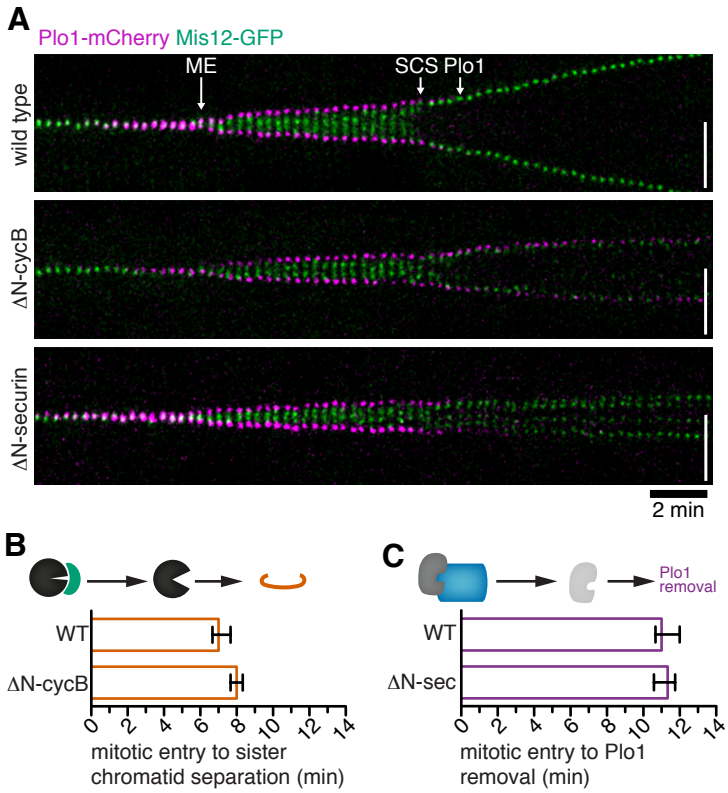
A
Plo1-mCherry Mis12-GFP
ME
SCS Plo1
wild type
ΔN-cycB
ΔN-securin
2 min
B
WT
ΔN-cycB
0 2 4 6 8 10 12 14
mitotic entry to sister chromatid separation (min)
C
Plo1 removal
WT
ΔN-sec
0 2 4 6 8 10 12 14
mitotic entry to Plo1 removal (min)

Figure 3

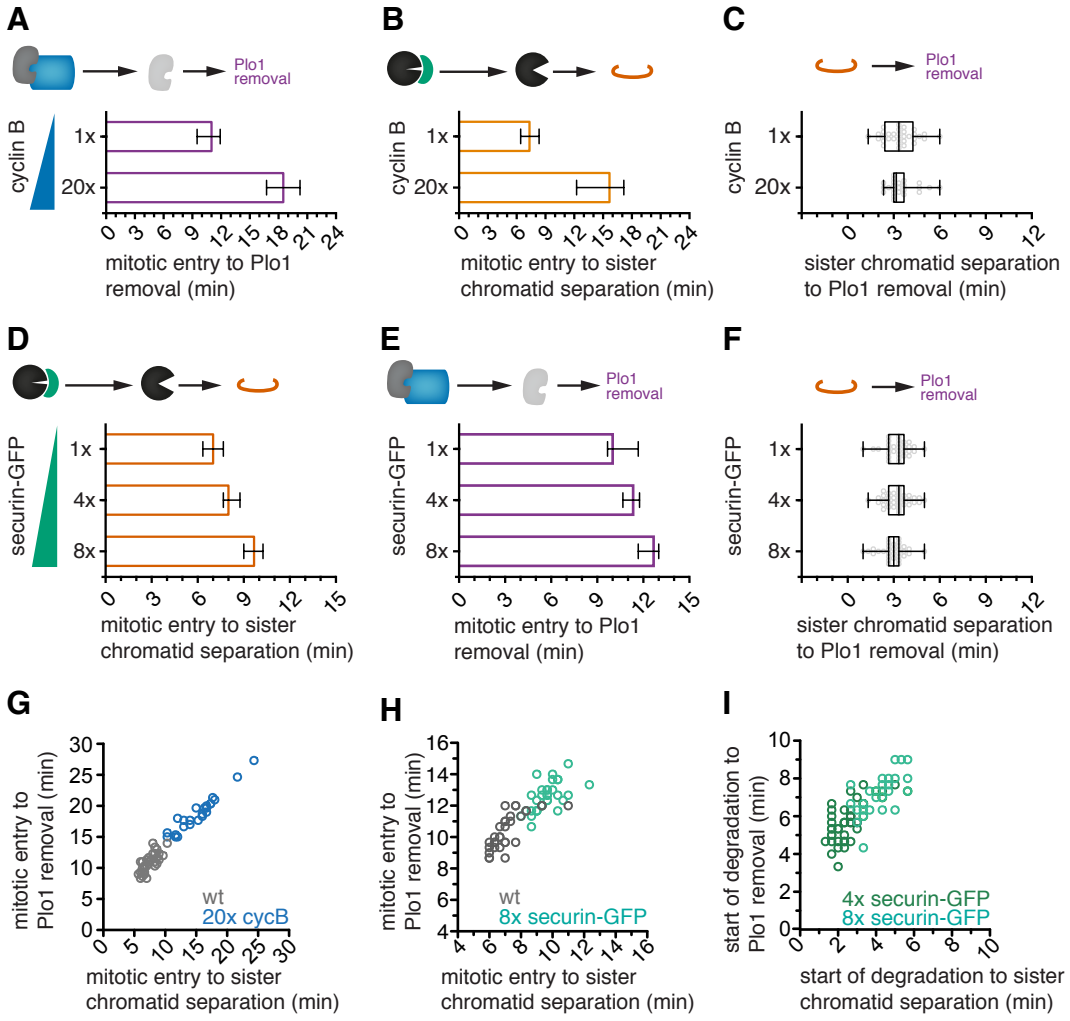
A
Plo1 removal
cyclin B
1x
20x
0 3 6 9 12 15 18 21 24
mitotic entry to Plo1 removal (min)
B
cyclin B
1x
20x
0 3 6 9 12 15 18 21 24
mitotic entry to sister chromatid separation (min)
C
Plo1 removal
cyclin B
1x
20x
0 3 6 9 12
sister chromatid separation to Plo1 removal (min)
D
securin-GFP
1x
4x
8x
0 3 6 9 12 15
mitotic entry to sister chromatid separation (min)
E
Plo1 removal
securin-GFP
1x
4x
8x
0 3 6 9 12 15
mitotic entry to Plo1 removal (min)
F
Plo1 removal
securin-GFP
1x
4x
8x
0 3 6 9 12
sister chromatid separation to Plo1 removal (min)
G
mitotic entry to Plo1 removal (min)
0 5 10 15 20 25 30
wt
20x cycB
mitotic entry to sister chromatid separation (min)
H
mitotic entry to Plo1 removal (min)
4 6 8 10 12 14 16
wt
8x securin-GFP
mitotic entry to sister chromatid separation (min)
I
start of degradation to Plo1 removal (min)
0 2 4 6 8 10
4x securin-GFP
8x securin-GFP
start of degradation to sister chromatid separation (min)

Figure 4

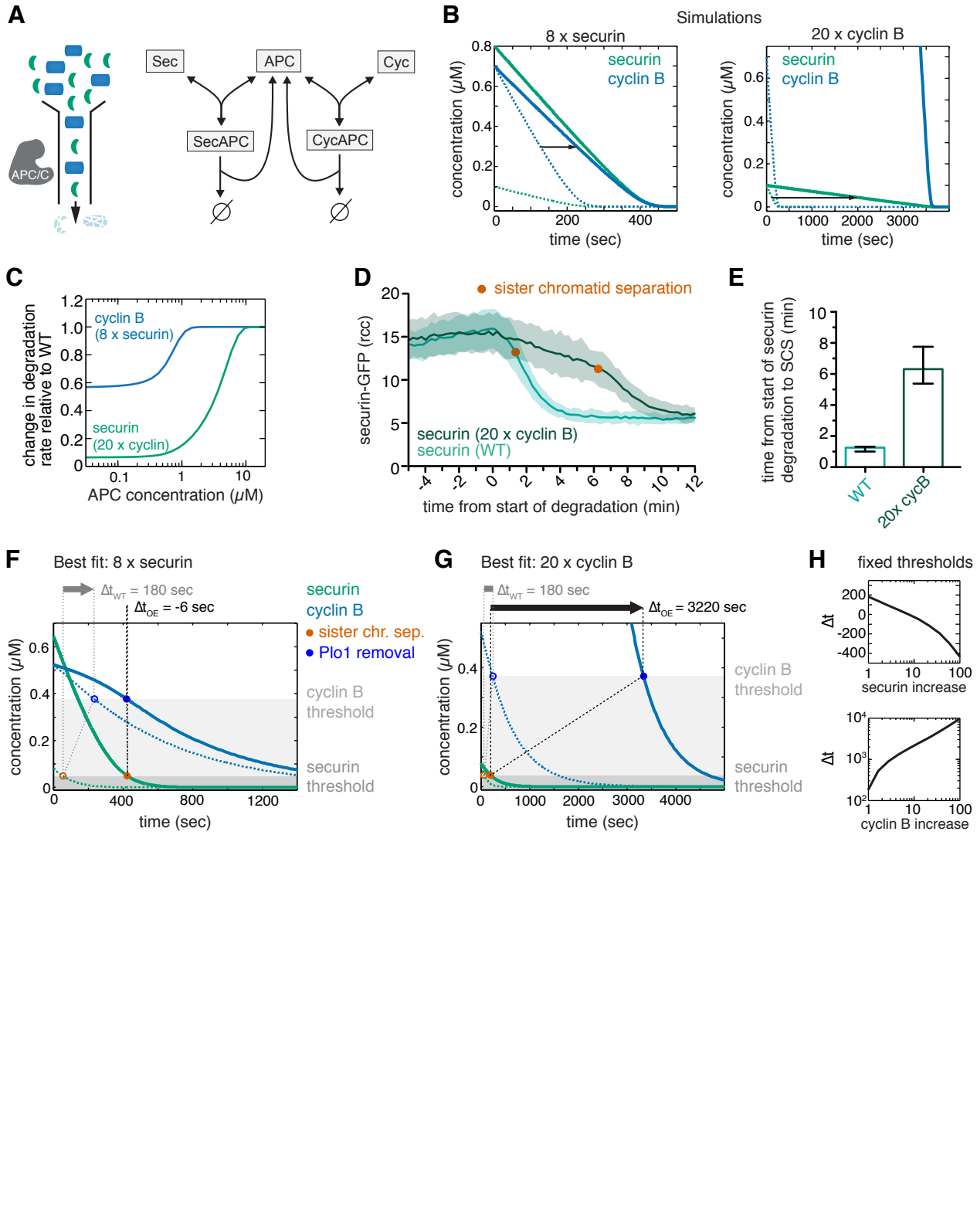
A
APC/C
Sec
APC
Cyc
SecAPC
CycAPC
B
Simulations
8 x securin
20 x cyclin B
securin
cyclin B
concentration (μM)
time (sec)
C
cyclin B
(8 x securin)
securin
(20 x cyclin)
change in degradation rate relative to WT
APC concentration (μM)
D
sister chromatid separation
securin-GFP (rcc)
securin (20 x cyclin B)
securin (WT)
time from start of degradation (min)
E
time from start of securin degradation to SCS (min)
WT
20x cycB
F
Best fit: 8 x securin
Δt_WT = 180 sec
Δt_OE = -6 sec
securin
cyclin B
sister chr. sep.
Plo1 removal
cyclin B threshold
securin threshold
concentration (μM)
time (sec)
G
Best fit: 20 x cyclin B
Δt_WT = 180 sec
Δt_OE = 3220 sec
cyclin B threshold
securin threshold
concentration (μM)
time (sec)
H
fixed thresholds
Δt
securin increase
cyclin B increase

Figure 5

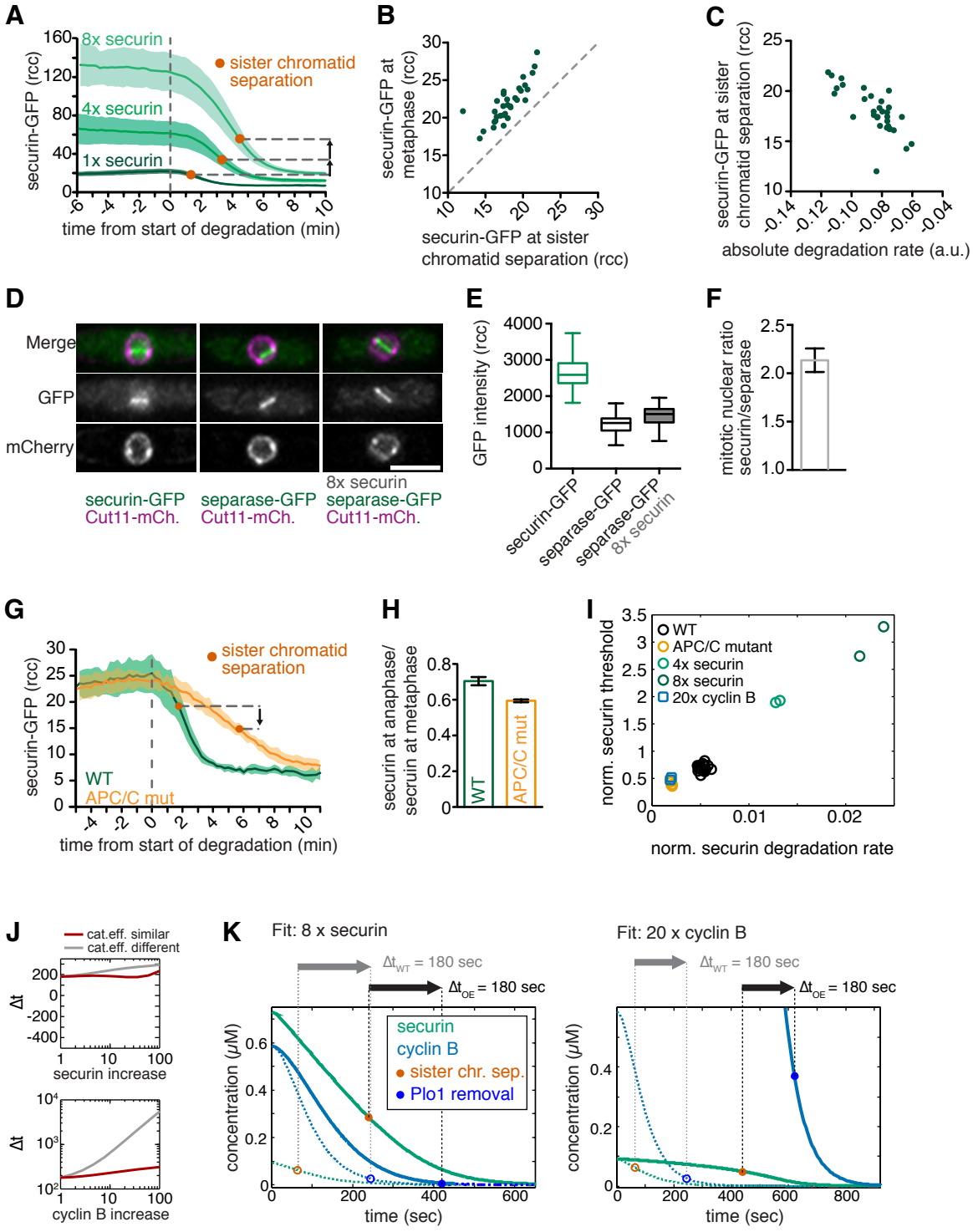
A
8x securin
4x securin
1x securin
sister chromatid separation
securin-GFP (rcc)
time from start of degradation (min)
B
securin-GFP at metaphase (rcc)
securin-GFP at sister chromatid separation (rcc)
C
securin-GFP at sister chromatid separation (rcc)
absolute degradation rate (a.u.)
D
Merge
GFP
mCherry
securin-GFP Cut11-mCh.
separase-GFP Cut11-mCh.
8x securin separase-GFP Cut11-mCh.
E
GFP intensity (rcc)
securin-GFP
separase-GFP
separase-GFP 8x securin
F
mitotic nuclear ratio securin/separase
G
sister chromatid separation
securin-GFP (rcc)
WT
APC/C mut
time from start of degradation (min)
H
securin at anaphase/ secruin at metaphase
WT
APC/C mut
I
WT
APC/C mutant
4x securin
8x securin
20x cyclin B
norm. securin threshold
norm. securin degradation rate
J
cat.eff. similar
cat.eff. different
Δt
securin increase
cyclin B increase
K
Fit: 8 x securin
Fit: 20 x cyclin B
Δt_WT = 180 sec
Δt_OE = 180 sec
securin
cyclin B
sister chr. sep.
Plo1 removal
concentration (μM)
time (sec)

Figure 6

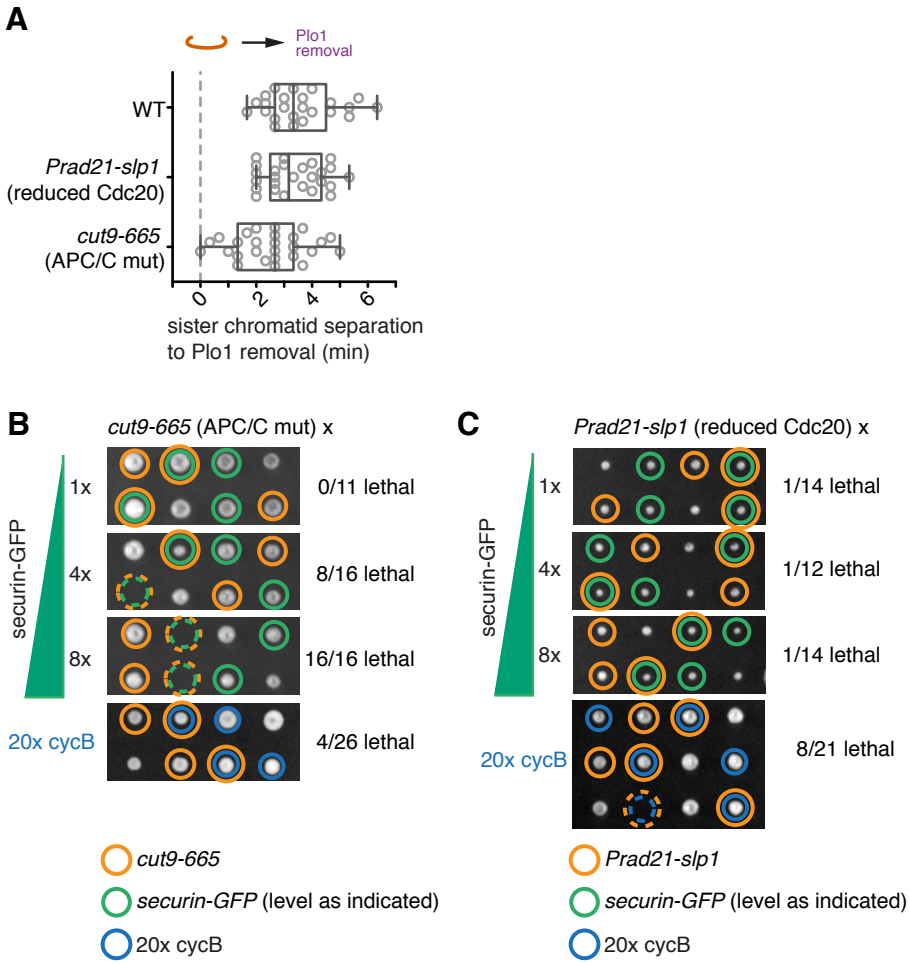
A
Plo1 removal
WT
Prad21-slp1 (reduced Cdc20)
cut9-665 (APC/C mut)
0
2
4
6
sister chromatid separation to Plo1 removal (min)
B
cut9-665 (APC/C mut) x
securin-GFP
1x
4x
8x
20x cycB
0/11 lethal
8/16 lethal
16/16 lethal
4/26 lethal
cut9-665
securin-GFP (level as indicated)
20x cycB
C
Prad21-slp1 (reduced Cdc20) x
securin-GFP
1x
4x
8x
20x cycB
1/14 lethal
1/12 lethal
1/14 lethal
8/21 lethal
Prad21-slp1
securin-GFP (level as indicated)
20x cycB

Figure S1

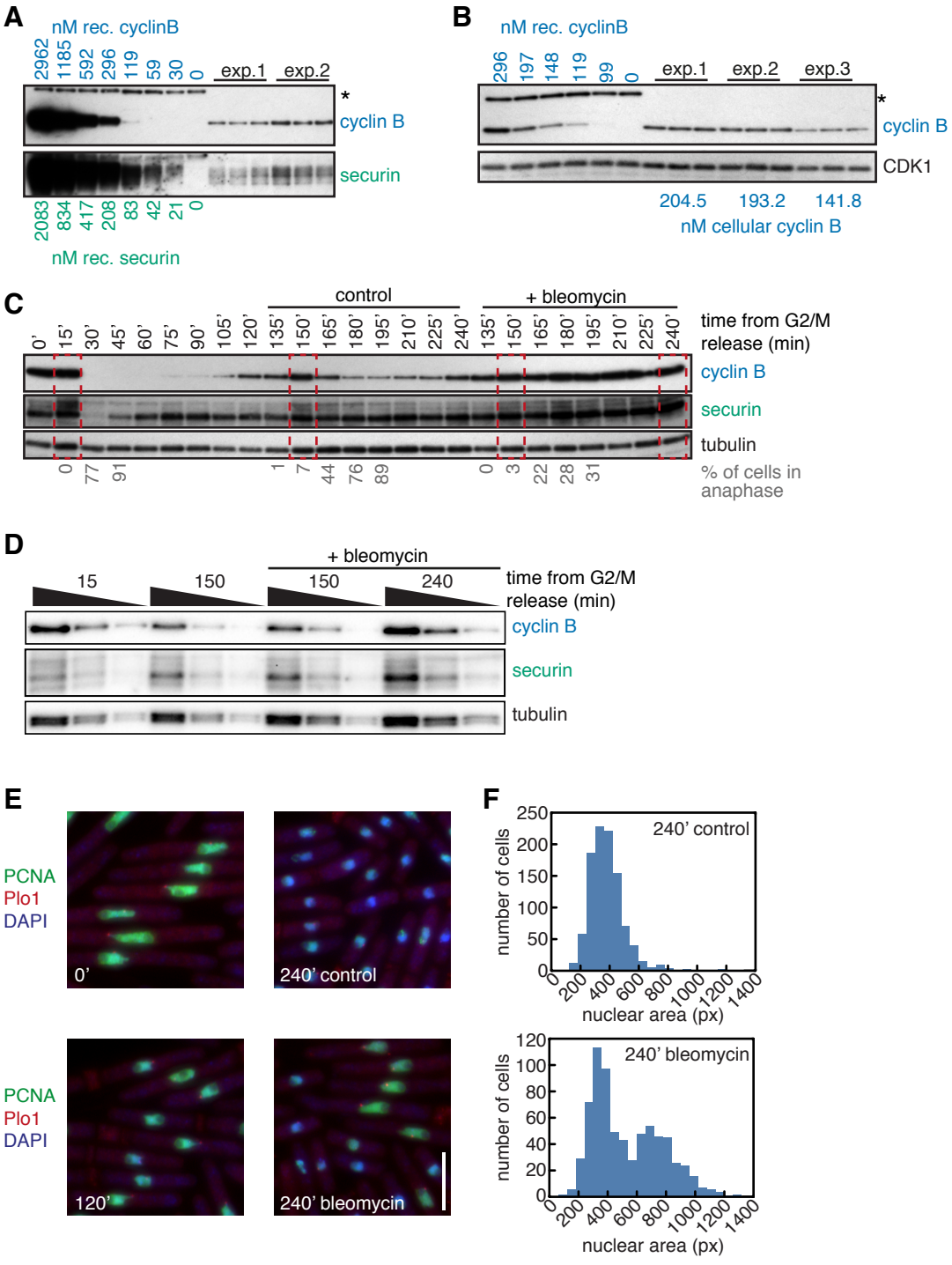
A
nM rec. cyclinB
2962 1185 592 296 119 59 30 0
exp.1 exp.2
*
cyclin B
securin
2083 834 417 208 83 42 21 0
nM rec. securin
B
nM rec. cyclinB
296 197 148 119 99 0
exp.1 exp.2 exp.3
*
cyclin B
CDK1
204.5 193.2 141.8
nM cellular cyclin B
C
control
+ bleomycin
0' 15' 30' 45' 60' 75' 90' 105' 120' 135' 150' 165' 180' 195' 210' 225' 240' 135' 150' 165' 180' 195' 210' 225' 240'
time from G2/M release (min)
cyclin B
securin
tubulin
0 77 91 1 7 44 76 89 0 3 22 28 31
% of cells in anaphase
D
+ bleomycin
15 150 150 240
time from G2/M release (min)
cyclin B
securin
tubulin
E
PCNA
Plo1
DAPI
0'
240' control
PCNA
Plo1
DAPI
120'
240' bleomycin
F
240' control
number of cells
0 50 100 150 200 250
0 200 400 600 800 1000 1200 1400
nuclear area (px)
240' bleomycin
number of cells
0 20 40 60 80 100 120
0 200 400 600 800 1000 1200 1400
nuclear area (px)

Figure S2

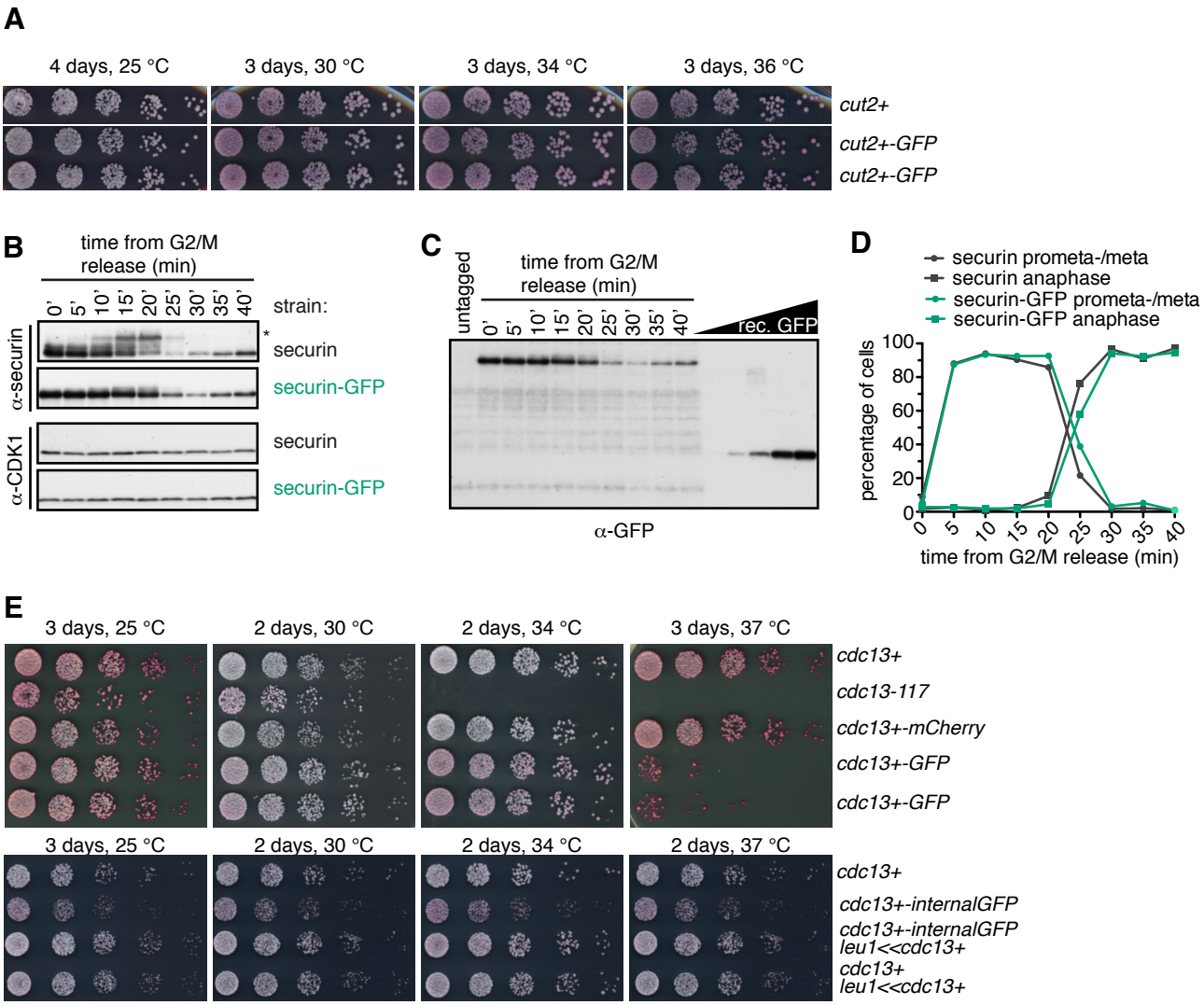
A
4 days, 25 °C
3 days, 30 °C
3 days, 34 °C
3 days, 36 °C
cut2+
cut2+-GFP
cut2+-GFP
B
time from G2/M release (min)
0'
5'
10'
15'
20'
25'
30'
35'
40'
strain:
α-securin
*
securin
securin-GFP
α-CDK1
securin
securin-GFP
C
untagged
time from G2/M release (min)
rec. GFP
α-GFP
D
securin prometa-/meta
securin anaphase
securin-GFP prometa-/meta
securin-GFP anaphase
percentage of cells
time from G2/M release (min)
E
3 days, 25 °C
2 days, 30 °C
2 days, 34 °C
3 days, 37 °C
cdc13+
cdc13-117
cdc13+-mCherry
cdc13+-GFP
cdc13+-GFP
2 days, 37 °C
cdc13+
cdc13+-internalGFP
cdc13+-internalGFP leu1<<cdc13+
cdc13+ leu1<<cdc13+

Figure S3

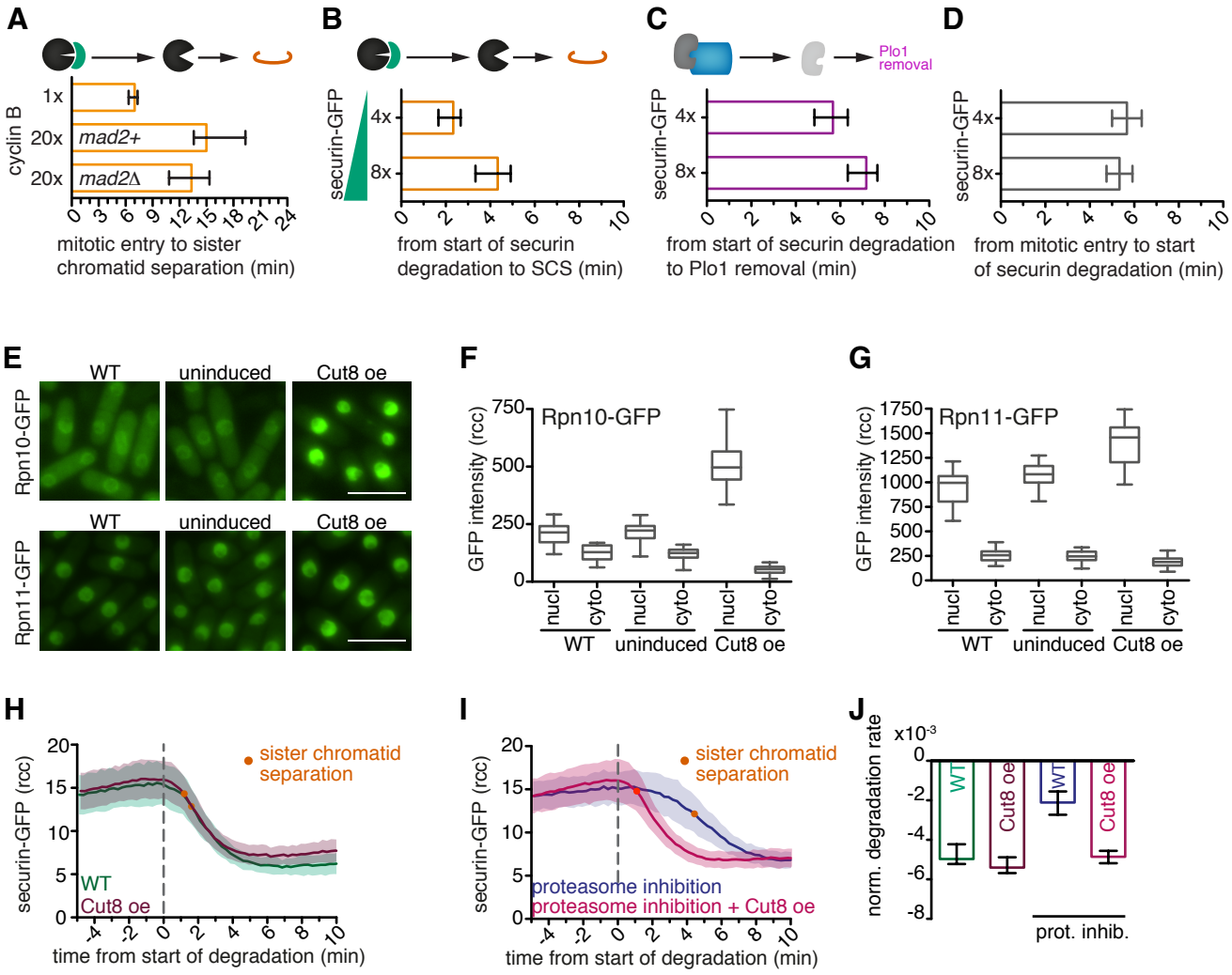
A
B
C
D
cyclin B
1x
20x
mad2+
20x
mad2Δ
mitotic entry to sister chromatid separation (min)
securin-GFP
4x
8x
from start of securin degradation to SCS (min)
Plo1 removal
from start of securin degradation to Plo1 removal (min)
from mitotic entry to start of securin degradation (min)
E
WT
uninduced
Cut8 oe
Rpn10-GFP
Rpn11-GFP
F
Rpn10-GFP
GFP intensity (rcc)
nucl
cyto
WT
uninduced
Cut8 oe
G
Rpn11-GFP
H
securin-GFP (rcc)
sister chromatid separation
WT
Cut8 oe
time from start of degradation (min)
I
proteasome inhibition
proteasome inhibition + Cut8 oe
J
norm. degradation rate
x10-3
prot. inhib.

Figure S4

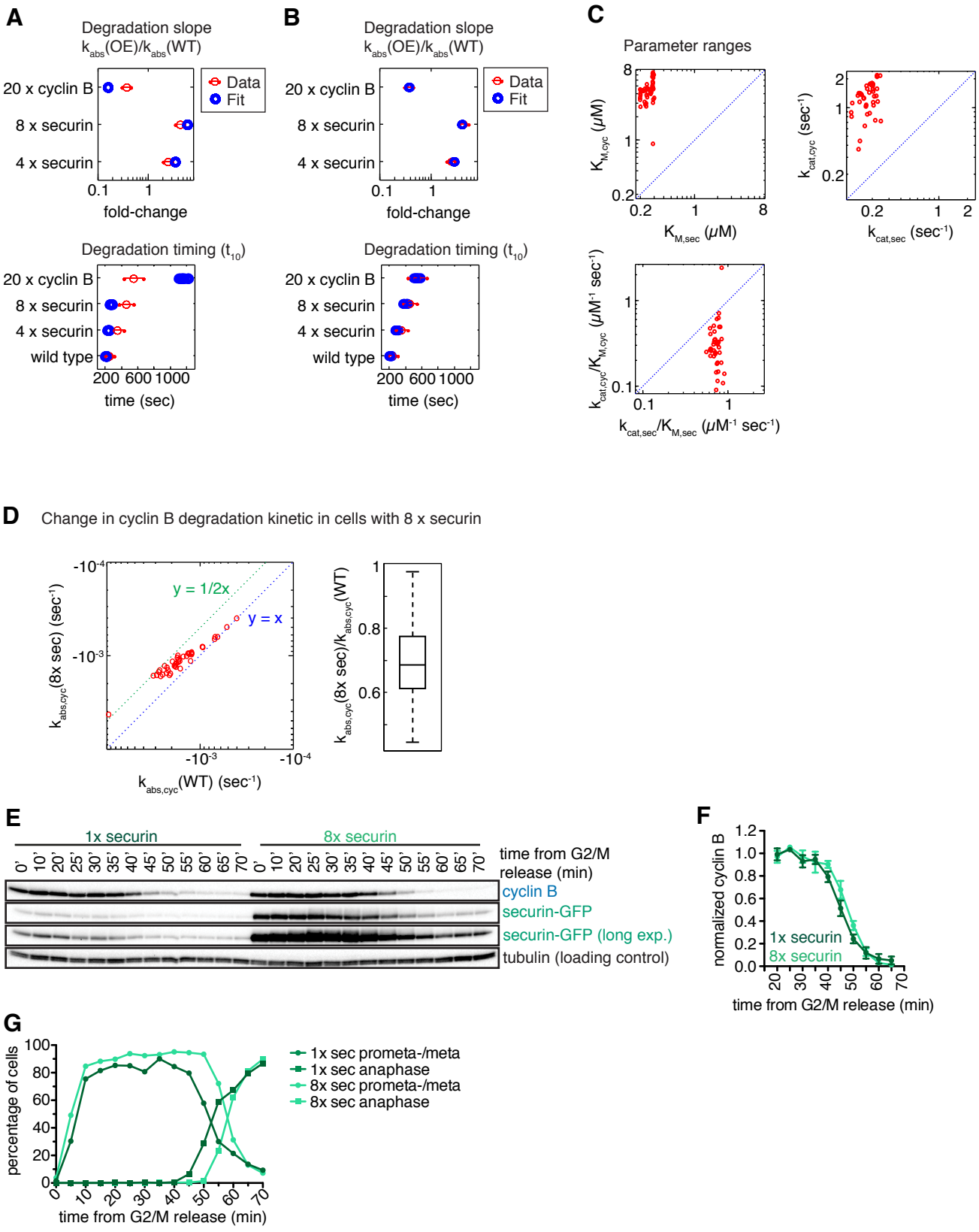
A
Degradation slope
k_{abs}(OE)/k_{abs}(WT)
20 x cyclin B
8 x securin
4 x securin
Data
Fit
0.1
1
fold-change
Degradation timing (t_{10})
wild type
200 600 1000
time (sec)
B
C
Parameter ranges
$K_{M,cyc}$ (μM)
$K_{M,sec}$ (μM)
$k_{cat,cyc}$ (sec^{-1})
$k_{cat,sec}$ (sec^{-1})
$k_{cat,cyc}/K_{M,cyc}$ (μM^{-1} sec^{-1})
$k_{cat,sec}/K_{M,sec}$ (μM^{-1} sec^{-1})
D
Change in cyclin B degradation kinetic in cells with 8 x securin
y = 1/2x
y = x
$k_{abs,cyc}$(8x sec) (sec^{-1})
$k_{abs,cyc}$(WT) (sec^{-1})
$k_{abs,cyc}$(8x sec)/$k_{abs,cyc}$(WT)
E
1x securin
8x securin
time from G2/M release (min)
cyclin B
securin-GFP
securin-GFP (long exp.)
tubulin (loading control)
F
normalized cyclin B
1x securin
8x securin
time from G2/M release (min)
G
percentage of cells
time from G2/M release (min)
1x sec prometa-/meta
1x sec anaphase
8x sec prometa-/meta
8x sec anaphase

Figure S5

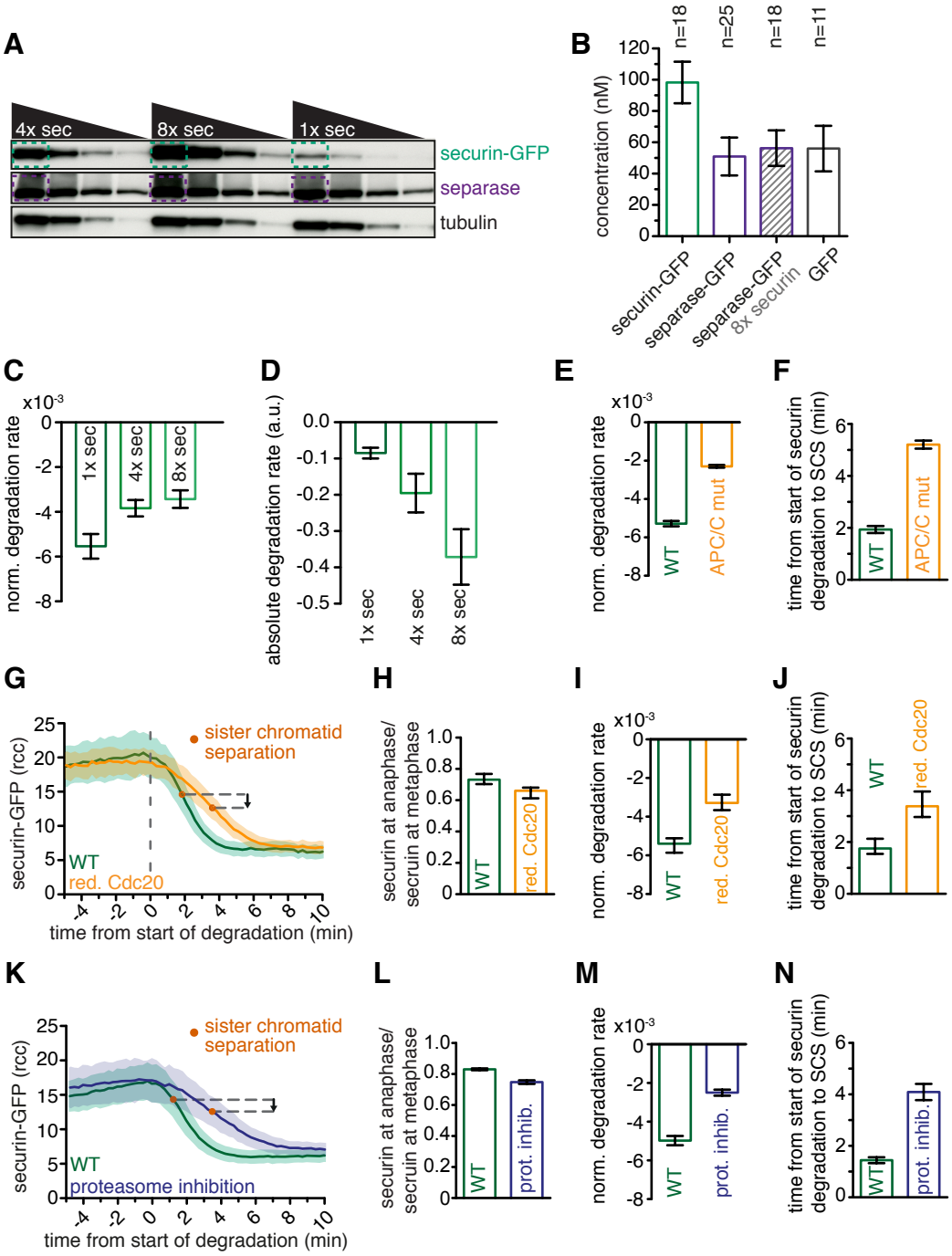
A
4x sec
8x sec
1x sec
securin-GFP
separase
tubulin
B
n=18
n=25
n=18
n=11
concentration (nM)
securin-GFP
separase-GFP
separase-GFP 8x securin
GFP
C
norm. degradation rate
1x sec
4x sec
8x sec
D
absolute degradation rate (a.u.)
E
norm. degradation rate
WT
APC/C mut
F
time from start of securin degradation to SCS (min)
G
securin-GFP (rcc)
sister chromatid separation
WT
red. Cdc20
time from start of degradation (min)
H
securin at anaphase/ secruin at metaphase
I
norm. degradation rate
J
time from start of securin degradation to SCS (min)
K
securin-GFP (rcc)
sister chromatid separation
WT
proteasome inhibition
time from start of degradation (min)
L
securin at anaphase/ secruin at metaphase
prot. inhib.
M
norm. degradation rate
N
time from start of securin degradation to SCS (min)

Supplementary Information for

Properties of the degradation machinery ensure temporal coupling during anaphase

by Julia Kamenz, Tamara Mihaljev, Armin Kubis, Stefan Legewie and Silke Hauf

Contents

Supplementary Figure Legends

Figure S1. Abundance of securin and cyclin B, related to Figure 1

(A) Quantification of securin and cyclin B from cell extracts of independently, asynchronously grown cell cultures in rich medium. Each cell extract was loaded in three replicates. Recombinant securin and cyclin B of defined concentrations were used as standards and were mixed into a cell extract from cells expressing securin and cyclin B as larger GFP or mCherry-fusion proteins, respectively. Proteins were detected by immunoblotting using antibodies against cyclin B (Cdc13) and securin (Cut2). The asterisk indicates the detection of the Cdc13-mCherry fusion protein in the cell extract of the standard. (B) Quantification of cyclin B as described in (A) from three independently grown cultures, but with a narrower concentration range for the recombinant protein. A summary of the quantification for securin in (A) and cyclin B in (B) are shown in Figure 1 B. (C) Immunoblot analysis of the protein abundances of securin and cyclin B during cell cycle progression after cells had been arrested at the G2/M transition using the temperature-sensitive *cdc25-22* allele. At 120 min, before cells entered the second mitosis, the culture was split and bleomycin was added to one of the cultures (see Figure 1C). For better quantification, cell extracts of the relevant time points (red, dashed rectangles) were reloaded as dilution series and analyzed by immunoblotting as shown in (D). Quantifications are shown in Figure 1C. (E) Microscopy images of cells from the time course experiment shown in (C). Cells were fixed with methanol and the DNA was stained with 4',6-diamidino-2-phenylindole (DAPI). Note the population of cells with large nuclei in the bleomycin-treated sample at 240 min, which indicates that a fraction of the cells did not undergo a second mitosis. (F) Analysis of the nuclear sizes within a cell population 240 min after release from G2/M arrest, with or without bleomycin treatment, as shown in (E). The nuclear area was defined using the PCNA-GFP signal.

Figure S2. Functionality tests for securin(Cut2)-GFP and cyclin B(Cdc13)-GFP

(A) Growth assays on rich medium and at the indicated temperature for a wild type strain and strains expressing the fluorescent fusion protein securin-GFP from the endogenous genomic locus. Cells have been grown on the same culture plate. (B) Cells expressing securin or securin-GFP were synchronized using the temperature-sensitive *cdc25-22*

allele and securin or securin-GFP degradation kinetics were followed by immunoblotting of the cell extracts from different time points after release from the arrest. No obvious delay in the degradation of the GFP-fusion protein was detected. The asterisk indicates the hyper-phosphorylated form of securin in mitosis (Kumada et al., 1998). The mobility shift is not as prominent for securin-GFP, most likely because of the increased size of the fusion protein. (C) Immunoblot for the cell extract from securin-GFP expressing cells as described in (B) but now probed with a GFP-antibody. Recombinant GFP (rec. GFP) was loaded for better comparison. No free GFP or smaller securin-GFP fragments could be detected in the extract during degradation. (D) Quantification of the mitotic progression for the synchronized cell cultures shown in (B,C). Prometaphase and metaphase was judged by the localization of Plo1-mCherry to the spindle pole bodies and a single DNA mass, anaphase was judged by the presence of two separated DNA masses. (E) Growth assays on rich medium and at the indicated temperature for a wild type strain, the temperature-sensitive *cdc13-117* strain and for strains expressing different fluorescent fusion proteins of cyclin B (Cdc13). Cdc13 was either tagged C-terminally with GFP or mCherry or internally between amino acid 224 and 225 with a circular permutated version of GFP (Baird et al., 1999; Tallini et al., 2006). The growth defect of the internally tagged Cdc13 version could be rescued by expressing *cdc13+* from an exogenous locus (*leu1<<cdc13+*).

Figure S3. The time between sister chromatid segregation and Plo1 removal is unaffected by variations of the securin to cyclin B ratio, related to Figure 3

(A) The mitotic delay observed in strains overexpressing cyclin B is largely independent of the spindle assembly checkpoint. Quantification of the time from mitotic entry to sister chromatid separation within single cells expressing endogenous levels of cyclin B (n=25), overexpressing cyclin B 20-times (n=14) or cells, where the mitotic checkpoint gene *mad2+* was deleted (*mad2Δ)* in addition to overexpressing cyclin B 20-times (n=25). Shown are the median (bar graph) and the interquartile range (error bars). (B-D) The time from the start of securin-GFP degradation to sister chromatid separation (B) or Plo1 removal (C) was quantified in single cells overexpressing securin-GFP 4-times or 8-times, respectively. The time from mitotic entry until the start of securin degradation does not increase with increasing securin-GFP expression (D). Shown are the median (bar

graph) and the interquartile range (error bars). Measurements were not possible for strains, which expressed securin-GFP from the endogenous promoter, because in this strain the securin-GFP signal was not sufficiently above the additional Mis12-GFP signal to allow reliable quantification. (E) Overexpression of the proteasome-associated protein Cut8 increases the nuclear concentration of proteasome subunits. Representative images of strains expressing GFP-fusion proteins of the proteasome subunits Rpn10 or Rpn11 in a wild type strain, before (uninduced) or after induction of the exogenous expression of Cut8-FLAG2 (Cut8 oe). Only images of strains expressing the same GFP-fusion protein are scaled the same (generally Rpn10-GFP seems to be expressed more weakly). Horizontal scale bar, 10 μm. (F, G) Quantification of the nuclear (nucl) and cytoplasmic (cyto) GFP intensities (in raw camera counts, rcc) for the strains shown in (E). 30 cells were quantified for each condition. Shown are Box-Whisker plots (the whiskers represent the minimum and maximum value). (H-J) Overexpression of Cut8-FLAG2 does not show a strong impact on the overall degradation kinetic of securin-GFP, but rescues the effect of proteasome inhibitor treatment. Securin-GFP degradation was followed by live cell imaging in wild type cells or after induction of Cut8-FLAG2 overexpression in the absence (H) or presence (I) of 10 μM of the proteasome inhibitor Bortezomib/Velcade. In (H): n(WT)= 19, n(Cut8 oe)=18, in (I): n(WT)=25, n(Cut8 oe)=29. The individual time courses of securin-GFP intensity (in raw camera counts, rcc) were aligned to sister chromatid separation and the time axis of the averaged time courses was shifted so that 0 min reflects the average time of the start of securin degradation. Shown is the average (solid line) +/- standard deviation of the cell population (filled area). Quantification of the normalized degradation rate is shown in (J) with the median (bar graph) and the interquartile range (error bars).

Figure S4. Substrate-specific degradation parameters need to be assumed to quantitatively describe the competition data, related to Figure 4

(A) Failure of the competition model (Fig. 4A, Eq. 1) to fit the securin degradation dynamics under the assumption of the same enzyme kinetic parameters for cyclin B and securin. The model was fitted to securin degradation slope changes in response to securin or cyclin B overexpression ($k_{abs}(OE)/k_{abs}(WT)$) and to the time at which securin was degraded to 10% of its initial value (t_{10}) as described in the Supplementary Note.

Red error bars indicate experimentally observed ranges, while blue circles indicate the simulation results for the 12 best fits obtained using a local multistart optimization strategy. (B) Improved model fit under the assumption of substrate-specific enzyme kinetic parameters. Representation similar to (A). Modified assumptions about parameter ranges are described in detail in the Supplemental Text. Blue circles show simulation results for the 40 best fits with a similar goodness-of-fit. (C) According to our fits, cyclin B is predicted to be a low-affinity substrate for the APC/C when compared to securin ($K_{M,Cyc} > K_{M,Sec}$), but ubiquitinylated with a higher catalytic rate constant ($k_{cat,Cyc} > k_{cat,Sec}$). Scatter plots show K_M, k_{cat} and k_{cat}/K_M of securin (x-axis) and cyclin (y-axis) for the top 40 fits of a local multi-start optimization (described in B). (D) Securin overexpression is predicted to only moderately shift the cyclin B degradation kinetics. Red circles show the degradation slopes of the top 40 fits (described in B) in wt (x-axis) and 8x securin overexpression conditions. All shifts are close to the intercept (dashed black line), and result in a less than two-fold change (dashed green line), as also indicated in the boxplot of the k_{abs}-ratio distribution of all fits (right). (E) Cells expressing securin or overexpressing securin to 8-times the wild type level were synchronized using the temperature-sensitive *cdc25-22* allele and securin and cyclin B degradation kinetics were followed by immunoblotting of the cell extracts from different time points after release from the arrest to 20 °C. For better comparison a short and a long-exposure (long exp.) of the detection using the anti-securin (anti-Cut2) antibody is shown. No obvious attenuation of the cyclin B degradation was detected. (F) Quantification of 3 reloads from the experiment shown in (E). Measurements of the single reloads were normalized to the 20 min time point. Shown is mean (filled circles) and standard deviation (error bars). The 25 min sample was only reloaded twice. (G) Quantification of mitotic stages of the experiment shown in (E). Prometaphase and metaphase was judged by the localization of Plo1-mCherry to the spindle pole bodies and a single DNA mass, anaphase was judged by the presence of two separated DNA masses.

Figure S5. An enzyme competition model with appropriate threshold shifts can create temporal invariance, related to Figure 5

(A) Overexpression of securin-GFP does not increase cellular separase level. Immunoblot of strains expressing securin-GFP from the endogenous promoter or

overexpressing securin-GFP to 4- or 8-times the wild type level, respectively. For the detection of separase, separase was fused to a 13xmyc epitope and detected with an antibody against the Myc moiety. Parts of the immunoblot have also been shown in Figure 1D and in (Kamenz and Hauf, 2014). (B) Relative nuclear protein abundances of the indicated GFP-fusion proteins and free GFP expressed from the *mad3* promoter were determined using wide-field fluorescence deconvolution microscopy. Previously, the absolute nuclear concentration for free GFP in this strain had been determined to be 56 nM (Heinrich et al., 2013) and all other values were calculated relative to this value. Shown are mean (bar graph) and standard deviation (error bars) of the single cell measurements. (C,D) Normalized and absolute securin-GFP degradation rate measured in single cells for securin-GFP and the securin-GFP overexpressions in Figure 5A. Shown is the mean of the single cell measurements (bar graph) and the standard deviation (error bars). (E,F) Quantification of the securin-GFP degradation rate and the time from the start of degradation to sister chromatid separation in the wild type and the strain carrying the temperature-sensitive allele of the APC/C subunit APC6 (*cut9-665*). Shown are the mean (bar graph) and the standard error of the mean (error bars) for 3 (wild type) and 5 (APC/C mutant) independent experiments. (G-J) A strain, which exhibits a reduced expression of the APC/C co-activator Cdc20 (*Prad21-slp1+*) behaves similarly to the *cut9-665* mutant. (G) Securin-GFP degradation was followed by live cell imaging in wild type cells (n=17) or cells with reduced Cdc20 expression (n=22). The individual time courses of securin-GFP intensity (in raw camera counts, rcc) were aligned to sister chromatid separation and the time axis of the averaged time courses was shifted so that 0 min reflects the average time of the start of securin degradation. Shown is the average (solid line) +/- standard deviation of the cell population (filled area). The relative amount of securin at the time of sister chromatid separation (H), the normalized degradation rates (I) and the time from start of securin degradation to sister chromatid separation (J) were measured for the experiment in (G). For each quantification median (bar graph) and interquartile range (error bars) are shown. (K-N) Attenuating securin-GFP degradation by partial inhibition of the proteasome causes a threshold shift similar to the one observed in the APC/C mutants. (K) Securin-GFP degradation was followed by live cell imaging after addition of DMSO (WT, n=41) or 10 μM of the proteasome inhibitor Bortezomib/Velcade (n=27). The individual time courses of securin-GFP intensity (in raw camera counts, rcc) were aligned as described in (G). Shown is the

average (solid line) +/- standard deviation of the cell population (filled area). The relative amount of securin at the time of sister chromatid separation (L), the normalized degradation rates (M) and the time from start of securin degradation to sister chromatid separation (N) were measured for single cells. For each quantification the mean (bar graph) and the standard error of the mean (error bars) from three independent experiments is shown.

Supplementary experimental information

Construction of a strain expressing Cdc13 as an internally, fluorescently labeled fusion protein

To replace the endogenous genomic copy of *cdc13+* by a version, which carried an insertion of the circular permutated GFP (Baird et al., 1999; Tallini et al., 2006) between amino acids 224 and 225 (located in an unstructured loop), we first integrated a second copy of *cdc13+* into the *leu1* locus of a strain carrying the recessive cycloheximide-resistant allele *rpl42::cyhR(sP56Q)* (Roguev et al., 2007). We next deleted the endogenous open reading frame of *cdc13+* by replacing it with the hygromycin-resistance and a cycloheximide-sensitive (*cyh^S*) allele, and subsequently replaced this resistance cassette by the *cdc13-internalGFP* construct selecting for cycloheximide resistance. The second copy of *cdc13+* at the *leu1* locus was then crossed out.

Overexpression of the proteasome-associated protein Cut8-FLAG2

For inducible overexpression of the proteasome-associated protein Cut8 fused to a FLAG2 epitope, the *cut8+* open reading frame was subcloned into the pDual-HFF vector (Matsuyama et al., 2006; Matsuyama et al., 2004) under the control of the *nmt1*-promotor and integrated into the *leu1* locus. Expression of *cut8-FLAG2* was repressed by the addition of 16 μM of thiamine to the medium and was induced by growing strains for 15 hours in minimal medium (EMM) without thiamine. For the quantification of the nuclear abundance of the proteasome subunits Rpn10 and Rpn11 fused to GFP, strains were grown in the absence or presence of thiamine. To correct for cellular autofluorescence, the strains were mixed with a strain expressing *cut11+-mCherry*, but not expressing GFP, prior to imaging. Images of living cells were taken with an

AxioImager M1 microscope (Zeiss) using a 63x/1.4 Plan Apochromat oil objective (Zeiss) driven by a Piezo motor. A z-stack of 14 planes spaced by 0.3 μm was acquired, the 4 most out-of-focus planes discarded and a sum projection of the stack calculated. A nuclear and a cytoplasmic region of interest (ROI) were defined for single cells and the mean average intensity for each ROI calculated. For each acquired picture the same number of cells not expressing a GFP fusion protein were measured and the mean cytoplasmic or nuclear intensity was subtracted from the single measurements of the cells expressing Rpn10- or Rpn11-GFP respectively.

Modeling of the dynamics of protein pools competing for a shared degradation machinery

Numerical modeling of substrate competition for the APC

***Model description*:** The model with enzyme competition is depicted in Figure 4A. Securin (Sec) and Cyclin B (Cyc) compete for binding to the APC/C (APC). The APC/C may be strongly sequestered in the enzyme-substrate complexes (SecAPC and CycAPC) if the APC concentration is much lower than the substrate concentration(s). Under these conditions, the degradation dynamics are not independent, but tightly coupled.

The differential equations describing this scenario are given by (1)

$$\frac{dSec}{dt} = -k_{on,SecAPC} \cdot Sec \cdot (APC_{tot} - SecAPC - CycAPC) + k_{off,SecAPC} \cdot SecAPC$$

$$\frac{dCyc}{dt} = -k_{on,CycAPC} \cdot Cyc \cdot (APC_{tot} - SecAPC - CycAPC) + k_{off,CycAPC} \cdot CycAPC$$

$$\frac{dSecAPC}{dt} = k_{on,SecAPC} \cdot Sec \cdot (APC_{tot} - SecAPC - CycAPC) - (k_{off,SecAPC} + k_{cat,SecAPC}) \cdot SecAPC$$

$$\frac{dCycAPC}{dt} = k_{on,CycAPC} \cdot Cyc \cdot (APC_{tot} - SecAPC - CycAPC) - (k_{off,CycAPC} + k_{cat,CycAPC}) \cdot CycAPC$$

The free APC species was not described explicitly, and enters the differential equations only in the form of the mass conservation relation APC = APC_{tot} - SecAPC - CycAPC, where APC_{tot} is the total active APC/C concentration.

***Numerical simulations*:** The ODE system in Eq. 1 was integrated numerically to generate the panels in Figure 4B. In the initial conditions, it was assumed that the active APC/C concentration was zero ($APC_{tot}(0) = 0$), and that no enzyme-substrate complexes exist (SecAPC(0) = 0, CycAPC(0) = 0). Consequently, all securin and cyclin B were assumed to be present in the free forms (Sec(0) = 0.1 μM and Cyc(0) = 0.7 μM). Anaphase was simulated by assuming a step-like increase in the total APC/C concentration from $APC_{tot}(0) = 0$ to APC_{tot}= 0.02 μM.

***Qualitative analysis of the model*:** The model was initially simulated with parameters derived from the literature and assuming the same enzyme kinetic parameters for securin and cyclin B degradation to determine at which range of APC/ concentrations

enzyme competition may be relevant (Figure 4B and C). The following parameters were assumed in Fig. 4B and C: Sec(0)= 0.1 μM; Cyc(0) = 0.1 μM; APC_{tot} = 0.02 μM (Figure 4 B) or APC_{tot} varied (Figure 4C); $k_{on,SecAPC} = k_{on,CycAPC}$ = 4 μM^{-1} sec^{-1}; $k_{off,SecAPC} = k_{off,CycAPC}$ = 0.01 sec^{-1}; $k_{cat,SecAPC} = k_{cat,CycAPC}$ = 0.01 sec^{-1}.

***Model fitting*:** The parameters in Eq. 1 were subsequently estimated by fitting the model simulations to experimental data (Figures 4D and 5A). Optimization was done using a multi-start local optimization strategy: 10^6 initial parameter vectors were generated within defined parameter boundaries using Latin-hypercube sampling. Local optimization of each starting parameter set was performed using a deterministic Trust-region optimization in the Matlab Optimization Toolbox (lsqnonlin). Fitting was done by minimizing the following cost function (2)

$$C = \sum_{i=1}^{N} \frac{1}{2}(t_i + |t_i|)$$

where (3)

$$t_i = |m_i - d_i| - r_i$$

This cost function is zero as long as $t_i < 0$, and increases linearly with t_i otherwise. t_i is negative if the model simulation m_i lies within a range r_i around the mean measurement value d_i. Hence, a deviation between model and mean measurement is not punished unless it exceeds the range r_i. This optimization strategy accommodates that single-cell measurements at different days gave qualitatively similar, but quantitatively different results for degradation dynamics (and, further below, for absolute SCS and Plo1 timing). Based on the variations between different days, we define reasonable ranges for the measured quantities, and performed a semi-quantitative model fitting over all N measurements.

***Model fitting to degradation dynamics*:** As shown in Supplementary Figure 4A and 4B, the model in Eq. 1 was fitted to degradation slope changes in response to securin or cyclin B overexpression (k_{abs}(OE)/k_{abs}(WT)) and to the time at which securin was degraded to 10% of its initial value (t_{10}). In Supplementary Figure 4A, we assumed the same enzyme kinetic parameters for the degradation reactions of securin and cyclin B, while different kinetics were allowed in Supplementary Figure 4B. The parameter ranges allowed during fitting and best-fit parameter values are given in Table S1. The blue

circles in in Supplementary Figure 4A and 4B show the goodness-of-fit for multiple fits obtained from local multi-start optimization.

The best-fit time courses of the model with substrate-specific degradation parameters are shown in Figure 4F and 4G, and the simulation results in Figure 4H were also generated using this best-fit model. The parameter values of the best 40 fits with substrate-specific degradation parameters obtained from local multi-start optimization are shown in Supplementary Figure 4C. The simulation results in Supplementary Figure 4D was also generated using these top 40 fits (red circles).

Parameter	**Unit**	**Range (Fig. S4A)**	**Best-fit (Fig. S4A)**	**Range (Fig. S4B)**	**Best-fit (Fig. 4B)**
[APC]	μM	0.016-0.024	0.018	0.016-0.024	0.019
[Sec(0)]	μM	0.08-1.2	0.11	0.08-1.2	0.08
[Cyc(0)]	μM	6-10x [Sec(0)]	6x [Sec(0)]	6-10x [Sec(0)]	6.49x [Sec(0)]
$k_{on,SecAPC}$	μM^{-1} sec^{-1}	1-100	1.17	1-100	1.05
$k_{off,SecAPC}$	sec^{-1}	0.01-1	0.22	0.01-1	0.064
$K_{cat,SecAPC}$	sec^{-1}	0.01-1	0.67	0.01-1	0.14
$k_{on,CycAPC}$	μM^{-1} sec^{-1}	fixed	= $k_{on,SecAPC}$	= 0.1-10x $k_{on,SecAPC}$	= 0.17x $k_{on,SecAPC}$
$k_{off,CycAPC}$	sec^{-1}	fixed	= $k_{off,SecAPC}$	= 0.1-10x $k_{off,SecAPC}$	= 5.8x $k_{off,SecAPC}$
$K_{cat,CycAPC}$	sec^{-1}	fixed	= $k_{cat,SecAPC}$	= 0.1-10x $k_{cat,SecAPC}$	= 2.57x $k_{cat,SecAPC}$

Table S1: Parameter ranges and best-fit parameter values for fitting to securin degradation dynamics

***Model fitting to degradation, SCS and Plo1 relocalization dynamics*:** We asked whether a competition model would be at the same time consistent with the degradation dynamics of securin (k_{abs}(OE)/k_{abs}(WT) and t_{10}) and with the timing of SCS as well as Plo1 relocalization. To this end, we extended our competition model with substrate-specific enzyme kinetic parameters by the additional assumption that SCS happens at the experimentally measured threshold levels in the wild type and overexpression conditions (Figure 5I). Plo1 removal was presumed to occur three minutes later to ensure temporal invariance under all experimental conditions. In this way, we could fit

the SCS and Plo1 timing to the corresponding experimental data (Figure 5K).

The fits were slightly better (compared to the model given by Eq. 1) if we added a proteasomal degradation step after APC-mediated ubiquitination. Such a two-step mechanism is likely to occur, because the kinetics of proteasomal degradation according to the literature (Luciani et al., 2005) are comparable to the time-scale of securin degradation in our experiment, implying that ubiquitination may not be the single rate-limiting step.

The differential equations corresponding to the model with proteasome degradation are given by (4)

$$\frac{dSec}{dt} = -k_{on,SecAPC} \cdot Sec \cdot (APC_{tot} - SecAPC - CycAPC) + k_{off,SecAPC} \cdot SecAPC$$

$$\frac{dCyc}{dt} = -k_{on,CycAPC} \cdot Cyc \cdot (APC_{tot} - SecAPC - CycAPC) + k_{off,CycAPC} \cdot CycAPC$$

$$\frac{dSecAPC}{dt} = k_{on,SecAPC} \cdot Sec \cdot (APC_{tot} - SecAPC - CycAPC) - (k_{off,SecAPC} + k_{cat,SecAPC}) \cdot SecAPC$$

$$\frac{dCycAPC}{dt} = k_{on,CycAPC} \cdot SecSep \cdot (APC_{tot} - SecAPC - CycAPC) - (k_{off,CycAPC} + k_{cat,CycAPC}) \cdot CycAPC$$

$$\frac{dSecU}{dt} = k_{cat,SecAPC} \cdot SecAPC - k_{Prot,Sec} \cdot SecU$$

$$\frac{dCycU}{dt} = k_{cat,CycAPC} \cdot CycAPC - k_{Prot,Cyc} \cdot CycU$$

We employed a local multi-start optimization strategy using the cost function described in Eq. 2 to fit this model to the data. The model was able to quantitatively fit securin degradation dynamics as before, but also correctly described the absolute timing of SCS and Plo1 removal (Figure 5K). The relationship between the securin thresholds and the securin degradation slope in the model was indistinguishable from the experimental data in Figure 5I (not shown). This further supports our hypothesis that enzyme competition combined with appropriate threshold shifts quantitatively accounts for temporal invariance. The time courses of the best-fit solution are shown in Fig. 5K, and the parameter values are listed in Table S2. The best-fit model predicted that the cyclin thresholds at which Plo1 relocalization occurs follow a scaling rule as well, i.e., they correlate well with the cyclin degradation rate (not shown).

Parameter	Unit	Range	Best-fit (Fig. 5K)
[APC]	μM	0.016-0.024	0.017
[Sec(0)]	μM	0.08-1.2	0.09
[Cyc(0)]	μM	6-10x [Sec(0)]	6.42x [Sec(0)]
$k_{on,SecAPC}$	μM^{-1} sec^{-1}	1-100	1.06
$k_{off,SecAPC}$	sec^{-1}	0.01-1	0.06
$K_{cat,SecAPC}$	sec^{-1}	0.01-1	0.18
$k_{on,CycAPC}$	μM^{-1} sec^{-1}	= 0.1-10x $k_{on,SecAPC}$	= 2.44x $k_{on,SecAPC}$
$k_{off,CycAPC}$	sec^{-1}	= 0.1-10x $k_{off,SecAPC}$	= 2.74x $k_{off,SecAPC}$
$k_{cat,CycAPC}$	sec^{-1}	= 0.1-10x $k_{cat,SecAPC}$	= 8.35x $k_{cat,SecAPC}$
$k_{prot,Sec}$	sec^{-1}	0.1-10	0.12
$k_{prot,Cyc}$	sec^{-1}	= 0.1-10x $k_{prot,Sec}$	= 0.14x $k_{prot,Sec}$

Table S2: Parameter ranges and best-fit parameter values for fitting to securin degradation dynamics, and to SCS as well as Plo1 relocalization timing

Analytical calculations for substrate competition for the APC

***Degradation timing*:** In analogy to classical Michaelis-Menten kinetics, we assume that the two enzyme-substrate complexes are in quasi-steady state, i.e. (2)

$$0 = Sec * (APC_{tot} - SecAPC - CycAPC) - K_{M,SecAPC} SecAPC$$

$$0 = Cyc * (APC_{tot} - SecAPC - CycAPC) - K_{M,CycAPC} CycAPC$$

The Michaelis-Menten constants $K_{M,SecAPC} = (k_{off,SecAPC} + k_{cat,SecAPC}) / k_{off,SecAPC}$ and $K_{M,CycAPC} = (k_{off,CycAPC} + k_{cat,CycAPC}) / k_{off,CycAPC}$ describe the affinity of the enzyme-substrate complexes. The initial degradation velocities at time t = 0 are given by $v_{Sec}(0) = k_{cat,SecAPC} SecAPC(0)$ and $v_{Cyc}(0) = k_{cat,CycAPC} CycAPC(0)$ which translates into the following equations (3)

$$v_{Sec}(0) = v_{max,Sec} \frac{\frac{Sec_{tot}}{K_{M,SecAPC}}}{1 + \frac{Sec_{tot}}{K_{M,SecAPC}} + \frac{Cyc_{tot}}{K_{M,CycAPC}}}$$

$$v_{Cyc}(0) = v_{max,Cyc}\frac{\frac{Cyc_{tot}}{K_{M,CycAPC}}}{1+\frac{Sec_{tot}}{K_{M,SecAPC}}+\frac{Cyc_{tot}}{K_{M,CycAPC}}}$$

where $v_{max,Sec} = k_{cat,SecAPC}APC_{tot}$ and $v_{max,Cyc} = k_{cat,CycAPC}APC_{tot}$. Sec_{tot} and Cyc_{tot} are the initial protein concentrations of the substrates. Using these equations, we can linearly approximate the time courses of securin and cyclin degradation as (4)

$$Sec(t) = Sec_{tot} - v_{Sec}(0)\cdot t$$

$$Cyc(t) = Cyc_{tot} - v_{Cyc}(0)\cdot t$$

Numerical simulations using the full set of ODEs (Eq. 1) confirm that this approximation works very well, especially if the APC is strongly saturated (Sec_{tot} >> $K_{M,SecAPC}$ and/or Cyc_{tot} >> $K_{M,CycAPC}$), since then the degradation time courses are approximately linear (zero-order degradation). In case of limited saturation, a very good match between approximation and exact numerical solution is restricted to the upper half of the degradation time course, owing to the curvature of exponential decays (first-order degradation).

By setting Sec(t) = 0 and Cyc(t) = 0 in Eq. 4, we see that the two proteins will always be coordinately degraded to a concentration (close to) zero at the same time (5)

$$t_0 = \frac{1}{v_{maxS}/K_{MS}}\left(1+\frac{Sec_{tot}}{K_{MS}}+\frac{Cyc_{tot}}{K_{MC}}\right)$$

This result indicates that enzyme competition effects coordinate the degradation dynamics of securin and cyclin.

***Timing of sister-chromatid separation and Plo1 relocalization*:** Using Eq. 4, the timing of SCS and Plo1 relocalization can be approximated. Let us assume that both events occur when a certain level of securin and cyclin B, respectively, remains, i.e. Sec(t) = Sec_{SCS} and Cyc(t) = Cyc_{Plo1}. Then, one derives the following timing equations (6)

$$t_{SCS} = \frac{Sec_{tot}-Sec_{SCS}}{v_{Sec}(0)} = \frac{1}{v_{max,Sec}/K_{M,Sec}}\left(1+\frac{Sec_{tot}}{K_{M,Sec}}+\frac{Cyc_{tot}}{K_{M,Cyc}}\right)\left(1-\frac{Sec_{SCS}}{Sec_{tot}}\right)$$

$$t_{Plo1} = \frac{Cyc_{tot}-Cyc_{Plo1}}{v_{Cyc}(0)} = \underbrace{\frac{1}{v_{max,Cyc}/K_{M,Cyc}}}_{\substack{catalytic\\efficiency}}\left(\underbrace{1+\frac{Sec_{tot}}{K_{M,Sec}}+\frac{Cyc_{tot}}{K_{M,Cyc}}}_{saturation}\right)\left(\underbrace{1-\frac{Cyc_{Plo1}}{Cyc_{tot}}}_{excess}\right)$$

As expected, it takes longer to achieve SCS and Plo1 relocalization if the catalytic

efficiency of the APC (V_{max}/K_M) is low, if the enzyme is strongly saturated ($Sec_{tot} >> K_{M,SecAPC}$ and/or $Cyc_{tot} >> K_{M,CycAPC}$), and if a large portion of the proteins needs to be degraded ($Sec_{SCS} << Sec_{tot}$ or $Cyc_{Plo1} << Cyc_{tot}$). The timing difference between SCS and Plo1 relocalization is given by (7)

$$\Delta t = t_{Plo1} - t_{SCS} = \underbrace{\left(1 + \frac{Sec_{tot}}{K_{M,Sec}} + \frac{Cyc_{tot}}{K_{M,Cyc}}\right)}_{I} \cdot \left(\frac{1 - \frac{Cyc_{Plo1}}{Cyc_{tot}}}{\underbrace{v_{max,Cyc}/K_{M,Cyc}}_{II}} - \frac{1 - \frac{Sec_{SCS}}{Sec_{tot}}}{\underbrace{v_{max,Sec}/K_{M,Sec}}_{III}} \right)$$

Assuming equal catalytic efficiency (V_{max}/K_M) of the APC for the degradation of the two substrates, this simplifies to (8)

$$\Delta t = t_{Plo1} - t_{SCS} = \frac{1}{v_{max}/K_M}\left(1 + \frac{Sec_{tot}}{K_M} + \frac{Cyc_{tot}}{K_M}\right) \cdot \left(\frac{Sec_{SCS}}{Sec_{tot}} - \frac{Cyc_{Plo1}}{Cyc_{tot}}\right)$$

Requirements for timing invariance

***Lack of Δt invariance in a model with fixed thresholds*:** In the following, we will apply Eq. 8 to the data assuming that SCS and cyclin-dependent events always happen at the same, fixed threshold levels, i.e. Sec_{SCS} = *const* and Cyc_{Plo1} = *const*. It will be shown that the fixed threshold assumption results in an inversion of temporal order for 8x Securin overexpression.

According to Eq. 8, Δt will be positive as long as (9)

$$\frac{Cyc_{Plo1}}{Cyc_{tot}} < \frac{Sec_{SCS}}{Sec_{tot}}$$

This expression implies that Cyc_{Plo1}/Cyc_{tot} needs to be at least 8-fold smaller than Sec_{SCS}/Sec_{tot} in order to maintain the order of events ($\Delta t > 0$) upon 8-fold securin overexpression.

From the WT data, we know that $Sec_{SCS}/Sec_{tot} = 0.7$ and $t_{Cyc} \approx 2.5 \cdot t_{SCS}$. According to Eq. 6 and assuming similar catalytic efficiencies for both substrates, both conditions can be fulfilled if (10)

$$\frac{Cyc_{Plo1}}{Cyc_{tot}} = 0.25$$

This disagrees with the requirement that Cyc_{Plo1}/Cyc_{tot} in wt needs to be at least 8-fold smaller than Sec_{SCS}/Sec_{tot}, suggesting that securin overexpression shifts timing

difference of SCS and Plo1 relocalization from positive to negative values.

Even for different catalytic efficiencies of the APC towards securin and cyclin B, Δt invariance in response to securin overexpression cannot be maintained: Term I and III in Eq. 7 always increase and decrease upon securin overexpression (increasing Sec_{tot}), respectively. Thus, increasing Sec_{tot} always increases Δt and timing invariance cannot be established.

***Timing invariance upon scaling of thresholds with initial degradation velocities*:** Δt invariance can be realized if the thresholds of SCS and Plo1 relocalization are not constant, but scale with the initial rates securin and and cyclin degradation, respectively. This means that (11)

$$Sec_{SCS} = a\, v_{Sec}(0)$$

$$Cyc_{Plo1} = b\, v_{Cyc}(0)$$

where a and b are constants. Then, the timing of the two branches (Eq. 6) is still dependent on the securin and cyclin concentrations (12)

$$t_{SCS} = \frac{Sec_{tot}}{v_{Sec}(0)} - a = \frac{1}{v_{max,Sec}/K_{M,Sec}}\left(1 + \frac{Sec_{tot}}{K_{M,Sec}} + \frac{Cyc_{tot}}{K_{M,Cyc}}\right) - a$$

$$t_{Plo1} = \frac{Cyc_{tot}}{v_{Cyc}(0)} - b = \frac{1}{v_{max,Cyc}/K_{M,Cyc}}\left(1 + \frac{Sec_{tot}}{K_{M,Sec}} + \frac{Cyc_{tot}}{K_{M,Cyc}}\right) - b$$

but the timing difference is invariant if the substrates are processed with the same catalytic efficiency (13)

$$\Delta t = t_{Cyc} - t_{SCS} = a - b$$

Numerical simulations under the assumption of threshold scaling (Eq. 11) confirm the near-complete invariance of Δt in the exact system (Figure 5K).

Notably, scaling is not the only solution for timing invariance. In fact, for each particular perturbation of the system (e.g., Securin or Cyclin overexpression) an infinite number of Sec_{SCS} and Cyc_{Plo1} threshold shift combinations exist to establish temporal invariance. However, the scaling rule in Eq. 11 represent a universal rule that may establish timing invariance for any strength of securin or cyclin overexpression, or for perturbations in the APC activity (V_{max}). The model thus predicts a strong correlation of the absolute securin degradation velocity and Sec_{SCS}, and this correlation is indeed seen in the data (Figure

5l).

***Slightly modified scaling rule in a system with uncoupled first-order decay*:** So far, it was assumed that protein degradation proceeds with (close-to) zero-order kinetics and the time courses can be approximated using a linear equation (Eq. 4). In the absence of strong enzyme saturation and competition, the kinetics of securin and cyclin degradation are described by simpler exponential decays (14)

$$Sec(t) = Sec(0) \cdot e^{-k_{Sec} \cdot t}$$

$$Cyc(t) = Cyc(0) \cdot e^{-k_{Cyc} \cdot t}$$

The time to decay to the thresholds Sec_{SCS} and Cyc_{Plo} is given by (15)

$$t_{SCS} = -\frac{ln\left(\frac{Sec_{SCS}}{Sec(0)}\right)}{k_{Sec}}$$

$$t_{Plo} = -\frac{ln\left(\frac{Cyc_{Plo}}{Cyc(0)}\right)}{k_{Cyc}}$$

The equation for the timing difference thus reads (16)

$$\Delta t = t_{Plo} - t_{SCS} = \frac{ln\left(\frac{Sec_{SCS}}{Sec(0)}\right)}{k_{Sec}} - \frac{ln\left(\frac{Cyc_{Plo}}{Cyc(0)}\right)}{k_{Cyc}}$$

It can be seen that temporal invariance towards securin or cyclin overexpression can already be realized if the SCS and Plo1 thresholds scale with the initial concentrations of securin and cyclin, respectively (17)

$$Sec_{SCS} = a\, Sec(0)$$

$$Cyc_{Plo1} = b\, Cyc(0)$$

Then, the timing difference is robust against protein overexpression, but not against fluctuations in the APC concentration (which enters into the rate constants k_{Cyc} and k_{Sec}). (18)

$$\Delta t = t_{Plo} - t_{SCS} = -\frac{ln(a)}{k_{Cyc}} + \frac{ln(b)}{k_{Sec}}$$

However, the system can even be partially invariant against APC fluctuations if the thresholds scale with the initial slope of degradation, i.e., (19)

$Sec_{SCS} = a\,Sec(0) \cdot k_{Sec}$

$Cyc_{Plo1} = b\,Cyc(0) \cdot k_{Cyc}$

Then the timing difference reads (20)

$$\Delta t = t_{Plo} - t_{SCS} = -\frac{ln(a \cdot k_{Cyc})}{k_{Cyc}} + \frac{ln(b \cdot k_{Sec})}{k_{Sec}}$$

APC fluctuations affect the degradation rate constants k_{Cyc} and k_{Sec} and therefore partially cancel out. Hence, in a system with first-order decay the temporal invariance towards securin and cyclin overexpression can already be explained by a simpler scaling rule (Eq. 17), but scaling with the initial velocity of degradation is still beneficial for the global robustness of the system.

Supplementary references

Baird, G.S., Zacharias, D.A., and Tsien, R.Y. (1999). Circular permutation and receptor insertion within green fluorescent proteins. Proceedings of the National Academy of Sciences of the United States of America *96*, 11241-11246.

Heinrich, S., Geissen, E.M., Kamenz, J., Trautmann, S., Widmer, C., Drewe, P., Knop, M., Radde, N., Hasenauer, J., and Hauf, S. (2013). Determinants of robustness in spindle assembly checkpoint signalling. Nature cell biology *15*, 1328-1339.

Kamenz, J., and Hauf, S. (2014). Slow checkpoint activation kinetics as a safety device in anaphase. Current biology : CB *24*, 646-651.

Kumada, K., Nakamura, T., Nagao, K., Funabiki, H., Nakagawa, T., and Yanagida, M. (1998). Cut1 is loaded onto the spindle by binding to Cut2 and promotes anaphase spindle movement upon Cut2 proteolysis. Current biology : CB *8*, 633-641.

Luciani, F., Kesmir, C., Mishto, M., Or-Guil, M., and de Boer, R.J. (2005). A mathematical model of protein degradation by the proteasome. Biophys J *88*, 2422-2432.

Matsuyama, A., Arai, R., Yashiroda, Y., Shirai, A., Kamata, A., Sekido, S., Kobayashi, Y., Hashimoto, A., Hamamoto, M., Hiraoka, Y.*, et al.* (2006). ORFeome cloning and global analysis of protein localization in the fission yeast Schizosaccharomyces pombe. Nat Biotechnol *24*, 841-847.

Matsuyama, A., Shirai, A., Yashiroda, Y., Kamata, A., Horinouchi, S., and Yoshida, M. (2004). pDUAL, a multipurpose, multicopy vector capable of chromosomal integration in fission yeast. Yeast *21*, 1289-1305.

Roguev, A., Wiren, M., Weissman, J.S., and Krogan, N.J. (2007). High-throughput genetic interaction mapping in the fission yeast Schizosaccharomyces pombe. Nat Methods *4*, 861-866.

Tallini, Y.N., Ohkura, M., Choi, B.R., Ji, G., Imoto, K., Doran, R., Lee, J., Plan, P., Wilson, J., Xin, H.B.*, et al.* (2006). Imaging cellular signals in the heart in vivo: Cardiac expression of the high-signal Ca2+ indicator GCaMP2. Proceedings of the National Academy of Sciences of the United States of America *103*, 4753-4758.

Supplementary Table S1 *S. pombe* strains

Figure 1B		
JY001	*h-*	*wild type*
ST541	*h-*	*leu1 ade6-M216 cut2+-GFP<<kanR cdc13+-mCherry<<kanR*
Figure 1C		
SM205	*h+*	*leu1-32::ura4+ lys1- plo1+-mCherry<<natR ura4::pcn1p::EGFP-pcn1 cdc25-22*
Figure 1D		
SM336	*h-*	*leu1 ade6-M216 cut2+-GFP<<kanR cut1+-13myc<<kanR*
SM330	*h-*	*leu1 ade6-M216 natNT2<<Padh1(M6)-cut2+-GFP<<kanR cut1+-13myc<<kanR*
Figure 1E		
SL249	*h-*	*leu1 ade6-M216 cut2+-GFP<<kanR dh1L<<ura4+<<tetO Z<<natR<<Padh31-tetR-tdTomato ade6-M216 leu1 natNT2<<Padh1-cdc13+ cut2+-GFP<<kanR dh1L<<ura4+<<tetO*
ST218'	*h-*	*Z<<natR<<Padh31-tetR-tdTomato*
Figure 1F		
SL248	*h-*	*leu1 ade6-M216 cut2+-GFP<<kanR*
SM329	*h-*	*leu1 ade6-M216 natNT2<<Padh1(M13)-cut2+-GFP<<kanR*
SM330	*h-*	*leu1 ade6-M216 natNT2<<Padh1(M6)-cut2+-GFP<<kanR*
Figure 1G		
JY336	*h+*	*ade6-M210 leu1*
ST215	*h+*	*ade6-M210 leu1 natNT2<<Padh1-cdc13+*
Figure 2A		
SP623	*h-*	*leu1 plo1+-mCherry<<natR cut2+-GFP<<kanR mis12+-GFP<<kanR*
ST530	*h-*	*leu1 leu1+>>Pnmt81-DN67-cdc13 plo1+-mCherry<<natR cut2+-GFP<<kanR mis12+-GFP<<kanR*
ST201	*h-*	*leu1 leu1+<<pDual Pnmt81-ΔN80-cut2 plo1+-mCherry<<natR cut2+-GFP<<kanR mis12+-GFP<<kanR*
Figure 2B		
SP623	*h-*	*leu1 plo1+-mCherry<<natR cut2+-GFP<<kanR mis12+-GFP<<kanR*
ST530	*h-*	*leu1 leu1+>>Pnmt81-DN67-cdc13 plo1+-mCherry<<natR cut2+-GFP<<kanR mis12+-GFP<<kanR*
Figure 2C		
SP623	*h-*	*leu1 plo1+-mCherry<<natR cut2+-GFP<<kanR mis12+-GFP<<kanR*
ST201	*h-*	*leu1 leu1+<<pDual Pnmt81-ΔN80-cut2 plo1+-mCherry<<natR cut2+-GFP<<kanR mis12+-GFP<<kanR*
Figure 3 A - C,G		
SP623	*h-*	*leu1 plo1+-mCherry<<natR cut2+-GFP<<kanR mis12+-GFP<<kanR*
ST223	*h-*	*leu1 natNT2<<Padh1-cdc13+ plo1+-mCherry<<natR cut2+-GFP<<kanR mis12+-GFP<<kanR*
Figure 3 D-F		
SP623'	*h-*	*leu1 plo1+-mCherry<<natR cut2+-GFP<<kanR mis12+-GFP<<kanR*
SP631'	*h-*	*ade6-M210 leu1 plo1+-mCherry<<natR natNT2<<Padh1(M13)-cut2+-GFP<<kanR mis12+-GFP<<kanR*
SP627'	*h-*	*leu1 ade6-M216 plo1+-mCherry<<natR natNT2<<Padh1(M6)-cut2+-GFP<<kanR mis12+-GFP<<kanR*
Figure 3 H		
SP623'	*h-*	*leu1 plo1+-mCherry<<natR cut2+-GFP<<kanR mis12+-GFP<<kanR*
SP627'	*h-*	*leu1 ade6-M216 plo1+-mCherry<<natR natNT2<<Padh1(M6)-cut2+-GFP<<kanR mis12+-GFP<<kanR*
Figure 3 I		
SP631'	*h-*	*ade6-M210 leu1 plo1+-mCherry<<natR natNT2<<Padh1(M13)-cut2+-GFP<<kanR mis12+-GFP<<kanR*
SP627'	*h-*	*leu1 ade6-M216 plo1+-mCherry<<natR natNT2<<Padh1(M6)-cut2+-GFP<<kanR mis12+-GFP<<kanR*
Figure 4D, E		
SL249	*h-*	*leu1 ade6-M216 cut2+-GFP<<kanR dh1L<<ura4+<<tetO Z<<natR<<Padh31-tetR-tdTomato ade6-M216 leu1 natNT2<<Padh1-cdc13+ cut2+-GFP<<kanR dh1L<<ura4+<<tetO*
ST218'	*h-*	*Z<<natR<<Padh31-tetR-tdTomato*
Figure 5A		
SL249	*h-*	*leu1 ade6-M216 cut2+-GFP<<kanR dh1L<<ura4+<<tetO Z<<natR<<Padh31-tetR-tdTomato*
ST619	*h-*	*leu1 ade6-M216 natNT2<<Padh1(M13)-cut2+-GFP<<kanR ura4-D18(?) dh1L<<ura4+<<tetO Z<<natR<<Padh31-tetR-tdTomato*
SM325	*h-*	*leu1 ade6-M216 natNT2<<Padh1(M6)-cut2+-GFP<<kanR ura4-D18(?) dh1L<<ura4+<<tetO Z<<natR<<Padh31-tetR-tdTomato*
Figure 5B,C		
SL249	*h-*	*leu1 ade6-M216 cut2+-GFP<<kanR dh1L<<ura4+<<tetO Z<<natR<<Padh31-tetR-tdTomato*
Figure 5D-F		
SM372	*h-*	*leu1 cut2+-GFP<<kanR cut11+-mCherry<<hphR gpi16+-mCherry<<<natR*
SK848	*h+*	*cut1+-GFP<<kanR cut11+-mCherry<<hphR*
ST533	*h-*	*cut1+-GFP<<kanR cut11+-mCherry<<hphR natNT2<<Padh1(M6)-cut2+*
Figure 5G,H		
SL249	*h-*	*leu1 ade6-M216 cut2+-GFP<<kanR dh1L<<ura4+<<tetO Z<<natR<<Padh31-tetR-tdTomato*
SL258'	*h-*	*leu1 ade6-M216 cut2+-GFP<<kanR dh1l<<ura4+<<tetO Z<<natR<<Padh131-tetR-tdTomato cut9-665*
Figure 6A		
SP632	*h-*	*leu1 plo1+-mCherry<<natR cut2+-GFP<<kanR mis12+-GFP<<kanR*
ST556	*h-*	*leu1 plo1+-mCherry<<natR cut2+-GFP<<kanR mis12+-GFP<<kanR Prad21-kanR-slp1*
ST558	*h-*	*leu1 plo1+-mCherry<<natR cut2+-GFP<<kanR mis12+-GFP<<kanR cut9-665*
Figure 6B		
JV037	*h-*	*leu1-32 ade6-M216 cut9-665*
SL248	*h-*	*leu1 ade6-M216 cut2+-GFP<<kanR*
SM329	*h-*	*leu1 ade6-M216 natNT2<<Padh1(M13)-cut2+-GFP<<kanR*
SM330	*h-*	*leu1 ade6-M216 natNT2<<Padh1(M6)-cut2+-GFP<<kanR*
ST215	*h+*	*ade6-M210 leu1 natNT2<<Padh1-cdc13+*
Figure 6C		
SI709	*h+*	*ade6-M216 Prad21-kanR-slp1*

SL248	*h-*	*leu1 ade6-M216 cut2+-GFP<<kanR*
SM329	*h-*	*leu1 ade6-M216 natNT2<<Padh1(M13)-cut2+-GFP<<kanR*
SM330	*h-*	*leu1 ade6-M216 natNT2<<Padh1(M6)-cut2+-GFP<<kanR*
ST553	*h-*	*leu1? ade6-M216 Prad21-kanR-slp1*
ST215	*h+*	*ade6-M210 leu1 natNT2<<Padh1-cdc13+*

Figure S1A,B

JY001	*h-*	*wild type*
ST541	*h-*	*leu1 ade6-M216 cut2+-GFP<<kanR cdc13+-mCherry<<kanR*

Figure S1C-F

SM205	*h+*	*leu1-32::ura4+ lys1- plo1+-mCherry<<natR ura4::pcn1p::EGFP-pcn1 cdc25-22*

Figure S2A

JY333	*h-*	*ade6-M216 leu1*
SL248, SL248'	*h-*	*leu1 ade6-M216 cut2+-GFP<<kanR*

Figure S2B,D

SL240	*h+*	*leu1 ade6-M210 plo1+-mCherry<<natR cdc25-22*
SM306'	*h-*	*leu1 ade6-M216 cdc25-22 cut2+-GFP<<kanR plo1+-mCherry<<natR*

Figure S2C

SM306'	*h-*	*leu1 ade6-M216 cdc25-22 cut2+-GFP<<kanR plo1+-mCherry<<natR*

Figure S2E

JY336	*h+*	*ade6-M210 leu1*
JZ686	*h-*	*cdc13-117*
SM390	*h+*	*leu1 ade6-M210 cdc13+-mCherry<<kanR*
JV358	*h-*	*cdc13-GFP<<kanr ade6-M216 leu1*
SI605	*h-*	*cdc13-GFP<<kanR ade6-M216 leu1*
ST207	*h-*	*leu1*
ST205	*h+*	*leu1 leu1+<<Pcdc13-cdc13 rpl42::cyhR(sP56Q)*
ST206	*h+*	*leu1 leu1+<<Pcdc13-cdc13 cdc13::cdc13-N224-cpGFP-225C*
ST204	*h-*	*leu1 rpl42::cyhR(sP56Q) cdc13::cdc13-N224-cpGFP-225C*

Figure S3A

SP623	*h-*	*leu1 plo1+-mCherry<<natR cut2+-GFP<<kanR mis12+-GFP<<kanR*
ST223	*h-*	*leu1 natNT2<<Padh1-cdc13+ plo1+-mCherry<<natR cut2+-GFP<<kanR mis12+-GFP<<kanR*
ST601	*h-*	*leu1 natNT2<<Padh1-cdc13+ plo1+-mCherry<<natR cut2+-GFP<<kanR mis12+-GFP<<kanR mad2Δ::hygR*

Figure S3B-D

SP631'	*h-*	*ade6-M210 leu1 plo1+-mCherry<<natR natNT2<<Padh1(M13)-cut2+-GFP<<kanR mis12+-GFP<<kanR*
SP627'	*h-*	*leu1 ade6-M216 plo1+-mCherry<<natR natNT2<<Padh1(M6)-cut2+-GFP<<kanR mis12+-GFP<<kanR*

Figure S3E

SP660	*h-*	*leu1 rpn10+-GFP<<hph*
SP661	*h-*	*leu1 rpn11+-GFP<<hph*
SP662	*h-*	*leu1 leu1+<<Pnmt1-cut8-FLAG2 rpn10+-GFP<<hph*
SP663	*h-*	*leu1 leu1+<<Pnmt1-cut8-FLAG2 rpn11+-GFP<<hph*

Figure S3F

SP660	*h-*	*leu1 rpn10+-GFP<<hph*
SP662	*h-*	*leu1 leu1+<<Pnmt1-cut8-FLAG2 rpn10+-GFP<<hph*

Figure S3G

SP661	*h-*	*leu1 rpn11+-GFP<<hph*
SP663	*h-*	*leu1 leu1+<<Pnmt1-cut8-FLAG2 rpn11+-GFP<<hph*

Figure S3H-J

SL249	*h-*	*leu1 ade6-M216 cut2+-GFP<<kanR dh1L<<ura4+<<tetO Z<<natR<<Padh31-tetR-tdTomato*
SP645	*h-*	*leu1 ade6-M216 cut2+-GFP<<kanR dh1L<<ura4+<<tetO Z<<natR<<Padh31-tetR-tdTomato leu1+<<Pnmt1-cut8-FLAG2*

Figure S4E-G

SM306	*h-*	*leu1 ade6-M216 cdc25-22 cut2+-GFP<<kanR plo1+-mCherry<<natR*
ST574	*h-*	*leu1 ade6-M210 plo1+-mCherry<<natR cdc25-22 natNT2<<Padh1(M6)-cut2+-GFP<<kanR*

Figure S5A

SM336	*h-*	*leu1 ade6-M216 cut2+-GFP<<kanR cut1+-13myc<<kanR*
SM330	*h-*	*leu1 ade6-M216 natNT2<<Padh1(M6)-cut2+-GFP<<kanR cut1+-13myc<<kanR*
SM332	*h-*	*leu1 ade6-M210 natNT2<<Padh1(M13)-cut2+-GFP<<kanR cut1+-13myc<<kanR*

Figure S5B

SM372'	*h-*	*leu1 cut2+-GFP<<kanR cut11+-mCherry<<hphR gpi16+-mCherry<<<natR*
SK848'	*h+*	*cut1+-GFP<<kanR cut11+-mCherry<<hphR*
ST533'	*h-*	*cut1+-GFP<<kanR cut11+-mCherry<<hphR natNT2<<Padh1(M6)-cut2+*
SM558	*h-*	*pDUAL-Pmad3+-GFP<<leu1+ cut11+-mCherry<<hphR*

Figure S5C,D

SL249	*h-*	*leu1 ade6-M216 cut2+-GFP<<kanR dh1L<<ura4+<<tetO Z<<natR<<Padh31-tetR-tdTomato*
ST619	*h-*	*leu1 ade6-M216 natNT2<<Padh1(M13)-cut2+-GFP<<kanR ura4-D18(?) dh1L<<ura4+<<tetO Z<<natR<<Padh31-tetR-tdTomato*
SM325	*h-*	*leu1 ade6-M216 natNT2<<Padh1(M6)-cut2+-GFP<<kanR ura4-D18(?) dh1L<<ura4+<<tetO Z<<natR<<Padh31-tetR-tdTomato*

Figure S5E,F

SL249	*h-*	*leu1 ade6-M216 cut2+-GFP<<kanR dh1L<<ura4+<<tetO Z<<natR<<Padh31-tetR-tdTomato*
SL258'	*h-*	*leu1 ade6-M216 cut2+-GFP<<kanR dh1l<<ura4+<<tetO Z<<natR<<Padh131-tetR-tdTomato cut9-665*

Figure S5G-J

SL249	*h-*	*leu1 ade6-M216 cut2+-GFP<<kanR dh1L<<ura4+<<tetO Z<<natR<<Padh31-tetR-tdTomato*
SM379	*h-*	*leu1 ade6-M216 cut2+-GFP<<kanR dh1L<<ura4+<<tetO Z<<natR<<Padh31-tetR-tdTomato Prad21-kanR-slp1*

Figure S5K-N

SL249	*h-*	*leu1 ade6-M216 cut2+-GFP<<kanR dh1L<<ura4+<<tetO Z<<natR<<Padh31-tetR-tdTomato*

2.3 Determinants of robustness in spindle assembly checkpoint signalling

Stephanie Heinrich[1], Eva-Maria Geissen[2], Julia Kamenz[1], Susanne Trautmann[3,8], Christian Widmer[1,4], Philipp Drewe[1,4], Michael Knop[3,5], Nicole Radde[2], Jan Hasenauer[6,7], Silke Hauf[1,*]

[1]*Friedrich Miescher Laboratory of the Max Planck Society, 72076 Tübingen, Germany*

[2]*Institute for Systems Theory and Automatic Control, University of Stuttgart, Germany*

[3]*EMBL, Heidelberg, Germany*

[4]*Computational Biology Center, Memorial Sloan-Kettering Cancer Center, New York, USA*

[5]*ZMBH, University of Heidelberg, Germany*

[6]*Institute of Computational Biology, Helmholtz Zentrum München, Germany*

[7]*Department of Mathematics, Technische Universität München, Germany*

[8]*Present address: PicoQuant GmbH, Berlin, Germany*

*Correspondence: silke.hauf@tuebingen.mpg.de

Published in **Nature Cell Biology**, Volume 15, p.1328–1339 (2013)
DOI: 10.1038/ncb2864

Author contributions:

I established the protocol for determining the protein abundances by quantitative immunoblotting including the purification of recombinant Slp1 and performed the Slp1 quantification in minimal medium. Additionally, I characterized the Mad1-RL/AG mutant and constructed plasmids and strains for the study.

Stephanie Heinrich designed and performed all other experiments, except the fluorescence correlation spectroscopy (FCS, performed by **Susanne Trautmann** and **Michael Knop**).

Eva Maria Geissen, Jan Hasenauer, Nicole Radde and **Silke Hauf** performed modelling and statistical evaluation.

Christian Widmer developed the automated nuclear tracking software with contributions from **Philipp Drewe**.

Silke Hauf supervised the study and wrote the manuscript together with Stephanie Heinrich, Eva-Maria Geissen, Jan Hasenauer and input from all other authors.

nature cell biology

Determinants of robustness in spindle assembly checkpoint signalling

Stephanie Heinrich[1], Eva-Maria Geissen[2], Julia Kamenz[1], Susanne Trautmann[3,8], Christian Widmer[1,4], Philipp Drewe[1,4], Michael Knop[3,5], Nicole Radde[2], Jan Hasenauer[6,7] and Silke Hauf[1,9]

The spindle assembly checkpoint is a conserved signalling pathway that protects genome integrity. Given its central importance, this checkpoint should withstand stochastic fluctuations and environmental perturbations, but the extent of and mechanisms underlying its robustness remain unknown. We probed spindle assembly checkpoint signalling by modulating checkpoint protein abundance and nutrient conditions in fission yeast. For core checkpoint proteins, a mere 20% reduction can suffice to impair signalling, revealing a surprising fragility. Quantification of protein abundance in single cells showed little variability (noise) of critical proteins, explaining why the checkpoint normally functions reliably. Checkpoint-mediated stoichiometric inhibition of the anaphase activator Cdc20 (Slp1 in *Schizosaccharomyces pombe*) can account for the tolerance towards small fluctuations in protein abundance and explains our observation that some perturbations lead to non-genetic variation in the checkpoint response. Our work highlights low gene expression noise as an important determinant of reliable checkpoint signalling.

Biological systems need to operate reliably under a variety of environmental conditions and need to buffer naturally occurring variations in the abundance of biomolecules (termed noise)[1,2]. The spindle assembly checkpoint (SAC) is a signalling pathway that protects genome integrity by detecting and responding to errors in chromosome attachment during mitosis[3,4]. The SAC is essential for the viability of mammals, and its function and components are conserved in eukaryotes[5]. As a guardian of genome integrity, the checkpoint should operate robustly. How this is accomplished is unknown.

SAC proteins accumulate on unattached kinetochores and start a signalling cascade that ultimately inhibits Cdc20 (called Slp1 in *S. pombe*), an essential cofactor of the anaphase-promoting complex/cyclosome (APC/C; refs 6,7). Mad1, Mad2, Mad3 (or BubR1, depending on the organism), Bub1, Bub3 and Mps1 (Mph1 in *S. pombe*) are considered the core components of the SAC. Mad1 and Mad2 form a complex, in which Mad2 adopts a closed conformation[8] (C-Mad2). According to the well-supported template model, Mad1-bound C-Mad2 dimerizes with a second molecule of Mad2 in the open (O-Mad2) conformation, and triggers binding of this second Mad2 molecule, now in the C-conformation, to Cdc20 (refs 9–11). Mad3 then binds C-Mad2:Cdc20. The proteins together form the mitotic checkpoint complex[12] (MCC), which is a potent inhibitor of the APC/C (Fig. 1b).

Requirements for robust checkpoint signalling have been evaluated theoretically[13], but not experimentally. We systematically probed SAC activity following changes in protein abundance or nutrient conditions in fission yeast. This allowed us to define the borders for reliable checkpoint function. Some alterations were tolerated well; other alterations shifted SAC signalling into one of two regimes: either the checkpoint failed entirely, or the cell population split into two genetically identical but phenotypically different populations with dissimilar SAC responses. As critical checkpoint proteins are kept within tight windows of abundance, cells normally do not reach these regimes.

RESULTS

Abundance of SAC proteins and APC/C subunits

SAC signalling involves a series of protein–protein interactions. Hence, signalling outcome should be affected by the abundance of SAC proteins. As a basis to assess how signalling varies with protein abundance, we measured the concentration of SAC proteins and APC/C subunits *in vivo* in single fission yeast cells. We expressed SAC genes as green

[1]Friedrich Miescher Laboratory of the Max Planck Society, 72076 Tübingen, Germany. [2]Institute for Systems Theory and Automatic Control, University of Stuttgart, 70550 Stuttgart, Germany. [3]EMBL, 69117 Heidelberg, Germany. [4]Computational Biology Center, Memorial Sloan-Kettering Cancer Center, New York 10065, USA. [5]Zentrum für Molekulare Biologie der Universität Heidelberg, Deutsches Krebsforschungszentrum, DKFZ-ZMBH Allianz, 69120 Heidelberg, Germany. [6]Institute of Computational Biology, Helmholtz Zentrum München, 85764 Neuherberg, Germany. [7]Department of Mathematics, Technische Universität München, 85748 Garching, Germany. [8]Present address: PicoQuant GmbH, 12849 Berlin, Germany.
[9]Correspondence should be addressed to S. Hauf (e-mail: silke.hauf@tuebingen.mpg.de)

Received 9 April 2013; accepted 20 September 2013; published online 27 October 2013; DOI: 10.1038/ncb2864

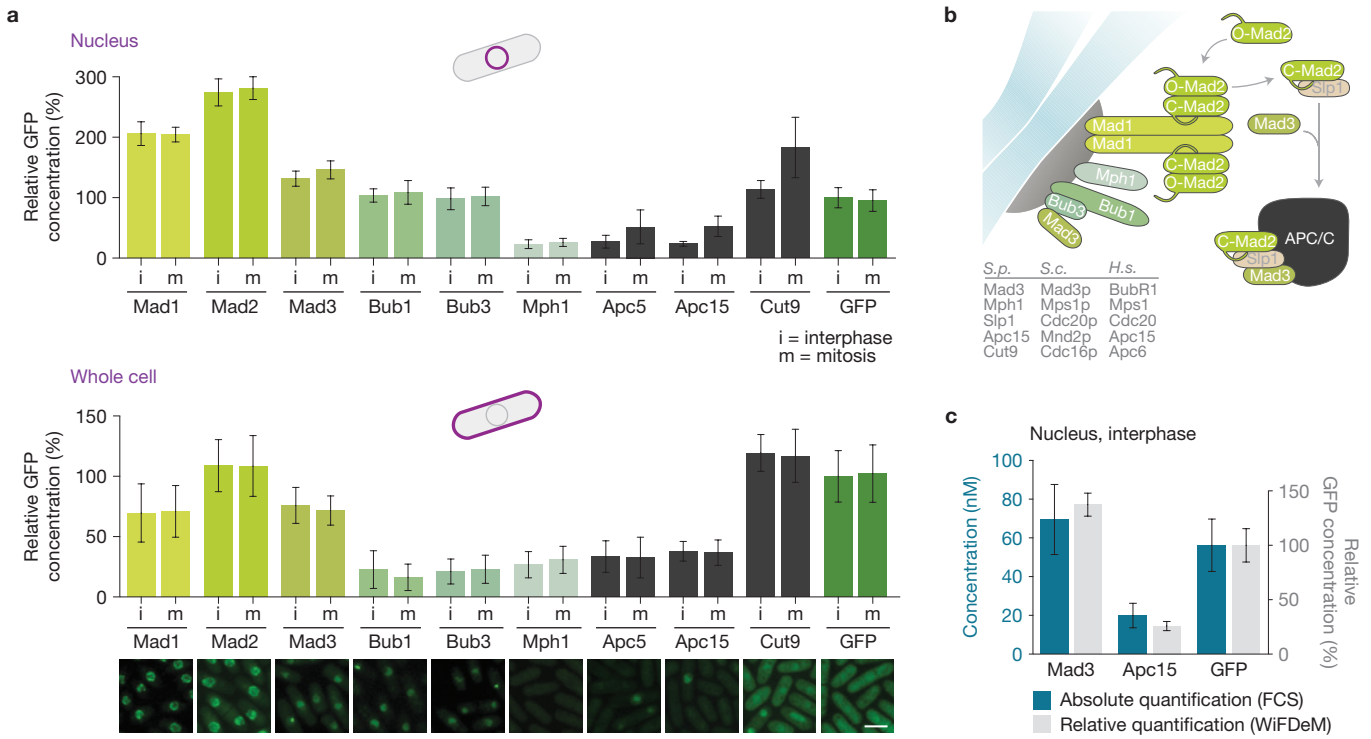

Figure 1 Abundance of SAC proteins and APC/C subunits. (**a**) Concentration of GFP-fusion proteins in the nucleus and the whole cell, normalized to the interphase concentration of free GFP expressed from the *mad3* promoter (GFP). Error bars, s.d. Statistics in Supplementary Table 1. Pictures show representative cells (scale bar, 5 μm). (**b**) Simplified schematic of the SAC signalling pathway. SAC proteins enrich at unattached kinetochores. Dimerization between Mad1-bound Mad2 and free Mad2 initiates binding of Mad2 to Cdc20 (*S. pombe* Slp1), followed by binding of Mad3 to form the mitotic checkpoint complex (MCC; template model[9]). When it is part of the MCC, Cdc20/Slp1 is unable to activate the APC/C. Protein names differ between organisms *(S.p., Schizosaccharomyces pombe; S.c., Saccharomyces cerevisiae; H.s., Homo sapiens).* (**c**) Average concentration of Mad3–GFP, Apc15–GFP and free GFP in the interphase nucleus determined by FCS (Supplementary Fig. 3). Relative abundances from **a** are shown for comparison.

fluorescent protein (GFP) fusions from the endogenous promoter at the endogenous locus, assessed their functionality (Supplementary Fig. 1) and quantified relative protein abundance both in the nucleus and in the entire cell by wide-field fluorescence deconvolution microscopy[14] (WiFDeM; Supplementary Fig. 2). SAC and APC/C protein abundances were similar between interphase and mitosis, but the APC/C became enriched in the nucleus during mitosis (Fig. 1a and Supplementary Table 1). The APC/C subunit Cut9 (Cdc16/Apc6 in other organisms) was more abundant than Apc5 and Apc15, presumably because it is present in the APC/C in two copies[15] and has an additional non-APC/C-bound pool[16]. According to the template model, Mad2 should be in excess over Mad1, which was the case (Fig. 1a). Bub1 and Bub3 showed similar abundances and nucleo-cytoplasmic distributions, fitting the complex formation between these proteins[17]. Furthermore, the low abundance of Mph1 was consistent with its catalytic role in the checkpoint[18,19]. Hence, our protein quantifications agree with existing knowledge on the molecular mechanisms of the SAC (Fig. 1b).

We measured absolute protein concentrations by fluorescence correlation spectroscopy (FCS) and quantitative immunoblotting in a strain that expresses freely diffusible GFP from the *mad3* promoter (*Pmad3–GFP*). FCS yielded a nuclear GFP concentration of 56 nM (Fig. 1c). On the basis of the relative quantification (Fig. 1a), this indicated nuclear concentrations between 13 nM (Mph1) and 154 nM (Mad2) for the SAC proteins (Supplementary Table 2). We also assessed the abundance of Mad3– and Apc15–GFP by FCS (Fig. 1c). FCS and WiFDeM found similar relative abundances between Mad3, Apc15 and free GFP, which cross-validates the methods. By quantitative immunoblotting, the free GFP concentration was 134 nM (Supplementary Fig. 3). Proteome-wide quantitative mass spectrometry determined values for SAC proteins that were lower or similar to those determined by FCS (Supplementary Table 2). We therefore consider the absolute concentrations derived from FCS of free GFP, in conjunction with relative abundance by WiFDeM, an adequate estimate.

SAC sensitivity to protein abundance changes

To determine which variations of checkpoint protein abundance are compatible with checkpoint activity, we modified the concentration of Mad1, Mad2 and Mad3 by promoter modifications (Supplementary Fig. 4 and Table 3). We assessed SAC activity by measuring mitosis time after preventing microtubule formation with a conditional tubulin mutation (*nda3-KM311*; ref. 20; Fig. 2a). Wild-type cells engage the SAC and remain in mitosis for longer than 5 h. Cells with a reduction of Mad1 to 30% of its wild-type level maintained a mitotic delay (Fig. 2b). Even reduction to about 10% of the original Mad1 level, which is hardly visible by fluorescence microscopy (Fig. 2e), did not fully abolish the SAC. As opposed to the strong reduction of Mad1 that was necessary to affect the SAC, already a slight reduction of Mad2 to 80% of the

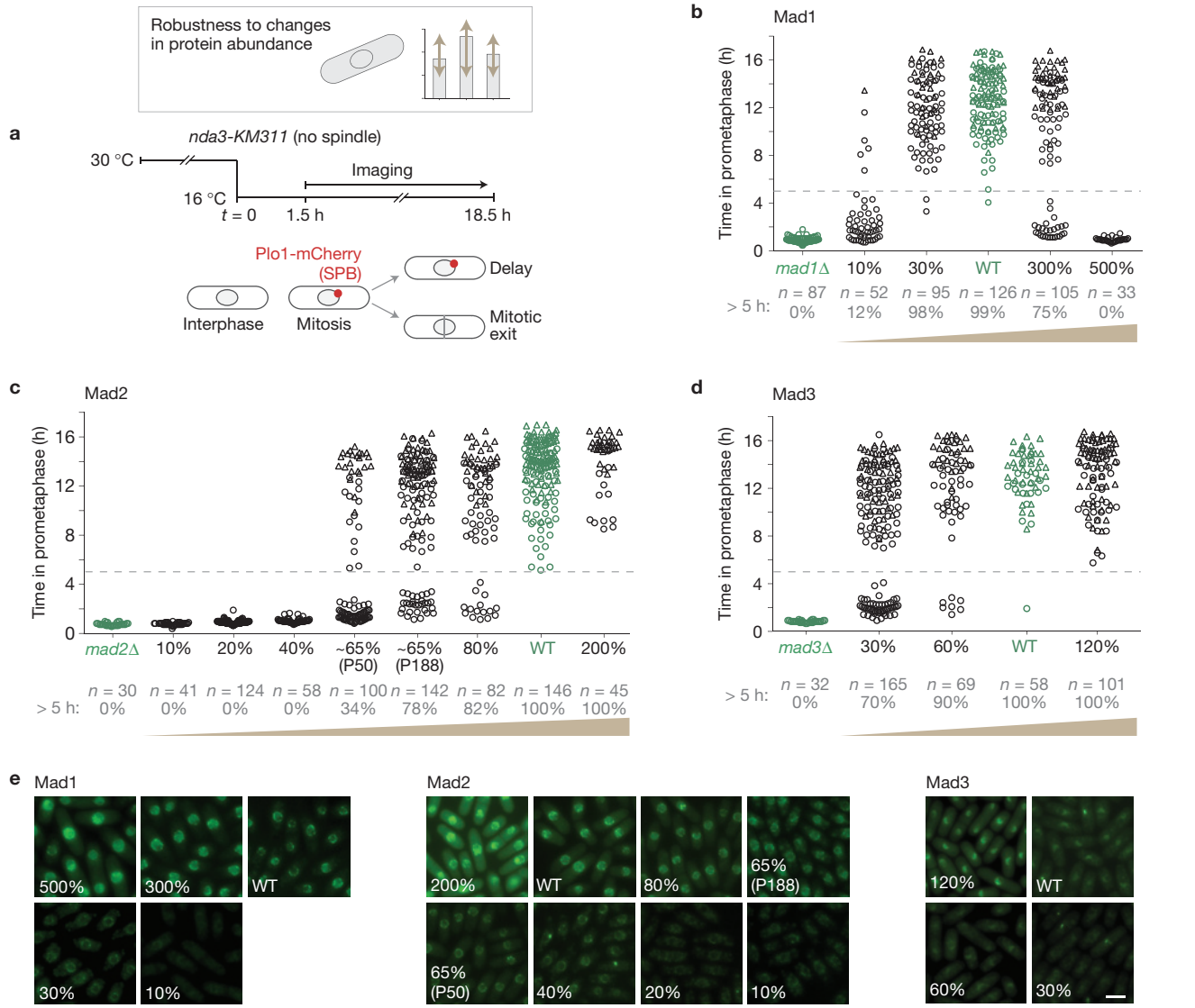

Figure 2 Sensitivity of the checkpoint to SAC protein abundance. (**a**) Cells expressing the tubulin mutant *nda3-KM311* and *plo1*$^{+}$*–mCherry* are shifted to the restrictive temperature for *nda3-KM311* to prevent microtubule formation, which is followed by live-cell imaging. The time in prometaphase, which indicates SAC functionality, is determined by the presence of Plo1–mCherry at spindle pole bodies (SPBs). (**b**–**d**) Mad1–GFP (**b**), Mad2–GFP (**c**) and Mad3–GFP (**d**) strains were followed by live-cell imaging as outlined in **a**. Percentages in black indicate the abundance of the respective protein relative to wild-type cells (Supplementary Fig. 4). Circles indicate cells in which the entire mitosis was recorded; triangles indicate cells that were still in mitosis when filming ended, so that only the lower bound of the mitosis time is known. Number of cells (*n*) and percentage of cells that delayed in mitosis for longer than 5 h are shown in grey. WT, wild type. (**e**) Representative GFP images from strains used in **b**–**d**. Imaging conditions and scaling are identical for strains expressing the same checkpoint protein, but differ between checkpoint proteins. Scale bar, 5 μm.

wild-type level impaired SAC function (Fig. 2c). Reduction to about 65% aggravated the effect, and at abundances of 40% or lower, cells lacked checkpoint activity. At about 65% of Mad2, the SAC response was noticeably different in two strains that had similar levels judged by immunoblotting (termed P188 and P50, Supplementary Fig. 4). This suggests a sharp decline in SAC activity at this level. Mad3 is required together with Mad2 to form the MCC and inhibit the APC/C (refs 12,21). Reduction of Mad3 to 60% slightly impaired the SAC, and reduction to 30% impaired the SAC roughly to a similar extent as 65% of Mad2 (Fig. 2d). Hence, the SAC exhibits distinct sensitivity to changes in the amounts of Mad1, Mad2 and Mad3, and the abundance of Mad2 is particularly critical.

Noise of SAC proteins and APC/C subunits

If a mere 20% reduction of Mad2 impairs SAC signalling (Fig. 2c), the cell-to-cell variability in Mad2 abundance must be small to ensure reliable signalling in wild-type cells. Our single-cell measurements (Fig. 1a) allowed us to estimate the protein noise (coefficient of variation (CV); standard deviation/mean×100(%)). The accuracy of the estimate increases with protein concentration (Supplementary Note). For nuclear Mad1 and Mad2, which have the highest concentration, we determine noise around 10% (Fig. 3a), which is low for proteins in this abundance range (Supplementary Note)[22,23]. Hence, it is indeed rare for wild-type cells to reach a level of 80% Mad2 relative to the population average that would perturb SAC signalling.

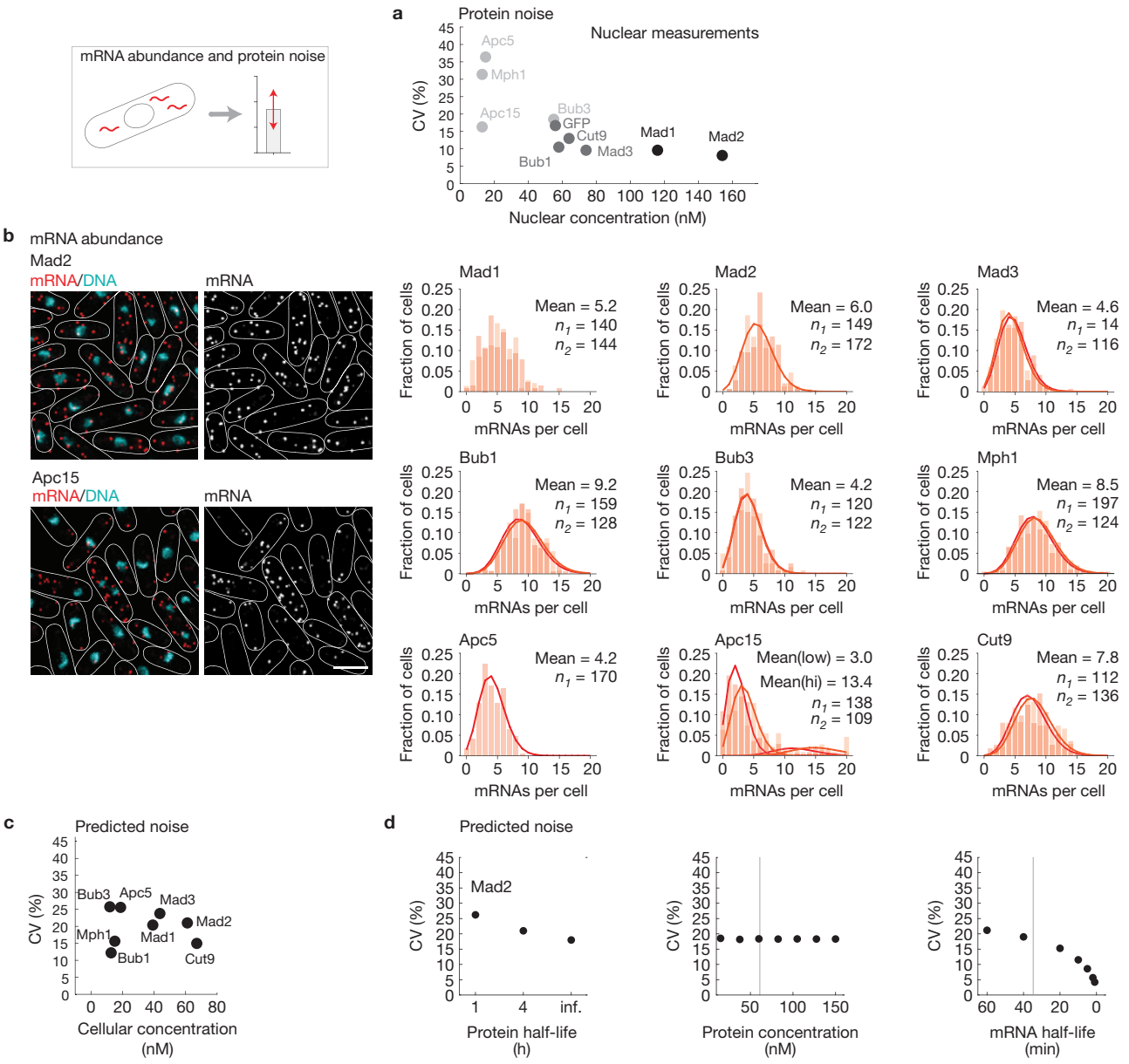

Figure 3 Expression noise of SAC proteins and APC/C subunits. (**a**) Protein noise (CV; standard deviation/mean×100 (%)) from nuclear measurements in Fig. 1a plotted against the nuclear concentration determined by FCS (Fig. 1c and Supplementary Table 2). Low GFP intensity leads to an overestimation of the noise (Supplementary Note). Darker grey indicates more reliable noise measurements. (**b**) Single-molecule FISH with probes against GFP mRNA in strains expressing fusions between the indicated proteins and GFP. Representative images for Mad2–GFP and Apc15–GFP mRNA are shown on the left (scale bar, 5 μm). The histograms show mRNA frequency distributions of two biological replicates (except for Apc5–GFP), and the corresponding fit assuming a Poisson distribution (curve), except for those samples where the *P* value determined from the statistics of the root-mean-square error between model and data, assessed using parametric bootstrapping, rejected the fit (n_1 or n_2 = number of cells in each replicate). Apc15 mRNA abundance fluctuated with cell cycle stage, in agreement with microarray analyses[60–62]; the mean for low and high (hi) expressing cells is given. (**c**) CVs for protein abundance were predicted by stochastic simulation assuming the measured protein concentration (Supplementary Table 2) and mRNA number (**b**), published mRNA half-life[25] and an estimate of 240 min for the protein half-life (Supplementary Note). CVs are plotted against the cellular protein concentration in interphase. (**d**) Protein half-life, protein synthesis rate and mRNA half-life were varied, and CVs were determined by stochastic simulation (Supplementary Note). Thin grey lines indicate measured values (Supplementary Table 2 and ref. 25).

Noise is influenced by messenger RNA number, protein concentration, and mRNA and protein degradation rate. Studies on cell populations determined an mRNA number of SAC genes of about 1 per cell[24] with half-lives between 15 and 35 min (refs 25,26). On the basis of these values, stochastic simulations predict noise of at least 45% for Mad1 and Mad2 (Supplementary Note), considerably higher than our measurement. We therefore assessed mRNA numbers for SAC proteins in single cells by fluorescence *in situ* hybridization[27] (FISH). We detected an average of 4–9 molecules (Fig. 3b), which decreases the expected checkpoint protein noise to 12–26% (Fig. 3c). However, for Mad2 the expected (21%) was still higher than the observed noise (8%). As all measurements that are required for the estimate are associated with uncertainty, we scanned a range of values (Fig. 3d). A longer protein half-life does not suffice for the observed noise, but a

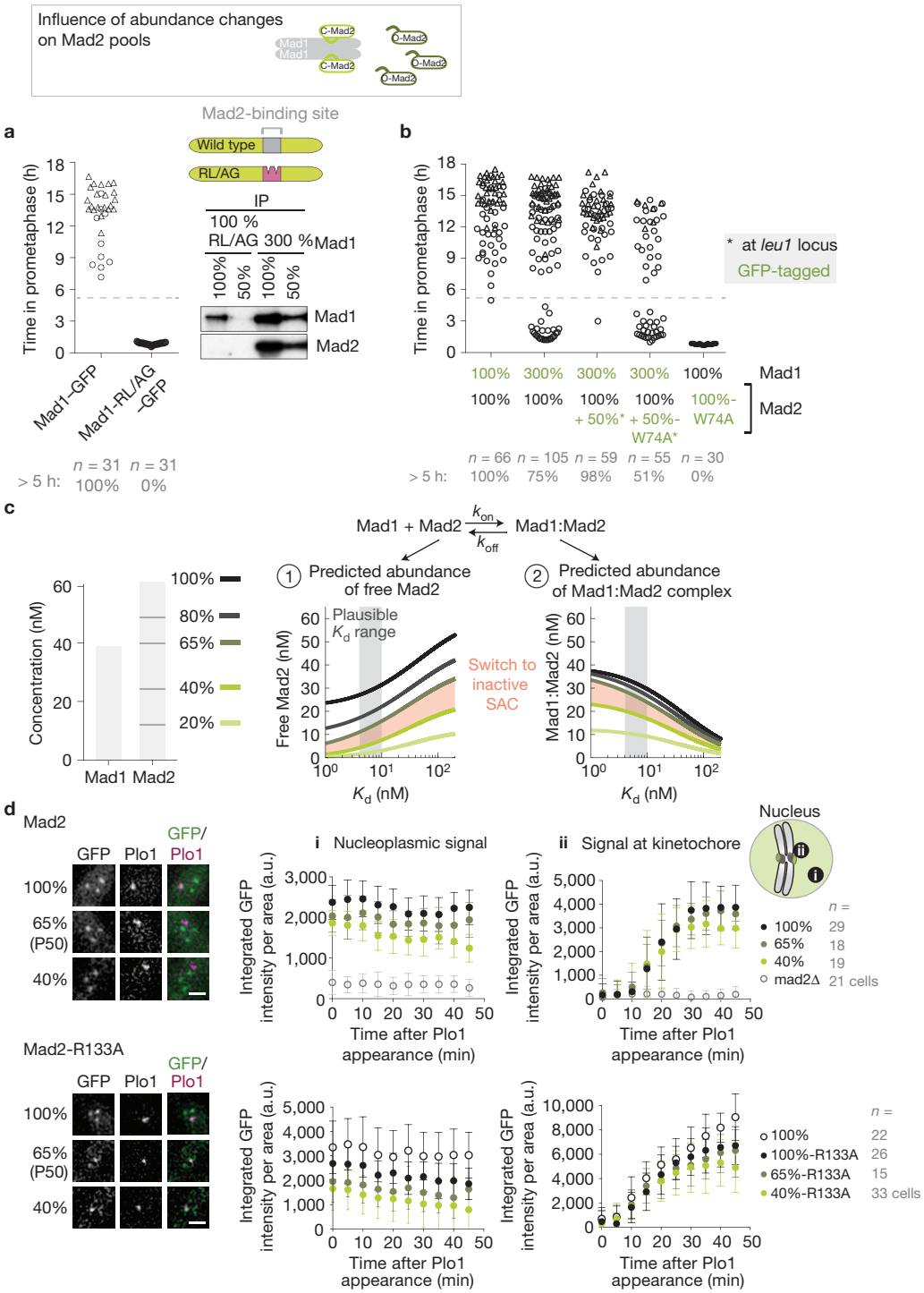

Figure 4 Influence of protein abundance changes on Mad1-bound and free pool of Mad2. (**a**) (Left) Strains were followed by live-cell imaging as in Fig. 2. Mad1-RL/AG contains two point mutations in the Mad2-binding site. (Right) Mad1 immunoprecipitations were analysed for the presence of Mad1 and Mad2. Input and flow through shown in Supplementary Fig. 5c. (**b**) Strains were followed by live-cell imaging as in Fig. 2. Protein abundances were determined by immunoblotting (Supplementary Figs 4a and 5f). Note that expression of 200% of Mad2–GFP is insufficient to delay mitosis or cause checkpoint activation in the absence of Mad1 (Supplementary Fig. 5h,i). Hence, the rescue is not due to artificial checkpoint activation by 150% Mad2. (**c**) Free Mad2 and Mad1:Mad2 abundance were computed from measured cellular concentrations of Mad1 and Mad2 in the wild type and in strains with altered protein abundance. Calculation was performed across a range of K_d values for Mad1:Mad2 complex formation. A plausible range of K_d values is indicated in grey (Supplementary Note). (**d**) The amount of Mad2–GFP or Mad2-R133A–GFP in the nucleoplasm (1) and at the kinetochore (2) was recorded as cells entered mitosis in the absence of microtubules (error bars, s.d.; statistical analysis: Supplementary Fig. 6f). Representative prometaphase nuclei are shown on the left. The dot-like GFP signals result from localization to the kinetochores of the three chromosomes. The dot-like Plo1 signal results from mitosis-specific localization to spindle pole bodies, which fail to separate in the absence of microtubules. Scale bars, 2 μm. Mad2-R133A has similar abundance as wild-type Mad2, but causes a checkpoint defect (Supplementary Fig. 6d,e). Uncropped images of blots are shown in Supplementary Fig. 9.

shorter mRNA half-life allows noise on the order of 10% (Fig. 3d). It is therefore possible that the discrepancy between measured (Fig. 3a) and predicted noise (Fig. 3c) is a consequence of inaccuracies in the existing measurements. Alternatively, yet undescribed feedback mechanisms control the abundance of checkpoint proteins and suppress noise.

SAC sensitivity to relative Mad1 and Mad2 abundance

The checkpoint is doubly sensitive to reduction of Mad2: even a slight reduction impairs checkpoint signalling; and reduction to 40%, which is still higher than the abundance of several other checkpoint proteins, abrogates checkpoint function (Fig. 2c). To address the molecular basis, we analysed the Mad1-bound and Mad1-unbound (free) pool of Mad2. Eliminating the Mad1-bound Mad2 pool by mutation of the binding site within Mad1 abolishes checkpoint signalling[28] (Fig. 4a), although the localization of Mad1 remains intact and Mad2 is present at normal levels (Supplementary Fig. 5). Overexpression of Mad1 to 300 and 500% reduces the free pool of Mad2 and impairs checkpoint signalling[29,30] (Figs 2b and 4b and Supplementary Fig. 5). Additional expression of wild-type Mad2 to about 150% re-increases the free Mad2 pool (Supplementary Fig. 5e) and rescues the checkpoint defect (Fig. 4b and Supplementary Fig. 5g), whereas additional expression of checkpoint-deficient Mad2 (Mad2-W74A; refs 31,32) does not (Fig. 4b). Together, these experiments confirm that both Mad2 pools are vital for checkpoint function.

We predicted the changes in the two Mad2 pools following reduction of Mad2, given the measured abundances of Mad1 and Mad2 (Fig. 4c). Lowering Mad2 to 80% or 65% should reduce the pool of free Mad2, but affect Mad1-bound Mad2 only little (Fig. 4c). Further reduction of Mad2 to 40 and 20% should continue to lower the pool of free Mad2, but should also decrease the abundance of Mad1:Mad2 (Fig. 4c). To test this prediction, we analysed the levels of Mad2 at kinetochores and in the nucleoplasm. As kinetochore localization of Mad2 crucially depends on Mad1 (ref. 33), the pool of Mad2 at kinetochores reflects the abundance of Mad1:Mad2. In contrast, the nucleoplasmic pool is additionally influenced by free Mad2. We measured wild-type Mad2 and the dimerization-deficient Mad2-R133A (ref. 34), which can be recruited to kinetochores only by direct binding to Mad1. Nucleoplasmic Mad2 decreased progressively as Mad2 was reduced to 65 and 40% Mad2 (Fig. 4d), which fitted our expectation for free Mad2. In contrast, the abundance of Mad2 at the kinetochore was less affected at 65% than at 40% (Fig. 4d) or 20% Mad2 (Supplementary Fig. 6a), in accordance with our prediction for Mad1:Mad2. To exclude that the reduction of Mad2 at kinetochores is influenced by the checkpoint failure in some strains, we tested Mad2 localization in cells lacking Mad3 or expressing Slp1 that is unable to bind Mad2 (*slp1-mr63*; ref. 35). Neither of these conditions reduced Mad2 kinetochore localization (Supplementary Fig. 6c). We conclude that reductions of Mad2 to 80 or 65% are likely to preferentially diminish the free pool of Mad2, leading to a partial checkpoint defect, mimicking the situation of 300% Mad1 (Supplementary Figs 5e and 6b). The checkpoint failure in cells with 40% or less Mad2 is unlikely to be solely due to the reduction of Mad1:Mad2, because cells with 30% Mad1 have less Mad1:Mad2 at kinetochores than cells with 40% Mad2 (Supplementary Fig. 6g), yet maintain checkpoint function (Fig. 2b). Instead, the checkpoint failure below 40% Mad2 could be due to either strong depletion of free Mad2 (Supplementary Fig. 6b), not leaving enough Mad2 to capture all Slp1, or could be due to a concomitant reduction of free Mad2 and Mad1:Mad2. Overall, the experiments underline the importance of appropriate relative levels between Mad1 and Mad2 (refs 29,36–39). Given this necessity, it is surprising that there is apparently no co-regulation of Mad1 and Mad2 abundance (Supplementary Figs 4–6).

SAC sensitivity to nutrient conditions

The checkpoint needs to be robust to fluctuations in intracellular conditions and to changes in the environment. We therefore probed SAC signalling in two different media (rich and minimal; Fig. 5). When chromosome attachment was prevented, wild-type cells delayed in mitosis in both media, suggesting robustness. In strains with altered SAC protein levels, however, the mitotic delay times differed between the two media (Fig. 5a). In cells with 30% Mad1, the checkpoint was markedly impaired in minimal medium, although largely functional in rich medium. This indicated that SAC signalling changes in response to nutrient conditions. We did not observe any difference in SAC protein or APC/C subunit abundance between the two media (Fig. 5b). However, the checkpoint target Slp1 accumulated to about twice the level in minimal compared with rich medium (Fig. 5c). This indicates that the environment alters SAC signalling, at least partly through changes in Slp1 abundance.

Tolerated Mad2 and Mad3 abundance set by Slp1 abundance

The SAC blocks APC/C activity by binding of Mad2 and Mad3 to Slp1, forming the MCC. The relative abundance between these proteins should therefore be an important determinant of checkpoint activity. As Slp1 (like other Cdc20 orthologues) has a short half-life[40,41] (Supplementary Fig. 3h), the comparably long maturation time of GFP (ref. 42) makes quantification through a GFP tag inaccurate. We therefore determined the abundance of endogenous Slp1 by quantitative immunoblotting (Fig. 6a and Supplementary Fig. 7). In cells synchronously undergoing mitosis, Slp1 accumulated to about 21 nM in rich medium (Fig. 6a) with slight enrichment (to about 30 nM) in the nucleus (Supplementary Fig. 7d). By single-molecule FISH, the number of Slp1 mRNAs varied between 0 (mean: 4.5) in interphase and up to more than 100 molecules in mitotic cells (Fig. 6b and Supplementary Fig. 7f). We confirmed that Slp1 is about twice as abundant in minimal medium (Supplementary Fig. 7). As we measured absolute Slp1 abundance by a different method from the absolute abundance of SAC proteins, we can compare the numbers only with some reservation. However, the amount of Mad3 (44 nM, Supplementary Table 2) and free Mad2 (around 30 nM, Fig. 4c) would be sufficient to capture 21 nM of Slp1.

To corroborate that the relative levels between Mad2, Mad3 and Slp1 matter, we decreased and increased Slp1. Decreasing Slp1 to about 40% fully rescued the checkpoint defect of cells with 30% Mad3, 65 or 40% Mad2, and of cells with both Mad2 and Mad3 reduced to 40 and 30%, respectively (Fig. 6c,d). Cells with 40% Slp1 and 20% Mad2 had an almost fully functional checkpoint, whereas the absence of Mad2 or Mad3 still caused a checkpoint failure. Increasing Slp1 abundance by inserting a second copy under its endogenous regulatory sequences (Fig. 6f) enhanced the effect of lowering Mad2 or Mad3, and the checkpoint was impaired even when Mad2 and Mad3 were unchanged (Fig. 6e). This was consistent with our abundance measurements, which suggested that Mad2 and Mad3 become limiting

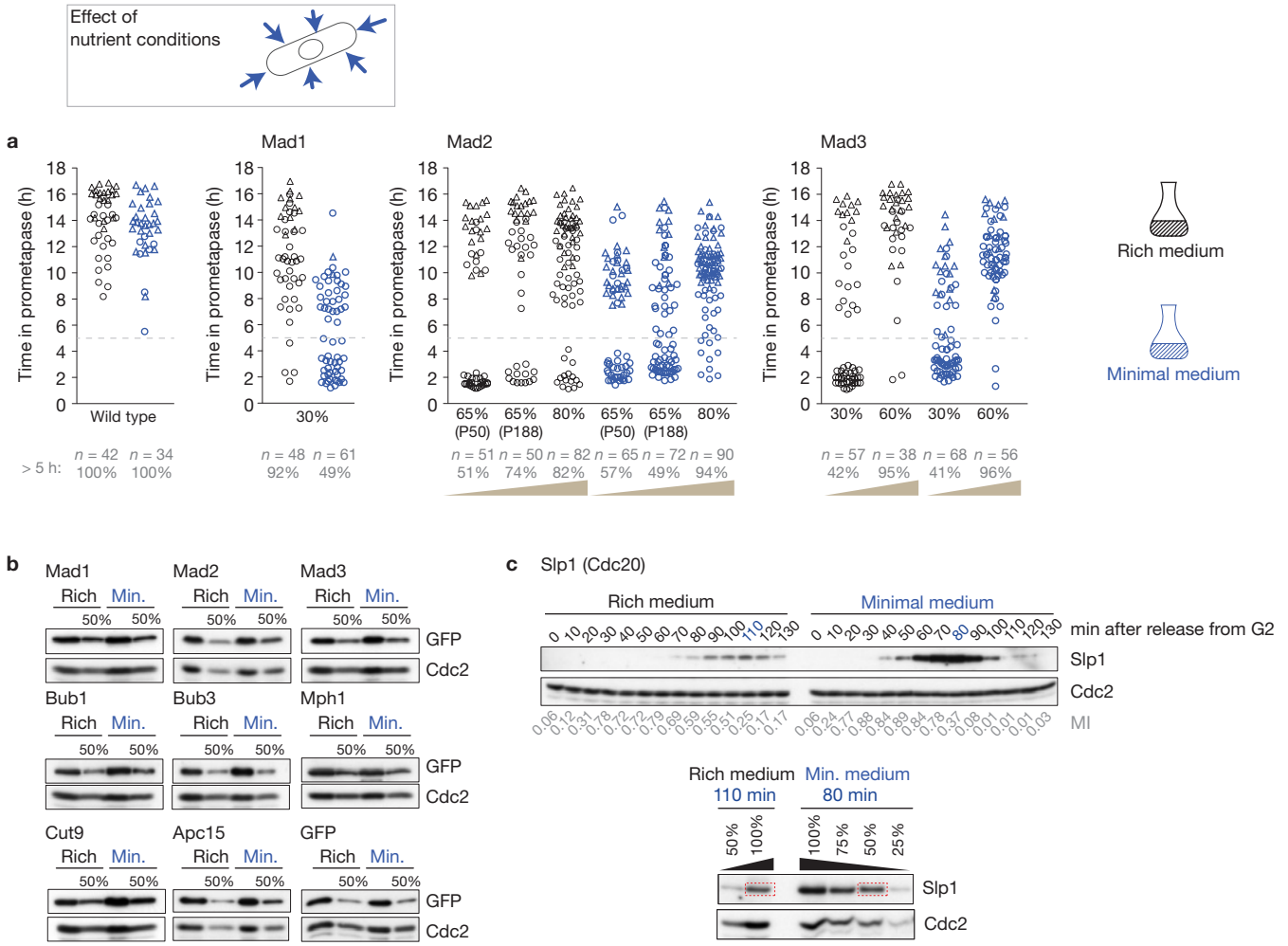

Figure 5 Alteration of the checkpoint response by growth medium. (**a**) Strains were followed by live-cell imaging as in Fig. 2 in either rich medium (black) or minimal medium (blue). (**b**) Strains expressing protein–GFP fusions from the endogenous locus were grown in rich or minimal (min.) medium. Extracts were analysed by immunoblotting using anti-GFP and anti-Cdc2 (loading control) antibodies. In every second lane, half the amount of extract was loaded (50%). (**c**) Cdc25-22 cells were cultured in rich or minimal medium, synchronized in G2 and released into mitosis at 16 °C. Samples were taken every 10 min and cell extracts were analysed for Slp1 abundance by immunoblotting with Cdc2 as the loading control. The mitotic index (MI; fraction of (pro)metaphase cells) is given below. The time point of maximal Slp1 signal was used to compare Slp1 abundance in rich and minimal medium (lower part). Percentages on top indicate how much of the extract was loaded. Dashed rectangles indicate bands with similar signal strength from which relative protein abundances were deduced. Uncropped images of blots are shown in Supplementary Fig. 9.

when Slp1 is increased to 200%, and with data from budding yeast showing that overexpression of the Slp1 orthologue by about threefold impaired the SAC (ref. 40). However, the result contrasted with the functional checkpoint observed in minimal medium for a similar abundance of Slp1 (Fig. 5). We suggest that additional, possibly post-translational modifications alter SAC signalling in minimal medium. Our experiments underline the importance of accurate relative levels both within checkpoint proteins and between checkpoint proteins and the checkpoint target Slp1.

Stoichiometric Slp1 inhibition as the cause of the population split

In several of our experiments the mitosis time of cells in a clonal population showed a bimodal distribution (for example, Fig. 2b–d), which we confirmed by statistical analysis (Fig. 7a and Supplementary Fig. 8a). We observed the split into two populations (which we call A and B (Fig. 7a)) when decreasing Mad2 or Mad3 (Fig. 2c,d) or increasing Slp1 (Fig. 6e). This hinted at a mechanism involving MCC formation. Stoichiometric binding reactions, such as MCC formation, can generate ultrasensitivity[43], which could be the source of the population split. To investigate this possibility, we analysed a model for MCC formation (model M1; Fig. 7b). In this model the amount of free Slp1 in the steady state can vary disproportionally with small changes (biological noise) in the Slp1 synthesis rate or the inhibitor concentration (Supplementary Note). We assumed that free Slp1 has to surpass a threshold to initiate anaphase and estimated the required parameters from the observed sizes of population A and B under different experimental conditions (Supplementary Note). Parameters within physiologically plausible boundaries reproduced our observations: free Slp1 stayed below the threshold in wild-type cells, despite varying levels of Slp1 synthesis and inhibitor (Fig. 7c), whereas in 30% Mad3 (Fig. 7c) or similar perturbations (Supplementary Note), Slp1 surpassed the threshold in the experimentally observed fraction of cells.

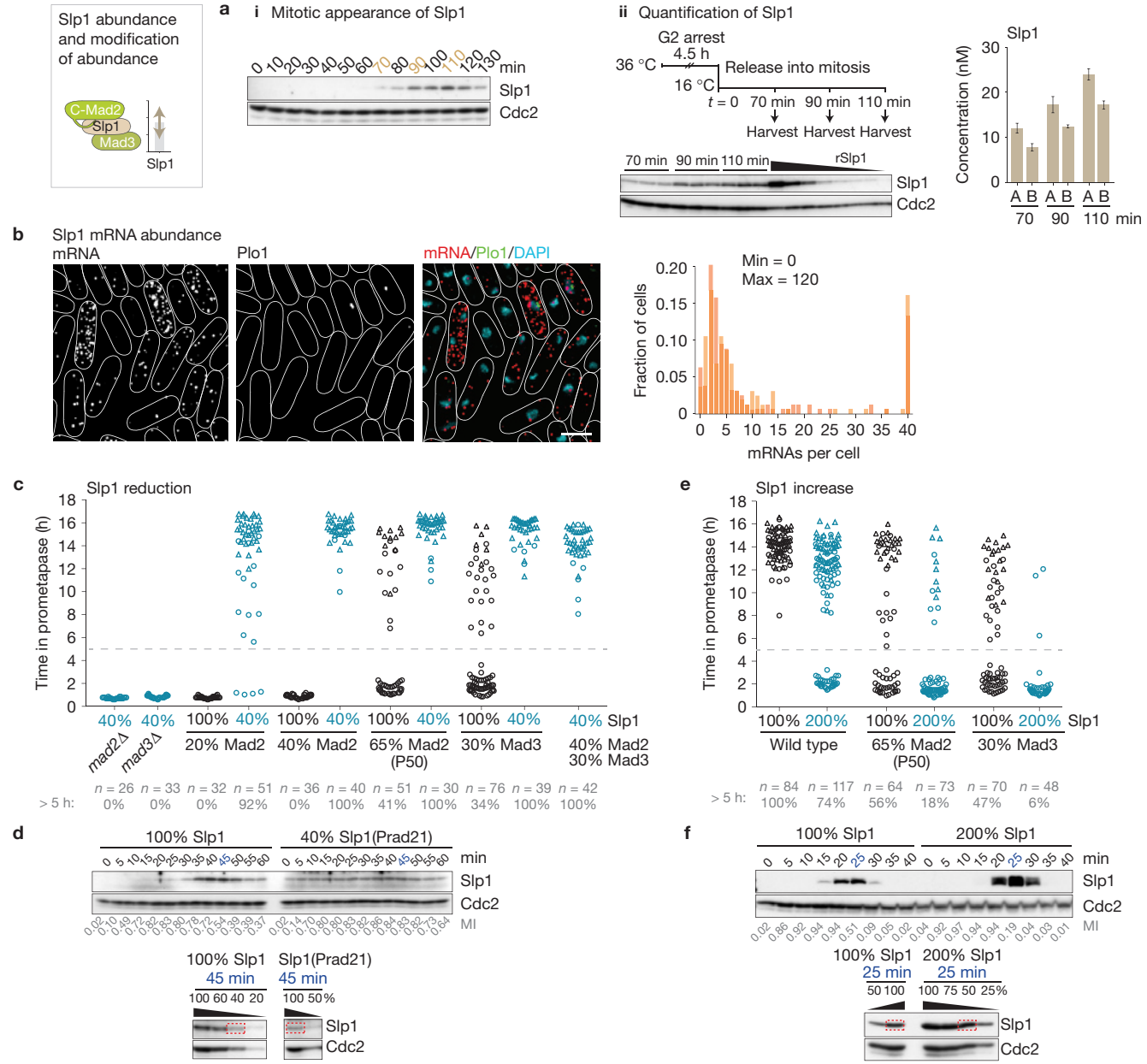

Figure 6 Influence of Slp1 abundance on the amount of Mad2 and Mad3 required for checkpoint function. (**a**) *Cdc25-22* cells were grown in rich medium, synchronized in G2 and released into mitosis at 16 °C. Immunoblotting shows an absence of Slp1 from G2 cells and accumulation in mitosis (**i**). To determine Slp1 concentration, three technical replicates were collected at the indicated time points and analysed by immunoblotting using anti-Slp1 and anti-Cdc2 (loading control) antibodies (**ii**). Recombinant His_6–Slp1 (rSlp1) was mixed with G2 extract and used as the standard for quantification. The graph on the right shows the average concentrations determined in two independent experiments (A, B; error bars, s.d. of technical replicates). (**b**) Single-molecule FISH of cells grown in rich medium with probes against Slp1 mRNA. A representative image is shown on the left (scale bar, 5 μm). Localized Plo1–GFP signals indicate cells in prometaphase. The histogram on the right depicts the mRNA frequency distribution of two replicates ($n = 158$ and 161 cells). (**c**–**f**) Slp1 abundance was altered and combined with changes in Mad2 or Mad3 abundance. (**c**,**e**) Strains were followed by live-cell imaging as in Fig. 2. (**d**,**f**) *Cdc25-22* cells were cultured in rich (**d**) or minimal (**f**) medium, synchronized in G2 and released into mitosis at 25 °C. Cell extracts taken at the indicated time points were analysed by immunoblotting using anti-Slp1 and anti-Cdc2 (loading control) antibodies. The mitotic index (MI; fraction of (pro)metaphase cells) is given below. The time point of maximal Slp1 signal was used to compare Slp1 abundances (lower part) as in Fig. 5c. Uncropped images of blots are shown in Supplementary Fig. 9.

The APC/C mediates MCC disassembly[44–46], which forms a double-negative feedback loop with the MCC-mediated inhibition of the APC/C. This could also cause ultrasensitivity and explain a population split. We therefore included the APC/C into the MCC formation model (model M2; Fig. 7d). Parameters within physiologically plausible boundaries could describe the population split through a bimodal distribution of the APC/C:Slp1 steady-state concentration; that is, although single cells differ only by typical protein noise, the resulting APC/C:Slp1 concentrations, and therefore the propensity to initiate anaphase, can show a bimodal distribution (Fig. 7e and Supplementary Note). Hence,

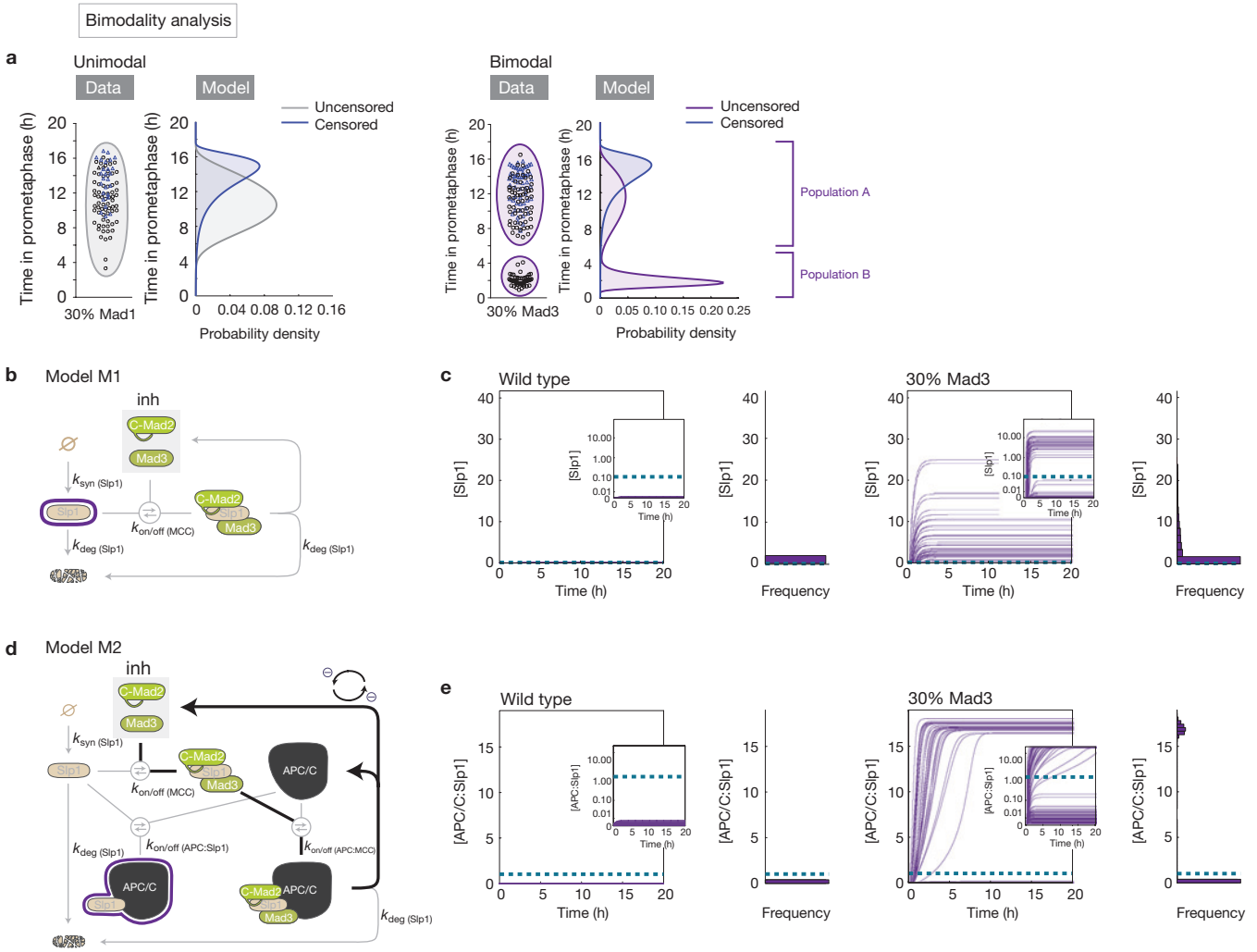

Figure 7 Models for core checkpoint reactions describing the occurrence of two populations. (**a**) Mitosis times were analysed by multi-experiment modelling for the occurrence of one or two subpopulations (Supplementary Fig. 8a). Examples for a unimodal (left, 30% Mad1) and a bimodal (right, 30% Mad3) distribution are shown. Uncensored (full mitosis time recorded) and censored mitosis times (recording stopped before mitosis ended) were modelled separately. (**b**) Reaction scheme for MCC formation. Slp1 is synthesized with rate $k_{syn(Slp1)}$ and degraded with rate $k_{deg(Slp1)}$. Mad2 and Mad3 act as stoichiometric inhibitors (inh) of Slp1 and bind with association rate $k_{on(MCC)}$ and dissociation rate $k_{off(MCC)}$. Slp1 within the complex is degraded with the same rate as free Slp1 (Supplementary Note). (**c**) The model in **b** was parameterized to fit the experimental data and simulated over time (Supplementary Note) for wild-type or 30% Mad3. Slp1 synthesis and inhibitor concentration are randomly sampled from log-normal distributions. The largest plot shows the concentration of free Slp1, [Slp1], over time (purple lines) with the frequency distribution at 20 h plotted on the right. The inset shows [Slp1] using a nonlinear *y* axis (Supplementary Note), which allows visualization of the trajectories around the threshold. When Slp1 stays below the threshold (dashed blue line), we consider this cell to arrest in mitosis (population A); when Slp1 passes the threshold, we assume that the cell exits mitosis (population B). (**d**) Reaction scheme for MCC formation and APC/C binding. In addition to the reactions in **b**, Slp1 binds the APC/C with $k_{on(APC:Slp1)}$ and $k_{off(APC:Slp1)}$, and MCC binds the APC/C with $k_{on(APC:MCC)}$ and $k_{off(APC:MCC)}$. Slp1 within the MCC bound to the APC/C is degraded with the same rate as Slp1, which leads to dissociation of Mad2 and Mad3 from the APC/C (Supplementary Note). APC/C inhibition by the MCC and MCC disassembly by the APC/C form a double-negative feedback loop (bold lines) that can lead to ultrasensitivity. (**e**) The model in **d** was parameterized to fit the experimental data and simulated over time as in **c**. The predicted concentration of APC/C:Slp1 in 30% Mad3 cells after 20 h shows a bimodal distribution.

our computational models suggest that known checkpoint reactions can explain the population split through protein noise.

Non-genetic variability in checkpoint signalling

To explore whether population A and B may indeed result from protein noise, we analysed the checkpoint activity of sister cells in situations where a population split was observed (Fig. 8a). As protein abundance in the mother cell is passed on to the daughter cells, sister cells resemble each other in protein abundance just after cell division but the similarity disappears over time owing to continuing noise[47–49]. We found that sister cells showed the same checkpoint behaviour more often than expected for unrelated cells (Fig. 8a). Hence, there is some correlation between sister cells, which is consistent with protein noise as the basis of the population split. About 20% of sister cell pairs differed in their checkpoint behaviour, which is strong evidence against a genetic cause. We conclude that non-genetic, stochastic variations in protein abundance may determine whether a cell shows the fate of population A or B.

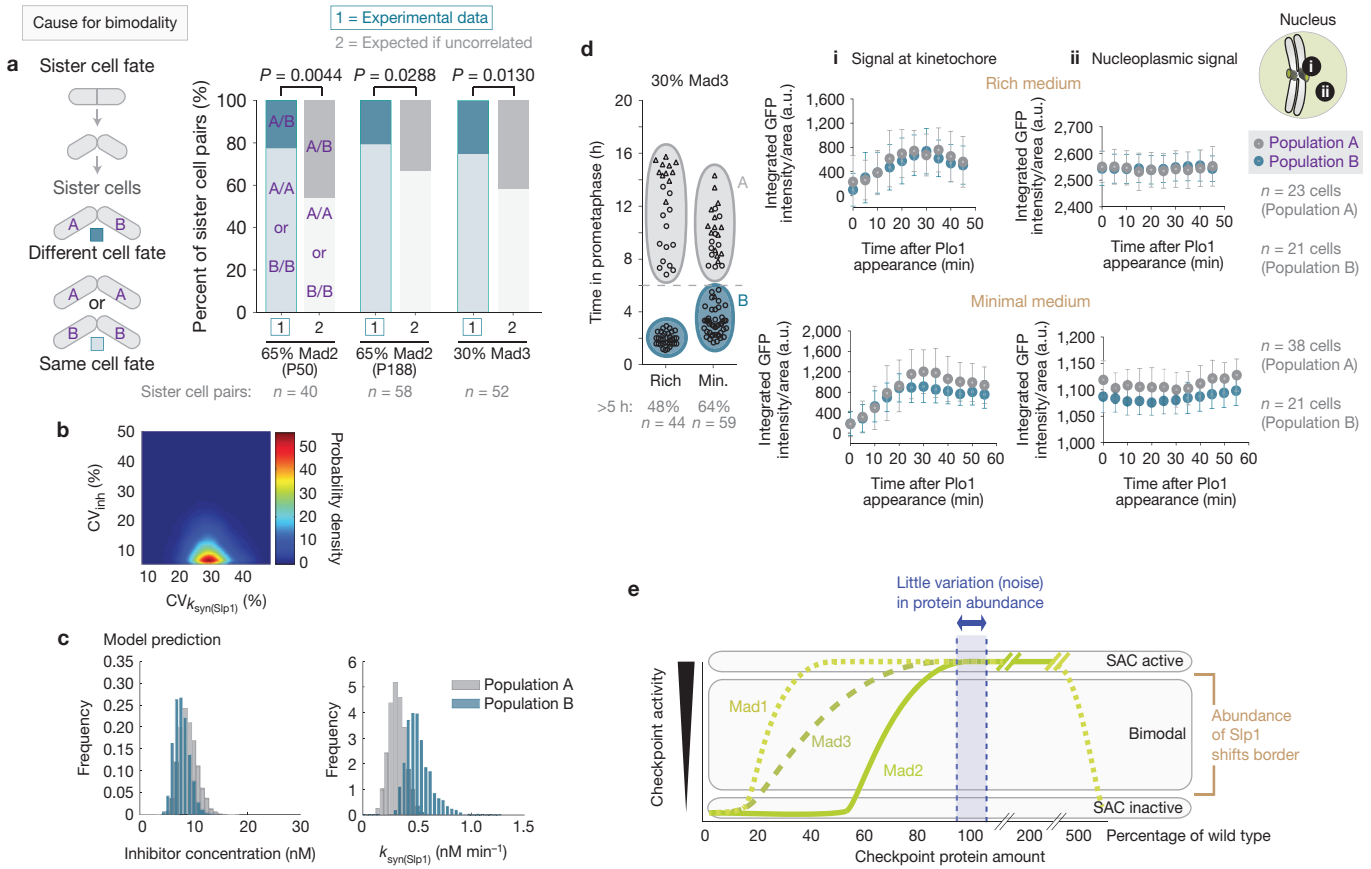

Figure 8 Non-genetic basis of the population split. (**a**) Sister cell pairs were followed by live-cell imaging as in Fig. 2. For each pair, we recorded whether it consisted of two cells with the same fate (A/A or B/B), or of two cells with different fates (A/B) (experimental data). The expected distribution for uncorrelated sister behaviour, which depends on the size of populations A and B, is shown in grey (expected if uncorrelated). Experimental result and expected outcome for uncorrelated behaviour were compared using a Chi-squared test. (**b**) The density distribution for the noise (CV) of Slp1 synthesis rate ($k_{syn(Slp1)}$) and inhibitor concentration was determined with model M1 (Supplementary Note). For wild-type cells, the model predicts lower noise in inhibitor concentration than in Slp1 synthesis. (**c**) The distributions of inhibitor concentration and Slp1 synthesis rate in populations A and B in cells with 30% Mad3 were predicted with model M2 (Supplementary Note). (**d**) Strains were followed by live-cell imaging as in Fig. 2 in either rich or minimal (min.) medium (left side). Mad3–GFP signals were quantified in each population (A and B) as cells entered mitosis (right side; a.u., arbitrary units; error bars, s.d). Statistical analysis: Supplementary Fig. 8d). Differences in Mad3 concentration between the two populations in minimal medium were statistically significant ($P < 0.05$). For rich medium, one representative out of two independent experiments is shown. (**e**) Sensitivity of the SAC to alterations in protein abundance. Checkpoint signalling is normally reliable, and all cells that encounter unattached chromosomes are delayed in mitosis (the SAC is active). Alterations in checkpoint protein abundance can shift checkpoint signalling into one of two other regimes: either only a fraction of cells responds reliably to unattached chromosomes (bimodal), or the checkpoint response is abolished in the entire population (SAC is inactive). To preserve reliable signalling, the abundance of some SAC proteins (for example, Mad2) can fluctuate only little. The abundance of Slp1 shifts the borders at which transition into another regime happens.

We used models M1 and M2 to investigate which extent of noise is required for the observed population split, while preserving a stable arrest in wild-type cells. Both models agreed that the noise for the inhibitor concentration in wild-type cells should be lower (CV: 5 and 9%, respectively) than for Slp1 synthesis (CV: 32 and 35%, respectively). An exhaustive exploration of the parameter space for model M1 confirmed this notion (Fig. 8b). This is consistent with the low noise of checkpoint proteins (Fig. 3), and we find it conceivable that the strong increase in transcription, and potentially translation, for Slp1 at the start of mitosis leads to a larger variability (Fig. 6). Model M2 indicated that the mean inhibitor concentration should differ little between population A and B, whereas the Slp1 synthesis rate should differ more (Fig. 8c). We cannot specifically measure the concentration of the active, inhibitory species of Mad2 and Mad3, but measured the total concentration as a substitute. The levels of Mad2 and Mad3 were highly similar between the two populations (Fig. 8d and Supplementary Fig. 8b–d). In minimal medium, we observed a slight tendency for higher Mad2 and Mad3 levels in the population of cells arresting for longer, consistent with the model prediction. When we vary Mad3 abundance in a strain with 65% Mad2, the fraction of cells in population A and B changes only little (Supplementary Fig. 8f), which confirms the relative insensitivity of the population split to changes in Mad3 abundance. As the pool of active Mad2 and Mad3 could be influenced by upstream checkpoint components, we analysed the amount of Bub1 in the two populations, but also found no significant difference (Supplementary Fig. 8e). Both experiments and model predictions therefore support that differences in the Slp1 synthesis rate play a stronger role in determining whether a cell is able to arrest following checkpoint activation or escapes the arrest. Overall, our results suggest that slight cell-to-cell variations can cause a

population split in the checkpoint response and that known checkpoint reactions can explain this split.

DISCUSSION

The SAC is crucial for genome integrity. How this checkpoint operates robustly is not understood. Here, we provide a comprehensive quantification of SAC proteins and perform an *in vivo* sensitivity analysis that evaluates checkpoint activity following changes in checkpoint protein abundance or nutrient conditions. We made several important observations: even small variations in checkpoint protein abundance can strongly impact signalling; the level of the relevant checkpoint proteins is kept within a narrow window; changes in protein abundance can cause non-genetic variability in the checkpoint response; and nutrient conditions influence the level of the checkpoint target Slp1, suggesting that cells modify SAC signalling in response to the environment.

Stoichiometric inhibition underlies robustness and fragility of SAC signalling

Robustness to perturbations is a key feature of many biological systems. Tight binding of an activator by an inhibitor can buffer variations in these components, as long as the inhibitor is in large enough excess[43]. A theoretical analysis of SAC signalling suggested that inhibition of the APC/C activator Slp1 (Cdc20) through sequestration by Mad2 and Mad3 provides robustness to fluctuations in Slp1 production[13]. Our experimental and theoretical analysis supports this mechanism (Figs 7 and 8). The robustness provided by stoichiometric inhibition, however, comes at a price. If the abundance of the inhibitor is reduced, the system output becomes variable, as is the case with 80% Mad2 or 60% Mad3. Hence, for the checkpoint to work reliably the abundance of these proteins should not fluctuate beyond certain borders, and indeed we observe low noise for Mad2 and Mad3 (Fig. 3). This level of noise is lower than is expected on the basis of measured protein and mRNA abundance and half-life (Supplementary Note). It remains an open question whether the discrepancy is due to incorrect measurements or whether yet undiscovered regulatory mechanisms, for example negative feedback between protein abundance and translation rate, control protein noise.

Reasons for narrow zone of reliable signalling

The fragility of the checkpoint to reduction of some of its components seems dangerous for cells and requires that these proteins are kept within tight windows of abundance (Fig. 8e). Slightly increasing the abundance of these proteins does not impair checkpoint signalling (Fig. 2), raising the question of why the level is not higher. The reason could be adaptability of the system. Alterations in the abundance of Slp1, as they are seen in different media, will not have a consequence on SAC signalling if the levels of critical SAC proteins are so high that these alterations are buffered. Hence, the system has to find a trade-off between reliable signalling in most situations, and the possibility to alter the system if needed. Alternatively, kinetic requirements may determine the levels. Higher levels of Mad2 or Mad3 may impair the ability to quickly and reliably silence the checkpoint. We expect that the levels of checkpoint proteins are under selection, and different organisms may operate with different relative and absolute levels. For example, for both budding yeast and vertebrate cells[29,50–56], there is evidence that the relative excess of Mad2 over Mad1 is higher than in fission yeast. Clearly, more work is needed to determine how different organisms regulate checkpoint levels and why certain levels are chosen.

Alteration of SAC signalling by changes in protein abundance

We show that SAC signalling can be both altered and abolished by changes in protein abundance. Such changes in abundance may occur in physiologic or pathologic situations. Modifications in checkpoint gene expression or protein abundance have been observed in different tissues (The Human Protein Atlas, ref. 57), during ageing[58], and in cancer cells (Oncomine database). In these situations, checkpoint signalling may be modified, and non-genetic variability in signalling could arise. Cancer cells show non-genetic variability in response to antimitotic drugs that activate the checkpoint[59]. Whether this is indeed related to altered checkpoint protein abundance remains to be examined. Overall, our results highlight both the robustness and the plasticity of SAC signalling and emphasize that checkpoint protein abundance is an important determinant in specifying the checkpoint response. □

METHODS

Methods and any associated references are available in the online version of the paper.

Note: Supplementary Information is available in the online version of the paper

ACKNOWLEDGEMENTS

We thank S. Umrania and G. Raetsch for help with developing image analysis software, M. Wachsmuth for FCS analysis software, D. Zenklusen and S-R. Imrazene for sharing their FISH protocol, B. Schwalb and A. Tresch for providing mRNA half-life measurements, N. Hustedt and J. Sauerwald for experiments, E. Illgen, E. Schwoerzer, J. Binder, F. Bolukbasi and W. Hauf for excellent technical help, T. Holder for data processing scripts, C. Liebig for advice on image processing, and F. Theis for support in developing the multi-experiment modelling. We are grateful to K. Gull and T. Matsumoto for antibodies, and to F. Bono, F. Herzog, M. Hothorn, S. Legewie and Y. Watanabe for comments on the manuscript. This work was supported by the Max Planck Society (S. Hauf, S. Heinrich, J.K., C.W. and P.D.), the Ernst Schering Foundation (fellowship to S. Heinrich), the Boehringer Ingelheim Fonds (fellowship to J.K.), the Memorial Sloan-Kettering Cancer Center (C.W. and P.D.), the Cluster of Excellence in Simulation Technology (EXC 310) of the German Research Foundation (DFG; N.R.), the Human Frontier Science Program (HFSP; postdoctoral fellowship to S.T.), the funding program for junior professors of the Ministry of Science, Research and Arts of Baden-Württemberg (E-M.G. and N.R.), and the Federal Ministry of Education and Research (BMBF) within the Virtual Liver project (Grant No. 0315766; J.H.).

AUTHOR CONTRIBUTIONS

S. Heinrich designed and performed all experiments, with the exception of FCS (by S.T. and M.K.), Slp1 quantification in EMM (J.K.), and characterization of the Mad1-RL/AG mutant (J.K.); S. Heinrich constructed plasmids and strains with contributions by J.K.; E-M.G., N.R., J.H. and S. Hauf performed modelling and statistical evaluation; C.W. developed the automated nuclear tracking approach with contributions from P.D.; S. Hauf devised the project and wrote the manuscript together with S. Heinrich and input from all authors.

COMPETING FINANCIAL INTERESTS

The authors declare no competing financial interests.

Published online at www.nature.com/doifinder/10.1038/ncb2864
Reprints and permissions information is available online at www.nature.com/reprints

1. Barkai, N. & Shilo, B. Z. Variability and robustness in biomolecular systems. *Mol. Cell* **28,** 755–760 (2007).
2. Raj, A. & van Oudenaarden, A. Nature, nurture, or chance: stochastic gene expression and its consequences. *Cell* **135,** 216–226 (2008).
3. Lara-Gonzalez, P., Westhorpe, F. G. & Taylor, S. S. The spindle assembly checkpoint. *Curr. Biol.* **22,** R966–R980 (2012).

4. Jia, L., Kim, S. & Yu, H. Tracking spindle checkpoint signals from kinetochores to APC/C. *Trends Biochem. Sci.* **38,** 302–311 (2013).
5. Vleugel, M., Hoogendoorn, E., Snel, B. & Kops, G. J. Evolution and function of the mitotic checkpoint. *Dev. Cell* **23,** 239–250 (2012).
6. Pines, J. Cubism and the cell cycle: the many faces of the APC/C. *Nat. Rev. Mol. Cell Biol.* **12,** 427–438 (2011).
7. Primorac, I. & Musacchio, A. Panta rhei: the APC/C at steady state. *J. Cell Biol.* **201,** 177–189 (2013).
8. Sironi, L. *et al.* Crystal structure of the tetrameric Mad1-Mad2 core complex: implications of a 'safety belt' binding mechanism for the spindle checkpoint. *EMBO J.* **21,** 2496–2506 (2002).
9. De Antoni, A. *et al.* The Mad1/Mad2 complex as a template for Mad2 activation in the spindle assembly checkpoint. *Curr. Biol.* **15,** 214–225 (2005).
10. Mapelli, M. & Musacchio, A. MAD contortions: conformational dimerization boosts spindle checkpoint signaling. *Curr. Opin. Struct. Biol.* **17,** 716–725 (2007).
11. Luo, X. & Yu, H. Protein metamorphosis: the two-state behavior of Mad2. *Structure* **16,** 1616–1625 (2008).
12. Chao, W. C., Kulkarni, K., Zhang, Z., Kong, E. H. & Barford, D. Structure of the mitotic checkpoint complex. *Nature* **484,** 208–213 (2012).
13. Doncic, A., Ben-Jacob, E. & Barkai, N. Noise resistance in the spindle assembly checkpoint. *Mol. Syst. Biol.* **2,** 1–6 (2006).
14. Wu, J. Q. & Pollard, T. D. Counting cytokinesis proteins globally and locally in fission yeast. *Science* **310,** 310–314 (2005).
15. Ohi, M. D. *et al.* Structural organization of the anaphase-promoting complex bound to the mitotic activator Slp1. *Mol. Cell* **28,** 871–885 (2007).
16. Yamashita, Y. M. *et al.* 20S cyclosome complex formation and proteolytic activity inhibited by the cAMP/PKA pathway. *Nature* **384,** 276–279 (1996).
17. Vanoosthuyse, V., Valsdottir, R., Javerzat, J. P. & Hardwick, K. G. Kinetochore targeting of fission yeast Mad and Bub proteins is essential for spindle checkpoint function but not for all chromosome segregation roles of Bub1p. *Mol. Cell Biol.* **24,** 9786–9801 (2004).
18. He, X., Jones, M. H., Winey, M. & Sazer, S. Mph1, a member of the Mps1-like family of dual specificity protein kinases, is required for the spindle checkpoint in *S. pombe*. *J. Cell Sci.* **111,** 1635–1647 (1998).
19. Zich, J. *et al.* Kinase activity of fission yeast Mph1 is required for Mad2 and Mad3 to stably bind the anaphase promoting complex. *Curr. Biol.* **22,** 296–301 (2012).
20. Hiraoka, Y., Toda, T. & Yanagida, M. The NDA3 gene of fission yeast encodes beta-tubulin: a cold-sensitive nda3 mutation reversibly blocks spindle formation and chromosome movement in mitosis. *Cell* **39,** 349–358 (1984).
21. Millband, D. N. & Hardwick, K. G. Fission yeast Mad3p is required for Mad2p to inhibit the anaphase-promoting complex and localizes to kinetochores in a Bub1p-, Bub3p-, and Mph1p-dependent manner. *Mol. Cell Biol.* **22,** 2728–2742 (2002).
22. Bar-Even, A. *et al.* Noise in protein expression scales with natural protein abundance. *Nat. Genet.* **38,** 636–643 (2006).
23. Newman, J. R. *et al.* Single-cell proteomic analysis of *S. cerevisiae* reveals the architecture of biological noise. *Nature* **441,** 840–846 (2006).
24. Marguerat, S. *et al.* Quantitative analysis of fission yeast transcriptomes and proteomes in proliferating and quiescent cells. *Cell* **151,** 671–683 (2012).
25. Amorim, M. J., Cotobal, C., Duncan, C. & Mata, J. Global coordination of transcriptional control and mRNA decay during cellular differentiation. *Mol. Syst. Biol.* **6,** 380 (2010).
26. Sun, M. *et al.* Comparative dynamic transcriptome analysis (cDTA) reveals mutual feedback between mRNA synthesis and degradation. *Genome Res.* **22,** 1350–1359 (2012).
27. Castelnuovo, M. *et al.* Bimodal expression of PHO84 is modulated by early termination of antisense transcription. *Nat. Struct. Mol. Biol.* **20,** 851–858 (2013).
28. Emre, D., Terracol, R., Poncet, A., Rahmani, Z. & Karess, R. E. A mitotic role for Mad1 beyond the spindle checkpoint. *J. Cell Sci.* **124,** 1664–1671 (2011).
29. Chung, E. & Chen, R. H. Spindle checkpoint requires Mad1-bound and Mad1-free Mad2. *Mol. Biol. Cell* **13,** 1501–1511 (2002).
30. Schuyler, S. C., Wu, Y. F. & Kuan, V. J. The Mad1-Mad2 balancing act—a damaged spindle checkpoint in chromosome instability and cancer. *J. Cell Sci.* **125,** 4197–4206 (2012).
31. Tipton, A. R. *et al.* BUBR1 and closed MAD2 (C-MAD2) interact directly to assemble a functional mitotic checkpoint complex. *J. Biol. Chem.* **286,** 21173–21179 (2011).
32. Yang, M. *et al.* Insights into mad2 regulation in the spindle checkpoint revealed by the crystal structure of the symmetric mad2 dimer. *PLoS Biol.* **6,** 643–655 (2008).
33. Heinrich, S., Windecker, H., Hustedt, N. & Hauf, S. Mph1 kinetochore localization is crucial and upstream in the hierarchy of spindle assembly checkpoint protein recruitment to kinetochores. *J. Cell Sci.* **125,** 4720–4727 (2012).
34. Sironi, L. *et al.* Mad2 binding to Mad1 and Cdc20, rather than oligomerization, is required for the spindle checkpoint. *EMBO J.* **20,** 6371–6382 (2001).
35. Kim, S. H., Lin, D. P., Matsumoto, S., Kitazono, A. & Matsumoto, T. Fission yeast Slp1: an effector of the Mad2-dependent spindle checkpoint. *Science* **279,** 1045–1047 (1998).
36. Barnhart, E. L., Dorer, R. K., Murray, A. W. & Schuyler, S. C. Reduced Mad2 expression keeps relaxed kinetochores from arresting budding yeast in mitosis. *Mol. Biol. Cell* **22,** 2448–2457 (2011).
37. Michel, L. S. *et al.* MAD2 haplo-insufficiency causes premature anaphase and chromosome instability in mammalian cells. *Nature* **409,** 355–359 (2001).
38. Iwanaga, Y. *et al.* Heterozygous deletion of mitotic arrest-deficient protein 1 (MAD1) increases the incidence of tumors in mice. *Cancer Res.* **67,** 160–166 (2007).
39. Ryan, S. D. *et al.* Up-regulation of the mitotic checkpoint component Mad1 causes chromosomal instability and resistance to microtubule poisons. *Proc. Natl Acad. Sci. USA* **109,** E2205–E2214 (2012).
40. Pan, J. & Chen, R. H. Spindle checkpoint regulates Cdc20p stability in *Saccharomyces cerevisiae*. *Genes Dev.* **18,** 1439–1451 (2004).
41. Sczaniecka, M. *et al.* The spindle checkpoint functions of Mad3 and Mad2 depend on a Mad3 KEN box-mediated interaction with Cdc20-anaphase-promoting complex (APC/C). *J. Biol. Chem.* **283,** 23039–23047 (2008).
42. Heim, R., Cubitt, A. B. & Tsien, R. Y. Improved green fluorescence. *Nature* **373,** 663–664 (1995).
43. Buchler, N. E. & Louis, M. Molecular titration and ultrasensitivity in regulatory networks. *J. Mol. Biol.* **384,** 1106–1119 (2008).
44. Reddy, S. K., Rape, M., Margansky, W. A. & Kirschner, M. W. Ubiquitination by the anaphase-promoting complex drives spindle checkpoint inactivation. *Nature* **446,** 921–925 (2007).
45. Mansfeld, J., Collin, P., Collins, M. O., Choudhary, J. S. & Pines, J. APC15 drives the turnover of MCC-CDC20 to make the spindle assembly checkpoint responsive to kinetochore attachment. *Nat. Cell Biol.* **13,** 1234–1243 (2011).
46. Uzunova, K. *et al.* APC15 mediates CDC20 autoubiquitylation by APC/C(MCC) and disassembly of the mitotic checkpoint complex. *Nat. Struct. Mol. Biol.* **19,** 1116–1123 (2012).
47. Sigal, A. *et al.* Variability and memory of protein levels in human cells. *Nature* **444,** 643–646 (2006).
48. Spencer, S. L., Gaudet, S., Albeck, J. G., Burke, J. M. & Sorger, P. K. Non-genetic origins of cell-to-cell variability in TRAIL-induced apoptosis. *Nature* **459,** 428–432 (2009).
49. Balazsi, G., van Oudenaarden, A. & Collins, J. J. Cellular decision making and biological noise: from microbes to mammals. *Cell* **144,** 910–925 (2011).
50. Chen, R. H., Brady, D. M., Smith, D., Murray, A. W. & Hardwick, K. G. The spindle checkpoint of budding yeast depends on a tight complex between the Mad1 and Mad2 proteins. *Mol. Biol. Cell* **10,** 2607–2618 (1999).
51. Fraschini, R. *et al.* Bub3 interaction with Mad2, Mad3 and Cdc20 is mediated by WD40 repeats and does not require intact kinetochores. *EMBO J.* **20,** 6648–6659 (2001).
52. Sudakin, V., Chan, G. K. & Yen, T. J. Checkpoint inhibition of the APC/C in HeLa cells is mediated by a complex of BUBR1, BUB3, CDC20, and MAD2. *J. Cell Biol.* **154,** 925–936 (2001).
53. Shah, J. V. *et al.* Dynamics of centromere and kinetochore proteins; implications for checkpoint signaling and silencing. *Curr. Biol.* **14,** 942–952 (2004).
54. Poddar, A., Stukenberg, P. T. & Burke, D. J. Two complexes of spindle checkpoint proteins containing Cdc20 and Mad2 assemble during mitosis independently of the kinetochore in *Saccharomyces cerevisiae*. *Eukaryot. Cell* **4,** 867–878 (2005).
55. Nilsson, J., Yekezare, M., Minshull, J. & Pines, J. The APC/C maintains the spindle assembly checkpoint by targeting Cdc20 for destruction. *Nat. Cell Biol.* **10,** 1411–1420 (2008).
56. Schwanhausser, B. *et al.* Global quantification of mammalian gene expression control. *Nature* **473,** 337–342 (2011).
57. Uhlen, M. *et al.* Towards a knowledge-based Human Protein Atlas. *Nat. Biotechnol.* **28,** 1248–1250 (2010).
58. Baker, D. J. *et al.* BubR1 insufficiency causes early onset of aging-associated phenotypes and infertility in mice. *Nat. Genet.* **36,** 744–749 (2004).
59. Gascoigne, K. E. & Taylor, S. S. Cancer cells display profound intra- and interline variation following prolonged exposure to antimitotic drugs. *Cancer Cell* **14,** 111–122 (2008).
60. Oliva, A. *et al.* The cell cycle-regulated genes of *Schizosaccharomyces pombe*. *PLoS Biol.* **3,** 1239–1260 (2005).
61. Rustici, G. *et al.* Periodic gene expression program of the fission yeast cell cycle. *Nat. Genet.* **36,** 809–817 (2004).
62. Peng, X. *et al.* Identification of cell cycle-regulated genes in fission yeast. *Mol. Biol. Cell* **16,** 1026–1042 (2005).

METHODS

***S. pombe* strains and culture conditions.** Strains are listed in Supplementary Table 4. The *bub3*$^{+}$*-S(GGGGS)3–GFP ≪ kanR*, *mad1–CRVLQHRS/CAV GQHRS (RL/AG)–GFP ≪ kanR*, *mad2-R133A–GFP ≪ kanR*, *mad2-W74A–GFP ≪ kanR* and *mad3*$^{+}$*–GFP–Y66L≪ kanR* strains were generated by PCR-based gene targeting[63]. GFP–Y66L is a non-fluorescent version[64]. To create a strain with doubled abundance of Slp1, the *slp1*$^{+}$ genomic region from 1,504 base pairs (bp) 5′ to 549 bp 3′ of the open reading frame was integrated into the *leu1* locus using the pDUAL system[65]. To create a strain with extra copies of *mad2*$^{+}$*–GFP–T(adh), mad2-W74A–GFP–T(adh)* or *mad2*$^{+}$*-T(mad2)*, the respective genomic region with 950 bp 5′ and 485 bp 3′ (for *mad2*$^{+}$*-Tmad2*) of the *mad2* open reading frame was integrated into the *leu1* locus using the pDUAL system[65]. Other *S. pombe* strains have been described previously: *nda3-KM311* (ref. 20), *cdc25-22* (ref. 66), *cut7-446* (ref. 67), *kanR ≪ Prad21-slp1*$^{+}$ (ref. 68), *mad1*$^{+}$*–GFP ≪ kanR, mad2*$^{+}$*–GFP ≪ kanR, mad3*$^{+}$*–GFP ≪ kanR, bub3*$^{+}$*-S(GGGGS)3–2xGFP ≪ kanR* (ref. 69), *mad1Δ::ura4*$^{+}$, *mad3Δ::ura4*$^{+}$ (ref. 17), *mad2Δ::ura4*$^{+}$ (refs 35,70), *gtb1-93* (ref. 71), *fin1Δ::ura4*$^{+}$ (refs 72,73) and *cut2-364* (refs 74,75).

Cells were grown in either YEA or EMM (ref. 76) containing the necessary supplements. Strains expressing *cdc25-22* were grown at 25 °C until they reached a concentration of 6×10^6 cells ml^{-1}, were arrested before mitosis by shifting to 36 °C for 4.5 h (YEA) or 5 h (EMM), and released by reducing the temperature.

Quantification of GFP signal intensity by WiFDeM. We took several precautions to ensure accuracy of the measurements: we examined functionality of the GFP-fused SAC proteins by analysing growth of the strains, by testing sensitivity to the microtubule-depolymerizing drug benomyl and by performing genetic interaction tests (Supplementary Fig. 1); we ensured that the microscope system responded in a linear fashion to changes in fluorescent protein concentration within the relevant range (Supplementary Fig. 2); we mounted cells in a microfluidics trapping device to ensure parallel orientation of the cells relative to the coverslip, which facilitated capture of the entire cell within the *z*-stack (Supplementary Fig. 2); we performed flat-fielding to eliminate variation caused by unequal illumination; we performed deconvolution to avoid losing out-of-focus light; we subtracted the contribution of autofluorescence by simultaneously measuring cells without GFP (Supplementary Fig. 2); we corrected for errors induced by loss of signal with sample depth[77]; we corrected for variations in lamp intensity between different imaging days by relating all measurements to the *cut9*$^{+}$*–GFP* strain, which was measured on each of the imaging days.

For quantification, asynchronously growing cells were cultured in EMM at 30 °C until they reached a concentration of 6–8 $\times$ 10^6 cells ml^{-1}. Cells containing GFP-labelled proteins were mixed with cells containing no GFP, loaded into Y04C plates (CellASIC) and incubated for 2 h at 30 °C on the microscope stage with a constant flow of fresh medium. Imaging was performed on a DeltaVision Core system (Applied Precision) equipped with a climate chamber (EMBL) set to 30 °C. We used a ×60/1.4 Plan Apo oil objective (Olympus) and recorded with a CoolSnap CCD (charge-coupled device) camera (Roper Scientific). *Z*-stacks of 4.8 μm thickness were acquired for both mCherry and GFP fluorescence, with single planes spaced by 0.2 μm. In addition, a differential interference contrast (DIC) reference image of the middle plane was acquired. The imaged area spanned 256 $\times$ 256 pixels with 2 $\times$ 2 binning. Uneven illumination of the imaged area was corrected by flat-fielding. All images were deconvolved using SoftWorx software. Out of the 24 planes acquired, the 20 central planes were used for further image processing. Only cells of a length above 11 μm were chosen for quantification. The nuclear rim localization of Cut11–mCherry was used as a nuclear marker, and the mitosis-specific localization of Cut11–mCherry to spindle pole bodies was used to differentiate between interphase and early mitotic cells. The nucleus was either tracked in single planes using the SoftWorx 2D polygon tool or by semi-automated segmentation in the *z*-stack using stacked ellipse fitting[78]. The segmentation of the nucleus was projected to the GFP channel and the sum of GFP intensity per sum of area was calculated. Images were corrected for errors introduced by loss of signal with sample depth[77]. To eliminate the contribution of autofluorescence to the signal, we subtracted the sum of intensity per sum of area determined for cells not expressing GFP. To determine the signal from the entire cell, *z*-stacks of 20 planes were sum-projected to a single image and fused to the corresponding DIC image. The outline of individual cells was delineated by hand in the DIC image, projected to the GFP channel and the sum of GFP intensity in this area was calculated. As both the cell width and the cap size are uniform between single cells (data not shown), we used average values for these to calculate the cellular volume from the two-dimensional shape determined by segmentation. The sum of GFP intensities was divided by this volume to determine the GFP concentration. The contribution of autofluorescence was eliminated by performing similar measurements on cells not expressing GFP. The nuclear/cytoplasmic ratio (Supplementary Table 1) was calculated with the measured concentrations in nucleus and whole cell, and with a nucleus to cell volume ratio of 0.08 (ref. 79).

Fluorescence correlation spectroscopy. Cells were cultured in EMM and immobilized on lectin-treated LabTek chambers (Nunc). Fluorescence correlation spectroscopy (FCS) measurements were conducted in the nucleus of G2 cells as judged by cell length (>11 μm) and Cut11–mCherry signal (no spindle pole body localization). Each FCS measurement was acquired for 90 s. The time trace was autocorrelated and fitted with a 1-component anomalous diffusion model, including terms for the photophysics of GFP, using the custom-made Fluctuation Analyser software[80,81]. The parameters resulting from the fit were corrected for background and bleaching. The background correction factor was determined on the basis of the mean fluorescence intensity in the nuclei of wild-type cells (no GFP) that were excited and detected under the same conditions as the experimental measurements. The bleaching correction factor was calculated for each trace as the ratio between the fluorescent intensity within the first 2 s of the measurement and the mean fluorescence intensity. Measurements that showed strong bleaching or strong fluctuations due to cellular movement, resulting in measurement outside the nucleus, were excluded from the analysis based on the time trace. Concentrations were calculated on the basis of the size of the detection volume, which was determined by measurements of the fluorophore Alexa 488 with a known diffusion coefficient of 400 μm^2 s^{-1} (M. Wachsmuth, personal communication).

Size determination of the nucleolus. Cells expressing *cut11*$^{+}$*–mCherry* and either *mad3*$^{+}$*–GFP* or *nuc1*$^{+}$–GFP were cultured in minimal medium (EMM) at 30 °C. Cells were either loaded into Y04C microfluidics plates (CellASIC) or mounted in # 1.5 glass-bottom culture dishes (Ibidi) that had been coated with 35 μg ml^{-1} lectin (Sigma, L-2380). Imaging was performed with conditions identical to those used for relative quantification. The nuclear rim localization of Cut11–mCherry was used as a nuclear marker and the approximate volume of the nucleus was determined by segmenting the nuclear area in each plane (SoftWorx 2D polygon tool) and summing up the areas multiplied by the plane distance of 0.2 μm. The volume of the nucleolus was approximated in a similar way by segmenting the areas occupied by the nucleolar protein Nuc1–GFP, or manually segmenting the areas that exclude Mad3–GFP.

Live-cell imaging to assess SAC functionality. Imaging on a DeltaVision Core system (Applied Precision/GE Healthcare) was performed as previously described[33], with the exception of using 35 μg ml^{-1} lectin (Sigma, L1395 or L-2380) for coating glass-bottom culture dishes (Ibidi).

Quantification of GFP signal in the nucleus and at the kinetochore. Quantification of GFP signal intensity at the kinetochore was performed as previously described[33]. GFP signal intensity in the nucleoplasm was determined by placing two similarly sized regions in the nucleoplasm and in the medium outside the cell. The total intensity measured in the GFP channel per area in the medium was subtracted from the total GFP intensity per area in the nucleoplasm. To analyse differences in kinetochore and nucleoplasmic signals between strains or between population A and B, we used the pooled component test[82]. This is a multivariate test statistic, which accounts for correlation and which can handle missing values. Normality is required for the pooled component test and was verified using the Kolmogorow–Smirnow test taking into account multiple testing by using Bonferroni's correction. As throughout the manuscript, *P* values <0.05 were considered statistically significant.

Single-molecule mRNA fluorescence *in situ* hybridization. Mixtures of DNA probes (Supplementary Table 5) coupled to CAL Fluor Red 610 (Stellaris, synthesized by BioCat) were used for *in situ* hybridization. Except for Slp1, probes were targeted against the GFP moiety of the fusion between gene and GFP coding sequence. Typically, 5×10^7–1×10^8 cells were used for one hybridization reaction. Cells from an asynchronously growing culture were fixed with 4% paraformaldehyde, washed with buffer B (1.2 M sorbitol, 100 mM $KHPO_4$ at pH 7.5, 4 °C) and stored overnight at 4 °C. Cell walls were digested for 45–75 min in spheroplast buffer (1.2 M sorbitol, 100 mM $KHPO_4$ at pH 7.5, 20 mM vanadyl

DOI: 10.1038/ncb2864

ribonuclease complex and 20 μM β-mercaptoethanol) with 1% 100T zymolyase (Medac, 120493-1). The reaction was stopped by washing with buffer B. Cells were incubated for 20 min in 0.01% Triton/1× PBS and washed with 10% formamide/2× SSC. Before hybridization, 25 ng of the probes was mixed with 4μl of a 1:1 mixture between yeast transfer RNA (10 mg ml^{-1}, Life Technologies, AM7119) and salmon-sperm DNA (10 mg ml^{-1}, Life Technologies, 15632-011) and the mixture was dried in a vacuum concentrator. Hybridization buffer F (20% formamide, 10 mM $NaHPO_4$ at pH 7.0; 50 μl per reaction) was added, and the probe/buffer F solution was incubated for 3 min at 95 °C. Buffer H (4× SSC, 4 mg ml^{-1} BSA (acetylated) and 20 mM vanadyl ribonuclease complex; 50 μl per reaction) was added in a 1:1 ratio to the probe/buffer F solution. Cells were resuspended in the mixture and incubated overnight at 37 °C. After three washing steps (10% formamide/2× SSC; 0.1% Triton/2x SSC; 1x PBS), cells were resuspended in 1× PBS and mounted for imaging. Twenty *Z*-planes spaced by 0.3 μm were acquired on a DeltaVision Core system (Applied Precision). We used a ×60/1.4 Plan Apo oil objective (Olympus) and recorded with a CoolSnap CCD camera (Roper Scientific). Images were deconvolved and analysed with FISH-quant software[83] to detect single fluorescent spots in three dimensions. Cells were segmented manually. Dot signals co-localizing with DNA were interpreted as potential transcription sites and excluded from the mRNA counts. Pre-detected spots were narrowed down by thresholds for amplitude, raw intensity and filtered intensity, which were set manually. Typically, the threshold was 1.5× standard deviations below the centre of the distribution of spots that were considered positive. The results were cross-checked by manual counting of a subset of cells. In images of cells not expressing GFP, between 0 and 0.2 spots were detected per cell using similar settings. The value for the number of Slp1 mRNAs in highly expressing cells is underestimated for two reasons: unlike in cells with a low number of mRNAs, fluorescent spots have a range of intensities, indicating that some spots represent more than one mRNA, although we counted these as one; spots close to another spot were sometimes not recognized by the software when the density was high. The frequency distribution of mRNA spots was fitted with a Poisson distribution. The appropriateness of the fits and the corresponding *P* values were determined from the statistics of the root-mean-square error between model and data[84], which were assessed using parametric bootstrapping. For data sets not described by a single Poisson distribution, we fitted a weighted mixture of two Poisson distributions. The appropriateness of the fit was again analysed using the statistics of the root-mean-square error between model and data. For the statistical comparison of the two models, one Poisson distribution and a mixture of two Poisson distributions, we employed the likelihood ratio test.

Immunostaining and fluorescence microscopy of fixed cells. Asynchronously growing cells were fixed with 4% paraformaldehyde (PFA) for 30 min at room temperature, washed three times for 20 min with PEM (100 mM PIPES (pH 6.9), 1 mM EGTA and 1 mM $MgSO_4$) with 0.1% Triton X-100 before resuspending in PEMS (PEM with 1.2 M sorbitol). Beta-mercaptoethanol (0.5%) and zymolyase 100T (1%; Medac, 120493-1) were added and the mixture was incubated for 1 h at 37 °C. Cells were washed once with PEMS, three times with PEM/0.1% Triton X-100 for 20 min each, resuspended in blocking solution PEM-NL (PEM with 5% normal goat serum, 100 mM L-lysine monohydrochloride, 0.1% NaN_3) and incubated for 30 min at room temperature. The primary antibody solution (PEM-NL $^+$ rabbit anti-HA (Cell Signaling 3724S, 1:250) and mouse anti-TAT1 (Gull laboratory, 1:500)) was added and incubated overnight at 4 °C. After washing three times for 20 min with PEM/0.1% Triton X-100, cells were blocked for 5 min with PEM-NL and incubated for 1.5 h with the secondary antibody solution (PEM-NL $^+$ anti-rabbit Alexa-488 (Invitrogen A-11034, 1:250) and anti-mouse Alexa-568 (Invitrogen A-11031, 1:1.000)). Cells were washed three times for 20 min with PEM/0.1% Triton X-100 and resuspended in PEM before imaging. Images were acquired on a Zeiss AxioImager microscope coupled to a CCD camera and were processed with MetaMorph software (Molecular Devices Corporation). Typically, a *z*-stack of about 3 μm thickness, with single planes spaced by 0.3 μm, was acquired and subsequently projected to a single image. To determine the nucleo-cytoplasmic ratio for Slp1–HA, an area was placed over the nucleus of mitotic cells that were identified by the presence of Slp1–HA and a short spindle stained by TAT1. An equally sized area was placed in the cytoplasm. The mean Slp1–HA–Alexa-488 signal measured in the nucleus was divided by the mean Slp1–HA–Alexa-488 signal measured in the cytoplasm. Background measured in interphase cells was subtracted.

Immunoprecipitation. Asynchronously growing cells were collected, washed with extraction buffer (50 mM HEPES at pH 7.5, mM NaCl, 2 mM EDTA and 0.5% NP-40) and frozen as droplets in liquid N_2. Cell extracts were prepared using a mixer mill (RETSCH MM400), followed by resuspension in extraction buffer supplemented with protease inhibitors (Complete EDTA-free, Roche, 1187358001) and phosphatase inhibitors (PhosSTOP, Roche, 4906837001) to a protein concentration of 10 mg ml^{-1}. The extract was spun down for 10 min at 16,600*g* at 4 °C and the supernatant was collected. Protein A-coated magnetic beads (Dynabeads, Invitrogen 10002D) were coupled to rabbit anti-Mad1 antibodies (25 μg per 100 μl beads) and incubated with the supernatant for 15 min at 4 °C. Samples were taken before (input) and after (flow through) incubation with the beads. The beads were washed 5 times with extraction buffer, and elution from the beads was performed by adding 2x SDS sample buffer (125 mM Tris at pH 6.8, 4% SDS, 0.02% bromophenol blue, 20% glycerol and 200 mM dithiothreitol). To quantify input, flow through and immunoprecipitation ratios, the background was subtracted from each band by measuring an equally sized region adjacent to this band. Each Mad1 or Mad2 intensity was normalized to the Cdc2 band intensity in the same lane. As, for each sample, two dilutions were available, ratios were always compared among the more concentrated or among the more diluted samples. The average and standard deviation of these comparisons are shown. As the dilutions of the input were 50 and 25%, whereas the dilutions of the flow through were 100 and 50%, the band intensities for the input were multiplied by two before calculating the ratios. To calculate the immunoprecipitation ratio of Mad2 to Mad1, normalized intensities of Mad2 were divided by normalized intensities of Mad1 individually for each lane. For each strain, the average and standard deviation of the ratios of the two different dilutions (100%, 50%) was then calculated.

Immunoblotting and antibodies. Protein extraction and immunoblotting was performed as previously described[33]. Proteins were detected by mouse anti-GFP (Roche, 11814460001), mouse anti-tubulin (Sigma, T5168), rabbit anti-Mad1 (this study, directed against peptide ADSPRDPFQSRSQL, specificity demonstrated in Supplementary Fig. 5f,i), rabbit anti-Mad2 (ref. 85), rabbit anti-Slp1 (ref. 35) or rabbit anti-Cdc2 (Santa Cruz, SC-53). Secondary antibodies were anti-mouse HRP conjugates (Dianova, 115-035-003) or anti-rabbit HRP conjugates (Dianova, 111-035-003) and were read out using chemiluminescence.

We found that immunoblotting efficiency for recombinant proteins differed when only the recombinant protein was loaded or when the recombinant protein was mixed with a whole-cell extract (data not shown). For quantitative measurement of GFP, we therefore mixed recombinant GFP (Clontech 632373) with a wild-type protein extract not containing GFP. For quantitative measurement of Slp1, we introduced recombinant Slp1 into an extract from G2 cells, which did not contain detectable levels of Slp1. The recombinant GFP that we used for quantification differs from the GFP that was used for tagging of SAC proteins or APC/C subunits by one amino acid (Ser 65 in recombinant GFP, Thr 65 in the fused GFP). The mixture of two monoclonal antibodies that was used for immunoblotting recognizes these two versions similarly well (Supplementary Fig. 3g). We measured the concentration of recombinant GFP both by FCS and by a BCA assay. Both values were in good agreement (0.79 mg ml^{-1} determined by FCS, 0.63 mg ml^{-1} by BCA assay) and were slightly lower than the concentration indicated by the manufacturer (1 mg ml^{-1}). We used the value determined by FCS for all further calculations. The concentration of 6xHis-tagged recombinant Slp1, which was purified under denaturing conditions in 8 M urea, was determined by a Bradford assay. Slp1 and GFP were quantified in *cdc25-22* synchronized mitotic populations. These cells have a larger volume than *cdc25$^+$* cells, which were used for quantification by microscopy. We determined the nuclear volume increase (Supplementary Fig. 7a), which scales with the cellular volume increase[79], and used this value to derive the presumed protein concentration in a *cdc25$^+$* cell.

63. Bahler, J. *et al.* Heterologous modules for efficient and versatile PCR-based gene targeting in *Schizosaccharomyces pombe*. *Yeast* **14,** 943–951 (1998).
64. Rosenow, M. A., Huffman, H. A., Phail, M. E. & Wachter, R. M. The crystal structure of the Y66L variant of green fluorescent protein supports a cyclization-oxidation-dehydration mechanism for chromophore maturation. *Biochemistry* **43,** 4464–4472 (2004).
65. Matsuyama, A. *et al.* pDUAL, a multipurpose, multicopy vector capable of chromosomal integration in fission yeast. *Yeast* **21,** 1289–1305 (2004).
66. Russell, P. & Nurse, P. cdc25+ functions as an inducer in the mitotic control of fission yeast. *Cell* **45,** 145–153 (1986).
67. Hagan, I. & Yanagida, M. Novel potential mitotic motor protein encoded by the fission yeast cut7+ gene. *Nature* **347,** 563–566 (1990).

68. Yokobayashi, S. & Watanabe, Y. The kinetochore protein Moa1 enables cohesion-mediated monopolar attachment at meiosis I. *Cell* **123,** 803–817 (2005).
69. Windecker, H., Langegger, M., Heinrich, S. & Hauf, S. Bub1 and Bub3 promote the conversion from monopolar to bipolar chromosome attachment independently of shugoshin. *EMBO Rep.* **10,** 1022–1028 (2009).
70. He, X., Patterson, T. E. & Sazer, S. The *Schizosaccharomyces pombe* spindle checkpoint protein mad2p blocks anaphase and genetically interacts with the anaphase-promoting complex. *Proc. Natl Acad. Sci. USA* **94,** 7965–7970 (1997).
71. Tange, Y. & Niwa, O. Novel mad2 alleles isolated in a *Schizosaccharomyces pombe* gamma-tubulin mutant are defective in metaphase arrest activity, but remain functional for chromosome stability in unperturbed mitosis. *Genetics* **175,** 1571–1584 (2007).
72. Krien, M. J. *et al.* A NIMA homologue promotes chromatin condensation in fission yeast. *J. Cell Sci.* **111,** 967–976 (1998).
73. Grallert, A. & Hagan, I. M. *Schizosaccharomyces pombe* NIMA-related kinase, Fin1, regulates spindle formation and an affinity of Polo for the SPB. *EMBO J.* **21,** 3096–3107 (2002).
74. Funabiki, H., Kumada, K. & Yanagida, M. Fission yeast Cut1 and Cut2 are essential for sister chromatid separation, concentrate along the metaphase spindle and form large complexes. *EMBO J.* **15,** 6617–6628 (1996).
75. Matsumura, T. *et al.* A brute force postgenome approach to identify temperature-sensitive mutations that negatively interact with separase and securin plasmids. *Genes. Cells* **8,** 341–355 (2003).
76. Moreno, S., Klar, A. & Nurse, P. Molecular genetic analysis of fission yeast *Schizosaccharomyces pombe*. *Methods Enzymol.* **194,** 795–823 (1991).
77. Johnston, K. *et al.* Vertebrate kinetochore protein architecture: protein copy number. *J. Cell Biol.* **189,** 937–943 (2010).
78. Widmer, C. *et al.* GRED: graph-regularized 3D shape reconstruction from highly anisotropic and noisy images. Preprint at http://arXiv.org/abs/1309.4426 (2013).
79. Neumann, F. R. & Nurse, P. Nuclear size control in fission yeast. *J. Cell Biol.* **179,** 593–600 (2007).
80. Capoulade, J., Wachsmuth, M., Hufnagel, L. & Knop, M. Quantitative fluorescence imaging of protein diffusion and interaction in living cells. *Nat. Biotechnol.* **29,** 835–839 (2011).
81. Schmidt, U. *et al.* Assembly and mobility of exon-exon junction complexes in living cells. *RNA* **15,** 862–876 (2009).
82. Wu, Y., Genton, M. G. & Stefanski, L. A. A multivariate two-sample mean test for small sample size and missing data. *Biometrics* **62,** 877–885 (2006).
83. Mueller, F. *et al.* FISH-quant: automatic counting of transcripts in 3D FISH images. *Nat. Methods* **10,** 277–278 (2013).
84. Perkins, W., Tygert, M. & Ward, R. Chi-square and classical exact tests often wildly misreport significance; the remedy lies in computers. Preprint at http://arXiv.org/abs/1108.4126 (2011).
85. Yamada, H. Y., Matsumoto, S. & Matsumoto, T. High dosage expression of a zinc finger protein, Grt1, suppresses a mutant of fission yeast slp1(+), a homolog of CDC20/p55CDC/Fizzy. *J. Cell Sci.* **113,** 3989–3999 (2000).

DOI: 10.1038/ncb2864

nature cell biology

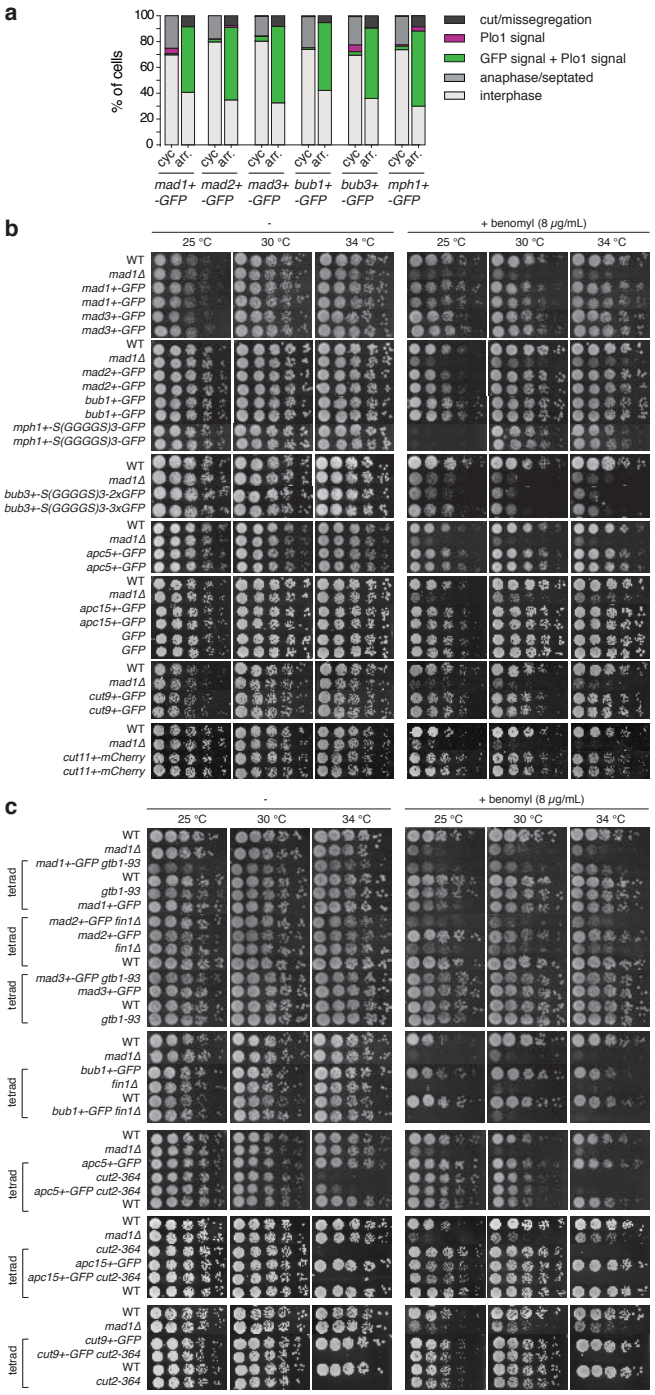

Figure S1 Functionality of GFP fusion proteins. **a** Strains with SAC protein-GFP fusions have a functional SAC. Cells were either grown at permissive temperature for the tubulin mutant *nda3-KM311* (30 °C; cyc; cycling cells) or at restrictive temperature (18 °C; arr.; cells arrested in mitosis) (n > 100 cells for each strain and condition). Plo1 localization to the spindle pole body (Plo1 signal) indicated that cells were in mitosis. Localization of the SAC protein-GFP fusions to kinetochores was additionally scored (GFP signal). Shown is one representative out of two independent experiments. **b** Strains expressing GFP-tagged SAC components grew similar to wild type (WT), with the exception of strains expressing *bub3+-GFP* and *mph1+-GFP*, whose growth was impaired on benomyl-containing medium. A serial dilution of cells was spotted and grown at the indicated temperatures on rich medium or rich medium supplemented with 8 µg/mL of the microtubule drug benomyl. **c** Strains expressing GFP-tagged SAC components were crossed to strains containing mutations that are known to cause a synthetic growth defect when combined with the respective SAC gene deletion. A growth assay of tetrads resulting from these crosses was performed as in (b). Except for the *mad1+-GFP gtb1-93* and *apc5+-GFP cut2-364* double mutant, which had slightly impaired growth, none of the double mutants showed a synthetic growth defect.

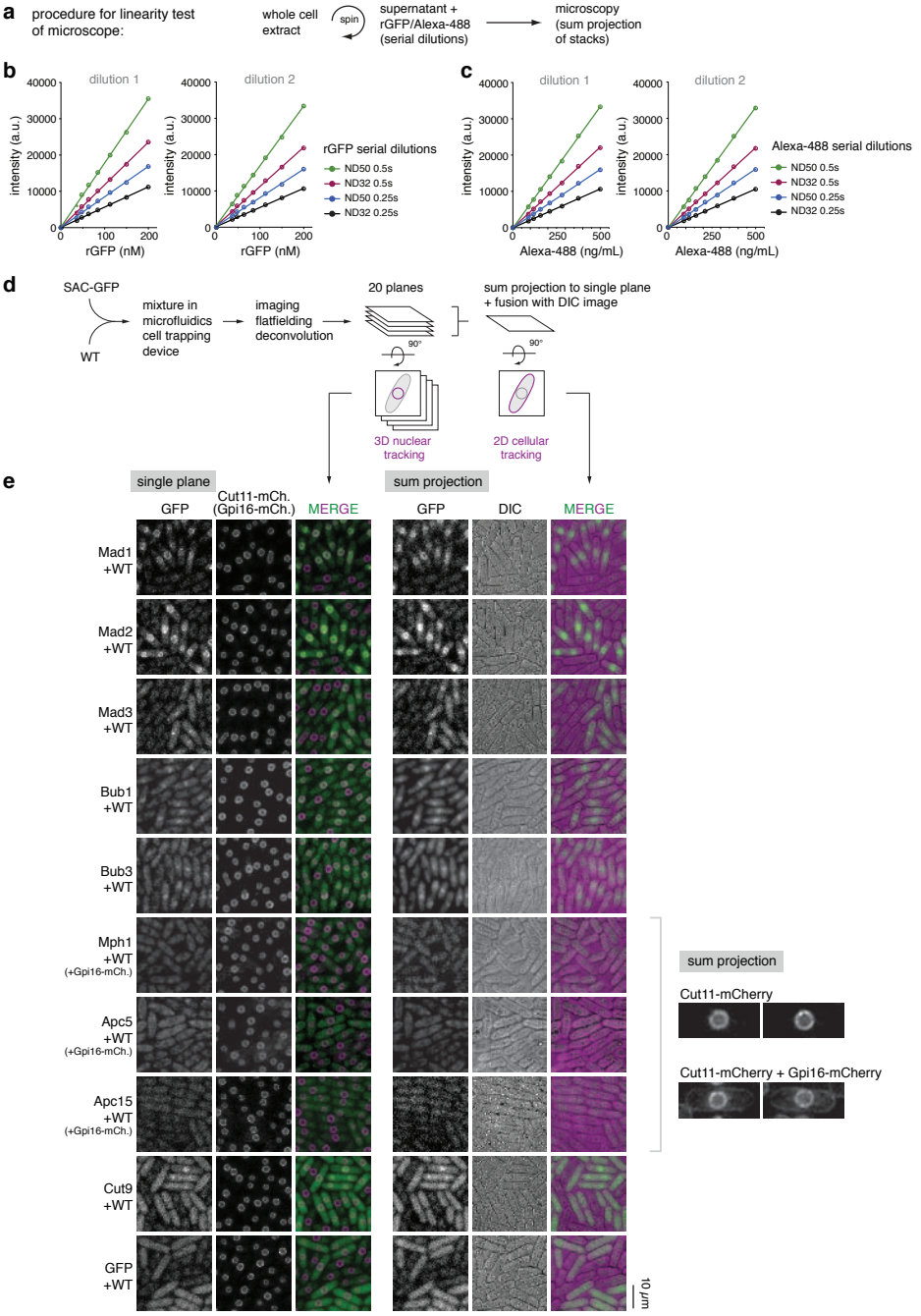

Figure S2 Imaging conditions for quantification by WiFDeM. **a-c** Microscope and camera respond linearly to signals in the relevant range. Protein extracts of wild type cells were mixed with serial dilutions of either recombinant GFP (rGFP; 3:4 dilutions starting from 200 nM) or Alexa-488 coupled antibodies (3:4 dilutions starting from 500 ng/mL). Two independent serial dilutions were imaged (dilution 1 and dilution 2) with different neutral density filters (ND) and different exposure times (0.25 s and 0.5 s). **d** Schematic representation of the quantitative imaging procedure. Cells containing GFP-labelled SAC proteins and cells without GFP (wild type; WT) were mixed and loaded into a microfluidics cell-trapping device. Cells were constantly supplied with fresh medium throughout the imaging process. Image stacks for GFP and mCherry fluorescence were acquired, and a DIC image was taken from the middle of the stack. Uneven illumination of the images was corrected by flatfielding and image stacks were deconvolved. 20 planes of the imaged stack were either used directly for 3D nuclear segmentation or sum-projected to a single plane and fused to the DIC image for 2D cellular segmentation. For 3D nuclear segmentation, the nuclear rim localization of Cut11-mCherry was used as marker. For 2D segmentation, the cellular outline in the DIC image was used and was converted to an estimate of cellular volume. **e** Representative single plane images and sum projections. To differentiate cells with a very weak GFP signal (Apc5-GFP, Apc15-GFP or Mph1-GFP) from cells that do not express GFP (wild type; WT), wild type cells in these cell mixtures expressed the membrane protein Gpi16-mCherry in addition to the nuclear marker Cut11-mCherry, as shown on the right side.

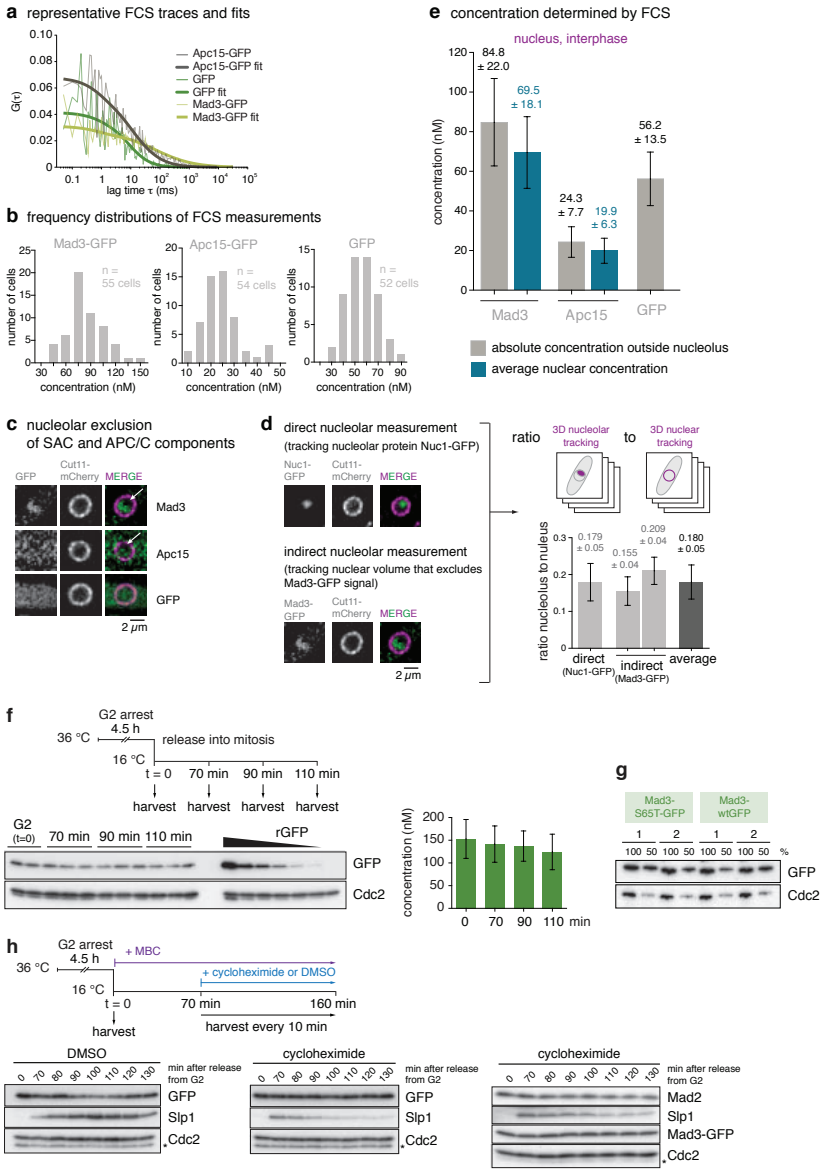

Figure S3 Absolute quantification of SAC proteins and APC/C subunits. **a,b** Quantification of free GFP, Apc15-GFP and Mad3-GFP by fluorescence correlation spectroscopy (FCS). Fluorescence fluctuations were determined in interphase nuclei. Shown in (a) are representative auto-correlation curves and the corresponding fit. The amplitude, G(0), of the autocorrelation curve is inversely proportional to the concentration of the fluorescent protein. The frequency distributions for the nuclear concentration in single cells are shown in (b). **c** Mad3-GFP and Apc15-GFP are excluded from the nucleolus (arrows), but free GFP is not. A single plane of representative nuclei in interphase is shown. GFP signals are differently scaled for different proteins to achieve good visibility. **d** The nucleolus occupies about ~18 % of the nuclear volume. The nucleolar volume was determined by segmentation of either Nuc1-GFP, which localizes to the nucleolus, or by segmentation of the region from which Mad3-GFP is excluded. (n=10 cells (Nuc1-GFP), n=9 and 11 cells (Mad3-GFP); error bars = s.d.). **e** Nuclear concentrations were measured by FCS outside the nucleolus (grey, data from (b)). The average concentration in the nucleus (blue) was calculated using the nucleolar volume determined in (d). (error bars = s.d.) **f** Quantification of free GFP by quantitative immunoblotting. *Cdc25-22* cells expressing *Pmad3-GFP* were arrested before mitosis in rich medium. Three technical replicates were harvested at the indicated time points after release and were analysed by immunoblotting using anti-GFP and anti-Cdc2 (loading control) antibodies. Recombinant GFP (rGFP, Clontech) was mixed with an extract from G2-arrested cells not expressing *Pmad3-GFP* as standard for quantification. The graph on the right shows the average concentration from 4 independent experiments, of which one is shown on the left. (error bars = s.d.; n = 4 experiments). **g** Equal detection of wtGFP and S65T-GFP with anti-GFP antibody. We used recombinant wild type GFP (wtGFP) for quantification of S65T-GFP-tagged checkpoint proteins (f). To confirm that the anti-GFP antibody detected wtGFP and S65T-GFP equally well, Mad3 was tagged with either wtGFP or S65T-GFP. Two independent strains (labelled 1 and 2) were compared by immunoblotting using anti-GFP and anti-Cdc2 (loading control) antibodies. Percentages on top of each lane indicate how much of the original extract was loaded. **h** Incomplete maturation of GFP is unlikely to account for the difference in GFP concentration determined by FCS and immunoblotting. We arrested cells in mitosis by the microtubule drug MBC and additionally treated with cycloheximide to block protein synthesis. GFP, but not Slp1, was stable for 60 min under these conditions. This indicates that protein turnover of GFP is low and that most of the GFP present at any given moment should have had enough time to form the fluorophore. In addition, GFP-tagged Mad3 as well as untagged Mad2 were similarly stable as GFP in cycloheximide-treated cells, indicating low turn-over of these SAC proteins. (*, antibody cross-reaction)

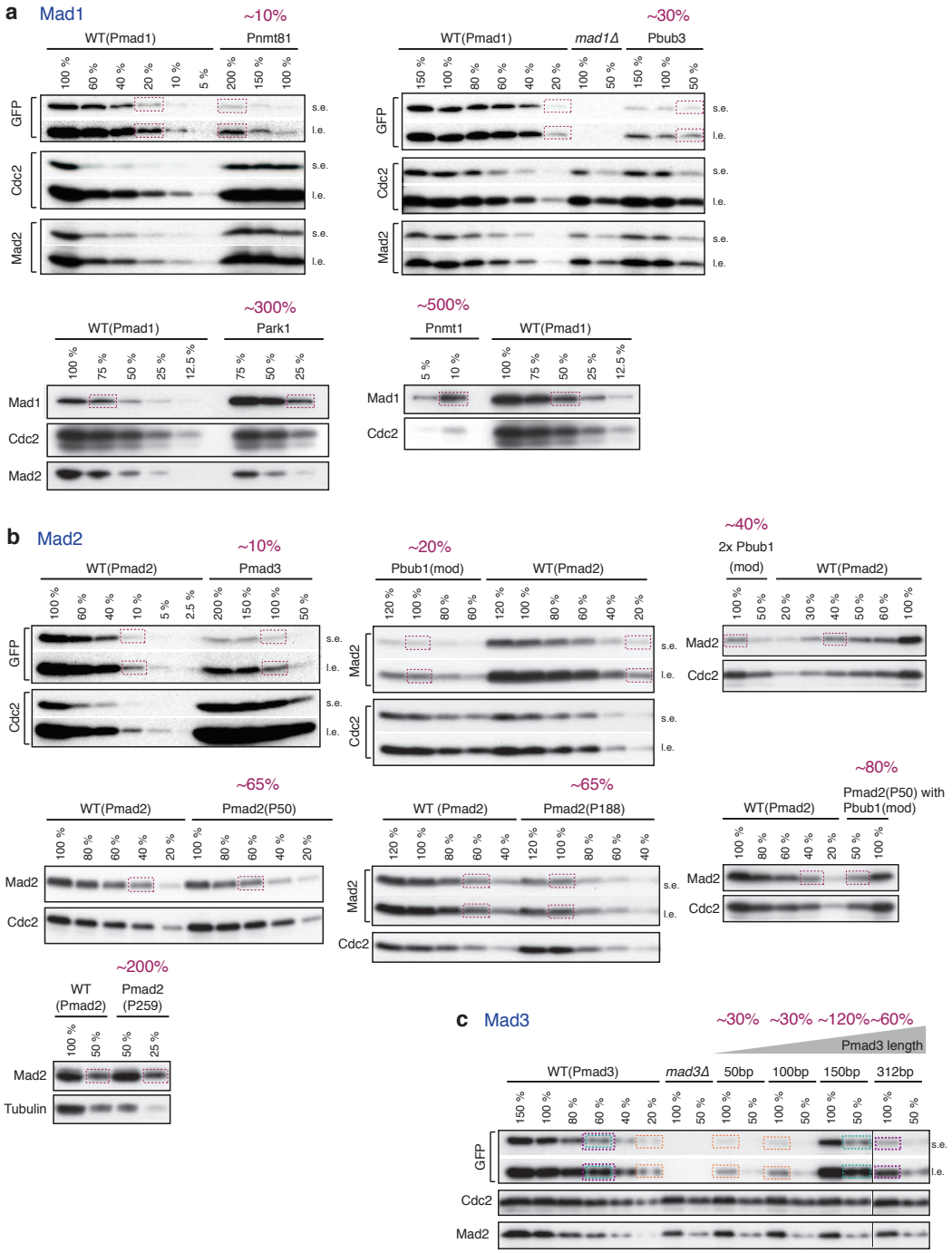

Figure S4 Abundance of Mad1-, Mad2- and Mad3-GFP after promoter modifications. Extracts from asynchronously growing cultures in rich medium were analysed by immunoblotting using anti-GFP, anti-Mad1, anti-Mad2 and either anti-Cdc2 or anti-tubulin antibodies (as loading controls). Mad1-GFP strains are shown in (a), Mad2-GFP strains in (b) and Mad3-GFP strains in (c). Percentages on top of each lane indicate how much of the original extract was loaded. Percentages in purple indicate the estimated protein abundance compared to wild type (WT). Dashed boxes indicate bands with similar signal strength from which protein abundances of the promoter-modified strains were deduced. Estimations of the abundance relative to wild type are typically based on several experiments, of which only one representative experiment is shown. (s.e. = short exposure, l.e. = long exposure, Pmad3 length = length of the remaining *mad3* promoter; see Supplementary Table S3 for the molecular changes in the promoter region).

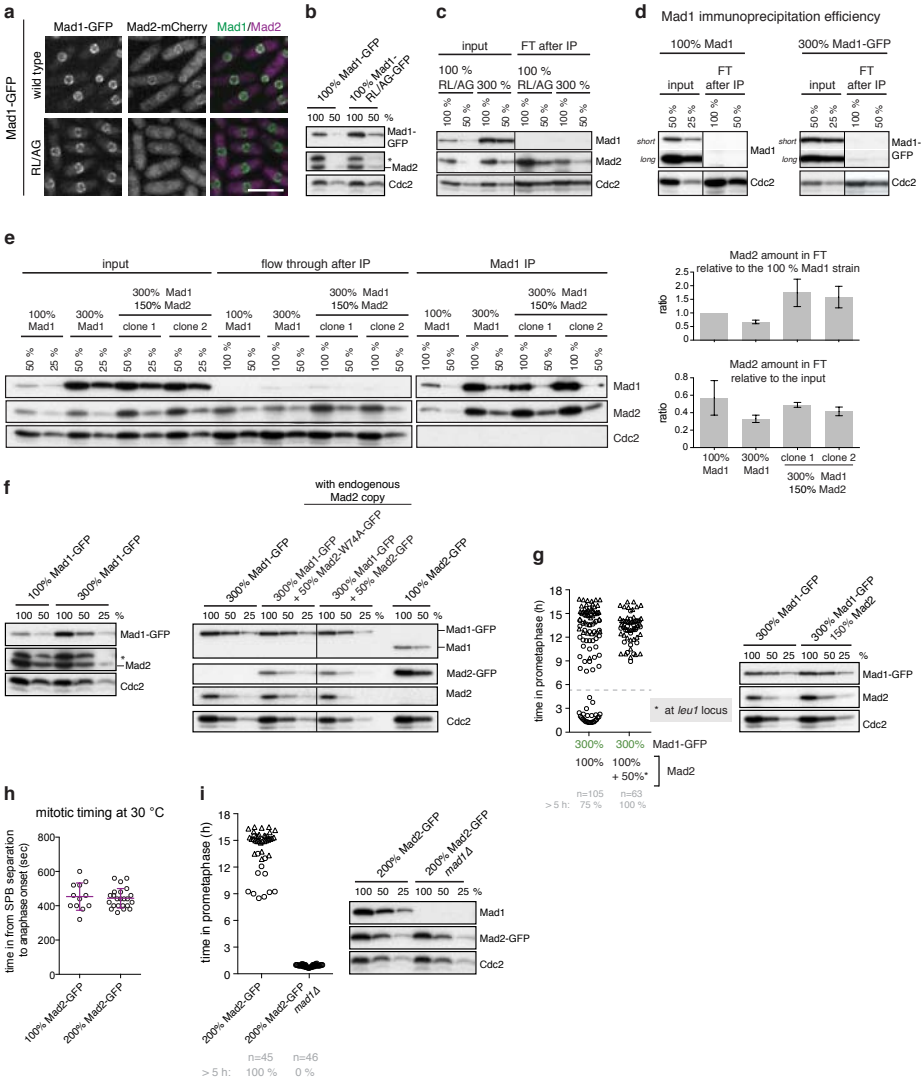

Figure S5 Analysis of the Mad1-RL/AG mutant as well as Mad1 and Mad2 overexpression. **a** Mad2-mCherry does not co-localise with Mad1 that contains two point mutations (CRVLQHRS to CAVGQHRS) in the Mad2-binding site (Mad1-RL/AG). Representative images from asynchronous cultures are shown. Scale bar: 10 µm. **b** Mad1-RL/AG is present at similar levels as wild type Mad1, and Mad2 abundance is unaffected. Extracts from asynchronously growing cultures in rich medium were analysed by immunoblotting using anti-Mad1, anti-Mad2 and anti-Cdc2 (as loading control) antibodies. Percentages on top of each lane indicate how much of the original extract was loaded. The asterisk indicates a cross-reacting band. **c** Input and flow-through of the immunoprecipitation shown in Fig. 4a. Extracts from asynchronously growing cultures in rich medium were used for immunoprecipitation (IP) of Mad1-RL/AG or Mad1-GFP (expressed to 300 %) using anti-Mad1 antibodies. Shown are immunoblots of the extract used for the IP (input) and of the flow through after immunoprecipitation (FT after IP). **d** High immunoprecipitation efficiency for Mad1 or Mad1-GFP. Extracts from asynchronously growing cultures in rich medium were used for immunoprecipitation of Mad1 or Mad1-GFP using anti-Mad1 antibodies and analysed for the amount of Mad1 remaining in the extract after IP (FT (flow through) after IP). **e** 50 % additional Mad2 increases free Mad2 in cells with 300 % Mad1-GFP. Extracts from asynchronously growing cultures in rich medium were used for immunoprecipitation of Mad1 using anti-Mad1 antibodies and analysed for co-immunoprecipitation of Mad2. The input and FT is 6.25 % of the amount used for the IP sample. Mad1 was largely depleted from the flow through after IP. Quantifications of the flow through are shown on the right (see Methods). The depletion of free Mad2 by increasing the Mad1 abundance to 300 % is not as strong as could be expected (Supplementary Note (B1)). Shown is one representative out of two independent experiments. **f** Mad1 and Mad2 abundance in the strains shown in Fig. 4b. Extracts from asynchronously growing cultures in rich medium were analysed by immunoblotting using anti-Mad1 (for Mad1 and Mad1-GFP detection), anti-GFP (for Mad2-GFP detection), anti-Mad2 (for Mad2 detection) and anti-Cdc2 antibodies (as loading control). The asterisk indicates a cross-reacting band. **g** Addition of 50 % untagged Mad2 rescues the checkpoint defect in cells with 300 % Mad1, similar to addition of 50 % Mad2-GFP (Fig. 4b). To determine SAC activity, cells were followed by live cell imaging at 16 °C as in Fig. 2 (left side). Extracts from asynchronously growing cultures from the same strains were analysed by immunoblotting (right side) using anti-Mad1, anti-Mad2 and anti-Cdc2 antibodies (as loading control). Shown is one representative out of two independent experiments. **h** Cells with 200 % Mad2-GFP stay in mitosis for a similar time as cells with 100 % Mad2-GFP. Cells were cultured in rich medium and followed by live cell imaging at 30 °C. The time in mitosis was determined from SPB separation to spindle elongation using Plo1-mCherry as marker for the SPBs. Each circle represents one cell. Shown in purple are mean and s.d. **i** 200 % Mad2-GFP cannot overcome the checkpoint defect of a *mad1* deletion. *nda3-KM311* strains were followed by live cell imaging at 16 °C and the time in mitosis was scored as in Fig. 2 (left side). Extracts from asynchronously growing cultures from the same strains were analysed by immunoblotting (right side) using anti-Mad1, anti-GFP and anti-Cdc2 antibodies (as loading control).

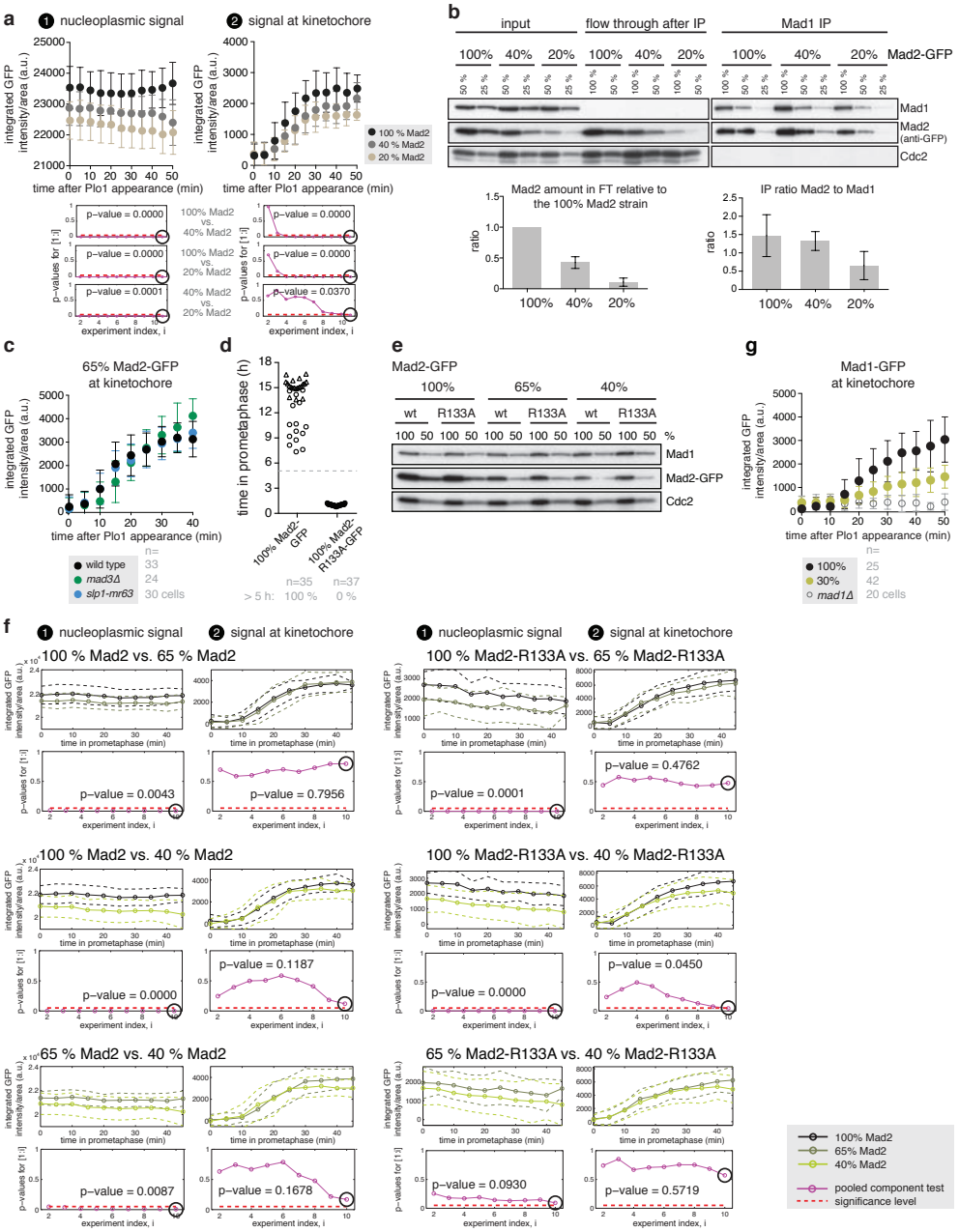

Figure S6 Analysis of Mad2 abundance at kinetochores, in the nucleoplasm and in complex with Mad1. **a** Abundance of 40 % and 20 % Mad2 in the nucleoplasm and at kinetochores. The amount of Mad2-GFP in the indicated strains was followed as cells entered mitosis in the absence of microtubules. (error bars = s.d.; n=41/38/29 cells for 100/40/20 % Mad2). We tested for similarity of the curves by pooled component test. The differences between strains for signals both at the kinetochore and in the nucleoplasm were statistically significant ($p < 0.05$). **b** Reduction of Mad2 to 20 % reduces the Mad1-bound and the free pool of Mad2. Extracts from asynchronously growing cultures in rich medium were used for immunoprecipitation (IP) of Mad1 using anti-Mad1 antibodies and analysed for co-immunoprecipitation of Mad2. Percentages on top of each lane indicate how much of the original extract or the immunoprecipitation was loaded. The input and flow through (FT) loaded is 15 % of the amount used for the IP sample. Quantifications of the flow through and the IP are shown on the right (see Methods). For 100 % and 40 % Mad2, one representative out of three independent experiments is shown. **c** Mad2-GFP recruitment to the kinetochore is not decreased in *mad3D* or *slp1-mr63*. The amount of Mad2-GFP at the kinetochore was recorded as cells entered mitosis in the absence of microtubules. (error bars = s.d.) **d** The Mad2-R133A mutation causes a checkpoint defect. Strains were followed by live cell imaging as in Fig. 2. **e** Mad2-R133A and abundance-reduced versions are present at similar levels as wild type Mad2. Extracts from asynchronously growing cultures in rich medium were analysed by immunoblotting using anti-Mad1, anti-GFP and anti-Cdc2 (as loading control) antibodies. Percentages on top of each lane indicate how much of the original extract was loaded. **f** Statistical analysis of Mad2 abundance in the nucleoplasm and at the kinetochore. Intensity curves for the Mad2-GFP and Mad2-R133A-GFP strains, also shown in Fig. 4d, were compared by a pooled component test. The cumulative p-value is plotted in pink. A p-value of 0.05 is shown as dashed red line. **g** Reduction of Mad1 to 30 % considerably decreases the Mad1 amount at unattached kinetochores. The amount of Mad1-GFP at the kinetochore in the indicated strains was followed as cells entered mitosis in the absence of microtubules (error bars = s.d.).

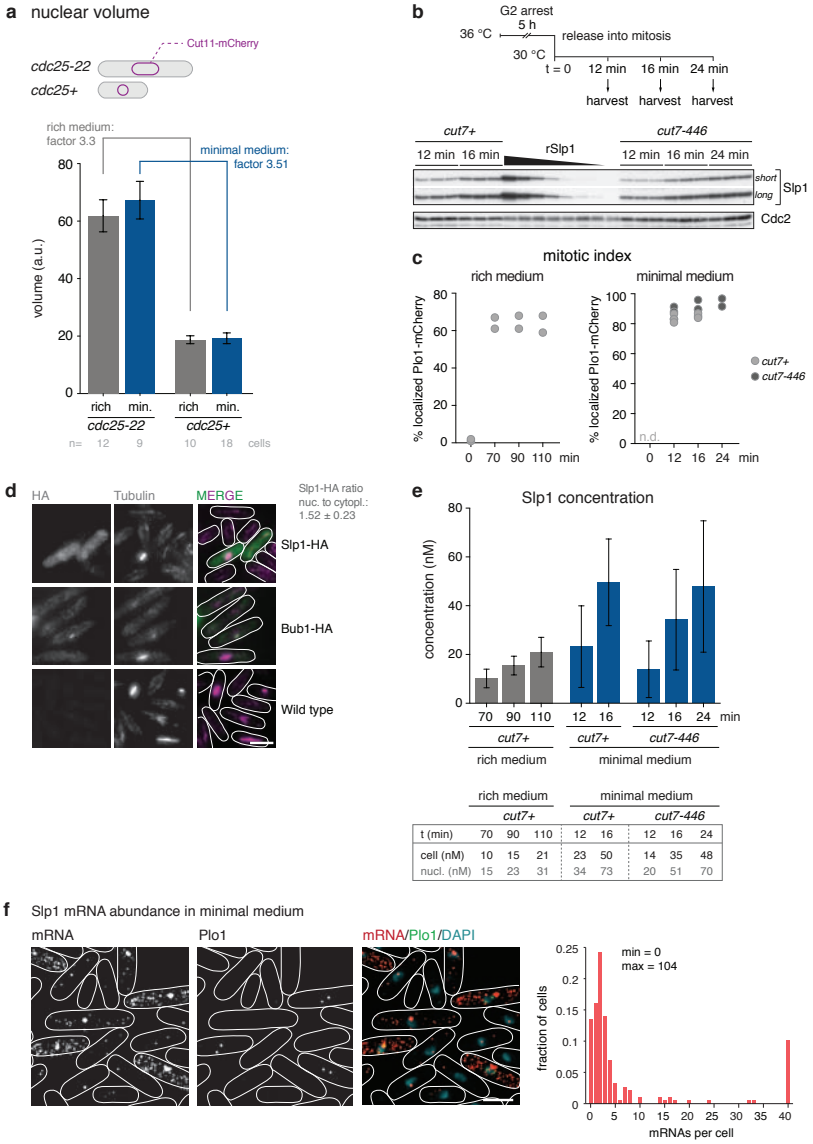

Figure S7 Quantification of Slp1 mRNA and protein abundance. **a** Nuclear volume increase in *cdc25-22* arrest. Cells expressing *cut11+-mCherry* were shifted for 4.5 hours (YEA) or 5 hours (EMM) to 36 °C for synchronization in G2. *Cdc25+* cells were mixed into the G2-arrested *cdc25-22* culture and the mixture was mounted on the microscope stage, which was pre-heated to 36 °C. The nuclear rim localization of Cut11-mCherry was used for nuclear segmentation. (a.u. = arbitrary units, error bars = s.d.) **b** Quantification of Slp1 in minimal medium by quantitative immunoblotting. *Cdc25-22* cells expressing either *cut7+* or the kinesin mutant *cut7-446* were grown in minimal medium (EMM). *Cut7-446* at restrictive temperature causes the formation of a monopolar spindle and activation of the spindle assembly checkpoint (SAC). Three technical replicates were harvested from the start of Slp1 expression until maximal abundance was reached and were analysed by immunoblotting using anti-Slp1 and anti-Cdc2 (loading control) antibodies. Recombinant His_6-Slp1 (rSlp1) was mixed with an extract from G2-arrested cells and was used as standard for quantification. (short = short exposure, long = long exposure) Shown is one representative out of two (*cut7+)* or three (*cut7-446*) independent experiments. **c** Mitotic index of samples used for Slp1 abundance determination by quantitative immunoblotting. Cells were grown in rich medium (for *cut7+* cells; see Fig. 6a) or minimal medium (EMM; for *cut7+* and *cut-446* cells; see (b) and (e) in this figure). After G2 arrest, cells in rich medium were released into mitosis at 16 °C, cells in minimal medium were released into mitosis at 30 °C. The mitotic index was determined from the percentage of cells showing a localized Plo1-mCherry signal at spindle pole bodies (SPBs). **d** Slp1-HA was detectable in mitotic cells and was distributed throughout the cell with a slight enrichment in the nucleus. Cells were immunostained for HA and tubulin. Cells expressing *bub1+-HA* and wild type cells served as specificity controls. The nucleo-cytoplasmic ratio for Slp1-HA was calculated by dividing the mean intensity in the nucleus (nuc.) by the mean intensity in the cytoplasm (cyto.). Background measured in interphase cells was subtracted. (n=30 cells; ± = s.d.) Scale bar: 5 µm. Shown is one representative out of two independent experiments. **e** Slp1 is approximately twice as abundant in minimal medium as in rich medium. Slp1 concentrations determined from the time course experiments shown in Fig. 6a and S6b. The graph shows average concentrations from two (*cut7+,* both rich and minimal medium) or three (*cut7-446*, minimal medium*)* independent experiments. (error bars = s.d.) The table below shows the values for cellular Slp1 concentration (cell) determined by immunoblotting and the estimated nuclear concentration (nucl.) based on the measured nucleo-cytoplasmic ratio (see d). **f** Slp1 mRNA abundance peaks in mitosis. Single molecule FISH was performed on an asynchronous cell culture grown in minimal medium with probes against Slp1 mRNA. A representative image is shown on the left (scale bar: 5 µm). Plo1-GFP indicates cells in prometaphase. The histogram on the right depicts the mRNA frequency distribution in this sample. (n=186 cells).

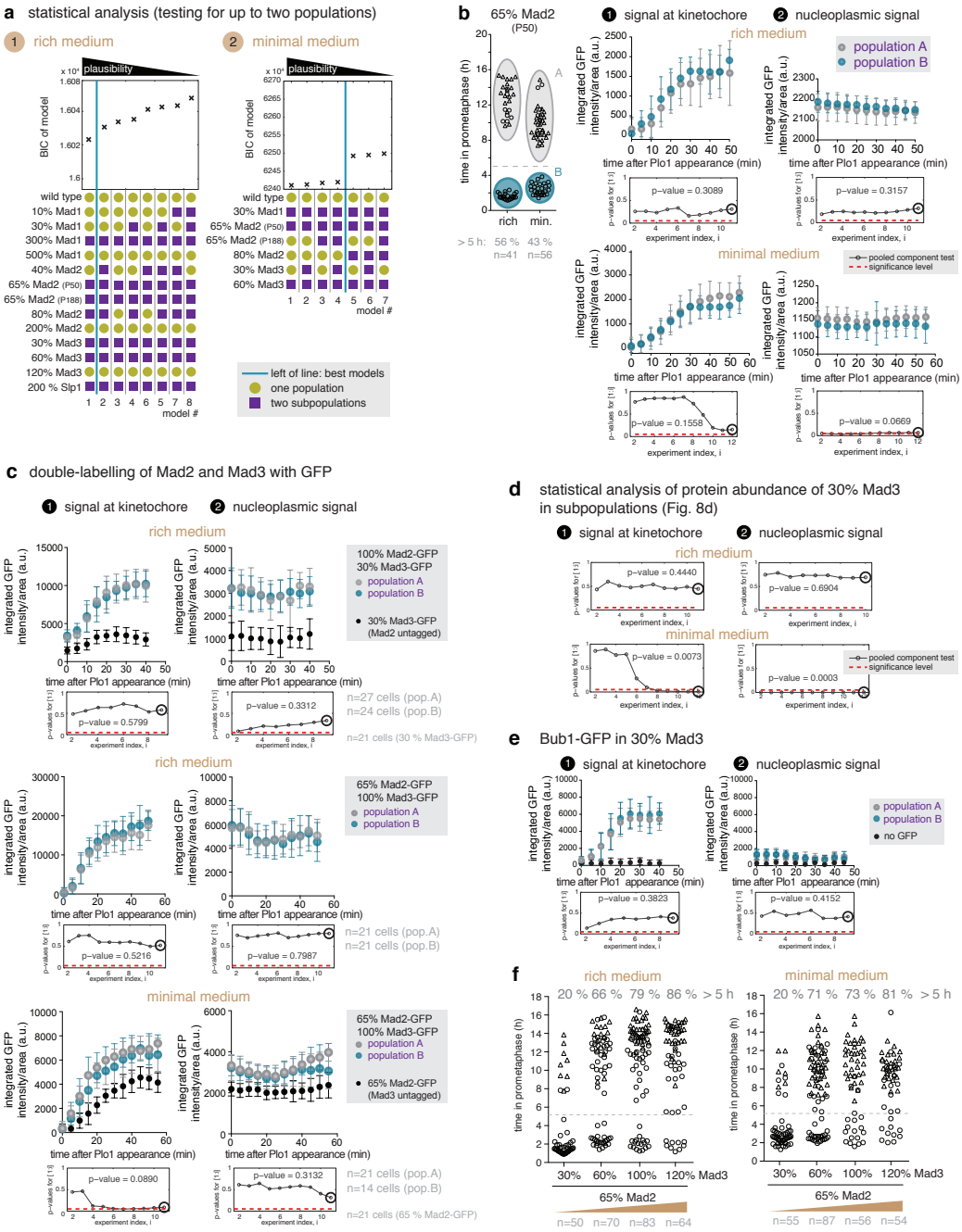

Figure S8 Statistical analysis of distribution of the mitosis times, and protein abundance measurements in the two subpopulations. **a** Distribution of mitosis times assessed by multi-experiment modelling (Supplementary Note). Mitosis times measured in strains with changed SAC protein abundance shown in Fig. 2 were analysed by multi-experiment modelling for the occurrence of up to two subpopulations. More plausible models have a lower Bayesian information criterion (BIC), and ranking of the models according to their BIC is shown. **b** In rich medium, no significant difference in Mad2 abundance was observed between the subpopulations. Strains were followed by live cell imaging as in Fig. 2 in either rich or minimal (min.) medium (left side). Mad2-GFP signals were quantified in each population (A and B) as cells entered mitosis (right side) (a.u. = arbitrary units; error bars = s.d.; n=23/18 cells for population A/B in rich medium; n=24/32 cells for population A/B in minimal medium). Intensity curves for population A and B were compared by a pooled component test. The cumulative p-value is plotted in grey. For rich medium, one representative out of two independent experiments is shown. **c** Combined Mad2 and Mad3 abundance are similar between population A and B. Strains expressing both Mad2- and Mad3-GFP in the indicated abundances were analysed as in (b) (a.u. = arbitrary units; error bars = s.d.). **d** Intensity curves for population A and B from Fig. 8d were compared by a pooled component test. The cumulative p-value is plotted in grey. A p-value < 0.05 is considered significant (dashed red line). Mad3 abundance in minimal medium is different between populations A and B. **e** Bub1-GFP signal intensity in a strain containing non-fluorescent 30 % Mad3-GFP-Y66L was analysed as in (b). ('no GFP' = 30 % Mad3-GFP-Y66L without Bub1-GFP; error bars = s.d.; n=19 cells (no GFP), n=24 cells (population A), n=22 cells (population B)). **f** Titration of Mad3 abundance in a 65 % Mad2-GFP background does not strongly affect the distribution of cells in the two subpopulations. Cells were followed by live cell imaging as in Fig. 2.

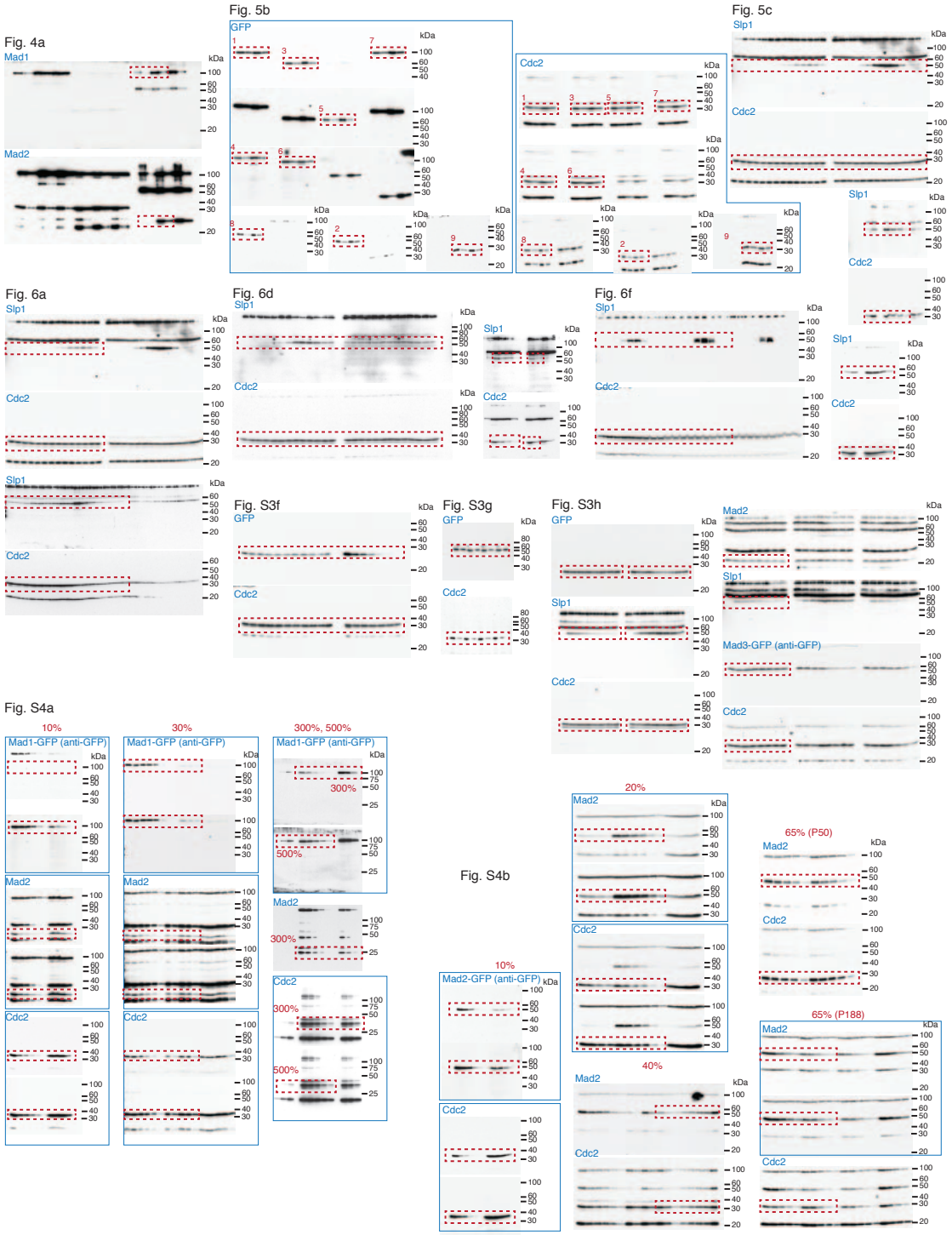

Figure S9 Entire membranes of cropped immunoblots. Blue labels on top indicate the antibody used for detection. Dashed red boxes show which regions of the immunoblot were cropped for the individual figures.

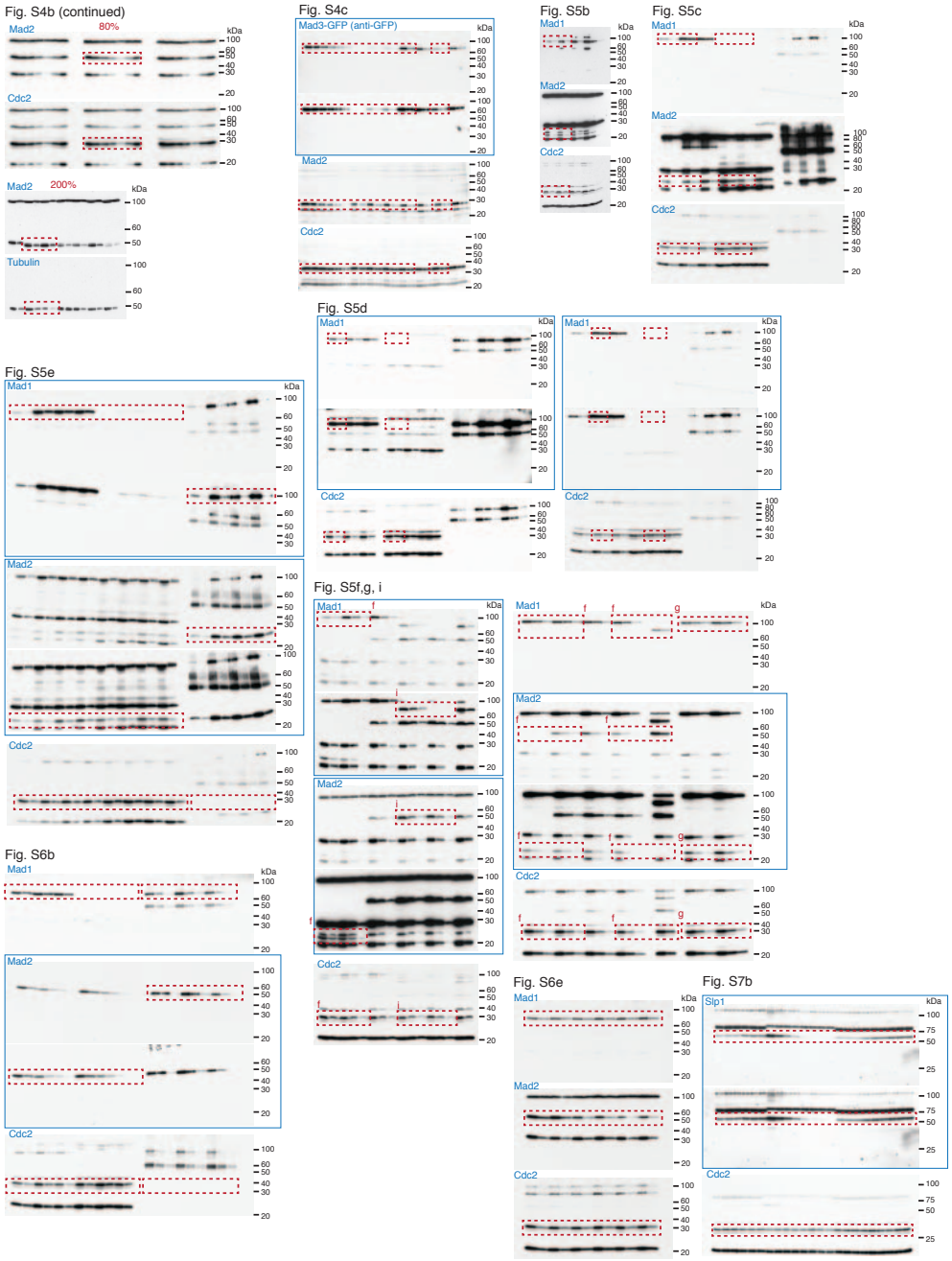

Figure S9 continued

Supplementary Table legends

Table S1 Relative SAC protein-GFP concentrations. SAC protein abundances measured in the nucleus or whole cell are given as relative (%) values with respect to the concentration of free GFP in interphase (GFP_i) (Fig. 1). (± = s.d.; CV, coefficient of variation =(standard deviation/mean) x 100 (%))

Table S2 Estimate of absolute SAC protein-GFP concentrations. Values for the nuclear concentration in interphase determined by FCS are from Fig. S3e, the value for GFP in mitosis determined by immunoblotting (IB) is from Fig. S3f. GFP is equally distributed between nucleus and cytoplasm, so that nuclear and cellular concentrations are assumed equal. The relative GFP concentrations measured in interphase (Fig. 1a) were used to derive absolute concentrations for SAC proteins and APC/C subunits. Values in parentheses for APC/C subunits denote mitotic values. For Slp1, the measured nucleo-cytoplasmic ratio (Fig. S7) was used to derive the nuclear concentration. Given is the maximum Slp1 concentration reached in rich medium in mitosis. For comparison, mass spectrometry-based quantification of selected checkpoint proteins by Marguerat *et al.*, 2012 (ref. 24), is shown. In addition, absolute cellular abundances of selected proteins were calculated using intensity based absolute quantification (iBAQ) (Schwanhausser *et al.*, 2011 (ref. 56)) applied to a global proteome analysis using SILAC (stable isotope labeling with amino acids in culture)-based quantification (A. Carpy, K. Krug, B. Macek, Proteome Center Tuebingen, personal communication). The iBAQ method correlates the protein mass spectrometric signal intensity to a spiked-in protein standard with known molar amounts and calculates the absolute cellular abundances for each identified protein.

Table S3 Promoter modifications to perturb protein abundance. List of modifications in the *mad1, mad2* and *mad3* genes that were used to change protein abundance. For two strains, 40% Mad2 and 80% Mad2, an extra copy of a modified *mad2* gene was integrated at the *leu1* locus.

Table S4 ***S. pombe*** strains. List of *Schizosaccharomyces pombe* strains employed in this study.

Table S5 mRNA FISH probes. List of DNA probes used in fluorescence *in situ* hybridization (FISH) to detect mRNAs of either gene-GFP fusions (through the GFP moiety) or of *slp1+*.

Supplementary Note for

Determinants of robustness in spindle assembly checkpoint signalling

Stephanie Heinrich, Eva-Maria Geissen, Julia Kamenz, Susanne Trautmann, Christian Widmer, Philipp Drewe, Michael Knop, Nicole Radde, Jan Hasenauer, Silke Hauf

(A) Analysis of noise in checkpoint protein abundance

(A1) Determination of protein noise by WiFDeM

Since we quantified the abundance of SAC proteins or APC/C subunits fused to GFP in single cells, we could determine the variability between cells, both for the nuclear and for the cellular measurements. We took the GFP measurements, from which the contribution of autofluorescence (based on wild type cells present in the same well) had been subtracted, and divided their standard deviation by the mean to obtain the coefficient of variation (CV).

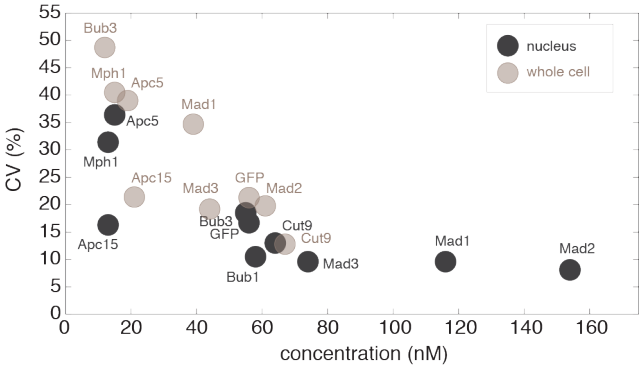

We noticed that noise values tended to be higher when the concentration was lower. This resulted in situations where, for the same cells, cellular noise was higher than nuclear noise (e.g. Mad1). However, in strains where the cellular and nuclear GFP concentration were similar (e.g. Cut9), the CV was also similar. We suspect that in samples with low GFP concentration, the protein noise is obscured by the underlying autofluorescence noise, which leads to an overestimation.

In brief, the fluorescence variability that we observe is a composite of the variability in autofluorescence and the variability in abundance of the GFP fusion protein.

The noise in autofluorescence is

(1) $CV_{AF} = \frac{\sigma_{AF}}{\mu_{AF}}$,

the noise of the GFP fusion protein is

(2) $CV_{GFP} = \frac{\sigma_{GFP}}{\mu_{GFP}}$,

with σ being the standard deviation and μ being the mean. While the noise of the autofluorescence can be measured in control experiments, the noise of the GFP concentration cannot be measured directly. We can merely measure noise of the combined fluorescence.

The combined fluorescence has a standard deviation of

(3) $\sigma_{tot} = \sqrt{{\sigma_{AF}}^2 + {\sigma_{GFP}}^2}$,

and, since we subtract the mean of the autofluorescence to obtain the GFP concentration, has a mean of $\mu_{tot} = \mu_{GFP}$.

We observe $CV_{tot} = \frac{\sigma_{tot}}{\mu_{GFP}}$, and are interested in CV_{GFP}. Equation (2) and (3) can be re-arranged to yield

(4) $$CV_{GFP} = \frac{\sqrt{{\sigma_{tot}}^2 - {\sigma_{AF}}^2}}{\mu_{GFP}} = \sqrt{{CV_{tot}}^2 - \frac{{\sigma_{AF}}^2}{{\mu_{GFP}}^2}}$$

Hence the observed noise (CV_{tot}) overestimates the noise of the SAC-GFP fusion proteins (CV_{GFP}) by a factor that depends on the noise of the autofluorescence and the mean GFP signal intensity. If the GFP signal is high, autofluorescence noise can be neglected and the observed noise will be close to the SAC-GFP fusion protein noise. We therefore grouped our measurements into three categories. Category 1 (darkest grey in Fig. 3a) contains samples, for which the mean GFP concentration is more than 2.5-times the mean autofluorescence concentration: this includes the nuclear measurements for Mad1 and Mad2. In this category, noise is determined quite accurately. Category 2 (intermediate grey intensity in Fig. 3a) contains samples, for which the mean GFP concentration is more than 1.5-times but less than 2.5-times the mean autofluorescence concentration: this includes the nuclear measurements for Mad3, Bub1, Cut9 and free GFP. Category 3 contains all other samples, including all cellular measurements, whose mean GFP concentration is less than 1.5-times the autofluorescence concentration. In those samples, we expect the measured noise to substantially overestimate the protein noise.

The standard deviation of the autofluorescence in the GFP-containing cells, which is needed in equation (4) is unknown, but we can use the standard deviation of the autofluorescence of wild type cells present in the same observation chamber as an estimate. If we perform this correction, the noise estimate of nuclear Mad1 and Mad2 changes only little, whereas the change is more substantial for measurements in category 2 and 3.

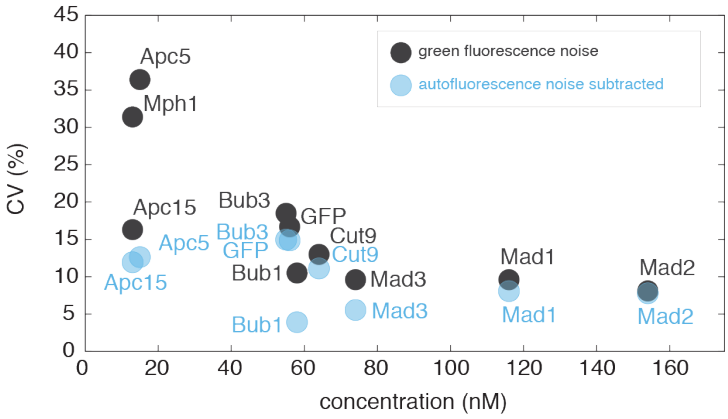

Mph1, whose fluorescence is only 5 % above the autofluorescence, could not be assessed in this way, because the standard deviation of the autofluorescence happened to be higher than the

standard deviation of the fluorescence signal in GFP cells, presumably due to chance variation. We conclude that the observed noise generally overestimates the protein noise and that the noise measurements are more accurate when the GFP concentration is higher, as is the case for Mad1 and Mad2 in the nucleus.

(A2) Comparison of coefficients of variation between our and published data

In budding yeast, low abundant proteins (as the ones we study here) have been reported to have coefficients of variation (CVs) in the order of 20 - 30 %[1,2], whereas our measured CVs for SAC proteins were as low as 8 % (Supplementary Table S1). For a comparison within the species, we plotted our data against a quantification of cytokinesis proteins in fission yeast[3], which used the same microscopy-based method that we used here. Those cytokinesis proteins that had low CVs of around 7 % were about a factor of 10 more abundant than SAC proteins, and those cytokinesis proteins with similar abundance as SAC proteins had higher CVs. This suggests that the cell-to-cell variability of some SAC proteins, including Mad1, Mad2 und Mad3, is remarkably low. Absolute protein abundances for the SAC proteins in the figure below are based on FCS measurements of GFP (Supplementary Table S2).

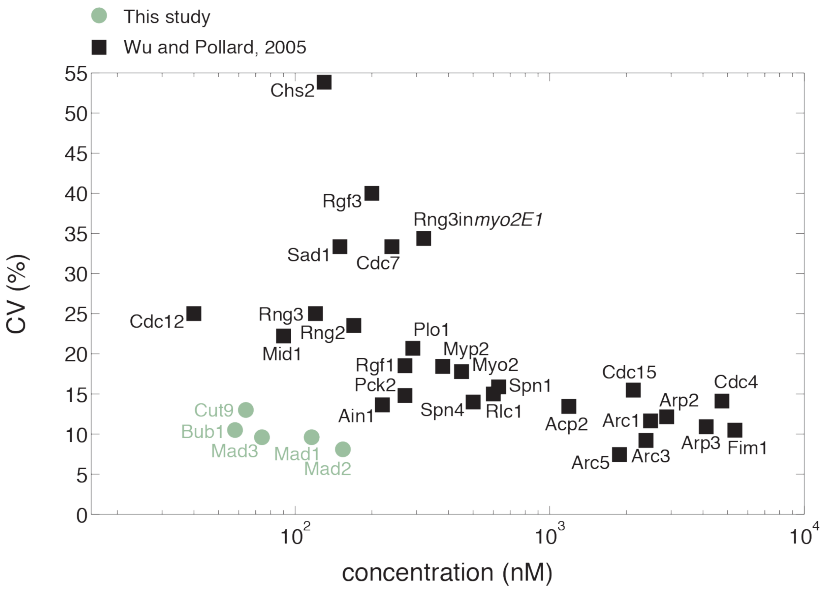

(A3) Stochastic model for the prediction of noise in protein concentration

To predict the minimal mRNA and protein abundance fluctuation of checkpoint proteins, we implemented a stochastic transcription-translation model[4,5], which takes both the stochasticity of biochemical reactions and cell cycle effects into account. The randomness of biochemical

reactions is modelled using the chemical master equation and simulated via Gillespie's simulation algorithm[6]. The reactions in a single cell are:

1. $G \rightarrow G + mRNA,\ w_1 = k_r[G]$ (transcription)
2. $mRNA \rightarrow \emptyset, w_2 = \gamma_r[mRNA]$ (mRNA degradation)
3. $mRNA \rightarrow mRNA + protein, w_3 = k_p[mRNA]$ (translation)
4. $protein \rightarrow \emptyset, w_4 = \gamma_p[protein]$ (protein degradation)

in which G denotes the gene, w_i denotes the reaction propensity of the i-th reaction and brackets denote molecule number of the respective chemical species. We assumed that rates are independent of cell volume. Furthermore, as DNA doubling in *S. pombe* takes place immediately after chromosome segregation[7], the number of gene copies remains constant. Hence, the common Gillespie algorithm can be employed. The transcription rate k_r, the mRNA degradation rate γ_r, the translation rate k_p and the degradation rate γ_p are chosen gene-specific.

The cell cycle introduces additional variability between cells, e.g. by differences in cell cycle length and stochastic partitioning of cell material at cell division. We assumed an inter-division time of 112.5 min (our measurement at 30 °C) and a CV of 10.8 %[8], with a linear increase in cell volume over time[9]. We assumed a log-normal distribution for the inter-division time. A growth rate of 0.632 fL/min (=(average volume increase per cell cycle)/(average cell cycle length) = 71.0 fL/112.5 min) is used, which yields an average cell size of 71.0 fL and 142.0 fL directly after and shortly before cell division, respectively. This is in agreement with our own measurements of the volume of dividing cells. The cell volume is assumed to partition symmetrically at division, yielding in our stochastic simulation cell size CVs of 6.26 % and 6.24 % at the beginning and the end of the cell cycle, respectively. Partitioning of the mRNAs and proteins into the daughter cells is assumed to be a stochastic process, resulting in a binomial distribution.

The simulation has been implemented in MATLAB exploiting fast simulation of the stochastic process using mex-files. Each simulation has been started with a single cell and ran for 40 times the mean inter-division time. This corresponds to roughly 40 generations, a time after which we observed equilibration of the stochastic process for all parameter values.

Simulation routines and parameter estimation routines are provided as supplementary MATLAB code.

(A4) Prediction of noise in protein concentration (Fig. 3c)

To determine protein noise, we required the kinetic parameters of the transcription-translation process. Experimental values for mRNA half-life have been reported[10,11]. We find that SAC proteins are stable for > 60 min (at least at less than 20 °C (Fig. S3)), similar to what others reported[12]. Since longer protein half-life reduces noise (Fig. 3d), we conservatively assumed a protein half-life of 240 min (Fig. 3c) or entirely stable protein (Fig. 3d) whose abundance is only

decreased by dilution in growing cells. The mRNA synthesis rate was estimated from our (Fig. 3b) or published[13] data on mRNA abundance. The protein synthesis rate was estimated from our measurement of protein abundance by FCS and WiFDeM (Fig. 1, Table S2).

As the stochastic process results in a stochastic objective function, we did not use classical gradient-based optimization routines but a simple, robust line search method. This method proved efficient and converged robustly to the global optimum. The optimization was considered converged when the measured values for mean mRNA number and protein concentration were within one standard error of the mean (SEM) interval ([mean-SEM, mean+SEM]) of the stochastic simulation. To ensure sufficient statistics we always averaged over more than 10,000 cells. The parameters were identifiable in all considered scenarios.

mRNA abundances and half-life from this and previous studies that were used in the simulations

	Mad1	Mad2	Mad3	Bub1	Bub3	Mph1	Apc5	Apc15	Cut9
mRNAs per cell[13]	1	0.84	1.4	2.6	0.44	1.9	0.73	2	0.94
mRNAs per cell (this study, Fig. 3b)*	5.2	6.0	4.6	9.2	4.2	8.5	4.2	3.0 13.4**	7.8
mRNA half-life (min)[10]	24.77	34.7	32.6	11.29	36.04	21.41	36.1	15.3	17.41
mRNA degradation rate (min^{-1})[11]	0.024	0.047	0.044	0.027	0.023	0.021	0.021	0.032	0.027

* All values are for the GFP mRNA moiety, i.e. the transcript coding for the quantified proteins.
** Apc15 mRNA counts in an asynchronous population show a bimodal distribution with the given means.

Predicted CV for protein concentration, with different assumptions for mRNA abundance and half-life

Predicted CV of protein conc. (%)	Mad1	Mad2	Mad3	Bub1	Bub3	Mph1	Apc5	Apc15	Cut9
mRNA number from Marguerat *et al.*[13] mRNA half-life from Amorim *et al.*[10]	46.3	56.3	43.0	22.2	76.6	44.6	60.6	n.d.	42.9
mRNA number determined in this study mRNA half-life from Amorim *et al.*[10]	20.4	21.0	23.8	12.2	25.8	15.6	25.6	n.d.	15.0
mRNA number determined in this study mRNA half-life from Sun *et al.*[11]	21.7	15.9	18.5	16.0	24.2	17.6	24.9	n.d.	17.1

All calculations assume a protein half-life of 240 min, and the cellular protein concentrations determined by FCS in this study (Supplementary Table S2). Estimates for Apc15 are not given, because the assumed mRNA half-life cannot reproduce the observed bimodal mRNA abundance distribution in the stochastic simulation.

As exemplified in the graphs for Mad2 below, the mean mRNA counts and the mean protein concentration agree well between measurement and simulation. However, the protein noise is overestimated by the simulation.

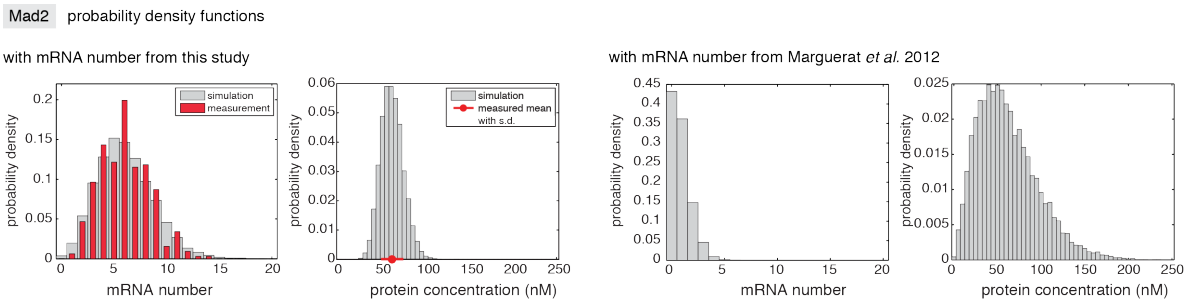

(A5) Comparison of mRNA number obtained in this and previous studies

Large scale studies in both budding and fission yeast have reported that many mRNAs are present in low copy number, often only one mRNA per cell on average[13,14]. Others have already noticed that it is difficult to explain the reliable operation of cell cycle regulatory networks with such low mRNA numbers[15]. For budding yeast, determination of mRNA numbers in single cells yielded slightly higher numbers per cell[16], as we observe it now for fission yeast.

(A6) Prediction of noise depending on protein half-life, protein synthesis rate or mRNA half-life (Fig. 3d)

To predict the changes in the CV of Mad2 protein concentration depending on different protein half-life (Fig. 3d, left), we assumed a mean protein concentration of 61 nM (Supplementary Table S2), a mean mRNA number of 6.03 (Fig. 3b) and an mRNA half-life of 34.7 min[10]. We tested protein half-lifes of 60 min, 240 min, and stable protein, whose abundance is only decreased by dilution in growing cells.

To predict the changes in the CV of Mad2 protein concentration depending on protein concentration (Fig. 3d, middle), we assumed stable protein, the same mean mRNA number and half-life as above, and varied the protein synthesis rate, so that protein concentrations between 15 and 150 nM were reached.

To predict the changes in the CV of Mad2 protein concentration depending on mRNA half-life (Fig. 3d, right), we assumed stable protein with a mean concentration of 61 nM (Supplementary Table S2) and the same mean mRNA number as above. The mRNA half-life was varied between 1 and 60 min.

(B) Computation of Mad1:Mad2 and free Mad2 abundance

The Mad1:Mad2 complex exists throughout interphase[17,18] and we find Mad1 and Mad2 abundance to be constant between interphase and mitosis (Fig. 1). Because Mad1-unbound Mad2 (free Mad2) enters the MCC in checkpoint-activated cells, it is possible that the equilibrium

shifts towards free Mad1 and Mad2 during a checkpoint-mediated mitotic delay. However, since the Mad1:Mad2 complex has repeatedly been shown to be very stable[17,19], we assume that this effect is negligible.

To assess the abundance of the different species in steady state as a function of the stability of the complex, we modelled complex formation

(5) Mad1 + Mad2 <-> Mad1:Mad2

assuming mass action kinetics. As a stability measure for the Mad1:Mad2 complex, we employ the dissociation constant (K_D),

(6) $K_D = \frac{[Mad1][Mad2]}{[Mad1{:}Mad2]}$.

The total protein abundances are assumed to be constant and we use the interphase protein concentrations estimated by FCS (Supplementary Table S2). Hence,

(7) $[Mad1_t] = [Mad1] + [Mad1{:}Mad2] = 39\ nM$

(8) $[Mad2_t] = [Mad2] + [Mad1{:}Mad2] = 61\ nM.$

By re-arranging (7) and (8) and substituting [Mad1] and [Mad2] in equation (6) we obtain

(9) $K_D = \frac{([Mad1_t]-[Mad1{:}Mad2])([Mad2_t]-[Mad1{:}Mad2])}{[Mad1{:}Mad2]}$.

This equation can be solved, which provides the steady-state concentrations of Mad1:Mad2 and Mad2,

(10) $[Mad1{:}Mad2] = \frac{([Mad1_t]+[\mathrm{Mad2}_t]+K_D)-\sqrt{([Mad1_t]+[\mathrm{Mad2}_t]+K_D)^2-4\times[Mad1_t][\mathrm{Mad2}_t]}}{2}$,

(11) $[Mad2] = \frac{([\mathrm{Mad2}_t]-[Mad1_t]-K_D)+\sqrt{([\mathrm{Mad2}_t]-[Mad1_t]-K_D)^2+4[\mathrm{Mad2}_t]K_D}}{2}$.

The abundances of Mad1:Mad2 and Mad2 as a function of dissociation constant are shown in Fig. 4c.

(B1) Plausible range of K_D values

Two pieces of evidence indicate that the K_D for Mad1:Mad2 complex formation is low:

(a) It has been shown that the complex is very stable[17,19,20] and

(b) it has been shown that almost all Mad1 is in complex with Mad2[12,17,21].

To fulfil these conditions, we conclude that the K_D should be 10 nM or lower (see Fig. 4c). Because we observe a reduction of free Mad2 when reducing Mad2 from 40 to 20 % (see Supplementary Fig. S6b), we consider a K_D of 4 nM a plausible, lower bound. We note that, given this low K_D, the expression of 300 % Mad1 should suppress free Mad2 to about one fourth the value in wild type (100 % Mad1) cells. The reduction that we observe is less pronounced (Supplementary Fig. S5e). The reason for the discrepancy is unclear at present, but we consider it possible that a factor like Tpr/Nup211[22] may become limiting in the Mad1 overexpression, so that Mad2 can be less efficiently captured and the soluble pool is less efficiently depleted.

(C) Multi-experiment mixture modelling to assess the distribution of mitosis times

When analysing mitosis time upon SAC activation in wild type or perturbed conditions, we observed strong inter-cell variability and in some situations a split into two subpopulations. For some cells both entry into and exit from mitosis were recorded, whereas for other cells only entry into mitosis was recorded within the observation interval (17 hours). Hence, for the latter cells, only a lower bound of the mitosis time is available. Furthermore cells are only recorded every five minutes. These two types of censoring complicate the statistical analysis. To statistically assess the number of populations and their distribution, we performed multi-experiment mixture modelling suited for censored data (Supplementary Fig. S8a).

To account for the observed inter cell variability we modelled the mitosis times as a stochastic process represented by the probability density function of a parametric distribution. The distribution of uncensored mitosis times was modelled by a log-normal distribution, $\log N(\mu,\sigma^2)$, whereas the distribution of censored times was modelled by a Johnson SU distribution $J(\gamma,\sigma,\lambda,\xi)$. After extensive testing, this combination of distributions was chosen because it resulted in the smallest values for the Bayesian information criterion (BIC). As exit from mitosis and censoring are mutually exclusive events, the realized mitosis and the censoring times depend on the convolution of the mitosis time distribution and censoring time distribution. By integrating these distributions over the inter-observation interval (in our experiments five minutes) we obtained the probability mass functions of the discrete time measurements of mitosis times and censoring times. These were used to derive the likelihood of the data given the model parameters using all perturbation conditions, which were used for fitting the parameters of the log-normal and Johnson SU distributions. Fitting was performed in MATLAB using a multi-start local optimization procedure.

(C1) Analysis for one or two populations

We implemented a mixture model in which every mitosis time distribution was a weighted mixture of up to two components, one for every potential subpopulation. The distribution of censoring times was assumed to be the same for all experimental conditions. To evaluate the different model alternatives and to determine the most parsimonious model still describing the data (evaluated using the BIC), we performed a backward selection. To analyse the distributions of mitosis times in rich medium (YEA), the data shown in Fig. 2b-d (excluding 10 % Mad2 and 20 % Mad2 for computational reasons) were used for the multi-experiment mixture modelling. The data for 200 % Slp1 were taken from Fig. 6e. To analyse the distributions of mitosis times in minimal medium (EMM), the data shown in Fig. 5a were used.

(C2) Comparison of the population A to wild type cells

We also tested the hypothesis that the subpopulation of cells arresting for longer (population A) behaves like the wild type population. In the corresponding mixture model, each dataset could comprise up to two mixture components: an independent, perturbation-caused subpopulation and one with the same parameter values as the wild type population. We considered this model to be favoured over the previous model (both subpopulations were unconstrained) when its BIC value was more than 6 points lower[23]. For rich medium, the hypothesis that population A behaves like the wild type population was favoured (BIC value 66 points lower); for minimal medium, the hypothesis was not supported (BIC value 6 points higher).

(D) Modelling of Slp1 synthesis and MCC formation using ODEs

(D1) Basic assumptions

We formulated a core model of MCC formation (M1; Fig. 7b) based on the following information:

(D1a) Slp1 is synthesized in mitosis[24].

(D1b) Slp1 is an unstable protein with a half-life in the range of 15 min (Supplementary Fig. S3h and Sczaniecka *et al.*[12]).

(D1c) Accumulation of Slp1 is not drastically different in cells with or without an active checkpoint (Supplementary Fig. S7 and data not shown). We therefore assume that the degradation rates of Slp1 and of Slp1 as part of the MCC are similar.

(D1d) Slp1 reaches approx. 20 nM (Fig. 6a and data not shown).

(D1e) Maximal Slp1 concentration is reached in about 120 min after start of mitosis at 16 °C (the temperature at which we assessed checkpoint activity) (Fig. 6a).

(D1f) Mad2 and Mad3 bind Slp1 as stoichiometric inhibitors[25-27].

(D1g) Mad2 and Mad3 are stable proteins (Supplementary Fig. S3h and Sczaniecka *et al.*[12]). Hence, synthesis and degradation can be neglected.

We extended this model by binding of Slp1 and the MCC to the APC/C (M2; Fig. 7d), with the following additional assumptions:

(D1h) APC/C is a stable complex[28]. Hence, synthesis and degradation can be neglected.

(D1i) APC/C is inhibited by binding to the MCC[25,29,30].

(D1j) APC/C is activated by Slp1[31,32].

(D1k) Slp1 is degraded as part of the MCC when bound to the APC/C[33-40].

(D1l) In analogy to M1, we assume APC/C-independent degradation of free Slp1, although the Slp1 ortholog Cdc20 is degraded in an APC/C-dependent manner[41].

(D2) Model M1 for MCC formation (Fig. 7b)

Using mass action kinetics, model M1 shown in Fig.7b is described by the following ordinary differential equations:

(12) $\frac{d[Slp1]}{dt} = k_{syn(Slp1)} - k_{\deg(Slp1)}[Slp1] - k_{on(MCC)}[Slp1][inh] + k_{off(MCC)}[MCC]$

(13) $\frac{d[inh]}{dt} = k_{\deg(Slp1)}[MCC] - k_{on(MCC)}[Slp1][inh] + k_{off(MCC)}[MCC]$

(14) $\frac{d[\mathrm{MCC}]}{dt} = k_{on(MCC)}[Slp1][inh] - k_{off(MCC)}[MCC] - k_{\deg(Slp1)}[MCC]$

in which [Slp1] denotes the concentration of Slp1, [inh] denotes the concentration of inhibitor and [MCC] denotes the concentration of the Slp1:inhibitor complex; $k_{syn(Slp1)}$ is the synthesis rate and $k_{deg(Slp1)}$ the degradation rate of Slp1; $k_{on(MCC)}$ and $k_{off(MCC)}$ are binding and dissociation rate of Slp1 and inhibitor. The degradation rate of Slp1 within the MCC is assumed to be equal to the degradation rate of free Slp1, $k_{deg(Slp1)}$ (see (D1c)). The inhibitor is analogous to Mad2/Mad3 that is competent to bind Slp1 ('active' Mad2/Mad3). The concentration of free Slp1, [Slp1], is considered the model output (Fig. 7b). It is unknown at which rate free Slp1 initiates anaphase. For simplicity, we assume that free Slp1 needs to reach a threshold for anaphase to occur. This is a common simplification[42-44], and is based on the assumption that very small amounts of free Slp1 are insufficient to initiate anaphase, because the system would otherwise not be robust. The threshold should be low, because even low levels of mammalian Cdc20 efficiently promote anaphase[45,46].

(D3) Model M2 for MCC formation with APC/C binding (Fig. 7d)

Using mass action kinetics, the model shown in Fig.7d is described by the following ordinary differential equations:

(15) $\frac{d[APC{:}MCC]}{dt} = \mathrm{v2} - \mathrm{v5}$

(16) $\frac{d[APC{:}Slp1]}{dt} = \mathrm{v1}$

(17) $\frac{d[MCC]}{dt} = -\mathrm{v2} + \mathrm{v3}$

(18) $\frac{d[Slp1]}{dt} = -\mathrm{v1} - \mathrm{v3} + \mathrm{v4} - \mathrm{v6}$

(19) $\frac{d[APC]}{dt} = -\mathrm{v1} - \mathrm{v2} + \mathrm{v5}$

(20) $\frac{d[inh]}{dt} = \mathrm{v5} - \mathrm{v3}$

with

(21) $\mathrm{v1} = k_{\mathrm{on}(APC:Slp1)}[APC][Slp1] - k_{\mathrm{off}(APC:Slp1)}[APC{:}Slp1]$

(22) $v2 = k_{\mathrm{on}(APC:MCC)}[APC][MCC] - k_{\mathrm{off}(APC:MCC)}[APC:MCC]$

(23) $v3 = k_{\mathrm{on}(MCC)}[inh][Slp1] - k_{\mathrm{off}(MCC)}[MCC]$

(24) $v4 = k_{\mathrm{syn(Slp1)}}$

(25) $v5 = k_{\mathrm{deg}(Slp1)}[APC:MCC]$

(26) $v6 = k_{\mathrm{deg}(Slp1)}[Slp1]$

in which [APC:MCC] denotes the concentration of the inhibited APC/C:MCC complex, [APC:Slp1] denotes the concentration of the active APC/C:Slp1 complex, [MCC] denotes the concentration of the Slp1:inhibitor complex MCC, [Slp1] denotes the concentration of free Slp1, [APC] denotes the concentration of APC/C, and [inh] denotes the concentration of the inhibitor. The inhibitor is analogous to Mad2/Mad3 that is competent to bind Slp1 ('active' Mad2/Mad3). The model parameters are the Slp1 synthesis and degradation rates, $k_{syn(Slp1)}$ and $k_{deg(Slp1)}$, and the binding and dissociation rates of different complexes, $k_{on(X)}$ and $k_{off(X)}$. The model fulfils the conservation relations

(27) $[APC_T] = [APC] + [APC:Slp1] + [APC:MCC]$

(28) $[inh_T] = [inh] + [MCC] + [APC:MCC]$

in which $[APC_T]$ denotes the total concentration of APC/C and $[inh_T]$ denotes the total concentration of inhibitor. The concentration of APC/C:Slp1, [APC:Slp1], is considered the model output (Fig. 7d). Anaphase is initiated when APC/C:Slp1 concentration exceeds a certain threshold.

The model includes a double negative feedback loop consisting of inhibition of the APC/C by binding to the MCC and disassembly (and therefore inhibition) of the MCC through the APC/C.

(D4) Parameter estimation for population model from phenotype data

As the models for the signalling pathway should reproduce cell-to-cell variability, the parameter estimation is highly non-trivial. A moment equation based method has been proposed[47], but the required moment closure introduces large errors for the system at hand, which renders it impractical. Furthermore, the measurement data are only phenotypic, namely whether the SAC is functional or dysfunctional, and hence very different from the common concentration measurements.

We employ maximum likelihood estimation to determine the optimal model parameters. We used the number of cells with active and inactive SAC under checkpoint-activating conditions from WT, 30 % Mad1, 65 % Mad2 and 30 % Mad3 strains with both 100 % and 200 % Slp1 and estimated the kinetic parameters (M1: k_{on}, k_{off}, $k_{deg(Slp1)}$; M2: $k_{on(APC:Slp1)}$, $k_{off(APC:Slp1)}$, $k_{on(APC:MCC)}$, $k_{off(APC:MCC)}$, $k_{on(MCC)}$, $k_{off(MCC)}$, $k_{deg(Slp1)}$) and the distribution parameters ($\mu_{k,syn(Slp1)}$, $\sigma_{k,syn(Slp1)}$, $\mu_{inhT,WT}$, $\sigma_{inhT,WT}$, $\mu_{inhT,30\%Mad1}$, $\sigma_{inhT,30\%Mad1}$, $\mu_{inhT,65\%Mad2}$, $\sigma_{inhT,65\%Mad2}$, $\mu_{inhT,30\%Mad3}$, $\sigma_{inhT,30\%Mad3}$).

For each strain:

n_A = number of cells in population A (functional SAC; output below threshold), and

n_B = number of cells in population B (dysfunctional SAC; output above threshold).

The probability of observing n_A and n_B follows a binomial distribution

$$p(n_A, n_A|\theta) = \frac{(n_A + n_B)!}{n_A!\, n_B!} p_A^{n_A}(\theta) p_B^{n_B}(\theta)$$

in which $p_A(\theta)$ is the probability that for a given parameterization θ the concentration of the active species (for M1: Slp1; M2: APC/C:Slp1) is below the threshold, while $p_B(\theta)$ is the probability that for a given parameterization the concentration exceeds the threshold, with $p_A(\theta) + p_B(\theta) = 1$. The binomial distribution provides the likelihood for each individual experiment. The overall likelihood is obtained by multiplying the likelihoods of the individual experiments. An independent optimization of the individual likelihoods is not possible, as the different experiments share the kinetic parameters, the threshold and the distribution parameters of the Slp1 synthesis rate.

The probabilities $p_A(\theta)$ and $p_B(\theta)$ for each strain can in principle be computed by simulating the model for different values of Slp1 synthesis rates and inhibitor concentrations, drawn from the corresponding distribution defined by $\mu_{k,syn(Slp1)}$, $\sigma_{k,syn(Slp1)}$, μ_{inhT} and σ_{inhT}. By evaluating for each simulated cell whether the threshold is reached or not, one obtains a Monte Carlo estimate of the probabilities $p_A(\theta)$ and $p_B(\theta)$. However, the number of simulations required to achieve a high precision is large and the resulting objective function would exhibit stochastic fluctuations. This renders application of efficient gradient-based methods impractical and the optimization of the process computationally intractable.

To estimate the parameters of the population model we developed a sigma-point based estimation method. Our method is based on the decomposition of the overall parameter distribution into smaller parts using mixtures of log-normal distributions. For the individual log-normal parameter distribution we approximate the mean and the variance of the systems states, e.g., the Slp1 concentration, using the sigma-point method[48]. Based on the means and variances provided by the sigma-point method, we construct an approximating normal distribution for each mixture component. By computing the weighted sum of the mixture components we obtain an approximation of the probability density of the state for the full parameter distribution. This approximation of the state density can directly be used to approximate the probabilities $p_A(\theta)$ and $p_B(\theta)$. While a high-quality estimate of $p_A(\theta)$ and $p_B(\theta)$ still requires the decomposition into many small distributions, which all have to be propagated forward by simulating the system, this method is still orders of magnitude faster than classical Monte Carlo integration. Furthermore, as the sigma-points are deterministic, we can derive the gradient of the objective function, resulting in a further acceleration of the optimization and in better convergence properties.

In addition to the computational speed-up provided by our sigma-point based method, we wanted

to ensure robustness of the model predictions with respect to the chosen threshold. To achieve this, we evaluated the objective function not only for the current threshold, but also for thresholds smaller and larger by a factor of 3.162. The likelihood functions obtained for these three thresholds are multiplied and the third root is computed. The resulting values can be interpreted as average likelihood function of the interval [1/3.162, 3.162] x threshold. This interval spans one order of magnitude. By using this average in the optimization, we search for parameter combinations for which $p_A(\theta)$ and $p_B(\theta)$ are not sensitive with respect to the threshold.

Using the likelihood function approximation based on sigma-points, for which we ensured a good approximation quality, we optimized M1 and M2. We employed multi-start local optimization using the MATLAB optimization routine fmincon.

Further details regarding the sigma point method and the implementation of the parameter estimation can be found in the supplementary MATLAB code and its documentations. Beyond the implementation of the estimation and the analysis of model 1 and model 2, we also provide illustrations of the sigma point approximation.

(D5) Parameter estimation for M1

The synthesis rate of Slp1 ($k_{syn(Slp1)}$) as well as [inh_T] in the different strains are assumed to be log-normally distributed with parameters μ and σ. This yields in total 14 parameters that we constrained to the following ranges:

- CV of $k_{syn(Slp1)}$ between 0.05 and 0.5
- lower bound of mean of $k_{syn(Slp1)}$: 0.17 mol/min; calculated from 20 nM Slp1 after 120 min (see (D1d) and (D1e)), assuming no degradation
- upper bound of mean of $k_{syn(Slp1)}$: 1.98 mol/min calculated from 20 nM Slp1 after 120 min, assuming the upper bound for the degradation rate
- degradation rates should result in a Slp1 half-life between 7 and 40 min (see (D1b))
- 1e-5 $nM^{-1}min^{-1} < k_{on} <$ 1e5 $nM^{-1}min^{-1}$
- 1e-5 nM < $K_d = k_{off}/k_{on}$ < 1e5 nM
- 1 nM < [inh_T] < 50 nM (Supplementary Table S2) with corresponding CV between 0.05 and 0.5
- Slp1 threshold for anaphase onset between 0.1 and 20 nM

The dissociation constant K_d and the CV and mean of the total inhibitor concentration [inh_T] are lumped parameters of several biological parameters that are not included in this simple model. Hence, these model parameters do not have an exact biological equivalent.

Parameter boundaries for estimation:

	$\sigma_{k,syn(Slp1)}$	$\mu_{k,syn(Slp1)}$	σ_{inhT}	μ_{inhT}	$k_{deg(Slp1)}$
min	0.04997	-1.793	0.04997	-0.1116	0.01733 min^{-1}
max	0.47238	0.5717	0.47238	3.9108	0.09902 min^{-1}

The optimization using the sigma-point method (D4) yields the following maximum likelihood estimates:

$\sigma_{k,syn(Slp1)}$	$\mu_{k,syn(Slp1)}$	$k_{deg(Slp1)}$	K_d	threshold
0.3096	-0.4077	0.0353 min^{-1}	6.6156 10^{-5} nM	0.1034 nM

$[inh_T]$	wild type	30 % Mad1	65 % Mad2	30 % Mad3
μ	3.8734	3.5366	2.9306	3.0791
σ	0.0507	0.0572	0.4719	0.2167

Based on these parameters the mean of the total inhibitor concentrations and of the synthesis rate $k_{syn(Slp1)}$ can be calculated together with the respective CVs.

	wild type $[inh_T]$	30 % Mad1 $[inh_T]$	65 % Mad2 $[inh_T]$	30 % Mad3 $[inh_T]$	$k_{syn(Slp1)}$
Mean	48.1675 nM	34.4063 nM	20.9464 nM	22.2551 nM	0.6978 nM min^{-1}
CV	0.0507	0.0573	0.4995	0.2192	0.3172

To assess how well the model describes the data parameterized with the maximum likelihood estimate found using our sigma-point method, we computed the probability density to measure the fraction of cells in population A and B for a particular strain. These probability densities can be computed from the binomial distribution (underlying the likelihood function) using the probabilities $p_A(\theta)$ and $p_B(\theta)$ computed by the model and the total number of measured cells. Using the probability densities, we evaluate the 98 % confidence interval of the measurement assuming that our model is correct. These 98 % confidence intervals are depicted below (light resp. dark grey area) for a range of threshold values around the best fit for each experimental condition. Bold lines indicate the resulting fraction of cells in population B when assuming the corresponding threshold.

We find that for the nominal threshold (x-axis value = 1) the experimentally observed fractions are inside the 98 % confidence intervals for all strains. By varying the threshold, we find that the model fit is not sensitive to the choice of the threshold. We conclude that M1 can describe the main characteristics of the process while satisfying our requirement to be robust with respect to the threshold for anaphase activation.

model analysis M1

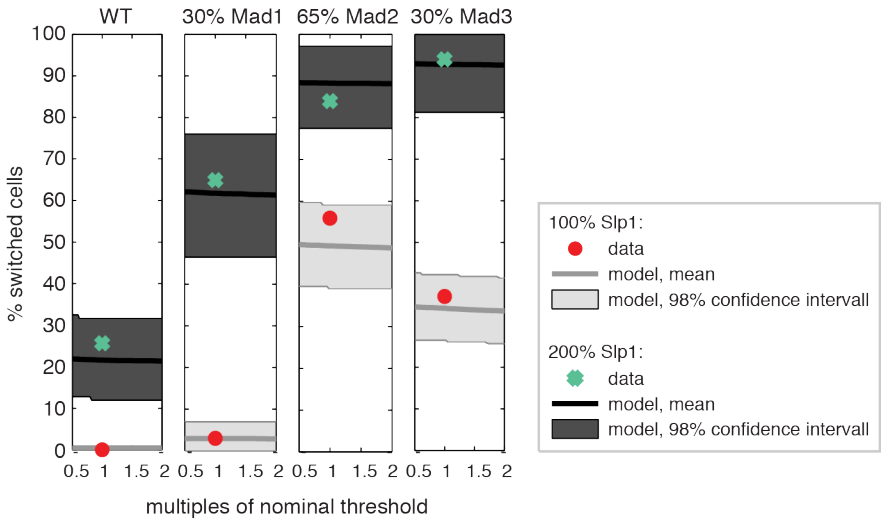

A representative sample of single-cell trajectories for model M1 is shown below and in Fig. 7c. We simulated 100 cells by sampling inhibitor concentration and Slp1 synthesis rate for each cell from the estimated distribution for each strain. In the large plot the time-dependent concentration of Slp1 in individual cells is shown. The frequency distribution is plotted on the right. The small plot shows the trajectories using a nonlinear y-axis, which is roughly linear for [Slp1] < 0.01 and becomes progressively logarithmic (Y = log([Slp1]+0.01)). The scale is related to the logicle scale used for the visualization of flow cytometry data[49].

The trajectory plots reveal that the Slp1 response is highly heterogeneous within the simulated populations. Depending on the strain, many cells keep very small values of [Slp1] (indicating a functional SAC, population A), while others reach high [Slp1] levels above the threshold (indicating a non-functional SAC, population B).

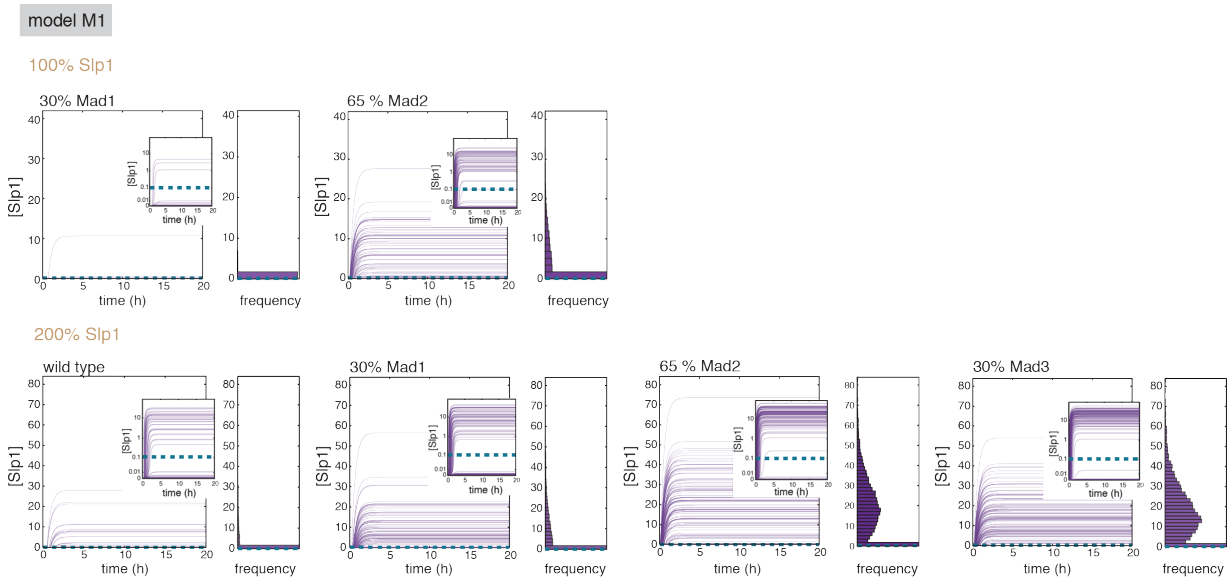

(D6) Bayesian uncertainty analysis for M1 using steady state assumption

Even with our sigma-point based method the parameter estimation for the time-dependent system is computationally intensive and a rigorous uncertainty analysis is currently impracticable. However, the estimation results in (D5) suggest that the system almost reached its steady state after 20 hours. We therefore decided to consider for the uncertainty analysis the steady state of M1, for which an analytical solution can be derived (see below). Using the analytical solution for the steady state of a single cell and the distribution of inhibitor and Slp1 synthesis rates, we can efficiently compute the probabilities $p_A(\theta)$ and $p_B(\theta)$. The efficient computation of $p_A(\theta)$ and $p_B(\theta)$ enables the fast evaluation of the likelihood function and thus a rigorous uncertainty analysis.

To study the uncertainty of the kinetic and distribution parameters of M1, we employed a Bayesian approach with a flat prior constraint to the parameter set specified above. To explore the parameter set we employed adaptive Markov chain Monte Carlo (adaptive MCMC) sampling. Using the MATLAB Toolbox DRAM (http://helios.fmi.fi/~lainema/mcmc/) we generated a converged MCMC sample and evaluated its statistics.

The MCMC sampling of the steady state version of M1 found the maximum a posteriori parameter estimate (the optimal parameters):

$\sigma_{k,syn(Slp1)}$	$\mu_{k,syn(Slp1)}$	$k_{deg(Slp1)}$	$K_D = k_{off} / k_{on}$	threshold
0.2908	0.3175	0.0716 min^{-1}	0.1066 nM	1.1788 nM

$[inh_T]$	wild type	30 % Mad1	65 % Mad2	30 % Mad3
μ	3.8945	3.5694	2.9338	3.1228
σ	0.0733	0.1058	0.4710	0.2882

This estimate is for many parameters surprisingly close to the estimate for the dynamic version of M1 and the fits of the observed data are almost indistinguishable. This substantiated our simplification and we analysed the parameter uncertainties based upon the MCMC sample.

The key finding of this analysis is that the variability in the inhibitor concentration in WT cells has to be small to explain the observed fraction of population A and B. Furthermore, the variability in the Slp1 synthesis rate is high compared to the variability of inhibitor concentrations in WT cells. The marginal for these two properties is illustrated in Fig. 8b.

(D7) Analysis of steady state ultrasensitivity of M1

Our analysis in (D5) revealed that the concentration of free Slp1 predicted by M1 is insensitive with respect to the threshold but yields two populations. To understand the underlying mechanism we analysed the steady state properties of M1 using methods developed by Buchler and Louis[50]. In particular, we analysed the steady state, the steady state fluxes and the point where the system changes its buffering behaviour (the equivalence point).

The *in vivo* dissociation constant[50] is

(29) $K_{\mathrm{D}} = \frac{k_{\mathrm{off}} + k_{\deg(Slp1)}}{k_{\mathrm{on}}}$.

In steady state, the fluxes are balanced,

(30) $k_{syn(Slp1)} = k_{\deg(Slp1)}[Slp1] + k_{\deg(Slp1)}[MCC]$.

As Mad2 and Mad3 are stable (see (D1g)), the overall inhibitor abundance is constant

(31) $[inh_T] = const. = [inh] + [MCC]$.

Employing these properties, we can determine an analytical expression for the steady state,

(32) $$k_{\deg\,(Slp1)}[Slp1] = \frac{k_{syn(Slp1)} - [inh_T]k_{\deg(Slp1)} - k_{\deg\,(Slp1)}K_D}{2} + \sqrt{\left(\frac{k_{syn(Slp1)} - [inh_T]k_{\deg(Slp1)} - k_{\deg\,(Slp1)}K_D}{2}\right)^2 + k_{syn(Slp1)}k_{\deg\,(Slp1)}K_D}$$

(33) $$k_{\deg\,(Slp1)}[inh] = \frac{-k_{syn(Slp1)} + [inh_T]k_{\deg(Slp1)} - k_{\deg(Slp1)}K_D}{2} + \sqrt{\left(\frac{-k_{syn(Slp1)} + [inh_T]k_{\deg(Slp1)} - k_{\deg(Slp1)}K_D}{2}\right)^2 + [inh_T]k_{\deg(Slp1)}k_{\deg(Slp1)}K_D}$$

(34) $$k_{\deg\,(Slp1)}[MCC] = \frac{k_{syn(Slp1)} + [inh_T]k_{\deg(Slp1)} + k_{\deg\,(Slp1)}K_D}{2} - \sqrt{\left(\frac{k_{syn(Slp1)} + [inh_T]k_{\deg(Slp1)} + k_{\deg\,(Slp1)}K_D}{2}\right)^2 - k_{syn(Slp1)}[inh_T]k_{\deg(Slp1)}}.$$

The comparison of these equations to equation (S4) from Buchler and Louis[50] yields the following relations:

(S4)	A	B	AB
our model	$k_{deg(Slp1)}$[Slp1]	$k_{deg(Slp1)}$[inh]	$k_{deg(Slp1)}$[MCC]

(S4)	A_T	B_T	K_D
our model	$k_{syn(Slp1)}$	$k_{deg(Slp1)}[inh_T]$	$k_{deg(Slp1)}K_D$

Thus, in analogy to Buchler and Louis[50], the system reaches its equivalence point when

(35) $k_{\mathrm{syn}\,(Slp1)} = k_{\mathrm{deg}\,(Slp1)}[inh_T]$

Slp1 synthesis rate $k_{syn(Slp1)}$, MCC degradation rate $k_{deg(Slp1)}$, and the amount of Slp1-inhibition competent Mad2/Mad3 ($[inh_T]$) define the regimes in which the checkpoint operates. Within the transition zone (regime II), the steady state of free Slp1 has high sensitivity with respect to changes in inhibitor concentration, i.e. it shows ultrasensitivity towards differences in the total amount of inhibitor. This sensitivity reaches its maximum at the so called equivalence point, which is the smallest total amount of inhibitor sufficient to roughly balance Slp1 synthesis given a certain rate for the degradation of Slp1 from the MCC. In Regime I, which is characterised by an excess of the inhibitor, changes are buffered and do not strongly influence the steady state. In Regime III, which is characterised by saturation of the inhibitor and an excess of free Slp1, changes in Slp1 synthesis rate or $[inh_T]$ result in equal fold changes of the steady state of Slp1.

Regime I **(buffering)**	**Regime II** **(transition zone)**	**Regime III** **(saturation)**
$k_{syn(Slp1)} \ll k_{deg(Slp1)}\,[inh_T]$	$k_{syn(Slp1)} \approx k_{deg(Slp1)}\,[inh_T]$	$k_{syn(Slp1)} \gg k_{deg(Slp1)}\,[inh_T]$

(D8) Parameter estimation for M2

To distinguish between qualitatively different outcomes (functional SAC vs. dysfunctional SAC) for different cells we assume that APC/C:Slp1 needs to reach a threshold for anaphase to occur.
The synthesis rate of Slp1($k_{syn(Slp1)}$) as well as $[inh_T]$ in the different strains are assumed to be log-normally distributed with parameters μ and σ. This yields in total 19 parameters that we constrained to the following ranges:

- CV of $k_{syn(Slp1)}$ between 0.05 and 0.5
- lower bound of mean of $k_{syn(Slp1)}$: 0.17 mol/min; calculated from 20 nM Slp1 after 120 min (see (D1d) and (D1e)), assuming no degradation
- upper bound of mean of $k_{syn(Slp1)}$: 1.98 mol/min calculated via 20 nM Slp1 after 120 min assuming maximum degradation rate
- degradation rates should result in a Slp1 half-life between 7 and 40 min (see (D1b))

- 1e-5 $nM^{-1}min^{-1} < k_{on} <$ 1e5 $nM^{-1}min^{-1}$
- 1e-5 nM $< K_d = k_{off}/k_{on} <$ 1e5 nM
- 1 nM $< [inh_T] <$ 50 nM (Supplementary Table S2) with corresponding CV between 0.05 and 0.5
- APC/C:Slp1 threshold for anaphase onset between 0.1 and 20 nM

Parameter boundaries for estimation:

	$\sigma_{k\_syn(Slp1)}$	$\mu_{k\_syn(Slp1)}$	σ_{inhT}	μ_{inhT}	$k_{deg(Slp1)}$
min	0.04997	-1.793	0.04997	-0.1116	0.01733 min^{-1}
max	0.47238	0.5717	0.47238	3.9108	0.09902 min^{-1}

Optimization using the sigma-point method (D4) yields the following maximum likelihood estimate for the model parameters:

$\sigma_{k,syn(Slp1)}$	$\mu_{k,syn(Slp1)}$	$k_{deg(Slp1)}$	$[APC_T]$	threshold
0.3446	-1.0654	0.0616 min^{-1}	19.2690 nM	1.0147 nM

$k_{on(Slp1:inh)}$	$K_{d(Slp1:inh)}$	$k_{on(APC:MCC)}$	$K_{d(APC:MCC)}$	$k_{on(APC:Slp1)}$	$K_{d(APC:Slp1)}$
1.4225e03 nM^{-1} min^{-1}	22.7780e-04 nM	1.9263 nM^{-1} min^{-1}	2.5582 nM	4.0955 nM^{-1} min^{-1}	0.2560 nM

$[inh_T]$	wild type	30 % Mad1	65 % Mad2	30 % Mad3
μ	3.2600	2.6577	1.9059	2.1000
σ	0.0922	0.0845	0.3854	0.2087

Based on these parameters the mean of the total inhibitor concentrations and of the synthesis rate $k_{syn(Slp1)}$ can be calculated as well as the respective CVs.

	wild type $[inh_T]$	30 % Mad1 $[inh_T]$	65 % Mad2 $[inh_T]$	30 % Mad3 $[inh_T]$	$k_{syn(Slp1)}$
Mean	26.1606 nM	14.3145 nM	7.2440 nM	8.3459 nM	0.3684 nM min^{-1}
CV	0.0924	0.0847	0.4002	0.2110	0.3551

For the maximum likelihood estimate we assess, as before, the fit of M2. The corresponding illustration is depicted below. As for M1, we find that M2 can describe the main characteristics of the process while satisfying our requirement to be robust with respect to the threshold for anaphase activation.

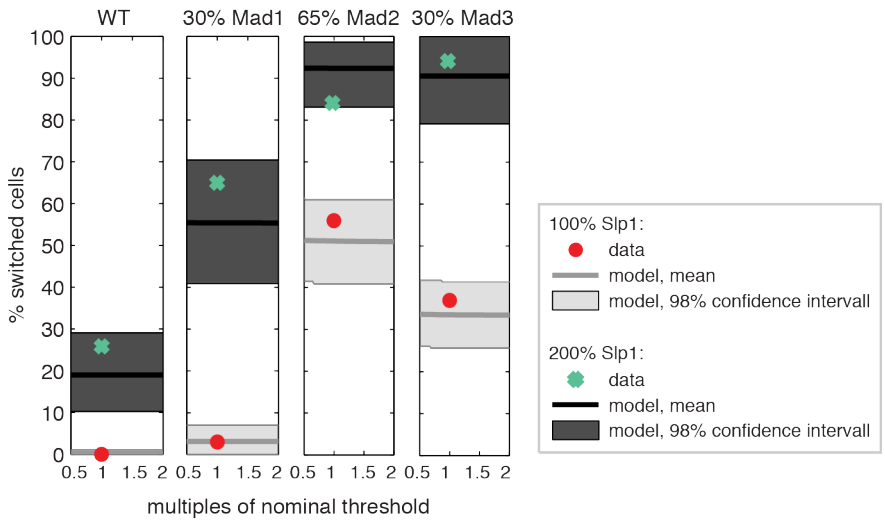

While the fits of the experimentally observed fractions of population A and B are similar for M1 and M2, the dynamics of the underlying pathways are quite different. This becomes apparent from exemplary trajectories of model M2 simulated with the maximum likelihood estimate. While M1 showed a long tail towards high concentrations of the active species ([Slp1]), which is a result of ultrasensitivity, M2 shows a bimodal distribution of the concentration of the active species ([APC:Slp1]). Individual cells either have [APC:Slp1] close to zero or have high [APC:Slp1] as depicted in the plot below and in Fig. 8e.

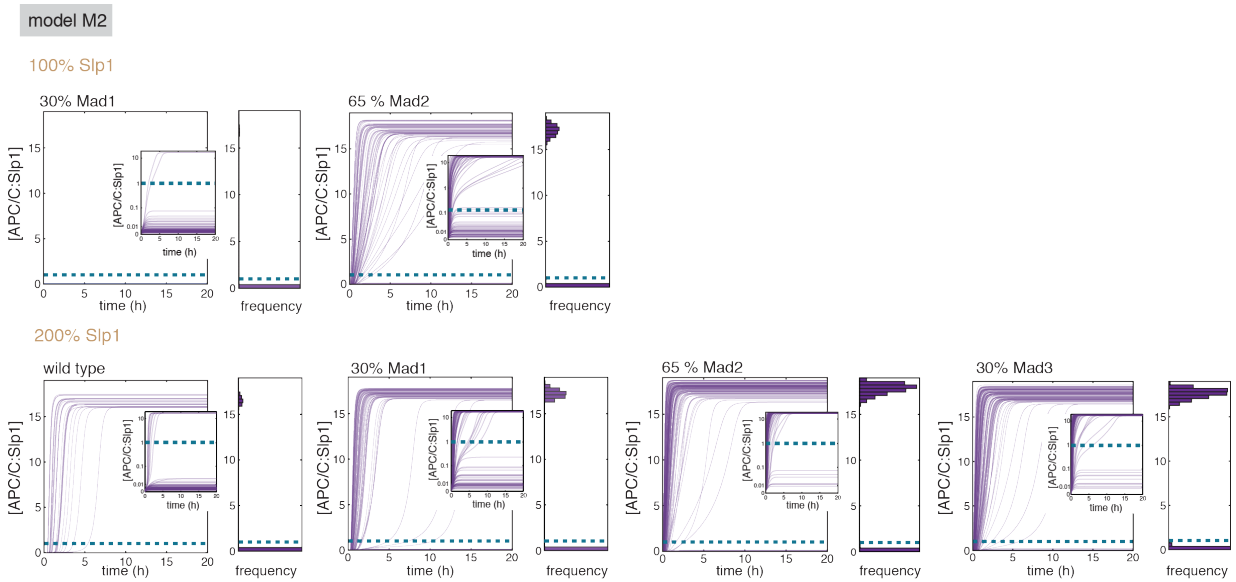

To analyse whether inhibitor concentration or Slp1 synthesis rate in populations A and B could be distinguished experimentally, we evaluated the parameter distributions corresponding to the individual populations. For [APC:Slp1] trajectories that exceeded or that remained below the threshold, we collected the inhibitor concentrations and the Slp1 synthesis rates and computed the corresponding frequency distributions. Shown in Fig. 8c are the histograms for a strain with 30 % Mad3 and 100 % Slp1. We find that the distributions of inhibitor concentrations differ only slightly between population A and B for most strains. The Slp1 synthesis rate allows for a better discrimination but this rate cannot be measured experimentally.

(D9) Bifurcation analysis for model M2

To understand the cause of the bimodality and the resulting robustness to threshold alterations we performed a bifurcation analysis using the maximum likelihood parameters and the estimated mean inhibitor concentration in WT cells. The resulting bifurcation diagram is shown below and revealed that: (1) For low $k_{syn(Slp1)}$, model M2 possesses a globally asymptotic stable steady state with low [APC:Slp1], corresponding to a functional SAC. (2) For high $k_{syn(Slp1)}$, there exists a globally asymptotic stable steady state with high [APC:Slp1] above the threshold, corresponding to a dysfunctional checkpoint. (3) For intermediate values of $k_{syn(Slp1)}$, M2 possesses three steady states of which two are stable and correspond to a functional and a dysfunctional SAC, respectively. This multi-stability allows for a threshold behaviour with respect to $k_{syn(Slp1)}$, meaning that below a certain Slp1 synthesis the SAC is functional, while above the threshold the SAC is deficient. For the maximum likelihood estimates of the parameters and the mean wild type inhibitor concentration, the critical Slp1 synthesis rate is 0.943 nM/min. Furthermore, the multi-stability and the switch-like change allow for robustness with respect to the threshold as lower and upper steady state are separated.

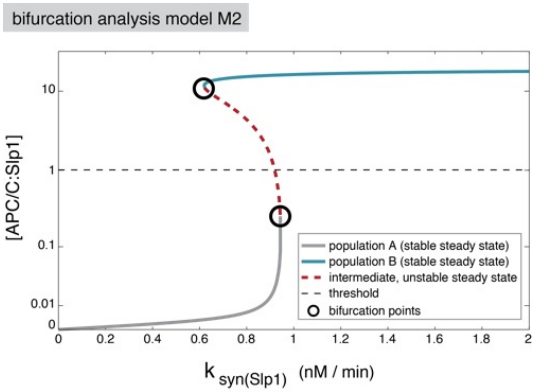

(E) References

1. Newman, J.R. *et al.* Single-cell proteomic analysis of S. cerevisiae reveals the architecture of biological noise. *Nature* **441**, 840-846 (2006).
2. Bar-Even, A. *et al.* Noise in protein expression scales with natural protein abundance. *Nature genetics* **38**, 636-643 (2006).
3. Wu, J.Q. & Pollard, T.D. Counting cytokinesis proteins globally and locally in fission yeast. *Science* **310**, 310-314 (2005).
4. Swain, P.S., Elowitz, M.B. & Siggia, E.D. Intrinsic and extrinsic contributions to stochasticity in gene expression. *Proc Natl Acad Sci U S A* **99**, 12795-12800 (2002).
5. Huh, D. & Paulsson, J. Non-genetic heterogeneity from stochastic partitioning at cell division. *Nature genetics* **43**, 95-100 (2011).
6. Gillespie, D.T. Exact Stochastic Simulation of Coupled Chemical-Reactions. *J Phys Chem-Us* **81**, 2340-2361 (1977).
7. Forsburg, S.L. & Nurse, P. Cell cycle regulation in the yeasts Saccharomyces cerevisiae and Schizosaccharomyces pombe. *Annual review of cell biology* **7**, 227-256 (1991).
8. Sveiczer, A., Novak, B. & Mitchison, J.M. The size control of fission yeast revisited. *J Cell Sci* **109 (Pt 12)**, 2947-2957 (1996).
9. Neumann, F.R. & Nurse, P. Nuclear size control in fission yeast. *J Cell Biol* **179**, 593-600 (2007).
10. Amorim, M.J., Cotobal, C., Duncan, C. & Mata, J. Global coordination of transcriptional control and mRNA decay during cellular differentiation. *Molecular systems biology* **6**, 380 (2010).
11. Sun, M. *et al.* Comparative dynamic transcriptome analysis (cDTA) reveals mutual feedback between mRNA synthesis and degradation. *Genome research* **22**, 1350-1359 (2012).
12. Sczaniecka, M. *et al.* The spindle checkpoint functions of Mad3 and Mad2 depend on a Mad3 KEN box-mediated interaction with Cdc20-anaphase-promoting complex (APC/C). *The Journal of biological chemistry* **283**, 23039-23047 (2008).
13. Marguerat, S. *et al.* Quantitative analysis of fission yeast transcriptomes and proteomes in proliferating and quiescent cells. *Cell* **151**, 671-683 (2012).
14. Holstege, F.C. *et al.* Dissecting the regulatory circuitry of a eukaryotic genome. *Cell* **95**, 717-728 (1998).
15. Kar, S., Baumann, W.T., Paul, M.R. & Tyson, J.J. Exploring the roles of noise in the eukaryotic cell cycle. *Proc Natl Acad Sci U S A* **106**, 6471-6476 (2009).
16. Zenklusen, D., Larson, D.R. & Singer, R.H. Single-RNA counting reveals alternative modes of gene expression in yeast. *Nature structural & molecular biology* **15**, 1263-1271 (2008).
17. Chen, R.H., Brady, D.M., Smith, D., Murray, A.W. & Hardwick, K.G. The spindle checkpoint of budding yeast depends on a tight complex between the Mad1 and Mad2 proteins. *Mol Biol Cell* **10**, 2607-2618 (1999).
18. Ikui, A.E., Furuya, K., Yanagida, M. & Matsumoto, T. Control of localization of a spindle checkpoint protein, Mad2, in fission yeast. *J Cell Sci* **115**, 1603-1610 (2002).
19. Sironi, L. *et al.* Mad2 binding to Mad1 and Cdc20, rather than oligomerization, is required for the spindle checkpoint. *Embo J* **20**, 6371-6382 (2001).
20. Vink, M. *et al.* In vitro FRAP identifies the minimal requirements for Mad2 kinetochore dynamics. *Curr Biol* **16**, 755-766 (2006).
21. Shah, J.V. *et al.* Dynamics of centromere and kinetochore proteins; implications for checkpoint signaling and silencing. *Curr Biol* **14**, 942-952 (2004).
22. Lee, S.H., Sterling, H., Burlingame, A. & McCormick, F. Tpr directly binds to Mad1 and Mad2 and is important for the Mad1-Mad2-mediated mitotic spindle checkpoint. *Genes Dev* **22**, 2926-2931 (2008).

23. Kass, R.E. & Raftery, A.E. Bayes Factors. *J Am Stat Assoc* **90**, 773-795 (1995).
24. Yamada, H.Y., Matsumoto, S. & Matsumoto, T. High dosage expression of a zinc finger protein, Grt1, suppresses a mutant of fission yeast slp1(+), a homolog of CDC20/p55CDC/Fizzy. *J Cell Sci* **113 (Pt 22)**, 3989-3999 (2000).
25. Fang, G. Checkpoint protein BubR1 acts synergistically with Mad2 to inhibit anaphase-promoting complex. *Mol Biol Cell* **13**, 755-766 (2002).
26. Burton, J.L. & Solomon, M.J. Mad3p, a pseudosubstrate inhibitor of APCCdc20 in the spindle assembly checkpoint. *Gene Dev* **21**, 655-667 (2007).
27. Chao, W.C., Kulkarni, K., Zhang, Z., Kong, E.H. & Barford, D. Structure of the mitotic checkpoint complex. *Nature* **484**, 208-213 (2012).
28. Schwanhausser, B. *et al.* Global quantification of mammalian gene expression control. *Nature* **473**, 337-342 (2011).
29. Herzog, F. *et al.* Structure of the anaphase-promoting complex/cyclosome interacting with a mitotic checkpoint complex. *Science* **323**, 1477-1481 (2009).
30. Sudakin, V., Chan, G.K. & Yen, T.J. Checkpoint inhibition of the APC/C in HeLa cells is mediated by a complex of BUBR1, BUB3, CDC20, and MAD2. *J Cell Biol* **154**, 925-936 (2001).
31. Fang, G., Yu, H. & Kirschner, M.W. Direct binding of CDC20 protein family members activates the anaphase-promoting complex in mitosis and G1. *Molecular cell* **2**, 163-171 (1998).
32. Kramer, E.R., Gieffers, C., Holzl, G., Hengstschlager, M. & Peters, J.M. Activation of the human anaphase-promoting complex by proteins of the CDC20/Fizzy family. *Curr Biol* **8**, 1207-1210 (1998).
33. Pan, J. & Chen, R.H. Spindle checkpoint regulates Cdc20p stability in Saccharomyces cerevisiae. *Genes Dev* **18**, 1439-1451 (2004).
34. Reddy, S.K., Rape, M., Margansky, W.A. & Kirschner, M.W. Ubiquitination by the anaphase-promoting complex drives spindle checkpoint inactivation. *Nature* **446**, 921-925 (2007).
35. Nilsson, J., Yekezare, M., Minshull, J. & Pines, J. The APC/C maintains the spindle assembly checkpoint by targeting Cdc20 for destruction. *Nat Cell Biol* **10**, 1411-1420 (2008).
36. Mansfeld, J., Collin, P., Collins, M.O., Choudhary, J.S. & Pines, J. APC15 drives the turnover of MCC-CDC20 to make the spindle assembly checkpoint responsive to kinetochore attachment. *Nat Cell Biol* **13**, 1234-1243 (2011).
37. Ma, H.T. & Poon, R.Y. Orderly inactivation of the key checkpoint protein mitotic arrest deficient 2 (MAD2) during mitotic progression. *J Biol Chem* **286**, 13052-13059 (2011).
38. Ge, S., Skaar, J.R. & Pagano, M. APC/C- and Mad2-mediated degradation of Cdc20 during spindle checkpoint activation. *Cell Cycle* **8**, 167-171 (2009).
39. Foster, S.A. & Morgan, D.O. The APC/C subunit Mnd2/Apc15 promotes Cdc20 autoubiquitination and spindle assembly checkpoint inactivation. *Molecular cell* **47**, 921-932 (2012).
40. Uzunova, K. *et al.* APC15 mediates CDC20 autoubiquitylation by APC/C(MCC) and disassembly of the mitotic checkpoint complex. *Nature structural & molecular biology* **19**, 1116-1123 (2012).
41. Foe, I.T. *et al.* Ubiquitination of Cdc20 by the APC occurs through an intramolecular mechanism. *Curr Biol* **21**, 1870-1877 (2011).
42. Doncic, A., Ben-Jacob, E. & Barkai, N. Evaluating putative mechanisms of the mitotic spindle checkpoint. *Proc Natl Acad Sci U S A* **102**, 6332-6337 (2005).
43. Doncic, A., Ben-Jacob, E. & Barkai, N. Noise resistance in the spindle assembly checkpoint. *Molecular systems biology* **2**, 2006 0027 (2006).
44. Mistry, H.B., MacCallum, D.E., Jackson, R.C., Chaplain, M.A. & Davidson, F.A. Modeling the temporal evolution of the spindle assembly checkpoint and role of Aurora B kinase. *Proc Natl Acad Sci U S A* **105**, 20215-20220 (2008).

45. Wolthuis, R. *et al.* Cdc20 and Cks direct the spindle checkpoint-independent destruction of cyclin A. *Molecular cell* **30**, 290-302 (2008).
46. Malureanu, L. *et al.* Cdc20 hypomorphic mice fail to counteract de novo synthesis of cyclin B1 in mitosis. *J Cell Biol* **191**, 313-329 (2010).
47. Zechner, C. *et al.* Moment-based inference predicts bimodality in transient gene expression. *Proc Natl Acad Sci U S A* **109**, 8340-8345 (2012).
48. Julier, S. & Uhlmann, J.K. New extension of the Kalman filter to nonlinear systems. *Proc. SPIE 3068, Signal Processing, Sensor Fusion, and Target Recognition VI* **182** (1997).
49. Parks, D.R., Roederer, M. & Moore, W.A. A new "Logicle" display method avoids deceptive effects of logarithmic scaling for low signals and compensated data. *Cytometry. Part A : the journal of the International Society for Analytical Cytology* **69**, 541-551 (2006).
50. Buchler, N.E. & Louis, M. Molecular titration and ultrasensitivity in regulatory networks. *J Mol Biol* **384**, 1106-1119 (2008).

2.4 Slow checkpoint activation kinetics as a safety device in anaphase

Julia Kamenz[1,*] and Silke Hauf[1,2,3*]

[1]*Friedrich Miescher Laboratory of the Max Planck Society, 72070 Tübingen, Germany*

[2]*Department of Biological Sciences and* [3]*Virginia Bioinformatics Institute, Virginia Tech, Blacksburg, VA 24061, USA*

*Correspondence: julia.kamenz@tuebingen.mpg.de, silke.hauf@vt.edu

Published in **Current Biology**, Volume 24, Issue 6, 17 March 2014, Pages 646-651
DOI: 10.1016/j.cub.2014.02.005

Author contributions:

I conceived the study together with Silke Hauf and designed, performed and analysed all experiments. Additionally, I contributed to writing the manuscript.

Silke Hauf supervised the study and contributed to writing the manuscript.

Please cite this article in press as: Kamenz and Hauf, Slow Checkpoint Activation Kinetics as a Safety Device in Anaphase, Current Biology (2014), http://dx.doi.org/10.1016/j.cub.2014.02.005

Current Biology 24, 1–6, March 17, 2014 ©2014 Elsevier Ltd All rights reserved http://dx.doi.org/10.1016/j.cub.2014.02.005

Report

Slow Checkpoint Activation Kinetics as a Safety Device in Anaphase

Julia Kamenz[1,*] and Silke Hauf[1,2,3,*]
[1]Friedrich Miescher Laboratory of the Max Planck Society, 72076 Tübingen, Germany
[2]Department of Biological Sciences, Virginia Tech, Blacksburg, VA 24061, USA
[3]Virginia Bioinformatics Institute, Virginia Tech, Blacksburg, VA 24061, USA

Summary

Chromosome attachment to the mitotic spindle in early mitosis is guarded by an Aurora B kinase-dependent error correction mechanism [1, 2] and by the spindle assembly checkpoint (SAC), which delays cell-cycle progression in response to errors in chromosome attachment [3, 4]. The abrupt loss of sister chromatid cohesion at anaphase creates a type of chromosome attachment that in early mitosis would be recognized as erroneous, would elicit Aurora B-dependent destabilization of kinetochore-microtubule attachment, and would activate the checkpoint [5, 6]. However, in anaphase, none of these responses occurs, which is vital to ensure progression through anaphase and faithful chromosome segregation. The difference has been attributed to the drop in CDK1/cyclin B activity that accompanies anaphase and causes Aurora B translocation away from centromeres [7–12] and to the inactivation of the checkpoint by the time of anaphase [10, 11, 13, 14]. Here, we show that checkpoint inactivation may not be crucial because checkpoint activation by anaphase chromosomes is too slow to take effect on the timescale during which anaphase is executed. In addition, we observe that checkpoint activation can still occur for a considerable time after the anaphase-promoting complex/cyclosome (APC/C) becomes active, raising the question whether the checkpoint is indeed completely inactivated by the time of anaphase under physiologic conditions.

Results and Discussion

Relocalization of Checkpoint Proteins to Kinetochores in Anaphase Does Not Prevent Degradation of APC/C Substrates

In several organisms, artificial maintenance of high cyclin B levels in anaphase results in recruitment of spindle assembly checkpoint proteins to kinetochores when sister chromatids split [7, 10, 12]. Yet, whether this kinetochore recruitment indeed creates a signal sufficient to inhibit the anaphase-promoting complex/cyclosome (APC/C) has remained unclear, and the observation that APC/C substrates are degraded in this situation suggests that it may not [15]. To systematically test this, we expressed physiologic amounts of nondegradable cyclin B (ΔN-Cdc13) in fission yeast (*S. pombe*) mitosis (Figure S1A available online). As expected [16], sister chromatids separated in anaphase but cells maintained short metaphase-like spindles (pseudometaphase; Figure S1B). The Aurora B kinase (*S.p.* Ark1) was retained on centromeres (Figure 1A), and the Polo kinase Plo1 was retained on spindle pole bodies (Figures S1B and S1C), indicating that CDK1 activity remained high [17, 18]. As had been observed in other cell types [7, 12, 15], kinetochore attachment became unstable, and centromeres frequently detached from the spindle poles (Figures S1B and S1D). Consistent with the destabilization of kinetochore attachment, the checkpoint proteins Mad1, Mad2, Mad3, and Bub3 localized to kinetochores of pseudometaphase cells (Figures 1A and 1B). Rebinding of Mad3 was almost immediate with anaphase onset and occurred even before detachment of kinetochores from the spindle poles was observed (Figures 1B, 1C, S1D, and S1F). However, the accumulation of checkpoint proteins did not appear to inhibit the APC/C, since degradation of the APC/C substrates cyclin B (*S.p.* Cdc13; Figure 1D) and securin (Figures 1D and 1E) continued unhindered. This suggested that the checkpoint does not detectably block APC/C activity when cyclin B is maintained, although checkpoint proteins enrich at kinetochores.

The MCC Forms in Anaphase when Nondegradable Cyclin B Is Present

To determine at which step checkpoint signaling may be blocked, we analyzed the formation of the mitotic checkpoint complex (MCC). The MCC is the ultimate inhibitor formed by the spindle assembly checkpoint [3] and consists of the APC/C activator Cdc20 (*S.p.* Slp1) and the checkpoint proteins Mad2 and Mad3. We synchronized cells expressing nondegradable cyclin B at the G2/M transition and immunoprecipitated the APC/C subunit Lid1 (Apc4) from cells in metaphase (20 min after release) or in pseudometaphase (28 min after release) (Figures 2A, S2A, and S2B). In pseudometaphase, but not in metaphase, Mad2 was clearly associated with APC/C and Slp1, indicative of MCC formation. In contrast, in the absence of nondegradable cyclin B, Mad2 did not accumulate on the APC/C during anaphase. The amount of MCC formed in pseudometaphase seemed substantial, as we coimmunoprecipitated less Slp1 and Mad2 from a culture where the checkpoint was engaged by treatment with the microtubule-destabilizing drug MBC (Figures S2C and S2D). Hence, MCC formation does take place when cyclin B levels remain high, but seems unable to prevent degradation of APC/C substrates.

Separase Activity Is Insufficient to Inactivate the Spindle Assembly Checkpoint

Separase overexpression overrides a mitotic checkpoint arrest in budding yeast [10, 13]. Because anaphase coincides with separase activation, we reasoned that separase might block a late step in checkpoint activity. To test this hypothesis, we conditionally overexpressed separase. In this situation, separase is not reliably inhibited by securin, and sister chromatids split almost instantaneously when cells enter mitosis (Figure 2B). Cohesin mutations that induce a similar precocious loss of cohesion cause a checkpoint-dependent delay in mitosis [19, 20]. If separase activity was sufficient to block checkpoint signaling, separase-mediated cohesion loss should not delay cells in mitosis [10]. However, we

*Correspondence: julia.kamenz@tuebingen.mpg.de (J.K.), silke.hauf@vt.edu (S.H.)

Please cite this article in press as: Kamenz and Hauf, Slow Checkpoint Activation Kinetics as a Safety Device in Anaphase, Current Biology (2014), http://dx.doi.org/10.1016/j.cub.2014.02.005

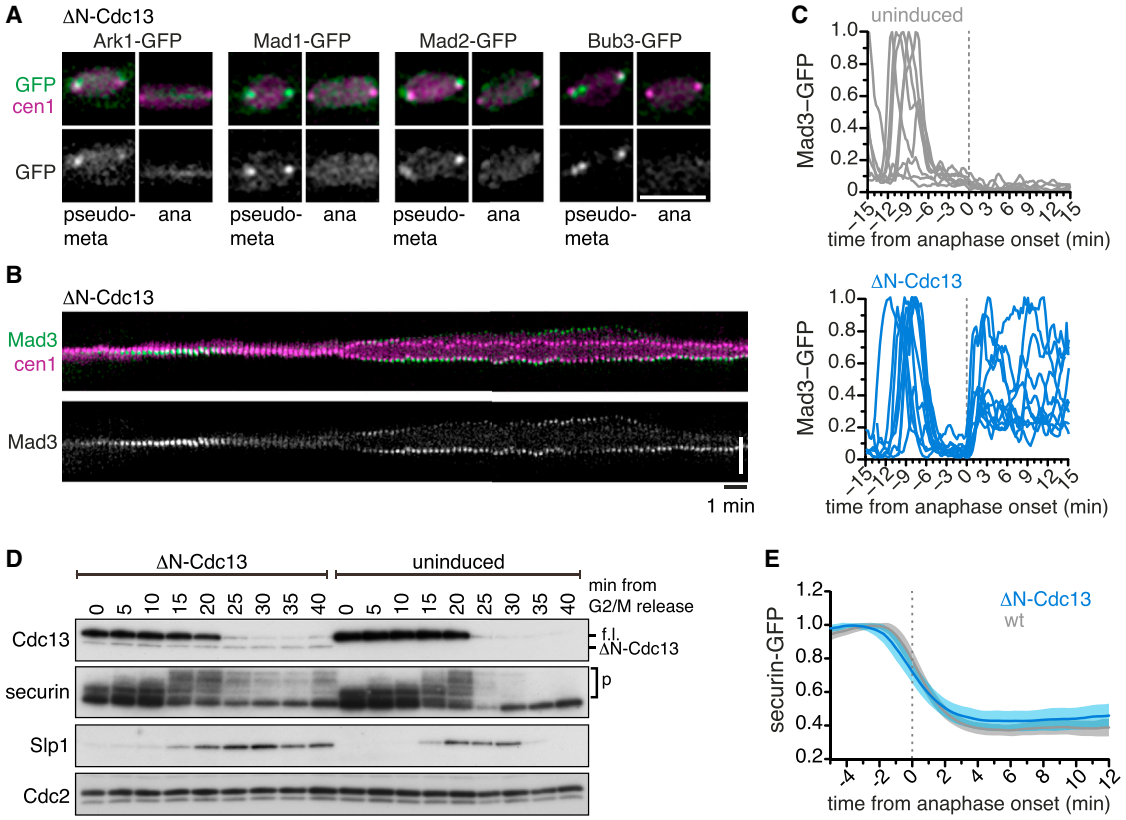

Figure 1. Securin and Cyclin B Are Degraded in Pseudometaphase Despite Fast Reaccumulation of Checkpoint Proteins at Kinetochores

(A and B) Expression of nondegradable cyclin B (ΔN-Cdc13) was induced in cells expressing the indicated proteins fused to GFP and a marker for the centromere of chromosome I (cen1). Mitotic progression was followed by live-cell imaging. Representative nuclei of cells 2 min after sister chromatid separation are shown in (A) (scale bar, 4 μm). Only cells exhibiting a pseudometaphase phenotype show localization of checkpoint components after anaphase onset. A representative kymograph of a cell expressing *mad3*$^{+}$*-GFP* and exhibiting a pseudometaphase phenotype is shown in (B) (vertical scale bar, 5 μm; see Figure S1E for comparison to the wild-type). Localized Mad3-GFP signal decreases in metaphase but reaccumulates quickly after anaphase when ΔN-Cdc13 is present (timing quantified in Figure S1F).

(C) Quantification of the experiment shown in (B). The maximal cellular Mad3-GFP signal was determined in individual cells, either without induction of ΔN-Cdc13 (gray, n = 8) or with induction of ΔN-Cdc13 and pseudometaphase phenotype (blue, n = 11). Individual time courses were aligned to the point of sister chromatid separation.

(D) *Cdc25-22* cells with or without induction of ΔN-Cdc13 were synchronized at the G2/M transition. Samples taken at the indicated time points were analyzed by immunoblotting using anti-Cdc13, anti-Cut2 (securin; antibody characterization in Figure S1G), anti-Slp1 and anti-Cdc2 (Cdk1, loading control) antibodies. p indicates mitotic phosphorylation of securin, f.l. marks the endogenous cyclin B, and ΔN-Cdc13 the shorter nondegradable version of Cdc13. Slp1 (*S.p.* ortholog of Cdc20) is stabilized as a result of the expression of ΔN-Cdc13. Endogenous Cdc13 accumulates in a *cdc25-22* arrest, so that in this experiment there is less ΔN-Cdc13 than f.l. Cdc13. See Figure S1A for a comparison in unsynchronized cells. Quantification of the cell-cycle stages is shown in Figures S1H and S1I.

(E) The abundance of securin-GFP was followed by live-cell imaging in wild-type cells (gray, n = 31) or in cells displaying a pseudometaphase phenotype after induction of ΔN-Cdc13 (blue, n = 22). The cen1 marker was used to determine the onset of anaphase and individual time courses were aligned to this point. Shown is the average (line) ±SD (filled area).

See also Figure S1.

observed a mitotic delay in separase-overexpressing cells, which furthermore was checkpoint dependent as deletion of the checkpoint gene *mad2*$^{+}$ abolished the delay (Figures 2B and 2C). Hence, we conclude that separase activity does not inactivate the spindle assembly checkpoint in fission yeast.

Checkpoint Reactivation in Anaphase Is Slow Relative to the Timing of Securin Degradation

The MCC formation in cells undergoing anaphase in the presence of nondegradable cyclin B (Figure 2A) suggested that checkpoint reactivation is not completely blocked, but that either the APC/C had become refractory to inhibition or that checkpoint reactivation is too slow to manifest in a block of securin degradation, i.e., the block in APC/C activity would only occur at a time when securin is completely degraded. To test the latter idea, we gave cells more time between the onset of anaphase and the completion of securin degradation. We overexpressed securin to about eight times its wild-type level (Figure S3A). This increased the total time of securin degradation from 5.5 min to 8.2 min (Figures 1E and 3A). However, the time between anaphase and complete securin degradation was still similar to wild-type cells (~3.7 min; Figures S3B and S3D). We therefore shifted the time of anaphase by co-overexpressing separase. As a result, anaphase occurred soon after the start of securin degradation and the time between the onset of anaphase and complete securin degradation was prolonged (7.6 min on average; Figures S3B and S3D). Interestingly, if we additionally stabilized cyclin B, securin degradation was halted before complete degradation (Figures 3A–3C). This depended on checkpoint

Please cite this article in press as: Kamenz and Hauf, Slow Checkpoint Activation Kinetics as a Safety Device in Anaphase, Current Biology (2014), http://dx.doi.org/10.1016/j.cub.2014.02.005

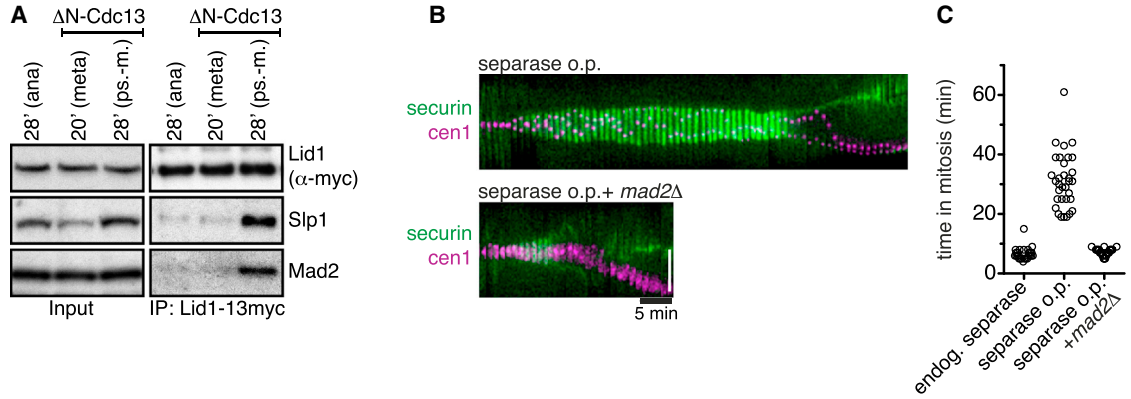

Figure 2. Expression of Nondegradable Cyclin B Results in Formation of the Mitotic Checkpoint Complex in Pseudometaphase

(A) *Cdc25-22* cells with or without induction of ΔN-Cdc13 were synchronized at the G2/M transition. Cells were harvested at the indicated time points after release, and the APC/C subunit Lid1 was immunoprecipitated and analyzed for coimmunoprecipitation of the MCC components Slp1 and Mad2 by immunoblotting. Quantification of the cell-cycle stages is shown in Figures S2A and S2B.

(B) Overexpression of separase was induced in cells carrying securin-GFP and a centromeric marker for chromosome I (cen1) in the presence or absence of the checkpoint protein Mad2. Mitotic progression was followed by live-cell imaging. Representative kymographs are shown (vertical scale bar, 5 μm).

(C) Quantification of the experiment in (B). The time in mitosis was determined by the presence of spindle-associated securin-GFP.

See also Figure S2.

activity, since deletion of the checkpoint gene *mad2*$^{+}$ allowed securin degradation to run to completion (Figures 3A–3C). Hence, the checkpoint indeed reactivates at anaphase if cyclin B is stabilized, but is slow in inhibiting the APC/C: it took between 3.5 min and 16 min (average 6.5 min) from anaphase to the stabilization of securin (Figure 3D). In cells solely expressing nondegradable cyclin B, which we had monitored earlier (Figure 1E), the time from anaphase to completion of securin degradation was only 1.5 min to 4.8 min (Figure S3D). Hence, securin degradation was completed or almost completed by the time the APC/C became inhibited, which explains our failure to observe securin stabilization in this background.

Since the time from anaphase onset to checkpoint protein recruitment was short (Figures 1B and 1C), this indicated that the time from checkpoint protein recruitment to APC/C inhibition is long. To test this directly, we monitored Mad2-mCherry signals in securin- and separase-overexpressing cells and related their kinetochore reoccurrence to the stabilization of securin (Figures 3E and 3F). As we had seen before, Mad2 enriched at kinetochores very soon after anaphase (0 to 60 s with an average of 30 s; see Figure 3E for an example), whereas it took 2.7 to 6 min (average 4.3 min) from the first enrichment of Mad2 until securin degradation was halted (Figure 3F). Hence, if anaphase occurs in the presence of nondegradable cyclin B, checkpoint protein rerecruitment to kinetochores is fast but APC/C inhibition is slow.

Checkpoint Reactivation Can Occur Once Cyclin B Degradation Has Started

Our results suggested that—although stabilization of cyclin B levels allows reactivation of the checkpoint in anaphase—reactivation is too slow to take effect before securin is degraded. It had previously been proposed that the checkpoint is completely inactivated by the time of anaphase [6, 14]. We therefore asked whether checkpoint activation became impossible or at least more inefficient when we allowed cyclin B levels to drop. To study this systematically, we turned to cells containing the kinesin-5 mutation *cut7-446* [21] and slightly impaired kinesin function by incubating at semipermissive temperature. We reasoned that this would cause spindle instability and frequent destabilization of chromosome attachments. Indeed, in some cells, we observed securin stabilization after the start of securin degradation (Figure 4). This stabilization appeared to be related to checkpoint signaling, because in the minutes preceding stabilization, strong Mad2 signals were observed, whereas in the minutes preceding securin degradation (either initially or when restarting), Mad2 signals were low (Figure 4C). This corroborates observations by the Pines and Gerlich groups, who showed that the checkpoint can still be activated after the APC/C has become active [22, 23]. Interestingly, the time between observing Mad2 signals and stabilization of securin levels was between 3 and 7 min (average 5.2 min), which is similar to the timing that we observed in cells with stabilized cyclin B (between 2.7 and 6 min; Figure 3F). When we plotted these values relative to the time that had elapsed since securin degradation started (Figure 4D), there was no obvious prolongation in the time needed for APC/C inhibition. This suggests that cyclin B degradation does not drastically alter the kinetics of checkpoint signaling, at least for about 2 min after the APC/C has become active. Because it takes around 2 min from the onset of securin degradation to anaphase in wild-type cells (Figure 1E), this raises the possibility that checkpoint signaling is still operational at anaphase. It should be noted that there is copious evidence that the checkpoint is inactivated at some point during mitotic exit, either through degradation of checkpoint proteins [14, 24–26] or through loss of CDK1-dependent phosphorylations [27–30]. However, when with respect to anaphase these mechanisms inactivate the checkpoint is largely unclear. Work from the Petronczki group indicates that recruitment of the checkpoint proteins Mad1 and Mad2 to kinetochores may be impaired by the time of anaphase in human cells [11].

Slow Checkpoint Activation May Protect Anaphase While Cyclin B Levels Are Still High

Our data suggest that the checkpoint remains operational at anaphase. Yet, in an unperturbed anaphase, rerecruitment of

Please cite this article in press as: Kamenz and Hauf, Slow Checkpoint Activation Kinetics as a Safety Device in Anaphase, Current Biology (2014), http://dx.doi.org/10.1016/j.cub.2014.02.005

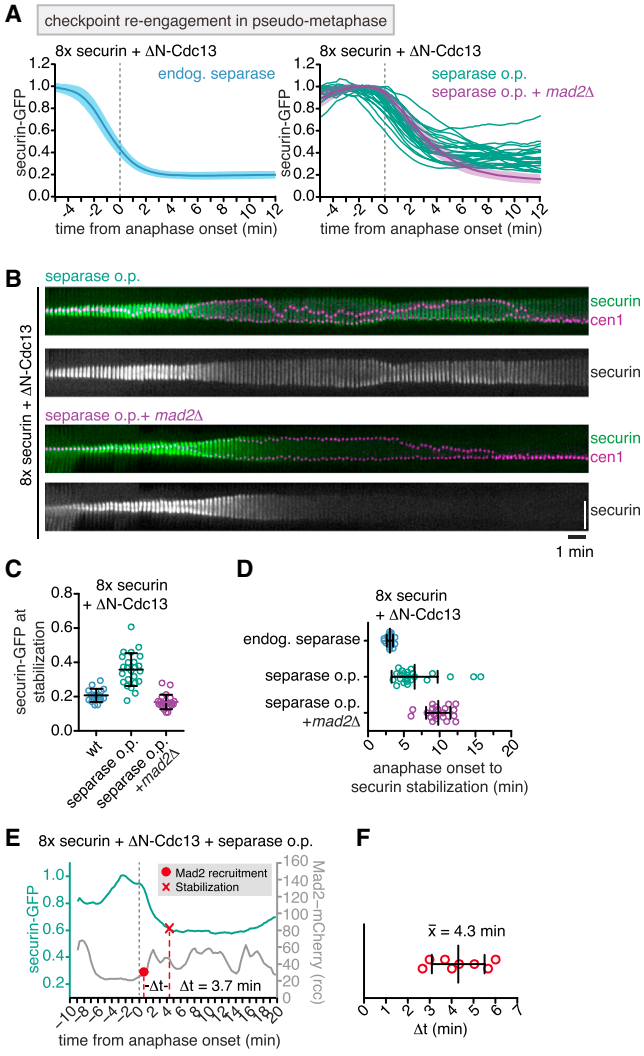

Figure 3. Checkpoint Re-engagement in Pseudometaphase Can Be Observed when the Time Period of Securin Degradation Is Prolonged

(A) Degradation kinetics of securin-GFP were assayed as in Figure 1E. In addition to nondegradable cyclin B (ΔN-Cdc13), cells overexpressed securin-GFP to about 8-fold (Figure S3A) (left, blue; n = 17), overexpressed securin-GFP and separase (right, green; n = 24), or overexpressed securin-GFP and separase and had *mad2* deleted (right, aubergine; n = 22). Given is the average (line) ±SD (filled area), except when single-cell data are shown (green).

(B) Representative kymographs of mitotic cells expressing ΔN-Cdc13 and overexpressing securin-GFP and separase with or without *mad2* deletion (vertical scale bar, 5 μm).

(C and D) Securin-GFP intensity at the time point of reflattening of the securin degradation curve ("securin stabilization") (C) and time between anaphase onset and securin stabilization (D) for the experiment shown in (A). Measurements from single cells (colored) with mean and SD (black lines) are shown.

(E) Representative curve showing checkpoint re-engagement from a cell expressing *mad2+-mCherry* in addition to nondegradable cyclin B and overexpression of securin-GFP and separase. For each time point, the normalized nuclear securin-GFP intensity (green) and the maximal cellular Mad2-mCherry signal in raw camera counts (rcc) (gray) is shown. Δt denotes the time difference between the start of Mad2-mCherry signal increase (red circle) and stabilization of securin-GFP (red cross).

(F) Time difference between start of Mad2-mCherry signal increase and stabilization of securin-GFP (Δt) as shown in (E). Single-cell measurements (red) with mean and SD (black lines) are shown.

See also Figure S3.

checkpoint proteins to kinetochores is typically not observed (Figures 1A, 1C, and S1E). This indicates that chromosome attachments remain stable, providing no possibility for the checkpoint to become engaged. This also indicates that persistent chromosome attachment is the primary mechanism that ensures unperturbed anaphase progression. Slow checkpoint activation (as we describe here) or an inability to activate the checkpoint in anaphase [11] will only become functionally important when the primary mechanism fails. This prompted us to ask how likely this is. Stability of chromosome attachment is thought to be regulated by centromere-localized Aurora B [2, 10, 11]. We therefore wanted to know when with respect to anaphase Aurora B translocates from the centromere to the midspindle and how variable this process is. Surprisingly, there was considerable variability and we found Aurora B on centromeres for up to 2 min after anaphase onset (Figures S4A and S4B), consistent with findings in vertebrate cells [31]. Hence, attachment remains stable despite the presence of Aurora B on centromeres, strengthening previous hints that an additional mechanism supports chromosome attachment stability in anaphase [11].

Like Aurora B translocation [8, 9], this other mechanism seems to require declining CDK1/cyclin B activity, because maintaining high cyclin B levels creates unstable chromosome attachments in anaphase (Figures S1B and S1D). Hence, anaphase is at risk as long as cyclin B levels are still (relatively) high. Checkpoint activation on the other hand is slow even when cyclin B levels are high (Figure 3), making it a suitable mechanism to protect anaphase in such a situation. The cells co-overexpressing securin and separase provide a means to test this idea. In these cells, anaphase occurs very early after the APC/C has become active and Aurora B translocates considerably later with respect to anaphase than in wild-type cells (Figure S4C). Hence, there should be a higher tendency for destabilization of chromosome attachments. Consistently, we sometimes see securin stabilization in these cells, indicating that an error was recognized during anaphase (Figure S4D). This needs to be corroborated by visualizing checkpoint proteins, which technical difficulties have so far rendered impossible for us. Most cells proceeded through anaphase unhindered, which suggests that slow checkpoint activation may be efficient in ensuring anaphase progression while cyclin B levels are still high.

Slow Checkpoint Activation Seems Evolutionary Conserved, Despite the Risks Associated

Since we found slow checkpoint activation kinetics at high cyclin B levels (mimicking the biochemical situation in prometaphase), checkpoint activation may be slow throughout prometaphase. This is surprising because the checkpoint is considered a crucial safety mechanism during that time of mitosis. Yet, this slowness seems evolutionary conserved since the Gerlich group recently reported similarly slow checkpoint activation kinetics during metaphase in human cells [22].

We asked whether such slow checkpoint activation is at all consistent with the timing of mitosis. In an unperturbed *S. pombe* mitosis, it takes on average 5.8 min from entry into mitosis (when chromosomes are initially unattached) to APC/C activation (Figures S4E and S4F). Apparently, this timing is set by checkpoint-independent mechanisms controlling APC/C activity, because deletions of checkpoint genes do not accelerate mitosis (Figure S4G). For the checkpoint to be able to protect chromosomes from missegregating, attachment errors must block APC/C activity in less than 5.8 min.

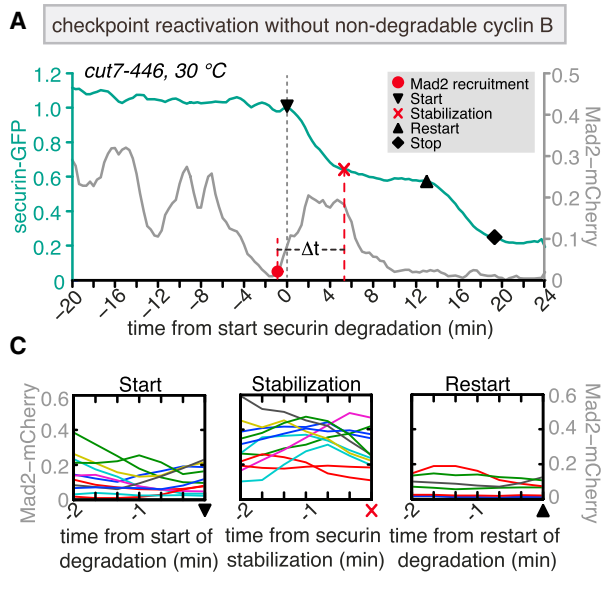

Figure 4. Checkpoint Re-engagement Triggered by Spindle Destabilization during the Metaphase-to-Anaphase Transition

(A) Normalized nuclear securin-GFP intensity (green) and normalized maximal cellular Mad2-mCherry intensity (gray) in a cell progressing through mitosis, expressing the temperature-sensitive kinesin-5 mutant allele *cut7-446* and overexpressing securin-GFP. Red circle, reincrease of Mad2; black head-down triangle, initial start of securin degradation; red cross, stabilization of securin-GFP abundance; black triangle, restart of securin degradation; black diamond, final stabilization of securin-GFP abundance; Δt, time between start of Mad2-mCherry signal increase and stabilization of securin-GFP abundance. A stabilization of securin abundance was observed in 11 cells, which are further analyzed in (B)–(D); only five of these cells showed a restart of securin degradation.

(B) Quantification of the normalized securin-GFP intensities at the different time points of anaphase as shown in (A). Average and SD are shown.

(C) Single-cell measurements of Mad2-mCherry intensities in the 2 min preceding the indicated points defined in (A).

(D) Time difference between start of Mad2-mCherry signal increase and restabilization of securin-GFP (Δt) with respect to the time that elapsed between the start of securin degradation and Mad2 rerecruitment. Shown are single-cell measurements (red circles) and regression line (black).

Our data indicate that it takes on average 4.3 min (in the presence of nondegradable cyclin B; Figure 3F). Hence, there is just enough time for chromosome attachment errors in early mitosis to prevent APC/C activity. In contrast, chromosome attachment errors that occur late in prometaphase may not have enough time to block APC/C activity. This is consistent with observations in human cells [22] and reveals a surprising vulnerability in the checkpoint mechanism. We can envision two possibilities why slow checkpoint activation nevertheless exists and is evolutionary conserved: either there is a biochemical constraint, which makes faster inhibition of the APC/C impossible, or the slowness has been evolutionary conserved because it provides a safety mechanism in anaphase, as our work here suggests.

Experimental Procedures

S. pombe Strains and Growth Conditions

Strains are listed in Table S1. PCR-based gene targeting [32] was used to replace genes by gene fusions at their endogenous loci. For overexpression of securin and separase, we replaced the endogenous promoters by the constitutive *Padh1* [33] and the thiamine-repressible *Pnmt1* promoter [34], respectively—except for Figures 2B and 2C, where separase overexpression was achieved by integration of *Pnmt1-cut1⁺-13myc-Tadh1* into the *leu1* locus. For inducible expression of *ΔN-cdc13*, the coding sequence for amino acids 68 to 482 of Cdc13 [16] was cloned into the pDual vector [35] under control of the *Pnmt81* promoter and integrated into the *leu1* locus. Unless stated differently, cells were grown at 30°C in Edinburgh minimal medium (EMM) with the necessary supplements. When applicable, the *nmt* promoter was suppressed by addition of 16 μM thiamine. Protein expression from the *nmt* promoter and its derivatives at 30°C was induced by culturing of the cells for 14–18 hr in EMM without thiamine. Rich medium (YEA) was used for asynchronously growing cells for protein extraction and immunoblotting. Detailed information can be found in the Supplemental Experimental Procedures.

Live-Cell Imaging

Cells were mounted in lectin-coated (35 μg/ml; Sigma L1395) culture dishes (8-well; Ibidi) and preincubated on the microscope stage for 30 min. Live-cell imaging was carried out at 30°C (if not stated otherwise) on a DeltaVision Core system (Applied Precision/GE Healthcare) equipped with a climate chamber (EMBL) using a 60×/1.4 Apo oil objective (Olympus). Images were deconvolved using SoftWorx software. For representative pictures, maximum-intensity projections were used if z stacks were acquired. All intensity measurements were performed using SoftWorx, and data analysis and kymograph assembly were performed using MatLab. Intensity was measured in units of raw camera counts. A detailed description of the imaging conditions and analysis can be found in the Supplemental Experimental Procedures.

Supplemental Information

Supplemental Information includes Supplemental Experimental Procedures, four figures, and one table and can be found with this article online at http://dx.doi.org/10.1016/j.cub.2014.02.005.

Author Contributions

J.K. and S.H. conceived the project and wrote the manuscript; J.K. designed, performed, and analyzed experiments.

Acknowledgments

We thank Tomohiro Matsumoto for antibodies, Yoshinori Watanabe for *S. pombe* strains, Mitsuhiro Yanagida for plasmids, Eva Illgen and Armin Kubis for excellent technical help, members of the Hauf lab for discussions, and Maria Vázquez-Novelle and Mark Petronczki for communicating results prior to publication. This work was supported by the Max Planck Society and the Boehringer Ingelheim Fonds (fellowship to J.K.).

Received: January 9, 2014
Revised: February 2, 2014
Accepted: February 4, 2014
Published: February 27, 2014

References

1. Lampson, M.A., and Cheeseman, I.M. (2011). Sensing centromere tension: Aurora B and the regulation of kinetochore function. Trends Cell Biol. *21*, 133–140.
2. Carmena, M., Wheelock, M., Funabiki, H., and Earnshaw, W.C. (2012). The chromosomal passenger complex (CPC): from easy rider to the godfather of mitosis. Nat. Rev. Mol. Cell Biol. *13*, 789–803.

3. Lara-Gonzalez, P., Westhorpe, F.G., and Taylor, S.S. (2012). The spindle assembly checkpoint. Curr. Biol. *22*, R966–R980.
4. Musacchio, A., and Salmon, E.D. (2007). The spindle-assembly checkpoint in space and time. Nat. Rev. Mol. Cell Biol. *8*, 379–393.
5. Oliveira, R.A., and Nasmyth, K. (2010). Getting through anaphase: splitting the sisters and beyond. Biochem. Soc. Trans. *38*, 1639–1644.
6. Vázquez-Novelle, M.D., Mirchenko, L., Uhlmann, F., and Petronczki, M. (2010). The 'anaphase problem': how to disable the mitotic checkpoint when sisters split. Biochem. Soc. Trans. *38*, 1660–1666.
7. Parry, D.H., Hickson, G.R., and O'Farrell, P.H. (2003). Cyclin B destruction triggers changes in kinetochore behavior essential for successful anaphase. Curr. Biol. *13*, 647–653.
8. Pereira, G., and Schiebel, E. (2003). Separase regulates INCENP-Aurora B anaphase spindle function through Cdc14. Science *302*, 2120–2124.
9. Hümmer, S., and Mayer, T.U. (2009). Cdk1 negatively regulates midzone localization of the mitotic kinesin Mklp2 and the chromosomal passenger complex. Curr. Biol. *19*, 607–612.
10. Mirchenko, L., and Uhlmann, F. (2010). Sli15(INCENP) dephosphorylation prevents mitotic checkpoint reengagement due to loss of tension at anaphase onset. Curr. Biol. *20*, 1396–1401.
11. Vázquez-Novelle, M.D., and Petronczki, M. (2010). Relocation of the chromosomal passenger complex prevents mitotic checkpoint engagement at anaphase. Curr. Biol. *20*, 1402–1407.
12. Oliveira, R.A., Hamilton, R.S., Pauli, A., Davis, I., and Nasmyth, K. (2010). Cohesin cleavage and Cdk inhibition trigger formation of daughter nuclei. Nat. Cell Biol. *12*, 185–192.
13. Tinker-Kulberg, R.L., and Morgan, D.O. (1999). Pds1 and Esp1 control both anaphase and mitotic exit in normal cells and after DNA damage. Genes Dev. *13*, 1936–1949.
14. Palframan, W.J., Meehl, J.B., Jaspersen, S.L., Winey, M., and Murray, A.W. (2006). Anaphase inactivation of the spindle checkpoint. Science *313*, 680–684.
15. Wolf, F., Wandke, C., Isenberg, N., and Geley, S. (2006). Dose-dependent effects of stable cyclin B1 on progression through mitosis in human cells. EMBO J. *25*, 2802–2813.
16. Yamano, H., Gannon, J., and Hunt, T. (1996). The role of proteolysis in cell cycle progression in Schizosaccharomyces pombe. EMBO J. *15*, 5268–5279.
17. Dischinger, S., Krapp, A., Xie, L., Paulson, J.R., and Simanis, V. (2008). Chemical genetic analysis of the regulatory role of Cdc2p in the S. pombe septation initiation network. J. Cell Sci. *121*, 843–853.
18. Mulvihill, D.P., Petersen, J., Ohkura, H., Glover, D.M., and Hagan, I.M. (1999). Plo1 kinase recruitment to the spindle pole body and its role in cell division in Schizosaccharomyces pombe. Mol. Biol. Cell *10*, 2771–2785.
19. Biggins, S., and Murray, A.W. (2001). The budding yeast protein kinase Ipl1/Aurora allows the absence of tension to activate the spindle checkpoint. Genes Dev. *15*, 3118–3129.
20. Windecker, H., Langegger, M., Heinrich, S., and Hauf, S. (2009). Bub1 and Bub3 promote the conversion from monopolar to bipolar chromosome attachment independently of shugoshin. EMBO Rep. *10*, 1022–1028.
21. Hagan, I., and Yanagida, M. (1990). Novel potential mitotic motor protein encoded by the fission yeast cut7+ gene. Nature *347*, 563–566.
22. Dick, A.E., and Gerlich, D.W. (2013). Kinetic framework of spindle assembly checkpoint signalling. Nat. Cell Biol. *15*, 1370–1377.
23. Hagting, A., Den Elzen, N., Vodermaier, H.C., Waizenegger, I.C., Peters, J.-M., and Pines, J. (2002). Human securin proteolysis is controlled by the spindle checkpoint and reveals when the APC/C switches from activation by Cdc20 to Cdh1. J. Cell Biol. *157*, 1125–1137.
24. Qi, W., and Yu, H. (2007). KEN-box-dependent degradation of the Bub1 spindle checkpoint kinase by the anaphase-promoting complex/cyclosome. J. Biol. Chem. *282*, 3672–3679.
25. King, E.M., van der Sar, S.J., and Hardwick, K.G. (2007). Mad3 KEN boxes mediate both Cdc20 and Mad3 turnover, and are critical for the spindle checkpoint. PLoS ONE *2*, e342.
26. Choi, E., Choe, H., Min, J., Choi, J.Y., Kim, J., and Lee, H. (2009). BubR1 acetylation at prometaphase is required for modulating APC/C activity and timing of mitosis. EMBO J. *28*, 2077–2089.
27. Chung, E., and Chen, R.H. (2003). Phosphorylation of Cdc20 is required for its inhibition by the spindle checkpoint. Nat. Cell Biol. *5*, 748–753.
28. D'Angiolella, V., Mari, C., Nocera, D., Rametti, L., and Grieco, D. (2003). The spindle checkpoint requires cyclin-dependent kinase activity. Genes Dev. *17*, 2520–2525.
29. Morin, V., Prieto, S., Melines, S., Hem, S., Rossignol, M., Lorca, T., Espeut, J., Morin, N., and Abrieu, A. (2012). CDK-dependent potentiation of MPS1 kinase activity is essential to the mitotic checkpoint. Curr. Biol. *22*, 289–295.
30. Yamaguchi, S., Decottignies, A., and Nurse, P. (2003). Function of Cdc2p-dependent Bub1p phosphorylation and Bub1p kinase activity in the mitotic and meiotic spindle checkpoint. EMBO J. *22*, 1075–1087.
31. Murata-Hori, M., Tatsuka, M., and Wang, Y.L. (2002). Probing the dynamics and functions of aurora B kinase in living cells during mitosis and cytokinesis. Mol. Biol. Cell *13*, 1099–1108.
32. Bähler, J., Wu, J.Q., Longtine, M.S., Shah, N.G., McKenzie, A., 3rd, Steever, A.B., Wach, A., Philippsen, P., and Pringle, J.R. (1998). Heterologous modules for efficient and versatile PCR-based gene targeting in Schizosaccharomyces pombe. Yeast *14*, 943–951.
33. McLeod, M., Stein, M., and Beach, D. (1987). The product of the mei3+ gene, expressed under control of the mating-type locus, induces meiosis and sporulation in fission yeast. EMBO J. *6*, 729–736.
34. Basi, G., Schmid, E., and Maundrell, K. (1993). TATA box mutations in the Schizosaccharomyces pombe nmt1 promoter affect transcription efficiency but not the transcription start point or thiamine repressibility. Gene *123*, 131–136.
35. Matsuyama, A., Shirai, A., Yashiroda, Y., Kamata, A., Horinouchi, S., and Yoshida, M. (2004). pDUAL, a multipurpose, multicopy vector capable of chromosomal integration in fission yeast. Yeast *21*, 1289–1305.

Current Biology, Volume *24*

Supplemental Information

Slow Checkpoint Activation Kinetics as a Safety Device in Anaphase

Julia Kamenz and Silke Hauf

Figure S1

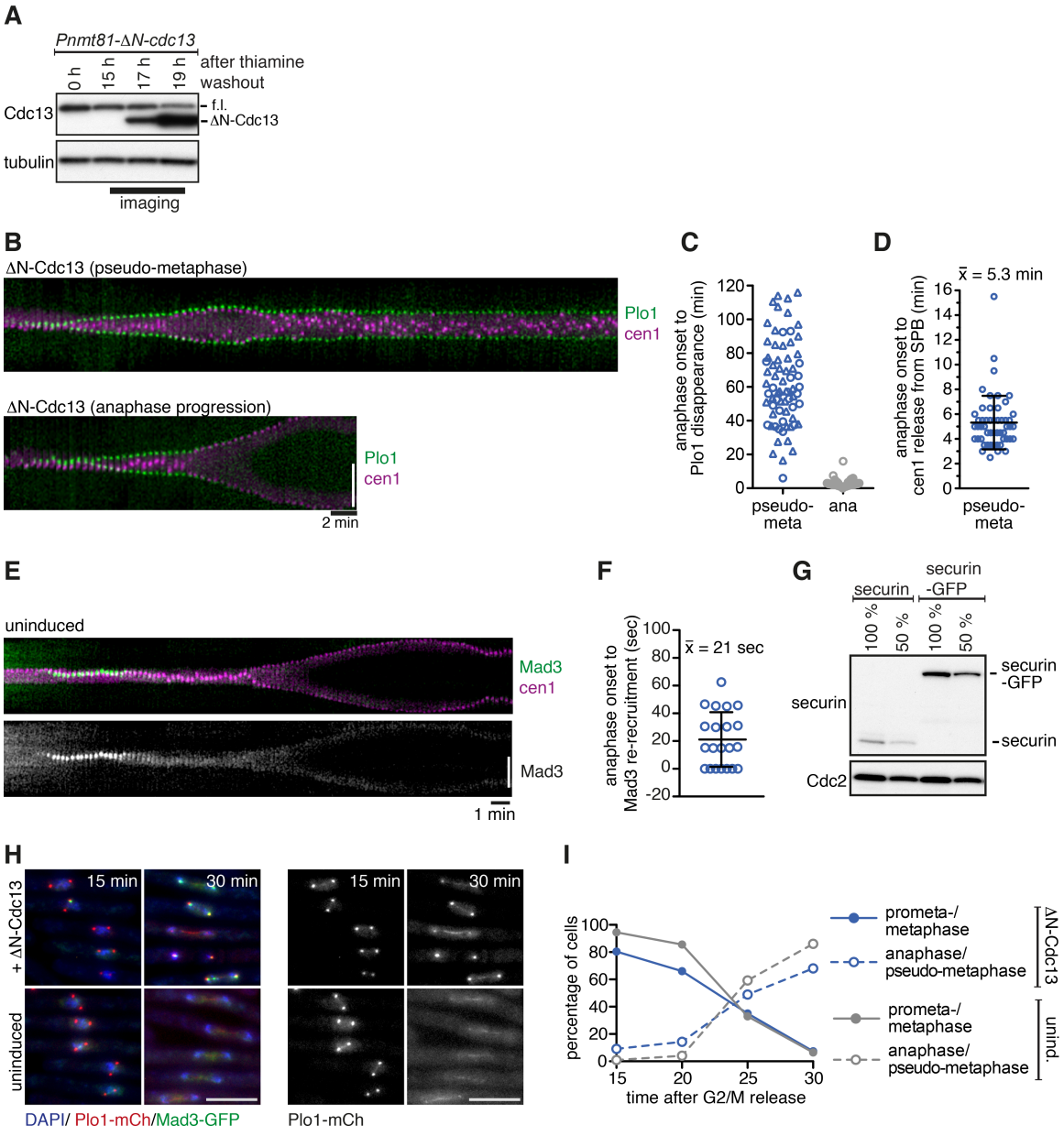

Figure S1.

Characterization of cells expressing non-degradable cyclin B (ΔN-Cdc13), related to Figure 1.

A Expression levels of non-degradable cyclin B (ΔN-Cdc13) at different time points after induction were analyzed by immunoblotting using antibodies against Cdc13 and alpha-tubulin (loading control). The black bar shows the time window for image acquisition. f.l. marks the endogenous Cdc13 and ΔN-Cdc13 the shorter non-degradable

version.

B Expression of ΔN-Cdc13 was induced in cells expressing *plo1+-GFP* and a marker for the centromere of chromosome I (cen1). Mitotic progression was followed by live cell imaging. Representative kymograph for cells exhibiting a pseudo-metaphase phenotype or cells with unperturbed anaphase progression (vertical scale bar: 5 μm). For cells exhibiting a pseudo-metaphase phenotype, persistent localization of Plo1-GFP to the spindle pole bodies as well as movement of centromeres along the spindle axis was observed.

C Quantification of the time between anaphase onset and the disappearance of Plo1-GFP from the spindle pole bodies for the cells shown representatively in (B). Circles indicate cells in which the entire time was recorded; triangles indicate cells that still exhibited localized Plo1-GFP signal when filming ended.

D Quantification of the time between anaphase onset and dissociation of the centromeric region of chromosome I (cen1) more than 1 μm away from the spindle pole body. Data from single cells (blue) with mean and standard deviation (black lines).

E Representative kymograph of mitotic progression of a cell expressing *mad3+-GFP* and a centromeric marker for chromosome I (cen1) without induction of non-degradable cyclin B (vertical scale bar: 5 μm, see Figure 1B for comparison to the expression of ΔN-Cdc13). Note that Mad3-GFP does not re-appear in anaphase.

F Quantification of the experiment in Figure 1B and 1C. Time between anaphase onset and the start of increasing Mad3-GFP signal. Data from single cells (blue) with mean and standard deviation (black lines).

G Characterization of the antibody raised against recombinant securin (Cut2). Protein extracts from asynchronous cultures of strains expressing endogenous securin or securin-GFP were analyzed by immunoblotting. Cdc2 was used as a loading control.

H Representative pictures of the cultures used in Figure 1D (scale bar: 5 μm).

I Quantification of the cell cycle stages during the time points of the metaphase to anaphase transition for the cultures used in Figure 1D (n>100 cells per time point).

Figure S2

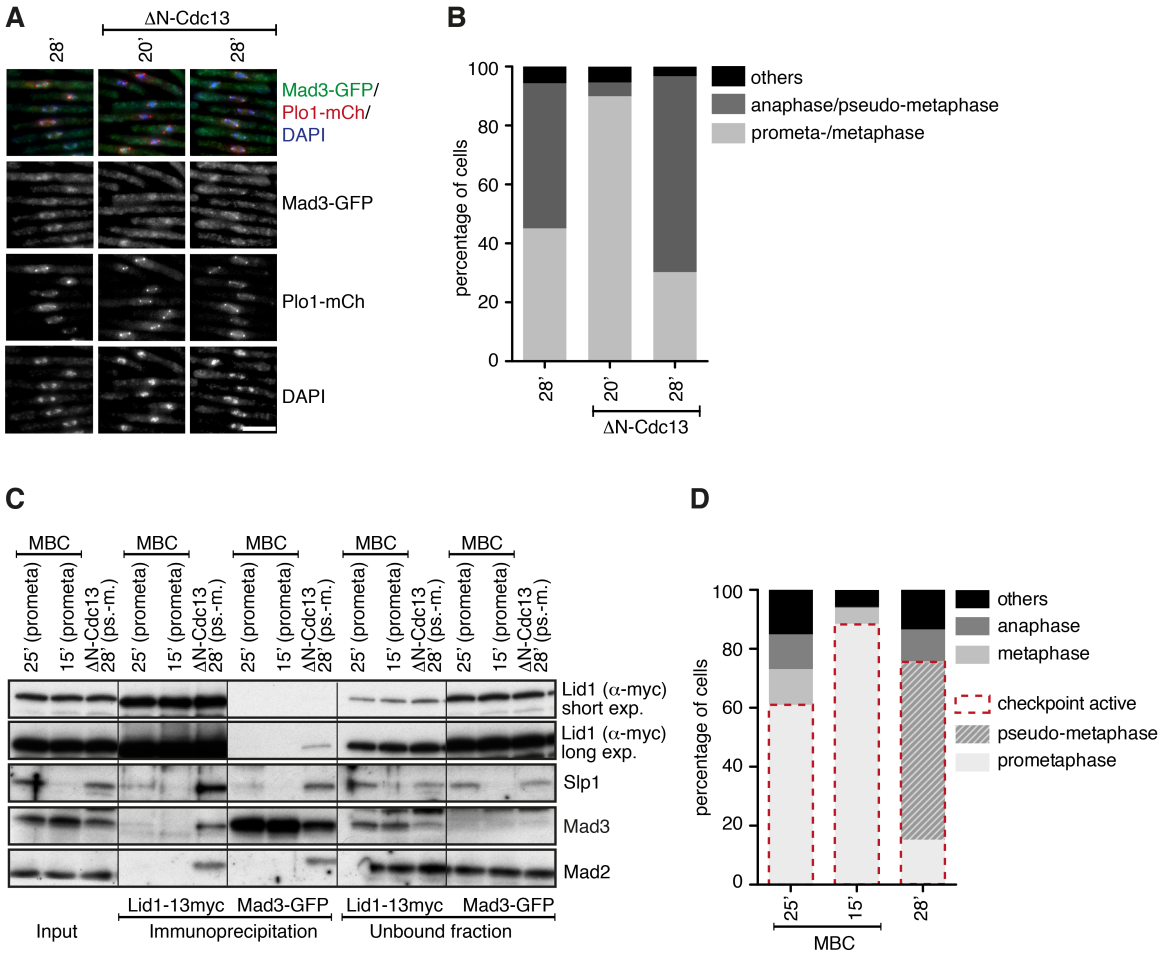

Figure S2.

Quantification of cell cycle stages and comparison of MCC formation between prometaphase and pseudo-metaphase, related to Figure 2A.

A Representative pictures of the cultures used in Figure 2A (scale bar: 5 μm).

B Quantification of cell cycle stages in the cultures used in Figure 2A (n>200 cells per time point).

C *Cdc25-22* cells with or without induction of ΔN-Cdc13 were synchronized at the G2/M transition. After release the microtubule-destabilizing drug MBC was added to the cultures without ΔN-Cdc13 induction. Cells were harvested at the indicated time points after release and the APC/C subunit Lid1-13myc or the MCC component Mad3-GFP were immunoprecipitated and analyzed by immunoblotting for co-immunprecipitation of Slp1, Mad2, and Mad3-GFP or Lid1-13myc, respectively. As Slp1 is not yet expressed at 15 min after release, this sample serves as a negative control.

D Quantification of cell cycle stages in the cultures used in Figure S2C (n>200 cells per time point). Cells exhibiting localized Mad3-GFP signal were considered as 'checkpoint active' (either prometaphase or pseudo-metaphase, respectively).

Figure S3

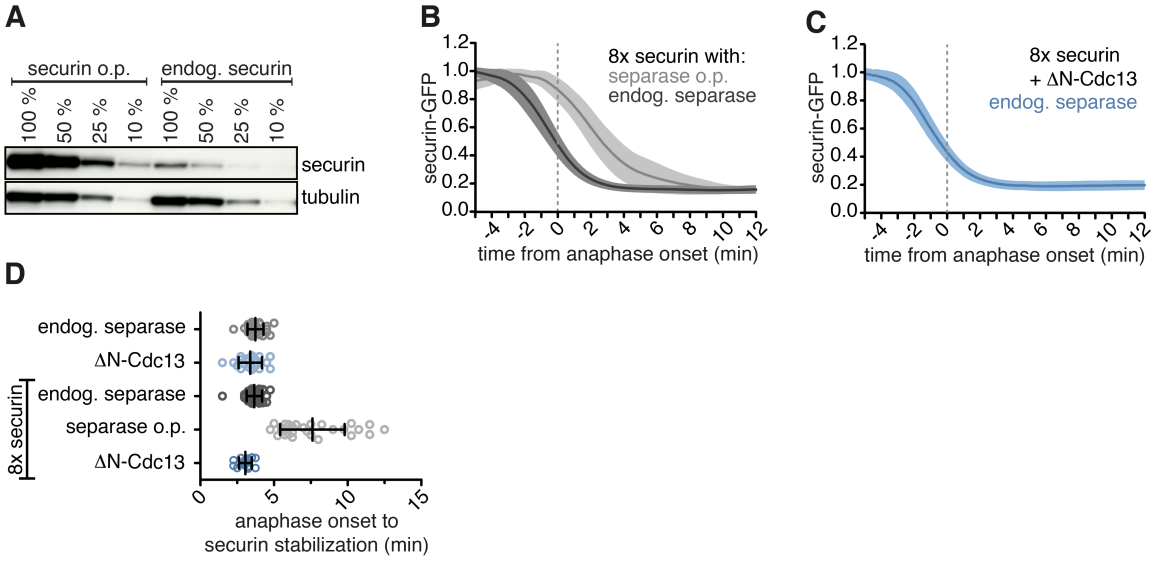

Figure S3.

Combined overexpression of securin-GFP and separase prolongs the time between anaphase onset and completion of securin-GFP degradation, related to Figure 3.

A Expression level of endogenous securin-GFP and securin-GFP overexpression (securin o.p.) were analyzed by immunoblotting using antibodies against Cut2 (securin) and alpha-tubulin (loading control). For comparison, serial dilutions of the cell extracts were loaded.

B Degradation kinetics of securin-GFP were assayed as described in Figure 1E. Cells either overexpressed securin-GFP alone (n=46, dark grey) or securin-GFP and separase (n=27, light grey). Shown is the average (line) +/- standard deviation (filled area).

C Degradation kinetics of overexpressed securin-GFP in the presence of non-degradable cyclin B. Same data as in Figure 3A, shown here for direct comparison to (B).

D Time between anaphase onset and securin stabilization for the cells from (B), (C) and Figure 1E. Single cell measurements with mean and standard deviation (black lines).

Figure S4

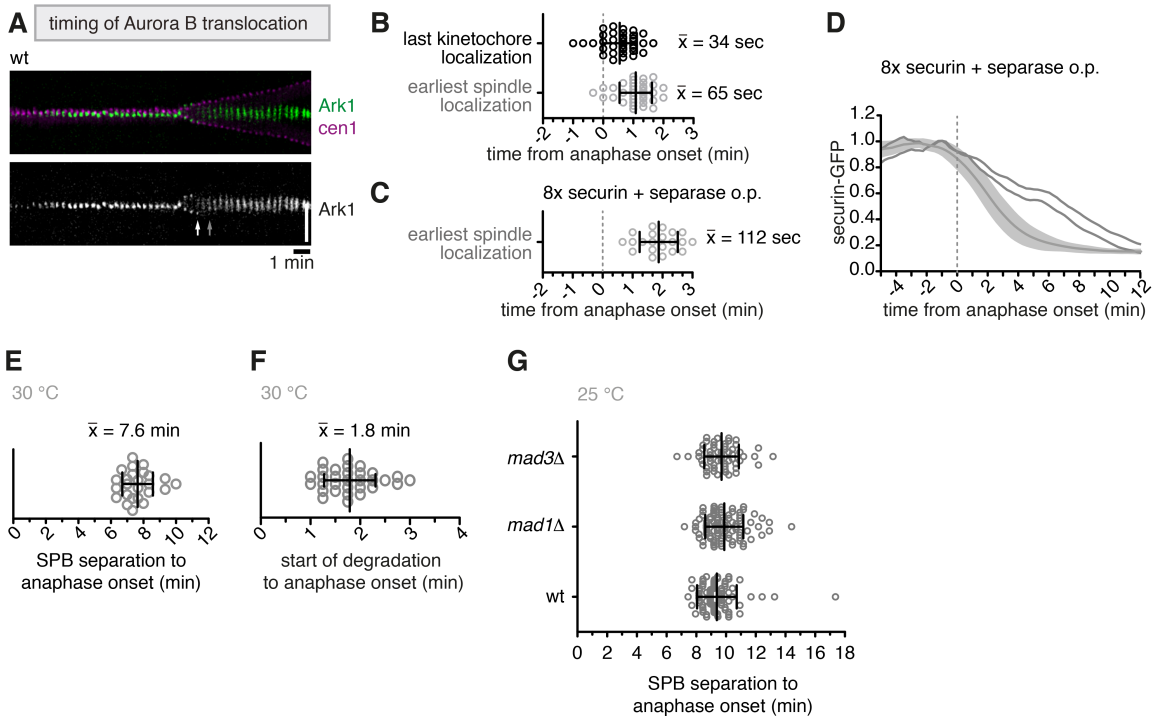

Figure S4.

Mitotic timing in an unperturbed mitosis, related to Results and Discussion.

A,B Timing of Aurora B translocation with respect to sister chromatid separation in cells expressing *ark1+-GFP* and a centromeric marker for chromosome I (cen1). A representative kymograph is shown in (A) (vertical scale bar: 5 μm). The white arrow marks the last time point at which Ark1-GFP still exhibits a localized, presumably centromere-associated signal. The grey arrow depicts the first clear localization of Ark1-GFP to the midspindle. Measurements from 36 cells are shown in (B) with mean and standard deviation (black lines).

C Timing of Aurora B translocation with respect to sister chromatid separation in cells overexpressing securin and separase (n=21; mean and standard deviation in black lines).

D Securin degradation kinetics for the combined overexpression of securin-GFP and separase as shown in Figure S3B. Shown are the single cell tracks for the two cells, which exhibited a differential behavior with stabilization of securin-GFP during the degradation. In addition, the averaged degradation (line) +/- standard deviation (filled area) for the remaining cells is shown.

E Time from SPB separation to anaphase onset in wild type cells (n=25) at 30 °C. Single cell measurements (grey) with mean and standard deviation (black lines).

F Time from the start of securin-GFP degradation to anaphase onset at 30 °C. Single cell measurements (grey, n=31) from the cells in Figure 1E with mean and

standard deviation (black lines). The time from mitotic entry to APC/C activation was estimated as the difference of the measurement in S3E and S3F.

G Comparison of the mitotic timing at 25 °C of a wild type strain (n=83) and strains carrying a deletion of the *mad1* (n=91) or *mad3* (n=53) gene, respectively. Mitotic entry was defined as the point of spindle pole body (SPB) separation, anaphase onset as the point of sister chromatid separation. Single cell measurements (grey) with mean and standard deviation (black lines). At 25 °C mitotic progression is slower than at 30 °C, which makes it easier to see potential differences in timing.

Supplemental Table S1.

S. pombe strains, related to Experimental Procedures.

Figure 1A		
SM304	*h90*	*ade6-M216 leu1 ark1+-GFP<<kanR ura4-D18(?) dh1L<<ura4+<<tetO Z<<natR<<Padh31-tetR-tdTomato leu1+<<Pnmt81-deltaN67-cdc13*
SM361	*h-*	*ade6-M216 leu1 mad1+-GFP<<kanR ura4-D18(?) dh1L<<ura4+<<tetO Z<<natR<<Padh31-tetR-tdTomato leu1+<<Pnmt81-deltaN67-cdc13*
SM362'	*h90*	*leu1 ade6-M210 mad2+-GFP<<kanR ura4-D18(?) dh1L<<ura4+<<tetO Z<<natR<<Padh31-tetR-tdTomato leu1+<<Pnmt81-deltaN67-cdc13*
SM363	*h90*	*ade6-M216 leu1 bub3+-S(GGGGS)3-doublemyeGFP<<kanR ura4-D18(?) dh1L<<ura4+<<tetO Z<<natR<<Padh31-tetR-tdTomato leu1+<<Pnmt81-deltaN67-cdc13*
Figure 1B,C		
ST512	*h90*	*leu1 ade6? ura4-D18 dh1L<<ura4+<<tetO Z<<natR<<Padh31-tetR-tdTomato mad3+-GFP<<kanR leu1+<<Pnmt81-deltaN67-cdc13*
Figure 1D		
SP700	*h+*	*leu1 mad3+-GFP<<kanR plo1+-mCherry<<natR cdc25-22 lid1+-13xmyc<<natR leu1+<<Pnmt81-deltaN67-cdc13*
Figure 1E		
SL249	*h-*	*leu1 ade6-M216 cut2+-GFP<<kanR dh1L<<ura4+<<tetO Z<<natR<<Padh31-tetR-tdTomato*
SL253	*h-*	*leu1 ade6-M216 cut2+-GFP<<kanR dh1L<<ura4+<<tetO Z<<natR<<Padh31-tetR-tdTomato leu1+<<Pnmt81-deltaN67-cdc13*
Figure 2A		
SP700	*h+*	*leu1 mad3+-GFP<<kanR plo1+-mCherry<<natR cdc25-22 lid1+-13xmyc<<natR leu1+<<Pnmt81-deltaN67-cdc13*
Figure 2B		
SP637	*h-*	*leu1 ade6-M216 cut2+-GFP<<kanR cut1+-13myc<<kanR dh1L<<ura4+<<tetO Z<<natR<<Padh31-tetR-tdTomato leu1+<<Pnmt1-cut1-13myc*
ST515	*h-*	*leu1 ade6-M216 cut2+-GFP<<kanR cut1+-13myc<<kanR dh1L<<ura4+<<tetO Z<<natR<<Padh31-tetR-tdTomato leu1+<<Pnmt1-cut1-13myc mad2D::hygR*
Figure 2C		
SM337	*h-*	*leu1 ade6-M216 cut2+-GFP<<kanR cut1+-13myc<<kanR dh1L<<ura4+<<tetO Z<<natR<<Padh31-tetR-tdTomato*
SP637	*h-*	*leu1 ade6-M216 cut2+-GFP<<kanR cut1+-13myc<<kanR dh1L<<ura4+<<tetO Z<<natR<<Padh31-tetR-tdTomato leu1+<<Pnmt1-cut1-13myc*
ST515	*h-*	*leu1 ade6-M216 cut2+-GFP<<kanR cut1+-13myc<<kanR dh1L<<ura4+<<tetO Z<<natR<<Padh31-tetR-tdTomato leu1+<<Pnmt1-cut1-13myc mad2D::hygR*
Figure 3A,C,D		
SP684'	*h-*	*leu1 ade6-M216 natNT2<<Padh1(#6)-cut2-GFP<<kanR ura4-D18(?) dh1L<<ura4+<<tetO Z<<natR<<Padh31-tetR-tdTomato leu1+<<Pnmt81-deltaN67-cdc13*
SP693'	*h-*	*leu1 ade6-M216 natNT2<<Padh1(#6)-cut2-GFP<<kanR ura4-D18(?) dh1L<<ura4+<<tetO Z<<natR<<Padh31-tetR-tdTomato leu1+<<Pnmt81-deltaN67-cdc13 hphNT1>>Pnmt1-cut1+*
ST504'	*h-*	*leu1 ade6-M216 natNT2<<Padh1(#6)-cut2-GFP<<kanR ura4-D18(?) dh1L<<ura4+<<tetO Z<<natR<<Padh31-tetR-tdTomato leu1+<<Pnmt81-deltaN67-cdc13 hphNT1>>Pnmt1-cut1+ mad2D<<hygR*
Figure 3B		
SP693'	*h-*	*leu1 ade6-M216 natNT2<<Padh1(#6)-cut2-GFP<<kanR ura4-D18(?) dh1L<<ura4+<<tetO Z<<natR<<Padh31-tetR-tdTomato leu1+<<Pnmt81-deltaN67-cdc13 hphNT1>>Pnmt1-cut1+*
ST504'	*h-*	*leu1 ade6-M216 natNT2<<Padh1(#6)-cut2-GFP<<kanR ura4-D18(?) dh1L<<ura4+<<tetO Z<<natR<<Padh31-tetR-tdTomato leu1+<<Pnmt81-deltaN67-cdc13 hphNT1>>Pnmt1-cut1+ mad2D<<hygR*
Figure 3E,F		
ST514	*h-?*	*leu1 ade6-M216 natNT2<<Padh1(#6)-cut2-GFP<<kanR ura4-D18(?) leu1+<<Pnmt81-deltaN67-cdc13 hphNT1>>Pnmt1-cut1+ mad2+-mCherry<<natR*
Figure 4A-D		
ST523	*h?*	*leu1 ade6? natNT2<<Padh1(#6)-cut2+-GFP<<kanR mad2+-mCherry<<natR cut7-446*

Figure S1A

SL274	*h+*	*leu1 ade6-M216 ura4-D18(?) cen2<<lacO-kanR-ura+ his7+<<dis1-GFP-lacI-NLS dh1L<<ura4+<<tetO Z<<natR<<Padh31-tetR-tdTomato leu1+<<Pnmt81-deltaN67-cdc13*

Figure S1B-D

SL298	*h-*	*leu1 ade6-M216 plo1+-GFP<<kanR ura4-D18(?) dh1L<<ura4+<<tetO Z<<natR<<Padh31-tetR-tdTomato leu1+<<Pnmt81-deltaN67-cdc13*

Figure S1E,F

ST512	*h90*	*leu1 ade? ura4-D18 dh1L<<ura4+<<tetO Z<<natR<<Padh31-tetR-tdTomato mad3+-GFP<<kanR leu1+<<Pnmt81-deltaN67-cdc13*

Figure S1G

JY333	*h-*	*leu1 ade6-M216*
SL248	*h-*	*leu1 ade6-M216 cut2+-GFP<<kanR*

Figure S1H,I

SP700	*h+*	*leu1 mad3+-GFP<<kanR plo1+-mCherry<<natR cdc25-22 lid1+-13xmyc<<natR leu1+<<Pnmt81-deltaN67-cdc13*

Figure S2A-D

SP700	*h+*	*leu1 mad3+-GFP<<kanR plo1+-mCherry<<natR cdc25-22 lid1+-13xmyc<<natR leu1+<<Pnmt81-deltaN67-cdc13*

Figure S3A

SM336	*h-*	*leu1 ade6-M216 cut2+-GFP<<kanR cut1+-13myc<<kanR*
SM333	*h-*	*leu1 ade6-M216 natNT2<<Padh1(#6)-cut2+-GFP<<kanR cut1+-13myc<<kanR*

Figure S3B

SM325'	*h-*	*leu1 ade6-M216 natNT2<<Padh1(#6)-cut2-GFP<<kanR ura4-D18(?) dh1L<<ura4+<<tetO Z<<natR<<Padh31-tetR-tdTomato*
ST519	*h+*	*leu1 ade6? natNT2<<Padh1(#6)-cut2-GFP<<kanR ura4-D18(?) dh1L<<ura4+<<tetO Z<<natR<<Padh31-tetR-tdTomato hphNT1>>Pnmt1-cut1+*

Figure S3C

SP684'	*h-*	*leu1 ade6-M216 natNT2<<Padh1(#6)-cut2-GFP<<kanR ura4-D18(?) dh1L<<ura4+<<tetO Z<<natR<<Padh31-tetR-tdTomato leu1+<<Pnmt81-deltaN67-cdc13*

Figure S3D

SL249	*h-*	*leu1 ade6-M216 cut2+-GFP<<kanR dh1L<<ura4+<<tetO Z<<natR<<Padh31-tetR-tdTomato*
SL253	*h-*	*leu1 ade6-M216 cut2+-GFP<<kanR dh1L<<ura4+<<tetO Z<<natR<<Padh31-tetR-tdTomato leu1+<<Pnmt81-deltaN67-cdc13*
SM325'	*h-*	*leu1 ade6-M216 natNT2<<Padh1(#6)-cut2-GFP<<kanR ura4-D18(?) dh1L<<ura4+<<tetO Z<<natR<<Padh31-tetR-tdTomato*
ST519	*h+*	*leu1 ade6? natNT2<<Padh1(#6)-cut2-GFP<<kanR ura4-D18(?) dh1L<<ura4+<<tetO Z<<natR<<Padh31-tetR-tdTomato hphNT1>>Pnmt1-cut1+*
SP684'	*h-*	*leu1 ade6-M216 natNT2<<Padh1(#6)-cut2-GFP<<kanR ura4-D18(?) dh1L<<ura4+<<tetO Z<<natR<<Padh31-tetR-tdTomato leu1+<<Pnmt81-deltaN67-cdc13*

Figure S4A,B

ST202	*h+*	*leu1 ade6-M210 ura4-D18(?) dh1L<<ura4+<<tetO Z<<natR<<Padh31-tetR-tdTomato plo1+-mCherry<<natR ark1+-GFP<<kanR*

Figure S4C

ST529	*h?*	*leu1 ade6? natNT2<<Padh1(#6)-cut2-GFP<<kanR ura4-D18(?) dh1L<<ura4+<<tetO Z<<natR<<Padh31-tetR-tdTomato hphNT1>>Pnmt1-cut1+ ark1+-mCherry<<natR*

Figure S4D

ST519	*h+*	*leu1 ade6? natNT2<<Padh1(#6)-cut2-GFP<<kanR ura4-D18(?) dh1L<<ura4+<<tetO Z<<natR<<Padh31-tetR-tdTomato hphNT1>>Pnmt1-cut1+*

Figure SE

SP623	*h-*	*leu1 plo1+-mCherry<<natR cut2+-GFP<<kanR mis12+-GFP<<kanR*

Figure S4F

SL249	*h-*	*leu1 ade6-M216 cut2+-GFP<<kanR dh1L<<ura4+<<tetO Z<<natR<<Padh31-tetR-tdTomato*

Figure S4G

SI546'	*h-*	*leu1 ade6-M216 plo1+-GFP<<kanR ura4-D18(?) dh1L<<ura4+<<tetO Z<<natR<<Padh31-tetR-tdTomato*
SI589	*h-*	*leu1 ade6-M216 plo1+-GFP<<kanR ura4-D18(?) dh1L<<ura4+<<tetO Z<<natR<<Padh31-tetR-tdTomato mad1D::ura4+*
SI548	*h-*	*leu1 ade6-M210 plo1+-GFP<<kanR ura4-D18(?) dh1l<<ura4+<<tetO Z<<natR<<Padh131-tetR-tdTomato mad3Δ::ura4+*

Supplemental Experimental Procedures

Literature references for published *S. pombe* strains

S. pombe strains with the following modifications and mutations have been described previously: *cdc25-22* [S1], *cut7-446* [S2], *mad2+-GFP<<kanR, mad3+-GFP<<kanR*, *bub3+-S(GGGGS)3-2GFP<<kanR* [S3], *plo1+-mCherry<<natR*, *ark1+*-GFP<<kanR [S4], *plo1+-GFP<<kanR* [S5], *cen1-tdTomato* [S6].

Cell synchronization

To synchronize at the G2/M transition, *cdc25-22* cells were cultured at 25 °C in thiamine-containing EMM. The culture was washed, split and continued in EMM with or without 16 μM thiamine, respectively. After 15 h, cells were shifted to the restrictive temperature of 36.5 °C for an additional 5 h to arrest at the G2/M transition. Cells were released from the arrest by quickly cooling the culture to 25 °C using an ice-water bath and were further incubated at 25 °C until harvesting. For arresting cells in prometaphase the microtubule-destabilizing drug methyl benzimidazole-2-yl-carbamate (MBC) was added at a concentration of 50 μg/mL directly after release from the arrest. For protein extraction and methanol fixation 1×10^7 cells, for immunoprecipitation 1.5×10^9 cells were harvested. The quality of the arrest was analyzed by microscopy of the methanol fixed cells as described previously [S7].

Immunoprecipitation

Native protein extraction and immunoprecipitation was performed following the previously reported protocol [S8] using rabbit anti-Myc antibody (71D10, Cell Signaling, #2278) covalently coupled to protein A-coated magnetic beads (12.5 μg/100 μl beads, Invitrogen, 10002D) or mouse anti-GFP antibody covalently coupled to protein G-coated

magnetic beads (8 μg/100 μl beads, Invitrogen, 10004D). Immunoprecipitates were eluted using 100 mM citric acid pH 2; pH was adjusted with 1 M Tris pH 9.2, and the elution boiled in 4x SDS buffer (250 mM Tris pH 6.8, 8 % w/v SDS, 0.04 % bromophenol blue, 40 % glycerole, 400 mM dithiothreitol).

Cell extracts, immunoblotting and antibodies

Protein extraction under denaturing conditions using trichchloroacetic acid (TCA) was performed as described [S7]. Mouse anti-Myc (Sigma, M4439), mouse anti-Cdc13 (Novus, NB200-576), rabbit anti-Cdc2 (Santa Cruz, SC-53), rabbit anti-Mad2 [S9], rabbit anti-Slp1 [S10] and rabbit anti-Cut2 (this study) antibodies were used as primary antibodies. The anti-Cut2 antibody has been raised against recombinant full-length protein purified from *E. coli* under denaturing conditions. Anti-mouse or anti-rabbit HRP-conjugates (Dianova, 115-035-003, 111-035-003) were used as secondary antibodies and were read out using chemiluminescence.

Imaging and quantification of checkpoint proteins labeled with GFP

For visualization of Ark1-GFP, Mad2-GFP, Mad3-GFP and Bub3-GFP a z-stack of 8 planes and a total thickness of 3.2 μm was acquired. Sum projections were used for quantification of the maximal cellular Mad3-GFP intensity. For each time point a region of interest (ROI) was defined by the cell outline and the maximum and average GFP intensity of the area were measured. To correct for bleaching, the average GFP intensity was subtracted from the maximum (background correction). The data were smoothed by calculating the average of 5 consecutive time points. The time derivative was computed by linear regression on 5 consecutive time points. The time point of Mad3-GFP signal reappearance was defined as the time point after anaphase onset at which the time

derivative increased above a noise threshold (0.5625 rcc s^{-1}). The noise threshold was set as 2 standard deviations of the time derivative after anaphase onset in the wild type. In Figure 1C, the single cell measurements have been normalized to the minimal and maximal signal intensity and the time axis was aligned to anaphase onset.

Imaging and quantification of securin degradation kinetics

Images were acquired using the 'optical axis integration' algorithm of the SoftWorx software. For each time point an ROI was defined using the nuclear background signal of tetR-tdTomato and the average GFP signal intensity for the ROI was determined. If there was more than one ROI (e.g. after nuclear division), the average of the two measurements was calculated. Each time point was corrected for background signal, for which the average signal intensity of three ROIs placed outside of the cell was calculated. The data were smoothed by calculating the average of 5 consecutive time points and the time derivative was computed by linear regression on 5 consecutive time points. The time points of start and stabilization of securin-GFP degradation were defined as the time points before and after anaphase onset at which the time derivative raised above a given threshold (> -0.1 rcc s^{-1} for endogenous securin, > -0.4 rcc s^{-1} for 8x securin). For depiction, single cell measurements were normalized to 1 by the value of securin-GFP intensity at the start of degradation and the time axis was aligned to anaphase onset.

Imaging and quantification of securin-GFP degradation and Mad2-mCherry localization

For following the Mad2-mCherry localization in addition to securin-GFP degradation z-stacks of 10 planes and a total thickness of 4 μm were acquired for both wavelengths, deconvolved and projected into a single plane. Securin-GFP degradation kinetics were

analyzed as described above, except that in this case the sum projections were used, the nuclear ROI was placed by hand for each time point and the threshold for the start of degradation was set to -0.2 rcc s^{-1}. The maximal cellular Mad2-mCherry signal was measured as described for the Mad3-GFP signal quantification, except that the maximum intensity projection was used and Mad2-mCherry appearance was defined as the time point after anaphase onset at which the time derivative increased above 0.1 rcc s^{-1}.

For experiments following the securin-GFP degradation kinetics and Mad2-mCherry localization in the background of the temperature-sensitive *cut7-446* allele, cells were grown at 25 °C and only shifted to semi-permissive temperature of 30 °C for live cell imaging. Z-stacks of 10 planes and a total thickness of 4 μm were acquired for both wavelengths, deconvolved and projected into a single plane. Sum projections were used for the analysis of the securin-GFP degradation kinetics, maximum projections for the analysis of Mad2-mCherry signals. Securin-GFP degradation kinetics were analyzed by placing an ROI around the nucleus by hand, determining the average signal intensity and subtracting the extracellular background. The data were smoothed by averaging 5 consecutive time points and the time derivative computed by linear regression of 9 consecutive time points. The local minima of the time derivative (points of fastest degradation) were determined and the nearest start of degradation and stabilization point was defined as the time points before and after the minimum at which the time derivative increased above the threshold of -1 rcc s^{-1}. The maximal cellular Mad2-mCherry signal was determined as described above, but the signal was normalized to the minimal and maximal signal. The threshold was set to 0.015.

Supplemental References

S1. Russell, P., and Nurse, P. (1986). cdc25+ functions as an inducer in the mitotic control of fission yeast. Cell *45*, 145-153.

S2. Hagan, I., and Yanagida, M. (1990). Novel potential mitotic motor protein encoded by the fission yeast cut7+ gene. Nature *347*, 563-566.

S3. Windecker, H., Langegger, M., Heinrich, S., and Hauf, S. (2009). Bub1 and Bub3 promote the conversion from monopolar to bipolar chromosome attachment independently of shugoshin. EMBO reports *10*, 1022-1028.

S4. Heinrich, S., Windecker, H., Hustedt, N., and Hauf, S. (2012). Mph1 kinetochore localization is crucial and upstream in the hierarchy of spindle assembly checkpoint protein recruitment to kinetochores. Journal of cell science *125*, 4720-4727.

S5. Kawashima, S.A., Tsukahara, T., Langegger, M., Hauf, S., Kitajima, T.S., and Watanabe, Y. (2007). Shugoshin enables tension-generating attachment of kinetochores by loading Aurora to centromeres. Genes & development *21*, 420-435.

S6. Kagami, A., Sakuno, T., Yamagishi, Y., Ishiguro, T., Tsukahara, T., Shirahige, K., Tanaka, K., and Watanabe, Y. (2011). Acetylation regulates monopolar attachment at multiple levels during meiosis I in fission yeast. EMBO reports *12*, 1189-1195.

S7. Koch, A., Rode, H.B., Richters, A., Rauh, D., and Hauf, S. (2012). A chemical genetic approach for covalent inhibition of analogue-sensitive aurora kinase. ACS chemical biology *7*, 723-731.

S8. Heinrich, S., Geissen, E.M., Kamenz, J., Trautmann, S., Widmer, C., Drewe, P., Knop, M., Radde, N., Hasenauer, J., and Hauf, S. (2013). Determinants of robustness in spindle assembly checkpoint signalling. Nature cell biology *15*, 1328-1339.

S9. Yamada, H.Y., Matsumoto, S., and Matsumoto, T. (2000). High dosage expression of a zinc finger protein, Grt1, suppresses a mutant of fission yeast slp1(+), a homolog of CDC20/p55CDC/Fizzy. Journal of cell science *113 (Pt 22)*, 3989-3999.

S10. Kim, S.H., Lin, D.P., Matsumoto, S., Kitazono, A., and Matsumoto, T. (1998). Fission yeast Slp1: an effector of the Mad2-dependent spindle checkpoint. Science *279*, 1045-1047.

3 Discussion

3.1 Synchronous sister chromatid splitting in anaphase without obligatory positive feedback (results part 2.1)

3.1.1 Synchronicity of sister chromatid separation

The abrupt splitting of sister chromatids at anaphase onset is one of the visually most striking events of the cell cycle. Interestingly, studies in several organisms suggested that the degradation of the main separase inhibitor securin occurs slowly compared to sister chromatid separation (Hagting et al., 2002; Lu et al., 2014). Which mechanism translates the slow degradation of securin into the switch-like behaviour of sister chromatid separation has remained largely unknown, but positive feedback has been suggested to play a role (Holt et al., 2008). We determined the degradation kinetics of securin relative to sister chromatid separation in single fission yeast cells. The measurements revealed that securin degradation takes about 3.5 minutes. Sister chromatid separation occurred after 1.5 – 2 minutes when 25 – 40 % of securin had been destroyed (part 2.1, Supplementary Figure 1 A – D). We next compared the securin degradation kinetics to the time window in which sister chromatids of different chromosomes split. To this end we fluorescently labelled the region close to the centromere of each chromosome with GFP or tdTomato (part 2.1, Figure 1 A – C) and measured the time window of separation for two chromosomes at a time. The measured values were normally distributed with a mean close to 0 seconds (reflecting simultaneous sister chromatid separation) and with a standard deviation of about 10 – 15 seconds (part 2.1, Figure 1 D and E). Hence, similar to other organisms sister chromatid separation occurs on a faster time scale than securin degradation. For several organisms it had been suggested that the segregation of chromosomes exhibits a certain degree of order (Gerlich et al., 2003; Holt et al., 2008; Vig, 1983); yet, the issue has remained controversial (Lyons and Morgan, 2011). The differential labelling of the chromosomes allowed us to determine the order in which the chromosomes segregated in fission yeast: For neither of the chromosome pairs that we studied we found a strict order. Nevertheless, we observed a slight but significant preference for chromosome I segregating earlier and chromosome III segregating later than chromosome II (part 2.1, Figure 1 E and Supplementary Figure 1 E). These findings suggested that stochastic processes

dominate the timing and order of sister chromatid separation, but that some intrinsic properties might create an additional bias in chromosome segregation.

3.1.2 Stochastic modelling of sister chromatid separation in fission yeast

In order to account for the stochasticity, we computationally modelled the loss of cohesin from two chromosomes. We assumed that the probability that a cohesin molecule on a chromosome is cleaved depends on the amount of separase, the number of cohesin molecules on each of the chromosomes and on the reaction constant of the cohesin cleavage. Sister chromatid separation for an individual chromosome is assumed to occur, when a defined threshold of cohesin molecules has been reached. Subsequently, the time difference between sister chromatid separation of the two chromosomes was calculated. Assuming an initially equal amount of cohesin on each chromosome, the simulation for the time window in which the chromosomes separated, yielded a Gaussian distribution with a mean of 0 seconds. Yet, we noticed that a model that allowed rapid diffusion of separase from one chromosome to the other exhibited very little variation in the time difference of sister chromatid separation between different chromosomes (part 2.1, Supplementary Figure 2 A – C). In such a model, variance created during the early steps of cohesin cleavage, when the number of active separase molecules is low, is efficiently buffered because separase cleavage is more likely to occur on the chromosome that is left with higher cohesin levels at a given time. The variance only significantly increases again when the number of cohesin molecules approaches zero and is determined by the level of active separase when the last few cohesin molecules are cleaved (part 2.1, Supplementary information and Supplementary Figure 2 C). As a consequence, we would need to assume that the chromosomes are stripped of virtually 100 % of cohesin before sister chromatid separation occurs in order to yield a variance comparable to the one we had observed in our experiments. Considering the spindle pulling forces acting on the kinetochore of each sister chromatid it seemed unlikely that a few cohesin complexes would be able to resist this force (Tanaka et al., 1999; Tanaka et al., 2000). This is further supported by findings that already partial depletion of cohesin subunits cause pronounced defects in sister chromatid cohesion (Feytout et al., 2011; Kawashima et al., 2007). Hence, we hypothesized that other processes contributed to the observed higher stochasticity in the timing of sister chromatid separation. Because the assumed free diffusion of separase acts as an efficient buffer against variability in our model, we decided to test a model were separase diffusion is restricted. Free separase is now

assumed to first stochastically associate with one of the chromosomes and only then the chromosome-associated pool of separase cleaves cohesin specific to this chromosome. This idea is supported by experimental findings in human cells that separase associates with chromosomal DNA, which enhances its ability to efficiently cleave cohesin (Sun et al., 2009). The stochastic association of separase to chromosomes induces strong variability early during the cohesin cleavage process and initial biases in separase load only become corrected slowly over time (see the time courses of cohesin loss shown in part 2.1, Supplementary Figure 2 E). Hence, the implemented changes resulted in a larger variance in the time of sister chromatid separation and the variance was now large independently of whether one assumed that sister chromatid separation occurred with 5 or 200 cohesin complexes remaining on the chromosome (part 2.1, Supplementary Figure 2 D – F). This model exhibits another interesting feature: Disparities in the amount of separase associated with each chromosome are more likely to occur when few separase molecules are available. Because initial disparities are only slowly compensated by the increasing amounts of separase on both chromosomes in this model, the variance associated with the initial release kinetic is propagated over a significant time period. Hence, the initial kinetic of separase release becomes a determinant of the variance. This stands in contrast to our first model, where the initial release kinetics of separase did not impact the variance observed when the chromosomes separate (part 2.1, Supplementary Figure 2 G). Whether the variability is created early and propagated or is a result of the separase availability at sister chromatid separation will not be trivial to distinguish experimentally. Most of the perturbations which alter the initial release kinetic might also subsequently alter the amount of available separase at the time of sister chromatid separation and hence might not be able to distinguish between the models. Yet, our simulations suggest that in particular the rate of securin association relative to the rate of cohesin cleavage determines which factor dominates the variance. If the association of separase with the chromosomes is relatively slow but cohesin cleavage is fast, the initial kinetic of separase release will be critical for the variance. If separase association/dissociation is fast and cohesin cleavage is slow, the level of separase at sister chromatid separation will be decisive. Hence, a promising approach might be to study the spatio-dynamical behaviour of separase in more detail. How much separase and how fast is separase associating with chromosomes? How stable is separase association with the chromosomes? Measuring the turnover of separase on chromosomes by employing fluorescence-

recovery after photobleaching (FRAP) and its nucleoplasmic dynamic using fluorescence loss in photobleaching (FLIP) might help to shed light into these questions. This approach might also help to understand, why the system exhibits a higher stochasticity than our simple model suggested to be necessary. Separase association with DNA has been suggested to increase its proteolytic activity towards cohesin (Sun et al., 2009). Maybe the association of separase with the chromosomes provides additional advantages, which outweigh the disadvantages of a higher variability created by an additional stochastic reaction step.

Additionally, in both models, separase activity (defined by the reaction constant) is another determining factor of the variance (part 2.1, Figure 1 F). This is consistent with our finding that a temperature-sensitive separase mutant (*cut1-206*) with impaired catalytic activity at 30 °C exhibits a significant broadening of the distribution of time differences of sister chromatid separation between different chromosomes *in vivo* (part 2.1, Figure 1 G).

3.1.3 Cyclin B degradation is largely dispensable for synchronous sister chromatid separation

In budding yeast, it has been proposed that a feedback loop enhances the synchronicity of sister chromatid separation (Holt et al., 2008): CDK1-mediated phosphorylation of securin attenuates its initial degradation. Once some separase becomes active, it releases Cdc14 from its nucleolar sequestration. Cdc14 subsequently dephosphorylates securin, thereby accelerating securin's degradation and the release of more separase. Two clear predictions for the system's behaviour in the presence of such a feedback can be derived: 1) If CDK1 activity persists, securin should be constitutively phosphorylated; this would lead to slower degradation of securin and hence, less synchronous sister chromatid separation. 2) If the phosphatase is never activated by separase securin degradation should be attenuated (part 2.1, Figure 2 D and E). We tested both these predictions in fission yeast. We expressed an N-terminally truncated version of cyclin B, which can not be targeted for proteasomal degradation. Expression of this non-degradable version of cyclin B blocks mitotic exit, but sister chromatids nevertheless separate (Yamano et al., 1996). The kinetics of securin degradation as well as the synchronicity of sister chromatid separation were only marginally changed in the presence of non-degradable cyclin B (part 2.1, Figure 2 A – C, Supplementary Figure 3 A). The slight broadening of the distribution, which we observed, might reflect a minor contribution of cyclin B degradation towards synchronous sister chromatid separation. On the

other hand the broadening might be the result of impaired velocity of the chromosome movement in anaphase A in the presence of high CDK1 activity as has been observed in flies (Oliveira et al., 2010). Furthermore, we can not exclude that the indestructible cyclin B version, despite lacking the main recognition site for APC/C^{Cdc20}-mediated degradation, is still weakly competing with securin for binding to the APC/C. Indeed factors independent of the N-terminus have been identified to enhance APC/C^{Cdc20} binding (Matsusaka et al., 2014). Expressing a non-degradable version of cyclin B, which is not able to bind CDK1 might be able to distinguish between these possibilities. If expression of this construct also leads to slightly less synchronous sister chromatid separation, then this effect is probably due to competition with securin degradation and is not a consequence of persistent CDK1 activity when expressing non-degradable cyclin B. Overall, we can at present not exclude that CDK1 plays a minor role, but in contrast to budding yeast (Holt et al., 2008) cyclin B degradation is largely dispensable for normal securin degradation and a high synchronicity of sister chromatid separation. We additionally addressed whether separase release influences the securin degradation kinetics by expressing a non-degradable version of securin. Despite the failure to separate their sister chromatids in the presence of the indestructible securin, cells degraded a wild type version of securin-GFP with kinetics that were indistinguishable from the kinetics in cells without non-degradable securin (part 2.1, Figure 2 F and G). Hence, even if CDK1 activity should play a minor role, we do not see any evidence for separase-mediated feedback (part 2.1, Figure 2 F and G).

3.1.4 Securin degradation kinetics influence the synchronicity of sister chromatid separation

Although we did not find any evidence supporting a positive feedback loop similar to the one described in budding yeast, it was still possible that some other mechanism was increasing the activity of separase after its initial release from securin, e.g. in human cells separase is not only cleaving cohesin but also cleaves itself (Chestukhin et al., 2003; Waizenegger et al., 2002; Zou et al., 2002) and in fission yeast large oligomers of separase have been isolated (Funabiki et al., 1996a). Although neither of these mechanisms has been described to influence separase activation or sister chromatid separation so far, they have the potential to introduce nonlinearity into separase activation. We reasoned that if any nonlinearity existed downstream of separase release, the synchronicity of sister chromatid separation should be more robust against changes in the securin degradation kinetics than in the absence of

feedback (part 2.1, Figure 3 A – F). We tested this prediction by attenuating securin degradation using either a temperature-sensitive mutant of one of the APC/C subunits (*cut9-665*) or by partially inhibiting the proteasome using a small molecule inhibitor (Velcade/Bortezomib). Both approaches resulted in a pronounced decrease in the velocity of securin degradation (part 2.1, Supplementary Figure 3 B – D), which was accompanied by a severe broadening of the distributions of time differences between two chromosomes separating (part 2.1, Figure G and H). The slower the kinetic of securin degradation the stronger was the broadening of the distribution (part 2.1, Figure I and Supplementary Figure 3 B – D). Hence, synchronicity of sister chromatid separation is strongly determined by the degradation kinetic of the separase inhibitor securin. These findings make nonlinear activation downstream of securin degradation unlikely. Clearly, if such nonlinear step in separase activation existed, it is not able to efficiently buffer the system against changes in the securin kinetics.

3.1.5 Attenuation of securin degradation increases the segregation bias

In wild type cells, we had observed a small but reproducible segregation bias for chromosome I segregating earlier than chromosome II and chromosome III segregating later than chromosome II. With a mean difference of 11 seconds the bias for chromosome III was slightly more prominent than the mean bias of 5-6 seconds between chromosome I and II. Interestingly, we observed a significant increase in the segregation bias between chromosome II and chromosome III, but not for chromosome I and II when separase activity or securin degradation was impaired (part 2.1, Figure 4 A and B). Using our stochastic model, we investigated potential factors, which could be responsible for the observed biases. We find that when we allow the number of cohesin molecules to vary between the two simulated chromosomes, the simulations still yield Gaussian distributions for the time difference between the two chromosomes segregating but the mean of the distribution is no longer 0. Instead the chromosome with the lower cohesin load segregates on average earlier. Furthermore, the bias increases with an increasing ratio between the cohesin loads on the different chromosomes (part 2.1, Figure 4 D). Varying the degradation kinetic in addition to the cohesin ratio showed that in such a scenario decreasing kinetics would also increase the mean difference in segregation (part 2.1, Figure 4 C and D). We can only speculate about whether differential cohesin loads on the chromosomes are indeed the source of the observed bias in chromosome segregation. Although chromosome I is the largest and chromosome III is the

smallest chromosome, the sizes of the centromeric regions inversely correlate with the sizes of the chromosomes. These heterochromatic regions have been found to be particularly rich in cohesin (Schmidt et al., 2009; Tomonaga et al., 2000). Because our fluorescent labels locate close to the centromeric regions, it is likely that we observe the differentially fast loss of cohesin from the centromeric regions with our assay. One could address this hypothesis by using an artificial chromosome with a smaller centromeric region (Hahnenberger et al., 1989) and asking whether this mini-chromosome indeed segregates earlier than the other chromosomes. Alternatively, one could try to specifically alter the cohesin load on one of the chromosomes. Artificially recruiting the cohesin loading complex Scc2/Scc4 has been shown to enrich cohesin at the specific genomic locus in budding yeast (Fernius et al., 2013). A similar approach could be adopted for fission yeast. Order in chromosome segregation has been observed in several other organisms (Vig, 1983; Vig and Zinkowski, 1986) and has been suggested to contribute to nuclear organization (Gerlich et al., 2003). Furthermore, a correlation between late segregating chromosomes and certain cancer karyotypes has been pointed out (Vig, 1981, 1983). Whether there is indeed a physiological relevance to the observed order in health or disease remains an intriguing question.

3.1.6 Feedback-independent mechanisms can sharpen separase release

Our findings suggested that feedback was not significantly contributing to the synchronous separation of sister chromatids. Hence, we asked whether feedback-independent mechanisms were able to increase the synchronicity of sister chromatid separation. Our experimental and theoretical considerations had demonstrated that the initial release kinetic of separase and separase activity were the main determinants of the overall variance with which sister chromatids separated. Hence, any mechanism capable of increasing the synchronicity of sister chromatid separation would need to improve one of these two parameters. Because we had not found evidence for a mechanism that enhanced separase activity downstream of its release from securin, we focused on mechanisms that could enhance the release kinetic of separase. Inhibitor sequestration has been shown to create ultrasensitive responses in other biological contexts (Buchler and Cross, 2009; Legewie et al., 2008). We reasoned that a similar mechanism could act on separase release: If the association constant is high, separase is quickly resequestered by free securin as long as the inhibitor securin is in excess over separase. Only after the access pool of securin is depleted separase is released. At this point the bound securin does not

have to compete with the unbound pool of securin anymore. Hence, the degradation of the remaining securin and with it the release of separase exhibit a faster kinetic (part 2.1, Figure 5 A and B). Alternatively, an increase in the release kinetic of separase can be achieved by a preferential degradation of the unbound, excess pool of securin. The preferential degradation of the excess pool of securin prevents that this pool competes with the bound securin pool for degradation later (part 2.1, Figure 5 D and E). Indeed, preferential degradation has been reported in human cells (Hellmuth et al., 2014). Both these mechanisms were able to increase the synchronicity of sister chromatid separation in our stochastic simulations. In addition to providing a higher synchronicity these mechanisms are also able to provide more robustness against precocious activation of separase. By ensuring that a significant amount of securin has to be degraded before separase is released, they might provide a buffer against weak, basal levels of APC/C activity in early prometaphase or inefficient inhibition of the APC/C by the spindle assembly checkpoint. So far it has remained unclear whether separase once released from securin can be rebound and whether the rebinding kinetics is sufficiently fast to be relevant during the metaphase to anaphase transition. We have tried to explore this question by immobilizing separase in the cell and then measuring the turn over of securin-GFP on the immobilized separase during the metaphase to anaphase transition. Despite promising initial trials technical challenges have hindered us from making reliable conclusions about the kinetics. Alternatively, one could try to measure directly how long and how much of the securin/separase complex persists after securin degradation has started. This has only been done in population experiments using separase immunoprecipitations from synchronized cell extracts in human cells (Hellmuth et al., 2014; Shindo et al., 2012). A single cell imaging assay would provide a better temporal resolution, e.g. following the amount of complex over time by techniques based on Foerster resonance energy transfer (FRET). Yet, in fission yeast separase is not very abundant (approximately 300 molecules in the mitotic nucleus, part 2.2, Figure Supplementary Figure 5B): whether despite this low abundance sufficient FRET signal will be detectable remains to be tested.

3.2 Properties of the degradation machinery ensure temporal coupling during the metaphase to anaphase transition (results part 2.2 and 2.3)

3.2.1 Robustness of the metaphase to anaphase transition in the absence of crosstalk

The APC/C-mediated degradation of securin and cyclin B drives the metaphase to anaphase transition. Destruction of securin releases separase from its inhibition and thereby promotes sister chromatid separation. Destruction of cyclin B on the other hand orchestrates a multitude of events during mitotic exit, including stabilization of the kinetochore-microtubule interactions, mitotic checkpoint inactivation, spindle elongation, chromosome decondensation and cytokinesis. Especially in the early phases of the metaphase to anaphase transition some of the events that depend on cyclin B degradation need to be tightly coordinated with sister chromatid separation. For example, it is thought that kinetochore-microtubule interactions need to be stabilized and the mitotic checkpoint inactivated prior to sister chromatid separation in order to prevent untimely actions of the mitotic checkpoint machinery in anaphase and loss of genomic integrity (Oliveira and Nasmyth, 2010; Vázquez-Novelle et al., 2010). Indeed, artificially stabilized CDK1 activity results in unstable kinetochore-microtubule interactions and untimely checkpoint signalling in anaphase (part 2.3, (Oliveira et al., 2010; Parry et al., 2003; Rattani et al., 2014; Vazquez-Novelle et al., 2014)). Other events driven by the loss of CDK1 activity, such as the establishment of the midspindle and spindle elongation in anaphase B have to occur shortly after sister chromatid separation (Sullivan and Morgan, 2007). Yet other events should only happen once the sister chromatids have been securely segregated into two newly arising daughter nuclei, e.g. the disassembly of the kinetochore or chromatin decondensation. Little is known about which mechanisms ensure the order in which these cyclin B degradation-dependent events occur and how the timing of these events is coordinated relative to sister chromatid separation. In budding yeast it was shown that the changing ratio between CDK1 activity and its counteracting phosphatase Cdc14 defines phosphorylation thresholds for distinct proteins. Proteins that need to become dephosphorylated early in order to drive events early in mitotic exit become readily desphosphorylated at high CDK1 activity and low Cdc14 level. On the other hand, proteins that are important for later processes exhibit low affinity towards Cdc14 and hence become dephosphorylated late (Bouchoux and Uhlmann,

2011). Similarly, for sister chromatid separation it seemed conceivable that the ratio between separase and its inhibitor securin, which is present in excess over separase (Hellmuth et al., 2014; Holland and Taylor, 2006; Shindo et al., 2012), sets the threshold at which sister chromatid separation occurs. Yet, if the ratios between cyclin B/CDK1 and the counteracting phosphatases on the one hand and securin and separase on the other hand define the timing of mitotic exit events and sister chromatid separation respectively, protein fluctuation affecting only one of the proteins will alter the timing of events in one pathway but not in the other. In this case, the temporal order of the events during the metaphase to anaphase transition might be lost and genomic integrity at risk. However, we found that fission yeast cells are astonishingly robust against changes in the protein levels of cyclin B and securin (part 2.2, Figure 1). Neither 8-fold overexpression of securin nor 20-fold overexpression of cyclin B impaired cell viability (part 2.2, Figure 1 F – G). This is consistent with a large-scale study in fission yeast, which had determined the expression limits at which cells start to lose fitness to be 32-times the wild-type amount of securin and 5-times the wild-type amount of cyclin B (Moriya et al., 2011). We also detected that the cyclin B protein level can vary considerably *in vivo*: Prolonged cell cycle arrest in G2, provoked by DNA damaging agents, or blocking the G2/M transition using the temperature-sensitive allele *cdc25-22*, increased the abundance of cyclin B up to 3-fold (part 2.2, Figure 1 C), whereas the abundance of securin was not greatly affected. Nevertheless, cells released from the arrest progress through mitosis normally (part 2.2, Supplementary Figure S1 C,F). Similarly, it was reported that stress induced by high osmolarity, salt or divalent cations resulted in a prominent increase in securin abundance (Kawasaki et al., 2006). In order to explain this astonishing robustness of the metaphase to anaphase transition against different securin and cyclin B protein levels, we hypothesized that additional mechanisms were in place to ensure that the temporal order of events during the metaphase to anaphase transition was maintained.

Several organisms have evolved crosstalk between the securin and the cyclin B degradation pathways: In budding yeast, separase directly activates the Cdc14 phosphatase, which is essential for mitotic exit (Stegmeier and Amon, 2004). In vertebrates, mutual inhibition of cyclin B and separase has been demonstrated (Gorr et al., 2005). Although in human cells the inhibition is not sufficiently strong to completely block sister chromatid separation in the presence of endogenous levels of non-degradable cyclin B (Wolf et al., 2006), inhibition of localized pools of cyclin

B/CDK1 might contribute to the temporal coordination of specific processes during the metaphase to anaphase transition (Shindo et al., 2012). Hence, both these mechanisms have the potential to maintain the order of securin and cyclin B degradation-dependent events, even if significant changes in protein abundance occur. In fission yeast, it was unclear whether crosstalk between the pathways was present. Previous studies had shown that sister chromatid separation takes place even when cyclin B is not degraded (Yamano et al., 1996), and vice versa cells undergo mitotic exit independently of sister chromatid separation when securin is not degraded (Funabiki et al., 1996b). Nevertheless, it was still possible that crosstalk existed: Maybe the crosstalk was not sufficiently strong to fully prevent sister chromatid separation in the presence of non-degradable cyclin B, but was still capable to induce a significant time delay in sister chromatid separation to allow the delayed cyclin B degradation to catch up. To address this question we developed a single cell imaging assay that allowed us to measure the timing of sister chromatid separation relative to a cyclin B-degradation dependent event (the removal of the polo-kinase Plo1 from the spindle pole bodies (Dischinger et al., 2008; Mulvihill et al., 1999)).

We detected a slight delay in sister chromatid separation after blocking mitotic exit by expressing a non-degradable version of cyclin B (ΔN-Cdc13, part 2.2, Figure 2 A and B). This is consistent with our previous results showing that the expression of the non-degradable cyclin B version causes a slight broadening in the time window of sister chromatid separation (part 2.1, Figure 2) and a slight decrease in the securin degradation rate (part 2.1, Supplementary Figure 3A). As discussed in chapter 3.1.3 we are not certain whether this effect is an indication for some weak cross-talk between the pathways or can be ascribed to a weak competition between the ΔN-Cdc13 construct and securin for binding the APC/C^{Cdc20}. On the other hand, preventing securin degradation and the release of active separase by expressing a non-degradable version of securin did not alter the timing of Plo1 removal (part 2.2, Figure 2 A, C). These data suggested that the pathways of securin and cyclin B degradation indeed act largely independently. Hence, mechanisms other than crosstalk might be responsible for the robustness of the metaphase to anaphase transition against protein fluctuations that others and we observed.

3.2.2 Events of the metaphase to anaphase transition maintain temporal order when cyclin B or securin levels are raised

Several scenarios could explain the robustness of the metaphase to anaphase transition against protein abundance fluctuations: 1) Changes in protein abundances do not result in a delay of the downstream events. 2) The downstream events are spaced far enough apart in time, so that protein fluctuations of one protein and the resulting delays of the downstream events do not jeopardize the overall order of anaphase events. 3) In contrast to our initial line of thought, a strict order of events does not need to be maintained. 4) The two pathways are coupled by a mechanism, which has not become evident in our experiments, when using the non-degradable versions of cyclin B and securin.

To distinguish between these possibilities we carefully measured the timing of sister chromatid separation relative to Plo1 removal in the strains overexpressing securin or cyclin B. We observed a pronounced delay in the removal of Plo1 from spindle pole bodies when cyclin B was overexpressed (part 2.2, Figure 3 A). Similarly, overexpression of securin resulted in a dose-dependent delay in sister chromatid separation (part 2.2, Figure 3 D). Hence, changes in protein abundance clearly delay the direct downstream events. Interestingly, cyclin B overexpression also resulted in a pronounced delay in sister chromatid separation and securin overexpression delayed Plo1 removal (part 2.2, Figure 3 B, E). As a consequence, the timing between sister chromatid separation and Plo1 removal remained almost constant in all strains, despite an overall delay of as long as 8 minutes in the cyclin B overexpression (part 2.2, Figure 3 C, F). This suggested that the timing of the events was coupled by some as yet uncharacterized mechanism. Consistent with this idea, we also found a correlation between the timing of sister chromatid separation and the timing of Plo1 removal within single cells (part 2.2, Figure 3 G and H). The observed temporal correlation between securin and cyclin B degradation-dependent events could theoretically be caused by a delayed onset of APC/C activity, e.g. because it takes these cells longer to achieve proper chromosome attachment. Importantly, the correlation was still seen when the time from the start of securin degradation to sister chromatid separation or Plo1 removal was determined (part 2.2, Figure 3 I and Supplementary Figure 2 B and C). This argued for a mechanism that directly acted during the metaphase to anaphase transition after the APC/C has become active.

3.2.3 Competition can provide temporal coupling

Competition for a shared enzymatic process has been suggested to establish crosstalk between two otherwise independent pathways (Cookson et al., 2011). If two protein species share the same degradation machinery and compete for binding to the degradation enzyme, a high abundance of one species is going to outcompete and thereby attenuate the degradation of the other species. As a consequence, the abundance of the second species increases until it is able to sufficiently compete with the first species. This mechanism can provide a fast, adaptive response to protein fluctuations and hence, co-regulate protein levels in the absence of direct crosstalk (Cookson et al., 2011; Prindle et al., 2014).

During interphase the levels of securin and cyclin B are determined by the basal rates of synthesis and degradation. Hence, competition for a shared basal degradation machinery could provide co-regulation of the securin and cyclin B abundances, which would subsequently result in correlated delays in sister chromatid separation and mitotic exit. Indeed in mouse oocytes it was noticed that the steady-state level of cyclin B and securin co-vary. Overexpression of securin increased the cyclin B level, whereas depletion of securin reduced the cyclin B level in interphase (Marangos and Carroll, 2008). We did not find evidence for a similar co-regulation of the steady-state level in fission yeast. Securin or cyclin B levels were unaltered in the strains overexpressing cyclin B or securin, respectively (part 2.2, Figure 1 C – E).

We hypothesized that even if co-regulation by competition did not act on the level of the basal turnover, it could still have a significant contribution during the APC/C-mediated degradation. To determine whether the abundances of securin, cyclin B, the APC/C and Slp1 (the *S. pombe* Cdc20 ortholog) are consistent with competition taking place, we measured their abundance on the population and single-cell level. Using quantitative immunoblotting against recombinant protein standards, we determined the concentrations for securin (18.5 nM +/- 6.6 nM, part 2.2 Figure 1 B and Supplementary Figure S1A), cyclin B (187.6 nM +/- 27.7 nM, part 2.2 Figure 1 B and Supplementary Figure S1A – B) and the APC/C co-activator Slp1 (49.5 nM +/- 17.8 nM, part 2.3, Supplementary Figure S7E). Furthermore, using comparative fluorescence microscopy of single cells we independently determined the nuclear mitotic concentrations of the fluorescently labelled versions of securin (98.2 nM +/- 13.3 nM, part 2.2, Supplementary Figure S5B), separase (51 nM +/- 12 nM, part 2.2, Supplementary Figure S5B), and the APC/C subunits Apc5 (52 nM +/- 28 nM, part 2.3, Figure 1 and Supplementary Table 1) and Apc15 (53 nM +/- 17 nM, part 2.3,

Figure 1 and Supplementary Table 1). We found that cyclin B is approximately in 10-fold excess over securin, which is consistent with previous large-scale studies employing mass spectrometric quantification methods (Carpy et al., 2014; Kulak et al., 2014; Marguerat et al., 2012). We were not able to determine the nuclear concentration of cyclin B, because all our attempts to generate a functional fluorescently labelled cyclin B-fusion protein failed (part 2.2, Supplementary Figure S1E). Yet, previous studies employing immunofluorescence suggested that, similar to securin, cyclin B is enriched in the mitotic nucleus (Alfa et al., 1990). We therefore assume that the overall ratio of securin and cyclin B will also be reflected in the nuclear concentrations. This would suggest there is about 1 μM of substrates and 20 – 50 nM of the APC/C^{Cdc20} present in the mitotic fission yeast nucleus.

Based on our kinetic measurements of securin degradation (part 2.1) and the protein concentration measurements we developed a deterministic model, in which securin and cyclin B compete for binding to the APC/C (part 2.2, Figure 4 A). Note that because the non-degradable versions of cyclin B and securin lack the N-terminal motifs that are essential for the interaction with the APC/C^{Cdc20} these constructs would not be able to compete and hence, consistent with our observations, would not show significant crosstalk. The model predicted that, with the given parameters, competition between securin and cyclin B resulted in an attenuation of securin degradation when the cyclin B level was increased and vice versa (part 2.2, Figure 4 B,C). We confirmed this prediction by showing that the securin degradation kinetic was indeed decreased when cyclin B was overexpressed (part 2.2, Figure 4 D). The observed decrease in degradation kinetics matched well with the previously observed delay in sister chromatid separation (compare part 2.2, Figure 3 B, 4 E and Supplementary Figure 3A).

3.2.4 Securin and cyclin B might exhibit different affinities towards the APC/C^{Cdc20}

The competition model that we developed was able to qualitatively account for the delay of sister chromatid separation in response to cyclin B overexpression and vice versa. In order to address whether such a model was also able to reflect the system's behaviour in quantitative terms, we estimated the free parameters to fit the kinetics of securin degradation in the different overexpressions of securin and cyclin B. Based on the similarity of the N-terminal recognition motifs, we had initially assumed equal affinities of securin and cyclin B towards the APC/C^{Cdc20}. In contrast, in order to fit the experimental data, a lower affinity (roughly a 5 – 6 times higher K_m value) of cyclin B

towards the APC/C^{Cdc20} was required. The enzymatic activity and affinity of the APC/C towards its substrates securin and cyclin B have been extensively studied (Matyskiela and Morgan, 2009; Rape et al., 2006; Zeng and King, 2012). Nevertheless comparative quantitative studies of the securin and cyclin B affinities towards the APC/^{Cdc20} are not available. For technical reasons many studies employ the more stable and more easily purifiable APC/C^{Cdh1} complex. Most studies also use only the N-terminal regions of either securin or cyclin B as substrate, although several studies have indicated that other factors and co-factors contribute to efficient substrate ubiquitinylation *in vivo* (Matsusaka et al., 2014; van Zon et al., 2010). Our model predicted that - as a consequence of the lower affinity of cyclin B - the 8-fold overexpression of securin would not strongly alter the cyclin B degradation kinetics. Because of the inability to label cyclin B fluorescently, we were only able to test this prediction by comparing the cyclin B degradation kinetics in the presence or absence of securin overexpression by immunoblotting extracts from a synchronized cell culture. We did not detect an obvious change in the kinetics (part 2.2, Supplementary Figure S4 E – G). Yet, due to the limitations in the temporal resolution of this approach, the result only indicates that no major delay in cyclin B degradation occurs but smaller delays are not ruled out.

To address the true affinities of the complexes *in vivo,* more sophisticated biochemical approaches will be necessary. One possible approach could be to immobilize recombinant, catalytically inactive APC/C on the surface of a flow cell and to incubate it with mitotic extracts from cells expressing securin- or cyclin B-GFP. By measuring the increase of signal on the surface one might be able to follow the binding reaction (similar to (Simonetta et al., 2009)). It needs to be tested, whether the signal intensity gained from the binding of the endogenously expressed proteins is sufficient to yield reliable measurements in such a set up.

3.2.5 Adaptive thresholds provide additional temporal robustness during the metaphase to anaphase transition

So far we had assumed that sister chromatid separation and Plo1 removal occur when securin and cyclin B level have been reduced to a defined threshold (see 3.2.1 for the reasoning). Under this assumption, securin overexpression delays sister chromatid separation exactly by the time that is required to degrade the additional excess of securin over the wild type amount. Hence, the time that it takes for cyclin B to reach the threshold for Plo1 removal would need to be delayed by the same amount of time, in order to explain the invariance in the timing between sister

chromatid separation and Plo1 removal in the securin overexpressions (part 2.2, Figure 3C and F). Yet, in all our models, overexpression of one protein was delaying the time of its direct downstream events more strongly than the events of the parallel pathway (part 2.2, Figure 4 F – G). Hence, under the assumption of defined concentration thresholds, a competition model provides some degree of temporal coupling, but is not able to ensure a robust timing and order of events over a larger range of protein abundance changes (part 2.2, Figure 4 H).

We therefore asked whether our assumption of fixed thresholds was correct. We measured the securin degradation dynamics relative to the occurrence of sister chromatid separation in the strains with differently high securin-GFP abundances. These measurements revealed that sister chromatid separation did not occur at a fixed concentration threshold of securin, instead the amount of securin remaining at the time of sister chromatid separation scaled with the initial amount of securin in metaphase. This correlation was observed not only on the population level but also on the single cell level (part 2.2, Figure 5 A and B). Intriguingly, in the strains overexpressing securin, sister chromatid separation occurred at a concentration of securin, which in a wild type cell would have been sufficient for robust inhibition of separase. Besides being the inhibitor of separase, securin also functions as a chaperone and mitotic import factor for separase in fission yeast (Kumada et al., 1998). Hence, it was possible that the increased level of securin also increased the nuclear concentration of separase in mitosis. If the nuclear separase level was increased concomitantly with the securin level then not as much securin would need to be degraded until separase was released and sister chromatid separation occurred. Yet, we did not detect an overall change in the cellular separase concentration in the strains overexpressing securin and only a slight increase in the nuclear concentration of separase (part 2.2, Figure 5 C – E and Supplementary Figure 5 A). This slight increase is insufficient to account for the considerable shifts in the threshold. The observed threshold shifts could also be explained if the degradation of securin-GFP generated a fluorescent, but non-functional degradation intermediate whose abundance depends on the initial securin-GFP level. We do not think that this is the case, because we did not detect any intermediate fragments of securin-GFP when following securin degradation of a synchronized cell culture by immunoblotting using a GFP antibody (part 2.2, Supplementary Figure 2C). Furthermore, we compared the mitotic progression of synchronized cell cultures that were either expressing untagged wild type securin or overexpressing untagged

securin to 8-fold the wild type level. Consistent with our imaging data, sister chromatid separation occurred at a higher cellular securin concentration in the strain overexpressing securin (part 2.2, Supplementary Figure 4 E and G).

The finding that the threshold at which sister chromatid separation occurs is variable has also been underscored by introducing other perturbations to the system: Attenuating the kinetics of securin degradation by APC/C inhibition, proteasome inhibition or cyclin B overexpression resulted in sister chromatid separation occurring at lower thresholds (part 2.2, Figure 5 G and H, Supplementary Figure 5 E, F, I and J, and Figure 4 D, respectively). In more general terms a faster securin degradation rate, e.g. as a consequence of higher initial securin level (see part 2.2, Supplementary Figure 5D), resulted in sister chromatid separation taking place at higher securin level, while a lower securin degradation rate resulted in sister chromatid separation taking place at lower securin level (part 2.2, Figure 5 I).

Interestingly, analytical considerations for how temporal invariance could be established on the basis of our competition model, exactly predicted these experimentally observed correlations (part 2.2, Supplementary Information and Figure 5 J and K). For example, in cells overexpressing securin this scaling of the thresholds in response to the faster degradation kinetic would result in an upshift of the threshold for sister chromatid separation (as observed). At the same time, the cyclin B degradation kinetics become attenuated because of the larger abundance of securin. As a consequence of the slower degradation of cyclin B the threshold at which Plo1 removal occurs is downshifted (part 2.2, Figure 5 K). In this way, the combination of competition for the degradation machinery and thresholds which adapt to the degradation kinetics of the upstream regulator have the potential to establish an invariant order of events during the metaphase to anaphase transition.

Currently, we are not able to demonstrate whether such a scaling of the threshold as we have observed for securin and securin degradation-dependent processes also exists for cyclin B and cyclin B degradation-dependent processes - as our theoretical considerations would suggest (see also part 2.2, Figure 5K). We have been unable to create a functional fusion protein between cyclin B and a fluorescent protein, which would enable us to follow the cyclin B degradation kinetic and the level at which certain downstream events occur by live cell imaging in single cells. Nevertheless, this would be an important experimental confirmation and alternative fusion constructs, where the GFP moiety is inserted into different internal sites of cyclin B, should be tested.

Furthermore, we have started to address the question which molecular mechanisms could be responsible for the observed threshold shifts and the temporal invariance. To this end, we have implemented a comprehensive computational model of the interactions and dynamics describing the metaphase to anaphase transition and screened for parameters capable of describing our experimental results. Two mechanisms are able to describe the observed shifts in the securin threshold at which sister chromatid separation occurs: a) slow rebinding kinetics of securin to separase or b) inactivation of securin by ubiquitinylation prior to its proteasomal degradation. These mechanisms have in common that the effective pool of inhibitory securin is decreased ahead of securin degradation. In the first case, due to the slow rebinding kinetics, separase released from its inhibition by securin is not effectively recaptured by free securin molecules that are still available. Therefore, separase becomes active despite the presence of free inhibitor. In the second case, ubiquitinylation of the excess securin renders a fraction of the inhibitor pool incapable of re-inhibiting the released separase and hence separase becomes active in the presence of a substantial amount of free securin. If securin is overexpressed these pools of securin would increase proportionally and therefore sister chromatid separation would take place at higher securin concentrations as we have observed. Gaining knowledge about the rebinding kinetics of securin to separase during the metaphase to anaphase transition, as discussed in part 3.1.6, would be of great help to distinguish between the different mechanisms. This could be substantiated by biochemical assays in which the ability of securin or ubiquitinylated securin to bind to free separase is tested *in vitro*. Furthermore, our preliminary analyses suggest that preferential degradation of the unbound pools of cyclin B and securin could also provide a mean to ensure temporal robustness against protein abundance fluctuations. This is particularly interesting because we have already discussed the potential of preferential degradation of the unbound securin pool in contributing to the synchronous splitting of sister chromatid separation (part 3.1). For fission yeast cyclin B it has been shown that a cyclin B-CDK1 fusion protein is viable (Coudreuse and Nurse, 2010). If indeed the preferential degradation of the free cyclin B pool was important for the robustness of the metaphase to anaphase transition, one would predict that a strain expressing the fusion protein might exhibit a higher sensitivity to changes in the protein abundances. Comparing the degradation kinetic of this constitutively complexed cyclin B to a version of cyclin B that is not able to bind

CDK1 could further give insight into whether the bound and unbound pool of cyclin B exhibit different degradation kinetics.

3.2.6 Universality of the observed temporal robustness

We have also started to address the question whether the invariant timing that we observed between sister chromatid separation and Plo1 removal is a universal feature. To this end, we have established an additional imaging assay, where we measure the timing of sister chromatid separation relative to the time of Ase1-GFP recruitment to the midspindle. Ase1 (PRC1 in other organisms) is a component important for proper establishment of the midspindle. Localization of Ase1 has been shown to depend on the dephosphorylation of several CDK1 sites (Fu et al., 2009). Preliminary results suggest that Ase1-GFP starts being recruited to the midspindle prior to sister chromatid separation and that this recruitment might also be delayed in response to securin overexpression (data not shown). Yet, the effect does not seem as pronounced as for Plo1 removal. It will be interesting to address in the future how different cyclin B degradation-dependent events are affected by changes in securin abundance. This will help to characterize the common features and differences in the regulation of different cyclin B degradation-dependent processes and will identify additional regulatory mechanisms that are important to coordinate the events during this important step in the cell cycle.

3.2.7 Limits to the temporal robustness of the metaphase to anaphase transition

We have observed that cyclin B can slow down securin degradation and have established that competition between securin and cyclin B for binding to the APC/C^{Cdc20} can theoretically make the order of events during the metaphase to anaphase transition more robust to abundance changes in the regulatory proteins. Yet, whether this mechanism is indeed important for temporal robustness *in vivo* was not clear. To address this question, we initially attempted to increase the cellular abundance of the APC/C. We hypothesized that a higher abundance of the APC/C would reduce competition between substrates and therefore uncouple the downstream events. Yet, we did not find a successful strategy to induce a higher expression of this multi-subunit complex. As an alternative, we studied the consequences of a temperature-sensitive mutation in the APC/C subunit APC6 (*cut9-665*, (Hirano et al., 1986)). Previous studies suggested that this allele specifically attenuated the degradation of securin (which we had confirmed), but not cyclin B

((Berry et al., 1999; Chang et al., 2001)). Indeed, the timing between sister chromatid separation and Plo1 removal in a strain carrying the mutant allele shortened (part 2.2, Figure 6A). We compared this result to a strain with a lower expression of the APC/C co-activator Cdc20. This strain attenuated securin degradation to a similar extent as the *cut9-665* mutation (part 2.2, Supplementary Figure 5 G and H), but because of the lower overall availability of the co-activator, it is likely to also impact the cyclin B degradation rate. This strain did not show a shortening in the timing (part 2.2, Figure 6 A). The constant timing in this strain suggests that competition is not only able to compensate for fluctuations in cyclin B and securin level, but that variability in the availability of the degradation machinery itself is also buffered.

Interestingly, the *cut9-665* allele exhibits a dose-dependent negative genetic interaction in combination with securin overexpression but not with cyclin B overexpression (part 2.2, Figure 6 B, (Matsumura et al., 2003)). Consistent with the observation that reductions of Cdc20 did not alter the timing, the strain with lower Cdc20 expression did not exhibit any negative interaction with securin or cyclin B. These findings suggest a model in which the affinities of cyclin B and securin are tuned to provide a maximal robustness against protein fluctuations. Altered affinities, as we suggest is the case in the strain expressing the *cut9-665* allele, drastically reduce the ability to compensate for these fluctuations. A securin construct carrying the N-terminal recognition motifs of cyclin B has been shown to rescue the temperature-sensitivity of a securin mutant in fission yeast, but the dynamics of this construct have not been studied (Funabiki et al., 1996b). Because these findings seemingly contradict our prediction that the affinities of securin and cyclin B differ, it would be interesting to study this construct and the inverse construct (the N-terminus of securin fused to cyclin B) in more detail. It is possible that - although essential for the recognition by the APC/C^{Cdc20} - the N-termini are not the pivotal factor that determines binding kinetics and other motifs or co-factors contribute. In this case, one would expect that the chimera do not show altered degradation kinetics. On the other hand, if the kinetics are indeed altered, it will be even more interesting how the system is able to compensate for these changes.

3.3 Slow checkpoint activation kinetics as a safety device in anaphase (results part 2.4)

3.3.1 The checkpoint reengages in anaphase in the presence of high CDK1 activity

In several organisms, preventing the loss of CDK1 activity arrests cells in pseudo-metaphase with short metaphase-like spindles but separated chromosomes (Gallant and Nigg, 1992; Hagting et al., 2002; Holloway et al., 1993; Parry and O'Farrell, 2001; Sigrist et al., 1995; Yamano et al., 1996). The oscillatory movements of the chromosomes that are observed in this situation suggest that kinetochore-microtubule interactions have become unstable. Consistently, proteins involved in spindle assembly checkpoint signalling have been found to enrich at kinetochores in this situation (Mirchenko and Uhlmann, 2010; Oliveira et al., 2010; Parry et al., 2003). Whether this enrichment also leads to the generation of the inhibitory mitotic checkpoint complex (MCC) and to the inactivation of the anaphase-promoting complex/cyclosome (APC/C) had remained controversial. In fission yeast, expression of a non-degradable version of cyclin B (ΔN-cyclin B) also results in a pseudo-metaphase arrest (Yamano et al., 1996). We showed that this arrest is accompanied by frequent dissociation of the chromosomes from the spindle poles indicating unstable MT-KT interactions, and by relocalization of the checkpoint components Mad1, Mad2, Mad3, and Bub3 to the kinetochore. The Aurora B kinase Ark1, which during an unperturbed anaphase translocates to the midspindle, remained associated with the centromeric region (part 2.4, Figure 1 A and B, Supplementary Figure S1), as had been seen in other organisms (Parry et al., 2003; Vazquez-Novelle et al., 2014). Despite these indications that, in the presence of high CDK1 activity, the loss of cohesion has been recognized as erroneous and at least a partial checkpoint response has been triggered, the degradation of the APC/C substrates securin and cyclin B proceeded with unaltered kinetics (part 2.4, Figure 1 D and E). Hence, we asked whether efficient checkpoint signalling was blocked downstream of kinetochore recruitment. However, neither the formation of the mitotic checkpoint complex nor its inhibitory association with the APC/C was abolished (part 2.4, Figure 2 A and Supplementary Figure S2). In budding yeast, separase overexpression is able to override a mitotic checkpoint arrest by precociously initializing the signalling cascade, which drives mitotic exit (Tinker-Kulberg and Morgan, 1999; Visintin et al., 1998). Although mitotic exit is regulated differently in fission and budding yeast

(Bardin and Amon, 2001; Simanis, 2003) and the exact mechanism might not be conserved, it was conceivable that separase activity directly interfered with efficient APC/C inhibition or that cohesin cleavage altered the kinetochore geometry thereby preventing efficient checkpoint signalling. Yet, precocious activation of separase and cohesin cleavage in prometaphase efficiently delayed mitotic progression in a checkpoint-dependent manner (part 2.4, Figure 2 B and C), which argues against a general role of separase in checkpoint inactivation in fission yeast.

As all experiments pointed towards an effective checkpoint signalling in response to high CDK1 activity in anaphase, we revisited our assay of monitoring APC/C activity by following securin degradation. In a wild type cell securin degradation continues for 2 – 4 minutes after sister chromatids separate. If re-inhibition of the APC/C occurrs later than this time window, securin degradation has already run to completion and we would have been unable to observe the inhibition. To extend the time window we increased securin abundance by 8-fold and overexpressed separase. Sister chromatid separation now occurred almost instantaneously with the start of securin degradation and the securin level declined for about 6 – 8 minutes before the substrate was exhausted (part 2.4 Supplementary Figure S3). Intriguingly, in the presence of non-degradable cyclin B securin degradation now stopped earlier and at a higher level of remaining securin, suggesting that APC/C activity was terminated prematurely (part 2.4, Figure 3 A – D). Indeed, abolishing spindle assembly checkpoint signalling by deletion of the checkpoint protein *mad2+* reversed the effect. These findings demonstrate that persistent CDK1 activity in anaphase is sufficient to fully reengage the mitotic checkpoint and block the activity of the APC/C. Similar results have concurrently been presented for human cells in culture (Vazquez-Novelle et al., 2014).

3.3.2 The checkpoint can reactivate after APC/C activation in the absence of non-degradable cyclin B

In the presence of persistent CDK1 activity the checkpoint is reactivated by the loss of tension between sister chromatids at anaphase onset (part 2.4, Figure 1-3, (Mirchenko and Uhlmann, 2010; Vazquez-Novelle et al., 2014)). Yet, during an unperturbed mitosis, when cyclin B is allowed to decline, reactivation of the checkpoint is not observed (part 2.4, Figure 1C and E, uninduced and control respectively). This has lead to the hypothesis that the declining level of cyclin B renders the spindle assembly checkpoint unresponsive by the time of anaphase. Nevertheless at least three studies in human cells suggested that the checkpoint is

able to reengage after cyclin B and securin levels have started to decrease (Clute and Pines, 1999; Dick and Gerlich, 2013; Hagting et al., 2002). We therefore investigated whether in the absence of non-degradable cyclin B it was possible to reengage the checkpoint during the metaphase to anaphase transition in fission yeast. Indeed, we were able to observe that for up to 2 minutes after the securin level had started to decline, destabilizing the mitotic spindle could cause relocalization of Mad2 to the kinetochore and inhibition of the APC/C (part 2.4, Figure 4). The inhibition kinetics were similar to the values we had measured in the presence of non-degradable cyclin B. Furthermore, the time from Mad2 enrichment at the kinetochore to the inhibition of the APC/C did not increase during these two minutes (part 2.4, Figure 4 D). Hence, the spindle assembly checkpoint remains fully responsive for at least some time during the metaphase to anaphase transition.

3.3.3 Error recognition and APC/C inhibition occur on different timescales

When we followed the relocalization of checkpoint proteins in the presence of non-degradable cyclin B in single cells, we had noticed that Mad3, which is most downstream in the recruitment hierarchy of checkpoint proteins (Heinrich et al., 2012), started to significantly enrich at the kinetochore within the first minute after sister chromatids separated. Detachment of chromosomes was only observed at a later time point (on average 5 minutes after separation) (part 2.4, Figure 1 C and Supplementary Figure S1 D). This suggests that the loss of tension due to cohesin cleavage is rapidly recognized and almost instantaneously translated into the recruitment of checkpoint proteins to the kinetochore. Yet, efficient inactivation of the APC/C was only detected after 6.5 minutes on average. This time difference was confirmed by simultaneously monitoring Mad2 relocalization and APC/C inhibition within the same cell (part 2.4, Figure 3 E and F) and in cells where the mitotic spindle was destabilized in early anaphase in the absence of non-degradable cyclin B (part 2.4, Figure 4 D). A recent study in human cells, where microtubule-kinetochore attachment was disrupted during metaphase and early anaphase, reported similarly slow kinetics for APC/C inhibition (Dick and Gerlich, 2013). Because in these situations cells still exhibit high CDK1 activity, it is tempting to speculate that the observed slow inhibition kinetic represents the universal kinetic of checkpoint signalling during prometa- and metaphase. This challenges the general idea that checkpoint signalling is a fast, immediate process. The slow inhibition might reflect kinetic constraints in the synthesis of the inhibitory signal, the mitotic checkpoint complex (MCC). The transition of the open, inactive confirmation of Mad2 into the

closed active confirmation, which binds Cdc20, has been shown to exhibit slow kinetics *in vitro* (Simonetta et al., 2009) and is likely to constitute the rate-limiting step in APC/C inhibition. So far it has not been possible to measure the *in vivo* kinetics of the different steps that lead to the inhibition of the APC/C, e.g. formation of the Mad2-Cdc20 complex, the Mad2-Cdc20-Mad3 complex, or association of the MCC with the APC/C. Biochemical assays to monitor the different complexes, e.g. immunoprecipitations or fractionation by size exclusion, require large amounts of extracts and hence, due to the limitation in synchronizing cell populations, fail to provide sufficient temporal resolution. Live cell imaging assays have the potential to overcome these limitations. Yet, in order to visualize protein-protein interactions over time, sophisticated techniques are required. Förster resonance energy transfer combined with fluorescence-lifetime imaging is a possibility (Sun et al., 2012), but comes with its own limitations and has yet to be applied successfully in the context of the spindle assembly checkpoint.

3.3.4 Timing of checkpoint inactivation

Data from our and other labs support the view that the spindle assembly checkpoint remains on the watch at least for some time during the metaphase to anaphase transition (part 2.4, Figure 4, (Clute and Pines, 1999; Dick and Gerlich, 2013; Hagting et al., 2002)). This raises the immediate question when and how the checkpoint is finally inactivated to keep it from interfering with anaphase progression. We did not find reactivation events later than two minutes into the degradation process or stabilization of securin at level lower than 45 % of the metaphase concentration. This might indicate that after 2 minutes the decline in cyclin B/CDK1 activity renders the checkpoint unresponsive to chromosome attachment errors. Yet, some technical aspects limit this conclusion: In our assay we were only able to identify those events with certainty, where we observed re-recruitment of Mad2 to the kinetochore and detected precocious termination of securin degradation. We would have missed events, where Mad2 was recruited, but securin degradation had already progressed too far for the slow APC/C inhibition to manifest in precocious stabilization of securin. Our time window of observation was limited to maximally 8 minutes and we measured that it takes about 4 – 7 minutes from the initial trigger to the inhibition of the APC/C (part 2.4, Figure 4 D). Hence, it is conceivable that checkpoint reactivation events, which occurred more than 2 minutes into the degradation process were not picked up by our assay. Furthermore, our assay relied on stochastically occurring spindle collapses, which we provoked by using a temperature-sensitive mutant of the

kinesin-5 Cut7. As we were not able to monitor the spindle integrity concomitantly with Mad2-mCherry and securin-GFP, we can not irrevocably demonstrate that at later time points spindle collapses did occur but were not recognized by the spindle assembly checkpoint. Hence, the measured 2 minutes only give us a lower bound for how long the checkpoint remains activatable during the transition.

Several approaches could provide a more satisfying answer to this question in the future: 1) Instead of relying on stochastic spindle collapses as the trigger for checkpoint signalling, one could treat cells with destabilizing microtubule drugs at defined time points during the metaphase to anaphase transition. This should be feasible, yet to yield sufficient quantitative data from such an assay, one would probably need to pre-synchronize cells. Furthermore, one would need to establish a reliable method to quickly and uniformly apply the microtubule drug to the dividing cells during the imaging process. Recent advances in the development of microfluidic devices make this possible (Charvin et al., 2008; Charvin et al., 2010). 2) The experiment that is discussed above is based on the idea to provide the initial trigger of checkpoint signalling (microtubule destabilization) at different time points during the metaphase to anaphase transition and to inquire whether the checkpoint is still capable to respond. Yet, one could approach the question from another angle: How long is checkpoint signalling maintained, when one provides a constant trigger for checkpoint signalling but allows CDK1 activity to decline? The constant trigger can be provided by permanently applying microtubule-destabilizing drugs. Under physiological conditions CDK1 activity will not decline in this situation, because the APC/C is inhibited by the spindle assembly checkpoint. Yet, the requirement for an active APC/C can be bypassed by using small molecule inhibitors for CDK1. At a sufficient level of CDK1 inhibition, the checkpoint will be inactivated and cells will progress into anaphase. However, it will be difficult to translate the inhibitor concentration into a physiologically meaningful unit, e.g. reduction in CDK1 activity or amount of degraded cyclin B. Hence, one will be restricted to relative comparisons about the temporal order of events, e.g. if less inhibitor is necessary to promote spindle assembly checkpoint inactivation than to promote anaphase B spindle elongation. 3) An approach, which could circumvent this problem, would be to not use CDK1 inhibitors but to delete the most downstream protein in the checkpoint signalling pathway, Mad3. Despite an unsatisfied checkpoint, cells would now progress into anaphase and the APC/C activity would naturally lead to a decline in cyclin B and CDK1 activity. This might provide an answer as of how much time

passes from the start of APC/C activity until kinetochore recruitment of the more upstream checkpoint proteins is lost. Despite the elegance of this approach, it is based on the assumption that the mechanism that disables the mitotic checkpoint in anaphase works via regulating the kinetochore recruitment of one of the upstream components. Whether or not this is true remains to be shown. Using the discussed CDK1 inhibitor approach one might be able to address this question to some extent: If after drug addition checkpoint proteins are removed from the kinetochore shortly before APC/C activation becomes detectable it might suggest some degree of causality. If instead checkpoint proteins only start to disappear from the kinetochore after the APC/C has become active it is more likely that the crucial step in checkpoint inactivation is located further downstream in the signalling cascade. Taken together, no single of the mentioned approaches might be able to unravel, when exactly the mitotic checkpoint is inactivated. Yet, synergistically, they could provide a comprehensive picture of the temporal dynamics of the checkpoint inactivation.

3.3.5 Mechanisms of checkpoint inactivation

Another open question in the field is which mechanisms render the checkpoint unresponsive. Aurora B is one of the most upstream components in the signalling cascade and cyclin B degradation-dependent translocation of Aurora B had been implicated in timely checkpoint inactivation (Vázquez-Novelle and Petronczki, 2010). Yet, when we followed the translocation dynamics of Aurora B relative to sister chromatid separation in unperturbed mitosis, I found that Aurora B only translocates about 30 seconds after sister chromatids have split (part 2.4, Supplementary Figure S4 A – C). Nevertheless, neither relocalization of checkpoint proteins to the kinetochore nor destabilization of kinetochore-microtubule interactions was observed in this situation. This is consistent with previous experiments in human cell lines, where is was shown that constitutive localization of Aurora B to the inner centromere during anaphase was not sufficient to provoke untimely checkpoint activation (Vázquez-Novelle and Petronczki, 2010). These findings argue that yet uncharacterized – potentially cyclin B degradation-dependent – processes contribute to checkpoint inactivation. Several steps in spindle assembly checkpoint signalling have been suggested to depend on CDK1 activity: kinetochore localization of Mps1 (Morin et al., 2012) and the Mad1/Mad2 complex (Ito et al., 2012; Morin et al., 2012), the checkpoint function of Bub1 (Yamaguchi et al., 2003), and the susceptibility of Cdc20 to checkpoint inhibition (D'Angiolella et al., 2003). Activation of the second APC/C co-activator Cdh1 by dephosphorylation during anaphase (Pesin and Orr-

Weaver, 2008) could further render the checkpoint inactive, because – unlike Cdc20 – Cdh1 is not targeted by the mitotic checkpoint (Fang, 2002; Fang et al., 1998). Among these mechanisms, recruitment of the Mad1/Mad2 complex might be a good candidate: Artificial tethering of the upstream kinases Mps1 or Ark1 recruits Bub1 and Bub3 but not Mad1 and Mad2 to the kinetochore when CDK1 activity is low (Vazquez-Novelle/Petronczki, 2010, Ito/Matsumoto, 2012), suggesting that Mad1/Mad2 localization requires CDK1 activity. Furthermore, artificial recruitment of Mad1 to the kinetochore during the metaphase to anaphase transition reengages the checkpoint in human cells arguing that the mechanisms downstream are still functional during this period (Kuijt/Kops, 2014). Whether recruitment of Mad1 is regulated by post-translational modifications of the protein itself or by regulation of the kinetochore receptor is unknown. In fission yeast other mechanisms might additionally contribute: although Mad1 recruitment to the kinetochore seems to be regulated in a cell cycle-dependent manner, artificial recruitment of Mad1 is not sufficient for checkpoint signalling (Heinrich et al., 2014). In any case, a first step would be the identification of the direct interactors of Mad1 at the kinetochore. As simple immunoprecipitations have not yielded good candidates so far, stabilizing the potential interactions by chemical crosslinking prior to the immunprecipitation or using novel proximity-dependent labelling approaches (Roux et al., 2012) might be more promising. Subsequently, potential CDK1 phosphorylation sites would need to be identified and their role be tested.

3.3.6 Stabilization of kinetochore-microtubule interaction in anaphase

We found that the checkpoint protein Mad2 can be re-recruited to kinetochores for at least 2 min after initiation of APC/C activity (part 2.4, Figure 4D). Yet, in normal anaphase, which occurs 1.5 to 2 min after initiation of APC/C activity, checkpoint proteins do not localize to kinetochores (part 2.4, Figure 1A,C and S1E) unless CDK1 activity is maintained (part 2.4, Figure 1 A-C). These observations suggest that the ability to recruit checkpoint proteins to the kinetochore may not have been inactivated by the time of normal anaphase. Instead one can hypothesize that kinetochore-microtubule attachment in normal anaphase does not become unstable, and therefore does not provide any platform to recruit checkpoint proteins. The stability of kinetochore-microtubule attachment should depend on declining CDK1 activity, because the initiation of sister chromatid separation in metaphase (when CDK1 activity is naturally high) or in anaphase under circumstances where CDK1 activity is maintained, both lead to unstable attachment and recruitment of checkpoint proteins

(Mirchenko and Uhlmann, 2010; Oliveira et al., 2010; Parry et al., 2003; Vazquez-Novelle et al., 2014).

Since Aurora B activity at the inner centromere is essential for the destabilization of kinetochore-microtubule interactions and its centromere interaction depends on CDK1 activity (Carmena et al., 2012), translocation of Aurora B had been thought to facilitate stable kinetochore-microtubule interactions. Yet, retaining Aurora B at the kinetochore in anaphase does not destabilize KT-MT attachment in human cells (Carmena et al., 2012; Hummer and Mayer, 2009; Vázquez-Novelle and Petronczki, 2010). Furthermore, our data suggests that Aurora B translocates too late in order to ensure stable attachment at anaphase onset (part 2.4, S4 A – C). This argues for an additional, cyclin B degradation-dependent mechanism, which promotes stable kinetochore-microtubule interaction. This mechanism might be distinct from the mechanism that regulates the activity of the mitotic checkpoint as none of the mechanisms discussed above has been implicated in stabilization of KT-MT interactions in anaphase. Consistently, engaging the mitotic checkpoint during the metaphase to anaphase transition in human cells by artificial kinetochore recruitment of Mad1 is not accompanied by destabilization of KT-MT interaction (Kuijt, 2014 #480, personal communication). I speculate that dephosphorylation of CDK1 target sites at the outer kinetochore is responsible for the stabilization of kinetochore-microtubule attachment by the time of anaphase. A targeted phospho-proteomic study could provide an initial list of candidates. Ideally, one would use a comparative approach, in which the phosphorylation status of kinetochore proteins isolated from prometaphase and metaphase are compared to the phosphorylation status of the proteins in early anaphase or shortly after drug-induced CDK1 inhibition. Additionally, it might be interesting to ask, whether any phosphatases are involved in this process. A candidate-based approach could address, whether phosphatases are specifically recruited to kinetochores at the metaphase to anaphase transition, thereby possibly promoting local dephosphorylation of CDK1 target sites even before a global reduction of CDK1 activity occurs.

3.3.7 Slow APC/C inhibition might protect anaphase

Experiments from others and us suggest that the APC/C inhibition kinetics is surprisingly slow and that this slowness might be a conserved feature of spindle assembly checkpoint signalling from yeast to humans (Dick and Gerlich, 2013). Consequently, errors that occur late in prometaphase or metaphase will not result in APC/C inhibition in time to block sister chromatid separation and mitotic progression.

Considering the elaborate nature of spindle assembly checkpoint signalling and importance of proper chromosome attachment for genomic stability it seems almost improvident to operate on such slow kinetics therefore putting anaphase progression at risk right before the end. It is possible that there are biophysical constraints, which do not allow the inhibition to occur faster, e.g. the aforementioned kinetics of the conformational change of Mad2 (Simonetta et al., 2009). On the other hand, slow inhibition of the APC/C could also reflect other physiological constraints onto checkpoint signalling. In some situations a delayed inhibition of the APC/C might be advantageous: In prometaphase, slow APC/C inhibition might ensure that a full checkpoint response and a significant delay in cell cycle progression is only triggered, if problems in establishing proper chromosome attachment persist. In anaphase a slow kinetic could provide a time buffer in which – even if initial checkpoint signalling occurs due to untimely high CDK1 activity at the time of sister chromatid separation – cyclin B degradation can continue to decline and inactivate the checkpoint in time to prevent the fatal inhibition of the APC/C. Consistent with this idea we have observed brief stabilization of the securin level during the degradation in two cases where sister chromatid separation occurred close to the start of degradation. Nevertheless, the cells then continued to degrade securin and correctly finished mitosis (part 2.4, Figure S4 D). It will be interesting to study whether indeed those events of brief stabilization are accompanied by recruitment of checkpoint proteins to the kinetochore. This would argue that inactivation of the mitotic checkpoint prior to sister chromatid separation is not absolutely crucial and that cells are able to compensate for untimely checkpoint signalling in anaphase to some extent. We will only be able to address to which degree cells are able to compensate, once the underlying mechanisms of checkpoint inactivation have been unravelled and means to prevent checkpoint inactivation despite declining CDK1 activity have been identified. Directly demonstrating that the slowness of checkpoint signalling is beneficial, will be an even more challenging task. It will require engineering a ‘faster’ checkpoint signalling and investigate the consequences of such accelerated signalling. Currently, we are still far from understanding what determines this kinetics on the molecular level and how to manipulate them appropriately.

4 References

Agromayor, M., and Martin-Serrano, J. (2013). Knowing when to cut and run: mechanisms that control cytokinetic abscission. Trends Cell Biol *23*, 433-441.

Alexandru, G., Zachariae, W., Schleiffer, A., and Nasmyth, K. (1999). Sister chromatid separation and chromosome re-duplication are regulated by different mechanisms in response to spindle damage. The EMBO journal *18*, 2707-2721.

Alfa, C.E., Ducommun, B., Beach, D., and Hyams, J.S. (1990). Distinct nuclear and spindle pole body population of cyclin-cdc2 in fission yeast. Nature *347*, 680-682.

Azzam, R., Chen, S.L., Shou, W., Mah, A.S., Alexandru, G., Nasmyth, K., Annan, R.S., Carr, S.A., and Deshaies, R.J. (2004). Phosphorylation by cyclin B-Cdk underlies release of mitotic exit activator Cdc14 from the nucleolus. Science *305*, 516-519.

Bardin, A.J., and Amon, A. (2001). Men and sin: what's the difference? Nature reviews Molecular cell biology *2*, 815-826.

Barr, F.A., and Gruneberg, U. (2007). Cytokinesis: placing and making the final cut. Cell *131*, 847-860.

Beach, D., Durkacz, B., and Nurse, P. (1982). Functionally homologous cell cycle control genes in budding and fission yeast. Nature *300*, 706-709.

Berry, L.D., Feoktistova, A., Wright, M.D., and Gould, K.L. (1999). The schizosaccharomyces pombe dim1(+) gene interacts with the anaphase-promoting complex or cyclosome (APC/C) component lid1(+) and is required for APC/C function. Mol Cell Biol *19*, 2535-2546.

Blanco, M.A., Sanchez-Diaz, A., de Prada, J.M., and Moreno, S. (2000). APC(ste9/srw1) promotes degradation of mitotic cyclins in G(1) and is inhibited by cdc2 phosphorylation. The EMBO journal *19*, 3945-3955.

Bouchoux, C., and Uhlmann, F. (2011). A quantitative model for ordered Cdk substrate dephosphorylation during mitotic exit. Cell *147*, 803-814.

Brust-Mascher, I., and Scholey, J.M. (2011). Mitotic motors and chromosome segregation: the mechanism of anaphase B. Biochemical Society transactions *39*, 1149-1153.

Buchler, N.E., and Cross, F.R. (2009). Protein sequestration generates a flexible ultrasensitive response in a genetic network. Mol Syst Biol *5*, 272.

Buffin, E., Emre, D., and Karess, R.E. (2007). Flies without a spindle checkpoint. Nature cell biology *9*, 565-572.

Burton, J.L., and Solomon, M.J. (2001). D box and KEN box motifs in budding yeast Hsl1p are required for APC-mediated degradation and direct binding to Cdc20p and Cdh1p. Genes & development *15*, 2381-2395.

Burton, J.L., Tsakraklides, V., and Solomon, M.J. (2005). Assembly of an APC-Cdh1-substrate complex is stimulated by engagement of a destruction box. Molecular cell *18*, 533-542.

Canman, J.C., Sharma, N., Straight, A., Shannon, K.B., Fang, G., and Salmon, E.D. (2002). Anaphase onset does not require the microtubule-dependent depletion of kinetochore and centromere-binding proteins. Journal of cell science *115*, 3787-3795.

Carmena, M., Wheelock, M., Funabiki, H., and Earnshaw, W.C. (2012). The chromosomal passenger complex (CPC): from easy rider to the godfather of mitosis. Nature reviews Molecular cell biology *13*, 789-803.

Carpy, A., Krug, K., Graf, S., Koch, A., Popic, S., Hauf, S., and Macek, B. (2014). Absolute proteome and phosphoproteome dynamics during the cell cycle of Schizosaccharomyces pombe (Fission Yeast). Mol Cell Proteomics *13*, 1925-1936.

Chang, D.C., Xu, N., and Luo, K.Q. (2003). Degradation of cyclin B is required for the onset of anaphase in Mammalian cells. The Journal of biological chemistry *278*, 37865-37873.

Chang, L., and Barford, D. (2014). Insights into the anaphase-promoting complex: a molecular machine that regulates mitosis. Current opinion in structural biology *29C*, 1-9.

Chang, L., Morrell, J.L., Feoktistova, A., and Gould, K.L. (2001). Study of cyclin proteolysis in anaphase-promoting complex (APC) mutant cells reveals the requirement for APC function in the final steps of the fission yeast septation initiation network. Mol Cell Biol *21*, 6681-6694.

Charvin, G., Cross, F.R., and Siggia, E.D. (2008). A microfluidic device for temporally controlled gene expression and long-term fluorescent imaging in unperturbed dividing yeast cells. PloS one *3*, e1468.

Charvin, G., Oikonomou, C., and Cross, F. (2010). Long-term imaging in microfluidic devices. Methods Mol Biol *591*, 229-242.

Cheeseman, I.M. (2014). The kinetochore. Cold Spring Harb Perspect Biol *6*, a015826.

Chestukhin, A., Pfeffer, C., Milligan, S., DeCaprio, J.A., and Pellman, D. (2003). Processing, localization, and requirement of human separase for normal anaphase progression. Proceedings of the National Academy of Sciences of the United States of America *100*, 4574-4579.

Chi, Y., Welcker, M., Hizli, A.A., Posakony, J.J., Aebersold, R., and Clurman, B.E. (2008). Identification of CDK2 substrates in human cell lysates. Genome Biol *9*, R149.

Chung, E., and Chen, R.H. (2003). Phosphorylation of Cdc20 is required for its inhibition by the spindle checkpoint. Nature cell biology *5*, 748-753.

Ciliberto, A., and Shah, J.V. (2009). A quantitative systems view of the spindle assembly checkpoint. The EMBO journal *28*, 2162-2173.

Cimini, D., Howell, B., Maddox, P., Khodjakov, A., Degrassi, F., and Salmon, E.D. (2001). Merotelic kinetochore orientation is a major mechanism of aneuploidy in mitotic mammalian tissue cells. The Journal of cell biology *153*, 517-527.

Ciosk, R., Zachariae, W., Michaelis, C., Shevchenko, A., Mann, M., and Nasmyth, K. (1998). An ESP1/PDS1 complex regulates loss of sister chromatid cohesion at the metaphase to anaphase transition in yeast. Cell *93*, 1067-1076.

Clute, P., and Pines, J. (1999). Temporal and spatial control of cyclin B1 destruction in metaphase. Nature cell biology *1*, 82-87.

Cohen-Fix, O., Peters, J.M., Kirschner, M.W., and Koshland, D. (1996). Anaphase initiation in Saccharomyces cerevisiae is controlled by the APC-dependent degradation of the anaphase inhibitor Pds1p. Genes & development *10*, 3081-3093.

Cookson, N.A., Mather, W.H., Danino, T., Mondragon-Palomino, O., Williams, R.J., Tsimring, L.S., and Hasty, J. (2011). Queueing up for enzymatic processing: correlated signaling through coupled degradation. Mol Syst Biol *7*, 561.

Coudreuse, D., and Nurse, P. (2010). Driving the cell cycle with a minimal CDK control network. Nature *468*, 1074-1079.

Cundell, M.J., Bastos, R.N., Zhang, T., Holder, J., Gruneberg, U., Novak, B., and Barr, F.A. (2013). The BEG (PP2A-B55/ENSA/Greatwall) pathway ensures cytokinesis follows chromosome separation. Molecular cell *52*, 393-405.

D'Angiolella, V., Mari, C., Nocera, D., Rametti, L., and Grieco, D. (2003). The spindle checkpoint requires cyclin-dependent kinase activity. Genes & development *17*, 2520-2525.

da Fonseca, P.C., Kong, E.H., Zhang, Z., Schreiber, A., Williams, M.A., Morris, E.P., and Barford, D. (2011). Structures of APC/C(Cdh1) with substrates identify Cdh1 and Apc10 as the D-box co-receptor. Nature *470*, 274-278.

den Elzen, N., and Pines, J. (2001). Cyclin A is destroyed in prometaphase and can delay chromosome alignment and anaphase. The Journal of cell biology *153*, 121-136.

Dick, A.E., and Gerlich, D.W. (2013). Kinetic framework of spindle assembly checkpoint signalling. Nature cell biology *15*, 1370-1377.

Dimova, N.V., Hathaway, N.A., Lee, B.H., Kirkpatrick, D.S., Berkowitz, M.L., Gygi, S.P., Finley, D., and King, R.W. (2012). APC/C-mediated multiple monoubiquitylation provides an alternative degradation signal for cyclin B1. Nature cell biology *14*, 168-176.

Dischinger, S., Krapp, A., Xie, L., Paulson, J.R., and Simanis, V. (2008). Chemical genetic analysis of the regulatory role of Cdc2p in the S. pombe septation initiation network. Journal of cell science *121*, 843-853.

Dohadwala, M., da Cruz e Silva, E.F., Hall, F.L., Williams, R.T., Carbonaro-Hall, D.A., Nairn, A.C., Greengard, P., and Berndt, N. (1994). Phosphorylation and inactivation of protein phosphatase 1 by cyclin-dependent kinases. Proceedings of the National Academy of Sciences of the United States of America *91*, 6408-6412.

Eme, L., Trilles, A., Moreira, D., and Brochier-Armanet, C. (2011). The phylogenomic analysis of the anaphase promoting complex and its targets points to complex and modern-like control of the cell cycle in the last common ancestor of eukaryotes. BMC Evol Biol *11*, 265.

Evans, T., Rosenthal, E.T., Youngblom, J., Distel, D., and Hunt, T. (1983). Cyclin: a protein specified by maternal mRNA in sea urchin eggs that is destroyed at each cleavage division. Cell *33*, 389-396.

Eytan, E., Moshe, Y., Braunstein, I., and Hershko, A. (2006). Roles of the anaphase-promoting complex/cyclosome and of its activator Cdc20 in functional substrate binding. Proceedings of the National Academy of Sciences of the United States of America *103*, 2081-2086.

Fang, G. (2002). Checkpoint protein BubR1 acts synergistically with Mad2 to inhibit anaphase-promoting complex. Molecular biology of the cell *13*, 755-766.

Fang, G., Yu, H., and Kirschner, M.W. (1998). The checkpoint protein MAD2 and the mitotic regulator CDC20 form a ternary complex with the anaphase-promoting complex to control anaphase initiation. Genes & development *12*, 1871-1883.

Felix, M.A., Labbe, J.C., Doree, M., Hunt, T., and Karsenti, E. (1990). Triggering of cyclin degradation in interphase extracts of amphibian eggs by cdc2 kinase. Nature *346*, 379-382.

Fernius, J., Nerusheva, O.O., Galander, S., Alves Fde, L., Rappsilber, J., and Marston, A.L. (2013). Cohesin-dependent association of scc2/4 with the centromere initiates pericentromeric cohesion establishment. Current biology : CB *23*, 599-606.

Feytout, A., Vaur, S., Genier, S., Vazquez, S., and Javerzat, J.P. (2011). Psm3 acetylation on conserved lysine residues is dispensable for viability in fission yeast but contributes to Eso1-mediated sister chromatid cohesion by antagonizing Wpl1. Mol Cell Biol *31*, 1771-1786.

Flemming, W. (1879). Beiträge zur Kenntniss der Zelle und ihrer Lebenserscheinungen. Arch Mikrosk Anat.

Flemming, W. (1882). Zellsubstanz, Kern und Zelltheilung (F. C. W. Vogel).

Floyd, S., Pines, J., and Lindon, C. (2008). APC/C Cdh1 targets aurora kinase to control reorganization of the mitotic spindle at anaphase. Current biology : CB *18*, 1649-1658.

Foe, I.T., Foster, S.A., Cheung, S.K., DeLuca, S.Z., Morgan, D.O., and Toczyski, D.P. (2011). Ubiquitination of Cdc20 by the APC occurs through an intramolecular mechanism. Current biology : CB *21*, 1870-1877.

Foster, S.A., and Morgan, D.O. (2012). The APC/C subunit Mnd2/Apc15 promotes Cdc20 autoubiquitination and spindle assembly checkpoint inactivation. Molecular cell *47*, 921-932.

Fu, C., Ward, J.J., Loiodice, I., Velve-Casquillas, G., Nedelec, F.J., and Tran, P.T. (2009). Phospho-regulated interaction between kinesin-6 Klp9p and microtubule bundler Ase1p promotes spindle elongation. Developmental cell *17*, 257-267.

Funabiki, H., Kumada, K., and Yanagida, M. (1996a). Fission yeast Cut1 and Cut2 are essential for sister chromatid separation, concentrate along the metaphase spindle and form large complexes. The EMBO journal *15*, 6617-6628.

Funabiki, H., Yamano, H., Kumada, K., Nagao, K., Hunt, T., and Yanagida, M. (1996b). Cut2 proteolysis required for sister-chromatid seperation in fission yeast. Nature *381*, 438-441.

Funabiki, H., Yamano, H., Nagao, K., Tanaka, H., Yasuda, H., Hunt, T., and Yanagida, M. (1997). Fission yeast Cut2 required for anaphase has two destruction boxes. The EMBO journal *16*, 5977-5987.

Gallant, P., and Nigg, E.A. (1992). Cyclin B2 undergoes cell cycle-dependent nuclear translocation and, when expressed as a non-destructible mutant, causes mitotic arrest in HeLa cells. The Journal of cell biology *117*, 213-224.

Gascoigne, K.E., and Cheeseman, I.M. (2013). CDK-dependent phosphorylation and nuclear exclusion coordinately control kinetochore assembly state. The Journal of cell biology *201*, 23-32.

Gautier, J., Minshull, J., Lohka, M., Glotzer, M., Hunt, T., and Maller, J.L. (1990). Cyclin is a component of maturation-promoting factor from Xenopus. Cell *60*, 487-494.

Gautier, J., Norbury, C., Lohka, M., Nurse, P., and Maller, J. (1988). Purified maturation-promoting factor contains the product of a Xenopus homolog of the fission yeast cell cycle control gene cdc2+. Cell *54*, 433-439.

Gavet, O., and Pines, J. (2010). Progressive activation of CyclinB1-Cdk1 coordinates entry to mitosis. Developmental cell *18*, 533-543.

Geley, S., Kramer, E., Gieffers, C., Gannon, J., Peters, J.M., and Hunt, T. (2001). Anaphase-promoting complex/cyclosome-dependent proteolysis of human cyclin A starts at the beginning of mitosis and is not subject to the spindle assembly checkpoint. The Journal of cell biology *153*, 137-148.

Genschik, P., Criqui, M.C., Parmentier, Y., Derevier, A., and Fleck, J. (1998). Cell cycle - dependent proteolysis in plants. Identification Of the destruction box pathway and metaphase arrest produced by the proteasome inhibitor mg132. Plant Cell *10*, 2063-2076.

Gerhart, J., Wu, M., and Kirschner, M. (1984). Cell cycle dynamics of an M-phase-specific cytoplasmic factor in Xenopus laevis oocytes and eggs. The Journal of cell biology *98*, 1247-1255.

Gerlich, D., Beaudouin, J., Kalbfuss, B., Daigle, N., Eils, R., and Ellenberg, J. (2003). Global chromosome positions are transmitted through mitosis in mammalian cells. Cell *112*, 751-764.

Ghislain, M., Udvardy, A., and Mann, C. (1993). S. cerevisiae 26S protease mutants arrest cell division in G2/metaphase. Nature *366*, 358-362.

Glotzer, M. (2005). The molecular requirements for cytokinesis. Science *307*, 1735-1739.

Glotzer, M., Murray, A.W., and Kirschner, M.W. (1991). Cyclin is degraded by the ubiquitin pathway. Nature *349*, 132-138.

Gorbsky, G.J., Chen, R.H., and Murray, A.W. (1998). Microinjection of antibody to Mad2 protein into mammalian cells in mitosis induces premature anaphase. The Journal of cell biology *141*, 1193-1205.

Gordon, C., McGurk, G., Dillon, P., Rosen, C., and Hastie, N.D. (1993). Defective mitosis due to a mutation in the gene for a fission yeast 26S protease subunit. Nature *366*, 355-357.

Gorr, I.H., Boos, D., and Stemmann, O. (2005). Mutual inhibition of separase and Cdk1 by two-step complex formation. Molecular cell *19*, 135-141.

Gourguechon, S., Holt, L.J., and Cande, W.Z. (2013). The Giardia cell cycle progresses independently of the anaphase-promoting complex. Journal of cell science *126*, 2246-2255.

Gruneberg, U., Neef, R., Honda, R., Nigg, E.A., and Barr, F.A. (2004). Relocation of Aurora B from centromeres to the central spindle at the metaphase to anaphase transition requires MKlp2. The Journal of cell biology *166*, 167-172.

Gurden, M.D., Holland, A.J., van Zon, W., Tighe, A., Vergnolle, M.A., Andres, D.A., Spielmann, H.P., Malumbres, M., Wolthuis, R.M., Cleveland, D.W.*, et al.* (2010). Cdc20 is required for the post-anaphase, KEN-dependent degradation of centromere protein F. Journal of cell science *123*, 321-330.

Hagting, A., Den Elzen, N., Vodermaier, H., Waizenegger, I., Peters, J.-M., and Pines, J. (2002). Human securin proteolysis is controlled by the spindle checkpoint and reveals when the APC/C switches from activation by Cdc20 to Cdh1. The Journal of cell biology *157*, 1125-1137.

Hahnenberger, K.M., Baum, M.P., Polizzi, C.M., Carbon, J., and Clarke, L. (1989). Construction of functional artificial minichromosomes in the fission yeast Schizosaccharomyces pombe. Proceedings of the National Academy of Sciences of the United States of America *86*, 577-581.

Hames, R.S., Wattam, S.L., Yamano, H., Bacchieri, R., and Fry, A.M. (2001). APC/C-mediated destruction of the centrosomal kinase Nek2A occurs in early mitosis and depends upon a cyclin A-type D-box. The EMBO journal *20*, 7117-7127.

Hartwell, L.H., Culotti, J., Pringle, J.R., and Reid, B.J. (1974). Genetic control of the cell division cycle in yeast. Science *183*, 46-51.

Hartwell, L.H., Culotti, J., and Reid, B. (1970). Genetic control of the cell-division cycle in yeast. I. Detection of mutants. Proceedings of the National Academy of Sciences of the United States of America *66*, 352-359.

Hartwell, L.H., and Weinert, T.A. (1989). Checkpoints: controls that ensure the order of cell cycle events. Science *246*, 629-634.

Hauf, S., Cole, R.W., LaTerra, S., Zimmer, C., Schnapp, G., Walter, R., Heckel, A., van Meel, J., Rieder, C.L., and Peters, J.M. (2003). The small molecule Hesperadin reveals a role for Aurora B in correcting kinetochore-microtubule attachment and in maintaining the spindle assembly checkpoint. The Journal of cell biology *161*, 281-294.

Heinrich, S., Sewart, K., Windecker, H., Langegger, M., Schmidt, N., Hustedt, N., and Hauf, S. (2014). Mad1 contribution to spindle assembly checkpoint signalling goes beyond presenting Mad2 at kinetochores. EMBO reports *15*, 291-298.

Heinrich, S., Windecker, H., Hustedt, N., and Hauf, S. (2012). Mph1 kinetochore localization is crucial and upstream in the hierarchy of spindle assembly checkpoint protein recruitment to kinetochores. Journal of cell science *125*, 4720-4727.

Hellmuth, S., Bottger, F., Pan, C., Mann, M., and Stemmann, O. (2014). PP2A delays APC/C-dependent degradation of separase-associated but not free securin. The EMBO journal *33*, 1134-1147.

Hershko, A., Ganoth, D., Pehrson, J., Palazzo, R.E., and Cohen, L.H. (1991). Methylated ubiquitin inhibits cyclin degradation in clam embryo extracts. The Journal of biological chemistry *266*, 16376-16379.

Higuchi, T., and Uhlmann, F. (2005a). Stabilization of microtubule dynamics at anaphase onset promotes chromosome segregation. Nature *433*, 171-176.

Higuchi, T., and Uhlmann, F. (2005b). Stabilization of microtubule dynamics at anaphase onset promotes chromosome segregation. Nature *433*, 171-176.

Hilioti, Z., Chung, Y.S., Mochizuki, Y., Hardy, C.F., and Cohen-Fix, O. (2001). The anaphase inhibitor Pds1 binds to the APC/C-associated protein Cdc20 in a destruction box-dependent manner. Current biology : CB *11*, 1347-1352.

Hirano, T., Funahashi, S., Uemura, T., and Yanagida, M. (1986). Isolation and characterization of Schizosaccharomyces pombe cutmutants that block nuclear division but not cytokinesis. The EMBO journal *5*, 2973-2979.

Hirano, T., Hiraoka, Y., and Yanagida, M. (1988). A temperature-sensitive mutation of the Schizosaccharomyces pombe gene nuc2+ that encodes a nuclear scaffold-like protein blocks spindle elongation in mitotic anaphase. The Journal of cell biology *106*, 1171-1183.

Holland, A.J., and Taylor, S.S. (2006). Cyclin-B1-mediated inhibition of excess separase is required for timely chromosome disjunction. Journal of cell science *119*, 3325-3336.

Holloway, S.L., Glotzer, M., King, R.W., and Murray, A.W. (1993). Anaphase is initiated by proteolysis rather than by the inactivation of maturation-promoting factor. Cell *73*, 1393-1402.

Holt, L.J., Krutchinsky, A.N., and Morgan, D.O. (2008). Positive feedback sharpens the anaphase switch. Nature *454*, 353-357.

Holt, L.J., Tuch, B.B., Villen, J., Johnson, A.D., Gygi, S.P., and Morgan, D.O. (2009). Global analysis of Cdk1 substrate phosphorylation sites provides insights into evolution. Science *325*, 1682-1686.

Hornig, N.C., Knowles, P.P., McDonald, N.Q., and Uhlmann, F. (2002). The dual mechanism of separase regulation by securin. Current biology : CB *12*, 973-982.

Hornig, N.C., and Uhlmann, F. (2004). Preferential cleavage of chromatin-bound cohesin after targeted phosphorylation by Polo-like kinase. The EMBO journal *23*, 3144-3153.

Hoyt, M.A., Totis, L., and Roberts, B.T. (1991). S. cerevisiae genes required for cell cycle arrest in response to loss of microtubule function. Cell *66*, 507-517.

Huang, X., Hatcher, R., York, J.P., and Zhang, P. (2005). Securin and separase phosphorylation act redundantly to maintain sister chromatid cohesion in mammalian cells. Molecular biology of the cell *16*, 4725-4732.

Hummer, S., and Mayer, T.U. (2009). Cdk1 negatively regulates midzone localization of the mitotic kinesin Mklp2 and the chromosomal passenger complex. Current biology : CB *19*, 607-612.

Irniger, S., Piatti, S., Michaelis, C., and Nasmyth, K. (1995). Genes involved in sister chromatid separation are needed for B-type cyclin proteolysis in budding yeast. Cell *81*, 269-278.

Ito, D., Saito, Y., and Matsumoto, T. (2012). Centromere-tethered Mps1 pombe homolog (Mph1) kinase is a sufficient marker for recruitment of the spindle checkpoint protein Bub1, but not Mad1. Proceedings of the National Academy of Sciences of the United States of America *109*, 209-214.

Ivanov, D., and Nasmyth, K. (2005). A topological interaction between cohesin rings and a circular minichromosome. Cell *122*, 849-860.

Izawa, D., and Pines, J. (2014). The mitotic checkpoint complex binds a second CDC20 to inhibit active APC/C. Nature.

Jager, H., Herzig, A., Lehner, C.F., and Heidmann, S. (2001). Drosophila separase is required for sister chromatid separation and binds to PIM and THR. Genes & development *15*, 2572-2584.

Jallepalli, P.V., Waizenegger, I.C., Bunz, F., Langer, S., Speicher, M.R., Peters, J.M., Kinzler, K.W., Vogelstein, B., and Lengauer, C. (2001). Securin is required for chromosomal stability in human cells. Cell *105*, 445-457.

Jaspersen, S.L., Charles, J.F., and Morgan, D.O. (1999). Inhibitory phosphorylation of the APC regulator Hct1 is controlled by the kinase Cdc28 and the phosphatase Cdc14. Current biology : CB *9*, 227-236.

Jensen, S., Segal, M., Clarke, D.J., and Reed, S.I. (2001). A novel role of the budding yeast separin Esp1 in anaphase spindle elongation: evidence that proper spindle association of Esp1 is regulated by Pds1. The Journal of cell biology *152*, 27-40.

Juang, Y.L., Huang, J., Peters, J.M., McLaughlin, M.E., Tai, C.Y., and Pellman, D. (1997). APC-mediated proteolysis of Ase1 and the morphogenesis of the mitotic spindle. Science *275*, 1311-1314.

Kaitna, S., Mendoza, M., Jantsch-Plunger, V., and Glotzer, M. (2000). Incenp and an aurora-like kinase form a complex essential for chromosome segregation and efficient completion of cytokinesis. Current biology : CB *10*, 1172-1181.

Kawasaki, Y., Nagao, K., Nakamura, T., and Yanagida, M. (2006). Fission yeast MAP kinase is required for the increased securin-separase interaction that rescues separase mutants under stresses. Cell Cycle *5*, 1831-1839.

Kawashima, S.A., Tsukahara, T., Langegger, M., Hauf, S., Kitajima, T.S., and Watanabe, Y. (2007). Shugoshin enables tension-generating attachment of kinetochores by loading Aurora to centromeres. Genes & development *21*, 420-435.

Khmelinskii, A., Lawrence, C., Roostalu, J., and Schiebel, E. (2007). Cdc14-regulated midzone assembly controls anaphase B. The Journal of cell biology *177*, 981-993.

Kimata, Y., Baxter, J.E., Fry, A.M., and Yamano, H. (2008). A role for the Fizzy/Cdc20 family of proteins in activation of the APC/C distinct from substrate recruitment. Molecular cell *32*, 576-583.

King, R.W., Glotzer, M., and Kirschner, M.W. (1996). Mutagenic analysis of the destruction signal of mitotic cyclins and structural characterization of ubiquitinated intermediates. Molecular biology of the cell *7*, 1343-1357.

King, R.W., Peters, J.M., Tugendreich, S., Rolfe, M., Hieter, P., and Kirschner, M.W. (1995). A 20S complex containing CDC27 and CDC16 catalyzes the mitosis-specific conjugation of ubiquitin to cyclin B. Cell *81*, 279-288.

Kirschner, M., and Mitchison, T. (1986). Beyond self-assembly: from microtubules to morphogenesis. Cell *45*, 329-342.

Kitagawa, R., Law, E., Tang, L., and Rose, A.M. (2002). The Cdc20 homolog, FZY-1, and its interacting protein, IFY-1, are required for proper chromosome segregation in Caenorhabditis elegans. Current biology : CB *12*, 2118-2123.

Kraft, C., Herzog, F., Gieffers, C., Mechtler, K., Hagting, A., Pines, J., and Peters, J.M. (2003). Mitotic regulation of the human anaphase-promoting complex by phosphorylation. The EMBO journal *22*, 6598-6609.

Kraft, C., Vodermaier, H.C., Maurer-Stroh, S., Eisenhaber, F., and Peters, J.M. (2005). The WD40 propeller domain of Cdh1 functions as a destruction box receptor for APC/C substrates. Molecular cell *18*, 543-553.

Kramer, E.R., Scheuringer, N., Podtelejnikov, A.V., Mann, M., and Peters, J.M. (2000). Mitotic regulation of the APC activator proteins CDC20 and CDH1. Molecular biology of the cell *11*, 1555-1569.

Krenn, V., Wehenkel, A., Li, X., Santaguida, S., and Musacchio, A. (2012). Structural analysis reveals features of the spindle checkpoint kinase Bub1-kinetochore subunit Knl1 interaction. The Journal of cell biology *196*, 451-467.

Krylov, D.M., Nasmyth, K., and Koonin, E.V. (2003). Evolution of eukaryotic cell cycle regulation: stepwise addition of regulatory kinases and late advent of the CDKs. Current biology : CB *13*, 173-177.

Kulak, N.A., Pichler, G., Paron, I., Nagaraj, N., and Mann, M. (2014). Minimal, encapsulated proteomic-sample processing applied to copy-number estimation in eukaryotic cells. Nat Methods *11*, 319-324.

Kumada, K., Nakamura, T., Nagao, K., Funabiki, H., Nakagawa, T., and Yanagida, M. (1998). Cut1 is loaded onto the spindle by binding to Cut2 and promotes anaphase spindle movement upon Cut2 proteolysis. Current biology : CB *8*, 633-641.

Kurasawa, Y., Earnshaw, W.C., Mochizuki, Y., Dohmae, N., and Todokoro, K. (2004). Essential roles of KIF4 and its binding partner PRC1 in organized central spindle midzone formation. The EMBO journal *23*, 3237-3248.

Kwon, Y.G., Lee, S.Y., Choi, Y., Greengard, P., and Nairn, A.C. (1997). Cell cycle-dependent phosphorylation of mammalian protein phosphatase 1 by cdc2 kinase. Proceedings of the National Academy of Sciences of the United States of America *94*, 2168-2173.

Lahav-Baratz, S., Sudakin, V., Ruderman, J.V., and Hershko, A. (1995). Reversible phosphorylation controls the activity of cyclosome-associated cyclin-ubiquitin ligase. Proceedings of the National Academy of Sciences of the United States of America *92*, 9303-9307.

Lara-Gonzalez, P., Westhorpe, F.G., and Taylor, S.S. (2012). The spindle assembly checkpoint. Current biology : CB *22*, R966-980.

Larionov, V.L., Karpova, T.S., Kouprina, N.Y., and Jouravleva, G.A. (1985). A mutant of Saccharomyces cerevisiae with impaired maintenance of centromeric plasmids. Curr Genet *10*, 15-20.

Legewie, S., Herzel, H., Westerhoff, H.V., and Bluthgen, N. (2008). Recurrent design patterns in the feedback regulation of the mammalian signalling network. Mol Syst Biol *4*, 190.

Leismann, O., Herzig, A., Heidmann, S., and Lehner, C.F. (2000). Degradation of Drosophila PIM regulates sister chromatid separation during mitosis. Genes & development *14*, 2192-2205.

Lewellyn, L., Carvalho, A., Desai, A., Maddox, A.S., and Oegema, K. (2011). The chromosomal passenger complex and centralspindlin independently contribute to contractile ring assembly. The Journal of cell biology *193*, 155-169.

Li, A., and Blow, J.J. (2004). Non-proteolytic inactivation of geminin requires CDK-dependent ubiquitination. Nature cell biology *6*, 260-267.

Li, R., and Murray, A.W. (1991). Feedback control of mitosis in budding yeast. Cell *66*, 519-531.

Lindon, C. (2008). Control of mitotic exit and cytokinesis by the APC/C. Biochemical Society transactions *36*, 405-410.

Lindon, C., and Pines, J. (2004). Ordered proteolysis in anaphase inactivates Plk1 to contribute to proper mitotic exit in human cells. The Journal of cell biology *164*, 233-241.

Lohka, M.J., Hayes, M.K., and Maller, J.L. (1988). Purification of maturation-promoting factor, an intracellular regulator of early mitotic events. Proceedings of the National Academy of Sciences of the United States of America *85*, 3009-3013.

London, N., and Biggins, S. (2014). Mad1 kinetochore recruitment by Mps1-mediated phosphorylation of Bub1 signals the spindle checkpoint. Genes & development *28*, 140-152.

London, N., Ceto, S., Ranish, J.A., and Biggins, S. (2012). Phosphoregulation of Spc105 by Mps1 and PP1 regulates Bub1 localization to kinetochores. Current biology : CB *22*, 900-906.

Lu, D., Hsiao, J.Y., Davey, N.E., Van Voorhis, V.A., Foster, S.A., Tang, C., and Morgan, D.O. (2014). Multiple mechanisms determine the order of APC/C substrate degradation in mitosis. The Journal of cell biology *207*, 23-39.

Luo, X., Tang, Z., Rizo, J., and Yu, H. (2002). The Mad2 spindle checkpoint protein undergoes similar major conformational changes upon binding to either Mad1 or Cdc20. Molecular cell *9*, 59-71.

Luo, X., Tang, Z., Xia, G., Wassmann, K., Matsumoto, T., Rizo, J., and Yu, H. (2004). The Mad2 spindle checkpoint protein has two distinct natively folded states. Nature structural & molecular biology *11*, 338-345.

Lyons, N.A., and Morgan, D.O. (2011). Cdk1-dependent destruction of Eco1 prevents cohesion establishment after S phase. Molecular cell *42*, 378-389.

Magalska, A., Schellhaus, A.K., Moreno-Andres, D., Zanini, F., Schooley, A., Sachdev, R., Schwarz, H., Madlung, J., and Antonin, W. (2014). RuvB-like ATPases Function in Chromatin Decondensation at the End of Mitosis. Developmental cell *31*, 305-318.

Maine, G.T., Sinha, P., and Tye, B.K. (1984). Mutants of S. cerevisiae defective in the maintenance of minichromosomes. Genetics *106*, 365-385.

Manchado, E., Eguren, M., and Malumbres, M. (2010a). The anaphase-promoting complex/cyclosome (APC/C): cell-cycle-dependent and -independent functions. Biochemical Society transactions *38*, 65-71.

Manchado, E., Guillamot, M., de Carcer, G., Eguren, M., Trickey, M., Garcia-Higuera, I., Moreno, S., Yamano, H., Canamero, M., and Malumbres, M. (2010b). Targeting mitotic exit leads to tumor regression in vivo: Modulation by Cdk1, Mastl, and the PP2A/B55alpha,delta phosphatase. Cancer cell *18*, 641-654.

Mansfeld, J., Collin, P., Collins, M.O., Choudhary, J.S., and Pines, J. (2011). APC15 drives the turnover of MCC-CDC20 to make the spindle assembly checkpoint responsive to kinetochore attachment. Nature cell biology *13*, 1234-1243.

Mapelli, M., and Musacchio, A. (2007). MAD contortions: conformational dimerization boosts spindle checkpoint signaling. Current opinion in structural biology *17*, 716-725.

Marangos, P., and Carroll, J. (2008). Securin regulates entry into M-phase by modulating the stability of cyclin B. Nature cell biology *10*, 445-451.

Maresca, T.J., and Salmon, E.D. (2009). Intrakinetochore stretch is associated with changes in kinetochore phosphorylation and spindle assembly checkpoint activity. The Journal of cell biology *184*, 373-381.

Maresca, T.J., and Salmon, E.D. (2010). Welcome to a new kind of tension: translating kinetochore mechanics into a wait-anaphase signal. Journal of cell science *123*, 825-835.

Marguerat, S., Schmidt, A., Codlin, S., Chen, W., Aebersold, R., and Bahler, J. (2012). Quantitative analysis of fission yeast transcriptomes and proteomes in proliferating and quiescent cells. Cell *151*, 671-683.

Masui, Y., and Markert, C.L. (1971). Cytoplasmic control of nuclear behavior during meiotic maturation of frog oocytes. J Exp Zool *177*, 129-145.

Matsumura, T., Yuasa, T., Hayashi, T., Obara, T., Kimata, Y., and Yanagida, M. (2003). A brute force postgenome approach to identify temperature-sensitive mutations that negatively interact with separase and securin plasmids. Genes to cells : devoted to molecular & cellular mechanisms *8*, 341-355.

Matsusaka, T., Enquist-Newman, M., Morgan, D.O., and Pines, J. (2014). Co-activator independent differences in how the metaphase and anaphase APC/C recognise the same substrate. Biol Open *3*, 904-912.

Matyskiela, M.E., and Morgan, D.O. (2009). Analysis of activator-binding sites on the APC/C supports a cooperative substrate-binding mechanism. Molecular cell *34*, 68-80.

Matyskiela, M.E., Rodrigo-Brenni, M.C., and Morgan, D.O. (2009). Mechanisms of ubiquitin transfer by the anaphase-promoting complex. J Biol *8*, 92.

McGrew, J.T., Xiao, Z.X., and Fitzgerald-Hayes, M. (1989). Saccharomyces cerevisiae mutants defective in chromosome segregation. Yeast *5*, 271-284.

Mei, J., Huang, X., and Zhang, P. (2001). Securin is not required for cellular viability, but is required for normal growth of mouse embryonic fibroblasts. Current biology : CB *11*, 1197-1201.

Meraldi, P., Draviam, V.M., and Sorger, P.K. (2004). Timing and checkpoints in the regulation of mitotic progression. Developmental cell *7*, 45-60.

Michaelis, C., Ciosk, R., and Nasmyth, K. (1997). Cohesins: chromosomal proteins that prevent premature separation of sister chromatids. Cell *91*, 35-45.

Mirchenko, L., and Uhlmann, F. (2010). Sli15(INCENP) dephosphorylation prevents mitotic checkpoint reengagement due to loss of tension at anaphase onset. Current biology : CB *20*, 1396-1401.

Mishima, M., Kaitna, S., and Glotzer, M. (2002). Central spindle assembly and cytokinesis require a kinesin-like protein/RhoGAP complex with microtubule bundling activity. Developmental cell *2*, 41-54.

Mishima, M., Pavicic, V., Gruneberg, U., Nigg, E.A., and Glotzer, M. (2004). Cell cycle regulation of central spindle assembly. Nature *430*, 908-913.

Mitchison, J.M. (2003). Growth during the cell cycle. Int Rev Cytol *226*, 165-258.

Mocciaro, A., and Schiebel, E. (2010). Cdc14: a highly conserved family of phosphatases with non-conserved functions? Journal of cell science *123*, 2867-2876.

Mochida, S., and Hunt, T. (2012). Protein phosphatases and their regulation in the control of mitosis. EMBO reports *13*, 197-203.

Mochida, S., Ikeo, S., Gannon, J., and Hunt, T. (2009). Regulated activity of PP2A-B55 delta is crucial for controlling entry into and exit from mitosis in Xenopus egg extracts. The EMBO journal *28*, 2777-2785.

Mollinari, C., Kleman, J.P., Jiang, W., Schoehn, G., Hunter, T., and Margolis, R.L. (2002). PRC1 is a microtubule binding and bundling protein essential to maintain the mitotic spindle midzone. The Journal of cell biology *157*, 1175-1186.

Morin, V., Prieto, S., Melines, S., Hem, S., Rossignol, M., Lorca, T., Espeut, J., Morin, N., and Abrieu, A. (2012). CDK-dependent potentiation of MPS1 kinase activity is essential to the mitotic checkpoint. Current biology : CB *22*, 289-295.

Moriya, H., Chino, A., Kapuy, O., Csikasz-Nagy, A., and Novak, B. (2011). Overexpression limits of fission yeast cell-cycle regulators in vivo and in silico. Mol Syst Biol *7*, 556.

Mulvihill, D.P., Petersen, J., Ohkura, H., Glover, D.M., and Hagan, I.M. (1999). Plo1 kinase recruitment to the spindle pole body and its role in cell division in Schizosaccharomyces pombe. Molecular biology of the cell *10*, 2771-2785.

Murray, A.W., and Kirschner, M.W. (1989a). Cyclin synthesis drives the early embryonic cell cycle. Nature *339*, 275-280.

Murray, A.W., and Kirschner, M.W. (1989b). Dominoes and clocks: the union of two views of the cell cycle. Science *246*, 614-621.

Murray, A.W., Solomon, M.J., and Kirschner, M.W. (1989). The role of cyclin synthesis and degradation in the control of maturation promoting factor activity. Nature *339*, 280-286.

Musacchio, A., and Salmon, E.D. (2007). The spindle-assembly checkpoint in space and time. Nature reviews Molecular cell biology *8*, 379-393.

Nannas, N.J., and Murray, A.W. (2014). Tethering sister centromeres to each other suggests the spindle checkpoint detects stretch within the kinetochore. PLoS genetics *10*, e1004492.

Nasmyth, K. (2002). Segregating sister genomes: the molecular biology of chromosome separation. Science *297*, 559-565.

Neef, R., Gruneberg, U., Kopajtich, R., Li, X., Nigg, E.A., Sillje, H., and Barr, F.A. (2007). Choice of Plk1 docking partners during mitosis and cytokinesis is controlled by the activation state of Cdk1. Nature cell biology *9*, 436-444.

Nezi, L., and Musacchio, A. (2009). Sister chromatid tension and the spindle assembly checkpoint. Curr Opin Cell Biol *21*, 785-795.

Nishiyama, A., Tachibana, K., Igarashi, Y., Yasuda, H., Tanahashi, N., Tanaka, K., Ohsumi, K., and Kishimoto, T. (2000). A nonproteolytic function of the proteasome is required for the dissociation of Cdc2 and cyclin B at the end of M phase. Genes & development *14*, 2344-2357.

Nurse, P., Thuriaux, P., and Nasmyth, K. (1976). Genetic control of the cell division cycle in the fission yeast Schizosaccharomyces pombe. Mol Gen Genet *146*, 167-178.

O'Donnell, K.L., Osmani, A.H., Osmani, S.A., and Morris, N.R. (1991). bimA encodes a member of the tetratricopeptide repeat family of proteins and is required for the completion of mitosis in Aspergillus nidulans. Journal of cell science *99 (Pt 4)*, 711-719.

Oliveira, R., and Nasmyth, K. (2010). Getting through anaphase: splitting the sisters and beyond. Biochemical Society transactions *38*, 1639-1644.

Oliveira, R.A., Hamilton, R.S., Pauli, A., Davis, I., and Nasmyth, K. (2010). Cohesin cleavage and Cdk inhibition trigger formation of daughter nuclei. Nature cell biology *12*, 185-192.

Parry, D., Hickson, G., and O'Farrell, P. (2003). Cyclin B destruction triggers changes in kinetochore behavior essential for successful anaphase. Current biology.

Parry, D.H., and O'Farrell, P.H. (2001). The schedule of destruction of three mitotic cyclins can dictate the timing of events during exit from mitosis. Current biology : CB *11*, 671-683.

Pauli, A., Althoff, F., Oliveira, R.A., Heidmann, S., Schuldiner, O., Lehner, C.F., Dickson, B.J., and Nasmyth, K. (2008). Cell-type-specific TEV protease cleavage reveals cohesin functions in Drosophila neurons. Developmental cell *14*, 239-251.

Pereira, A.J., and Maiato, H. (2012). Maturation of the kinetochore-microtubule interface and the meaning of metaphase. Chromosome research : an international journal on the molecular, supramolecular and evolutionary aspects of chromosome biology *20*, 563-577.

Pereira, G., and Schiebel, E. (2003). Separase regulates INCENP-Aurora B anaphase spindle function through Cdc14. Science (New York, NY) *302*, 2120-2124.

Pesin, J.A., and Orr-Weaver, T.L. (2008). Regulation of APC/C activators in mitosis and meiosis. Annual review of cell and developmental biology *24*, 475-499.

Peters, J.M. (2002). The anaphase-promoting complex: proteolysis in mitosis and beyond. Molecular cell *9*, 931-943.

Peters, J.M. (2006). The anaphase promoting complex/cyclosome: a machine designed to destroy. Nature reviews Molecular cell biology *7*, 644-656.

Pfleger, C.M., and Kirschner, M.W. (2000). The KEN box: an APC recognition signal distinct from the D box targeted by Cdh1. Genes & development *14*, 655-665.

Pfleger, C.M., Lee, E., and Kirschner, M.W. (2001). Substrate recognition by the Cdc20 and Cdh1 components of the anaphase-promoting complex. Genes & development *15*, 2396-2407.

Pines, J. (2006). Mitosis: a matter of getting rid of the right protein at the right time. Trends Cell Biol *16*, 55-63.

Pines, J., and Hagan, I. (2011). The Renaissance or the cuckoo clock. Philos Trans R Soc Lond B Biol Sci *366*, 3625-3634.

Potapova, T.A., Daum, J.R., Byrd, K.S., and Gorbsky, G.J. (2009). Fine tuning the cell cycle: activation of the Cdk1 inhibitory phosphorylation pathway during mitotic exit. Molecular biology of the cell *20*, 1737-1748.

Potapova, T.A., Daum, J.R., Pittman, B.D., Hudson, J.R., Jones, T.N., Satinover, D.L., Stukenberg, P.T., and Gorbsky, G.J. (2006). The reversibility of mitotic exit in vertebrate cells. Nature *440*, 954-958.

Primorac, I., and Musacchio, A. (2013). Panta rhei: the APC/C at steady state. The Journal of cell biology *201*, 177-189.

Primorac, I., Weir, J.R., Chiroli, E., Gross, F., Hoffmann, I., van Gerwen, S., Ciliberto, A., and Musacchio, A. (2013). Bub3 reads phosphorylated MELT repeats to promote spindle assembly checkpoint signaling. eLife *2*, e01030.

Prindle, A., Selimkhanov, J., Li, H., Razinkov, I., Tsimring, L.S., and Hasty, J. (2014). Rapid and tunable post-translational coupling of genetic circuits. Nature *508*, 387-391.

Queralt, E., Lehane, C., Novak, B., and Uhlmann, F. (2006). Downregulation of PP2A(Cdc55) phosphatase by separase initiates mitotic exit in budding yeast. Cell *125*, 719-732.

Rahmani, Z., Gagou, M.E., Lefebvre, C., Emre, D., and Karess, R.E. (2009). Separating the spindle, checkpoint, and timer functions of BubR1. The Journal of cell biology *187*, 597-605.

Rape, M., Reddy, S.K., and Kirschner, M.W. (2006). The processivity of multiubiquitination by the APC determines the order of substrate degradation. Cell *124*, 89-103.

Rattani, A., Vinod, P.K., Godwin, J., Tachibana-Konwalski, K., Wolna, M., Malumbres, M., Novak, B., and Nasmyth, K. (2014). Dependency of the spindle assembly checkpoint on Cdk1 renders the anaphase transition irreversible. Current biology : CB *24*, 630-637.

Reddy, S.K., Rape, M., Margansky, W.A., and Kirschner, M.W. (2007). Ubiquitination by the anaphase-promoting complex drives spindle checkpoint inactivation. Nature *446*, 921-925.

Robbins, J.A., and Cross, F.R. (2010). Regulated degradation of the APC coactivator Cdc20. Cell Div *5*, 23.

Roux, K.J., Kim, D.I., Raida, M., and Burke, B. (2012). A promiscuous biotin ligase fusion protein identifies proximal and interacting proteins in mammalian cells. The Journal of cell biology *196*, 801-810.

Rudner, A.D., and Murray, A.W. (2000). Phosphorylation by Cdc28 activates the Cdc20-dependent activity of the anaphase-promoting complex. The Journal of cell biology *149*, 1377-1390.

Sanchez, A., Choubey, S., and Kondev, J. (2013). Regulation of noise in gene expression. Annual review of biophysics *42*, 469-491.

Saurin, A.T., van der Waal, M.S., Medema, R.H., Lens, S.M., and Kops, G.J. (2011). Aurora B potentiates Mps1 activation to ensure rapid checkpoint establishment at the onset of mitosis. Nature communications *2*, 316.

Schmidt, C.K., Brookes, N., and Uhlmann, F. (2009). Conserved features of cohesin binding along fission yeast chromosomes. Genome Biol *10*, R52.

Schmitz, M.H., Held, M., Janssens, V., Hutchins, J.R., Hudecz, O., Ivanova, E., Goris, J., Trinkle-Mulcahy, L., Lamond, A.I., Poser, I.*, et al.* (2010). Live-cell imaging RNAi screen identifies PP2A-B55alpha and importin-beta1 as key mitotic exit regulators in human cells. Nature cell biology *12*, 886-893.

Schuyler, S.C., Liu, J.Y., and Pellman, D. (2003). The molecular function of Ase1p: evidence for a MAP-dependent midzone-specific spindle matrix. Microtubule-associated proteins. The Journal of cell biology *160*, 517-528.

Sczaniecka, M., Feoktistova, A., May, K.M., Chen, J.S., Blyth, J., Gould, K.L., and Hardwick, K.G. (2008). The spindle checkpoint functions of Mad3 and Mad2 depend on a Mad3 KEN box-mediated interaction with Cdc20-anaphase-promoting complex (APC/C). The Journal of biological chemistry *283*, 23039-23047.

Severson, A.F., Hamill, D.R., Carter, J.C., Schumacher, J., and Bowerman, B. (2000). The aurora-related kinase AIR-2 recruits ZEN-4/CeMKLP1 to the mitotic spindle at metaphase and is required for cytokinesis. Current biology : CB *10*, 1162-1171.

Shepperd, L.A., Meadows, J.C., Sochaj, A.M., Lancaster, T.C., Zou, J., Buttrick, G.J., Rappsilber, J., Hardwick, K.G., and Millar, J.B. (2012). Phosphodependent recruitment of Bub1 and Bub3 to Spc7/KNL1 by Mph1 kinase maintains the spindle checkpoint. Current biology : CB *22*, 891-899.

Shindo, N., Kumada, K., and Hirota, T. (2012). Separase sensor reveals dual roles for separase coordinating cohesin cleavage and cdk1 inhibition. Developmental cell *23*, 112-123.

Sigrist, S., Jacobs, H., Stratmann, R., and Lehner, C.F. (1995). Exit from mitosis is regulated by Drosophila fizzy and the sequential destruction of cyclins A, B and B3. The EMBO journal *14*, 4827-4838.

Simanis, V. (2003). The mitotic exit and septation initiation networks. Journal of cell science *116*, 4261-4262.

Simonetta, M., Manzoni, R., Mosca, R., Mapelli, M., Massimiliano, L., Vink, M., Novak, B., Musacchio, A., and Ciliberto, A. (2009). The influence of catalysis on mad2 activation dynamics. PLoS Biol *7*, e10.

Skoufias, D.A., Indorato, R.L., Lacroix, F., Panopoulos, A., and Margolis, R.L. (2007). Mitosis persists in the absence of Cdk1 activity when proteolysis or protein phosphatase activity is suppressed. The Journal of cell biology *179*, 671-685.

Stegmeier, F., and Amon, A. (2004). Closing mitosis: the functions of the Cdc14 phosphatase and its regulation. Annual review of genetics *38*, 203-232.

Stegmeier, F., Rape, M., Draviam, V.M., Nalepa, G., Sowa, M.E., Ang, X.L., McDonald, E.R., 3rd, Li, M.Z., Hannon, G.J., Sorger, P.K.*, et al.* (2007). Anaphase initiation is regulated by antagonistic ubiquitination and deubiquitination activities. Nature *446*, 876-881.

Stegmeier, F., Visintin, R., and Amon, A. (2002). Separase, polo kinase, the kinetochore protein Slk19, and Spo12 function in a network that controls Cdc14 localization during early anaphase. Cell *108*, 207-220.

Stemmann, O., Zou, H., Gerber, S.A., Gygi, S.P., and Kirschner, M.W. (2001). Dual inhibition of sister chromatid separation at metaphase. Cell *107*, 715-726.

Stratmann, R., and Lehner, C.F. (1996). Separation of sister chromatids in mitosis requires the Drosophila pimples product, a protein degraded after the metaphase/anaphase transition. Cell *84*, 25-35.

Strunnikov, A.V. (2006). SMC complexes in bacterial chromosome condensation and segregation. Plasmid *55*, 135-144.

Sudakin, V., Ganoth, D., Dahan, A., Heller, H., Hershko, J., Luca, F.C., Ruderman, J.V., and Hershko, A. (1995). The cyclosome, a large complex containing cyclin-selective ubiquitin

ligase activity, targets cyclins for destruction at the end of mitosis. Molecular biology of the cell *6*, 185-197.

Sullivan, M., and Morgan, D.O. (2007). Finishing mitosis, one step at a time. Nature reviews Molecular cell biology *8*, 894-903.

Sullivan, M., and Uhlmann, F. (2003). A non-proteolytic function of separase links the onset of anaphase to mitotic exit. Nature cell biology *5*, 249-254.

Sun, Y., Hays, N.M., Periasamy, A., Davidson, M.W., and Day, R.N. (2012). Monitoring protein interactions in living cells with fluorescence lifetime imaging microscopy. Methods in enzymology *504*, 371-391.

Sun, Y., Kucej, M., Fan, H.Y., Yu, H., Sun, Q.Y., and Zou, H. (2009). Separase is recruited to mitotic chromosomes to dissolve sister chromatid cohesion in a DNA-dependent manner. Cell *137*, 123-132.

Surana, U., Amon, A., Dowzer, C., McGrew, J., Byers, B., and Nasmyth, K. (1993). Destruction of the CDC28/CLB mitotic kinase is not required for the metaphase to anaphase transition in budding yeast. The EMBO journal *12*, 1969-1978.

Tanaka, T., Cosma, M.P., Wirth, K., and Nasmyth, K. (1999). Identification of cohesin association sites at centromeres and along chromosome arms. Cell *98*, 847-858.

Tanaka, T., Fuchs, J., Loidl, J., and Nasmyth, K. (2000). Cohesin ensures bipolar attachment of microtubules to sister centromeres and resists their precocious separation. Nature cell biology *2*, 492-499.

Thrower, J.S., Hoffman, L., Rechsteiner, M., and Pickart, C.M. (2000). Recognition of the polyubiquitin proteolytic signal. The EMBO journal *19*, 94-102.

Tinker-Kulberg, R.L., and Morgan, D.O. (1999). Pds1 and Esp1 control both anaphase and mitotic exit in normal cells and after DNA damage. Genes & development *13*, 1936-1949.

Tomonaga, T., Nagao, K., Kawasaki, Y., Furuya, K., Murakami, A., Morishita, J., Yuasa, T., Sutani, T., Kearsey, S.E., Uhlmann, F.*, et al.* (2000). Characterization of fission yeast cohesin: essential anaphase proteolysis of Rad21 phosphorylated in the S phase. Genes & development *14*, 2757-2770.

Tugendreich, S., Tomkiel, J., Earnshaw, W., and Hieter, P. (1995). CDC27Hs colocalizes with CDC16Hs to the centrosome and mitotic spindle and is essential for the metaphase to anaphase transition. Cell *81*, 261-268.

Ubersax, J.A., Woodbury, E.L., Quang, P.N., Paraz, M., Blethrow, J.D., Shah, K., Shokat, K.M., and Morgan, D.O. (2003). Targets of the cyclin-dependent kinase Cdk1. Nature *425*, 859-864.

Uchida, K.S., Takagaki, K., Kumada, K., Hirayama, Y., Noda, T., and Hirota, T. (2009). Kinetochore stretching inactivates the spindle assembly checkpoint. The Journal of cell biology *184*, 383-390.

Uhlmann, F. (2001). Secured cutting: controlling separase at the metaphase to anaphase transition. EMBO reports *2*, 487-492.

Uhlmann, F. (2003). Separase regulation during mitosis. Biochem Soc Symp, 243-251.

Uhlmann, F., Lottspeich, F., and Nasmyth, K. (1999). Sister-chromatid separation at anaphase onset is promoted by cleavage of the cohesin subunit Scc1. Nature *400*, 37-42.

Uhlmann, F., Wernic, D., Poupart, M.A., Koonin, E.V., and Nasmyth, K. (2000). Cleavage of cohesin by the CD clan protease separin triggers anaphase in yeast. Cell *103*, 375-386.

Uzunova, K., Dye, B.T., Schutz, H., Ladurner, R., Petzold, G., Toyoda, Y., Jarvis, M.A., Brown, N.G., Poser, I., Novatchkova, M.*, et al.* (2012). APC15 mediates CDC20 autoubiquitylation by APC/C(MCC) and disassembly of the mitotic checkpoint complex. Nature structural & molecular biology *19*, 1116-1123.

Vagnarelli, P., Hudson, D.F., Ribeiro, S.A., Trinkle-Mulcahy, L., Spence, J.M., Lai, F., Farr, C.J., Lamond, A.I., and Earnshaw, W.C. (2006). Condensin and Repo-Man-PP1 co-operate in the regulation of chromosome architecture during mitosis. Nature cell biology *8*, 1133-1142.

Vagnarelli, P., Ribeiro, S., Sennels, L., Sanchez-Pulido, L., de Lima Alves, F., Verheyen, T., Kelly, D.A., Ponting, C.P., Rappsilber, J., and Earnshaw, W.C. (2011). Repo-Man coordinates chromosomal reorganization with nuclear envelope reassembly during mitotic exit. Developmental cell *21*, 328-342.

Van Voorhis, V.A., and Morgan, D.O. (2014). Activation of the APC/C ubiquitin ligase by enhanced E2 efficiency. Current biology : CB *24*, 1556-1562.

van Zon, W., Ogink, J., ter Riet, B., Medema, R.H., te Riele, H., and Wolthuis, R.M. (2010). The APC/C recruits cyclin B1-Cdk1-Cks in prometaphase before D box recognition to control mitotic exit. The Journal of cell biology *190*, 587-602.

Varma, D., and Salmon, E.D. (2012). The KMN protein network--chief conductors of the kinetochore orchestra. Journal of cell science *125*, 5927-5936.

Vázquez-Novelle, M., Mirchenko, L., Uhlmann, F., and Petronczki, M. (2010). The 'anaphase problem': how to disable the mitotic checkpoint when sisters split. Biochemical Society transactions *38*, 1660-1666.

Vázquez-Novelle, M., and Petronczki, M. (2010). Relocation of the chromosomal passenger complex prevents mitotic checkpoint engagement at anaphase. Current biology : CB *20*, 1402-1407.

Vazquez-Novelle, M.D., Sansregret, L., Dick, A.E., Smith, C.A., McAinsh, A.D., Gerlich, D.W., and Petronczki, M. (2014). Cdk1 inactivation terminates mitotic checkpoint surveillance and stabilizes kinetochore attachments in anaphase. Current biology : CB *24*, 638-645.

Verbrugghe, K.J., and White, J.G. (2004). SPD-1 is required for the formation of the spindle midzone but is not essential for the completion of cytokinesis in C. elegans embryos. Current biology : CB *14*, 1755-1760.

Vig, B.K. (1981). Sequence of centromere separation: analysis of mitotic chromosomes in man. Hum Genet *57*, 247-252.

Vig, B.K. (1983). Sequence of centromere separation: occurrence, possible significance, and control. Cancer Genet Cytogenet *8*, 249-274.

Vig, B.K., and Zinkowski, R.P. (1986). Sequence of centromere separation: a mechanism for orderly separation of dicentrics. Cancer Genet Cytogenet *22*, 347-359.

Visintin, R., Craig, K., Hwang, E.S., Prinz, S., Tyers, M., and Amon, A. (1998). The phosphatase Cdc14 triggers mitotic exit by reversal of Cdk-dependent phosphorylation. Molecular cell *2*, 709-718.

Vodermaier, H.C., Gieffers, C., Maurer-Stroh, S., Eisenhaber, F., and Peters, J.M. (2003). TPR subunits of the anaphase-promoting complex mediate binding to the activator protein CDH1. Current biology : CB *13*, 1459-1468.

Waizenegger, I., Gimenez-Abian, J.F., Wernic, D., and Peters, J.M. (2002). Regulation of human separase by securin binding and autocleavage. Current biology : CB *12*, 1368-1378.

Walczak, C.E., Cai, S., and Khodjakov, A. (2010). Mechanisms of chromosome behaviour during mitosis. Nature reviews Molecular cell biology *11*, 91-102.

Wang, E., Ballister, E.R., and Lampson, M.A. (2011). Aurora B dynamics at centromeres create a diffusion-based phosphorylation gradient. The Journal of cell biology *194*, 539-549.

Wang, Z., Yu, R., and Melmed, S. (2001). Mice lacking pituitary tumor transforming gene show testicular and splenic hypoplasia, thymic hyperplasia, thrombocytopenia, aberrant cell cycle progression, and premature centromere division. Mol Endocrinol *15*, 1870-1879.

Wasserman, W.J., and Smith, L.D. (1978). The cyclic behavior of a cytoplasmic factor controlling nuclear membrane breakdown. The Journal of cell biology *78*, R15-22.

Welburn, J.P., Vleugel, M., Liu, D., Yates, J.R., 3rd, Lampson, M.A., Fukagawa, T., and Cheeseman, I.M. (2010). Aurora B phosphorylates spatially distinct targets to differentially regulate the kinetochore-microtubule interface. Molecular cell *38*, 383-392.

Wojcik, C., Schroeter, D., Stoehr, M., Wilk, S., and Paweletz, N. (1996). An inhibitor of the chymotrypsin-like activity of the multicatalytic proteinase complex (20S proteasome) induces arrest in G2-phase and metaphase in HeLa cells. European journal of cell biology *70*, 172-178.

Wolf, F., Wandke, C., Isenberg, N., and Geley, S. (2006). Dose-dependent effects of stable cyclin B1 on progression through mitosis in human cells. The EMBO journal *25*, 2802-2813.

Wolthuis, R., Clay-Farrace, L., van Zon, W., Yekezare, M., Koop, L., Ogink, J., Medema, R., and Pines, J. (2008). Cdc20 and Cks direct the spindle checkpoint-independent destruction of cyclin A. Molecular cell *30*, 290-302.

Wu, J.Q., Guo, J.Y., Tang, W., Yang, C.S., Freel, C.D., Chen, C., Nairn, A.C., and Kornbluth, S. (2009). PP1-mediated dephosphorylation of phosphoproteins at mitotic exit is controlled by inhibitor-1 and PP1 phosphorylation. Nature cell biology *11*, 644-651.

Wurzenberger, C., and Gerlich, D.W. (2011). Phosphatases: providing safe passage through mitotic exit. Nature reviews Molecular cell biology *12*, 469-482.

Yaakov, G., Thorn, K., and Morgan, D.O. (2012). Separase biosensor reveals that cohesin cleavage timing depends on phosphatase PP2A(Cdc55) regulation. Developmental cell *23*, 124-136.

Yamada, H.Y., Matsumoto, S., and Matsumoto, T. (2000). High dosage expression of a zinc finger protein, Grt1, suppresses a mutant of fission yeast slp1(+), a homolog of CDC20/p55CDC/Fizzy. Journal of cell science *113 (Pt 22)*, 3989-3999.

Yamagishi, Y., Yang, C.H., Tanno, Y., and Watanabe, Y. (2012). MPS1/Mph1 phosphorylates the kinetochore protein KNL1/Spc7 to recruit SAC components. Nature cell biology *14*, 746-752.

Yamaguchi, S., Decottignies, A., and Nurse, P. (2003). Function of Cdc2p-dependent Bub1p phosphorylation and Bub1p kinase activity in the mitotic and meiotic spindle checkpoint. The EMBO journal *22*, 1075-1087.

Yamamoto, A., Guacci, V., and Koshland, D. (1996). Pds1p, an inhibitor of anaphase in budding yeast, plays a critical role in the APC and checkpoint pathway(s). The Journal of cell biology *133*, 99-110.

Yamano, H., Gannon, J., and Hunt, T. (1996). The role of proteolysis in cell cycle progression in Schizosaccharomyces pombe. The EMBO journal *15*, 5268-5279.

Yang, Q., and Ferrell, J.E., Jr. (2013). The Cdk1-APC/C cell cycle oscillator circuit functions as a time-delayed, ultrasensitive switch. Nature cell biology *15*, 519-525.

Zachariae, W., Schwab, M., Nasmyth, K., and Seufert, W. (1998). Control of cyclin ubiquitination by CDK-regulated binding of Hct1 to the anaphase promoting complex. Science *282*, 1721-1724.

Zeng, X., and King, R.W. (2012). An APC/C inhibitor stabilizes cyclin B1 by prematurely terminating ubiquitination. Nat Chem Biol *8*, 383-392.

Zhu, C., and Jiang, W. (2005). Cell cycle-dependent translocation of PRC1 on the spindle by Kif4 is essential for midzone formation and cytokinesis. Proceedings of the National Academy of Sciences of the United States of America *102*, 343-348.

Zhu, C., Lau, E., Schwarzenbacher, R., Bossy-Wetzel, E., and Jiang, W. (2006). Spatiotemporal control of spindle midzone formation by PRC1 in human cells. Proceedings of the National Academy of Sciences of the United States of America *103*, 6196-6201.

Zou, H., McGarry, T.J., Bernal, T., and Kirschner, M.W. (1999). Identification of a vertebrate sister-chromatid separation inhibitor involved in transformation and tumorigenesis. Science *285*, 418-422.

Zou, H., Stemman, O., Anderson, J.S., Mann, M., and Kirschner, M.W. (2002). Anaphase specific auto-cleavage of separase. FEBS Lett *528*, 246-250.

Zur, A., and Brandeis, M. (2001). Securin degradation is mediated by fzy and fzr, and is required for complete chromatid separation but not for cytokinesis. The EMBO journal *20*, 792-801.

Zur, A., and Brandeis, M. (2002). Timing of APC/C substrate degradation is determined by fzy/fzr specificity of destruction boxes. The EMBO journal *21*, 4500-4510.

CURRICULUM VITAE

Personal

Name Julia Kamenz

Education

1996 – 2003 High School, Schadow Oberschule, Berlin, Germany

2003 – 2008 Studies in Biochemistry, Diploma, Eberhard Karls University Tuebingen, Germany
Diploma thesis: 'Functional analysis of Condensin's ATPase head domains *in vivo*'
Supervisor: Dr. Frank Uhlmann, London Research Institute, Lincoln's Inn Fields, CRUK, London, UK

2009 – 2014 Graduate studies, Eberhard Karls University Tuebingen, Germany
PhD thesis: 'Temporal coordination of the metaphase to anaphase transition'
Supervisor: Dr. Silke Hauf, Friedrich Miescher Laboratory of the Max Planck Society, Tuebingen, Germany (now: Virginia Polytechnic Institute and State University)

LIST OF PUBLICATIONS

Accepted manuscripts

1. **Kamenz, J**., and Hauf, S. (2014). Slow checkpoint activation kinetics as a safety device in anaphase. Curr Biol *24*, 646-651.

2. Heinrich, S., Geissen, E.M., **Kamenz, J.**, Trautmann, S., Widmer, C., Drewe, P., Knop, M., Radde, N., Hasenauer, J., and Hauf, S. (2013). Determinants of robustness in spindle assembly checkpoint signalling. Nat Cell Biol *15*, 1328-1339.

3. Fromm, S.A., **Kamenz, J.**, Noldeke, E.R., Neu, A., Zocher, G., and Sprangers, R. (2014). In vitro reconstitution of a cellular phase-transition process that involves the mRNA decapping machinery. Angew Chem Int Ed Engl *53*, 7354-7359.

4. Fromm, S.A., Truffault, V., **Kamenz, J.**, Braun, J.E., Hoffmann, N.A., Izaurralde, E., and Sprangers, R. (2012). The structural basis of Edc3- and Scd6-mediated activation of the Dcp1:Dcp2 mRNA decapping complex. Embo J *31*, 279-290.

Submitted manuscripts

1 Kamenz, J., Mihaljev, T., Legewie, S., and Hauf, S.
Synchronous sister chromatid splitting in anaphase without occurs without obligatory feedback, *Journal of Cell Biology*

Manuscript in preparation

1 Kamenz, J., Mihaljev, T., Kubis, A., Legewie, S., and Hauf, S.
Properties of the degradation machinery ensure temporal coupling during anaphase, *to be submitted to Molecular Cell*